Efficient prediction of the fluvial dike failure dynamics: hydraulic prediction of breach discharge.

Auteur : Wylock, Grégoire
Promoteur(s) : Dewals, Benjamin
Faculté : Faculté des Sciences appliquées
Diplôme : Master en ingénieur civil des constructions, à finalité spécialisée en "civil engineering"
Année académique : 2020-2021
URI/URL : http://hdl.handle.net/2268.2/11551

University of Liège - Faculty of Applied Sciences

Efficient prediction of the fluvial dike failure dynamics: *hydraulic prediction of breach discharge*

Master's thesis carried out to obtain the degree of Master of Science in Civil Engineering

Author
WYLOCK Grégoire

Supervisor
Mr. DEWALS Benjamin (ULiège)

Jury members
Mr. ERPICUM Sébastien (ULiège)
Mr. PIROTTON Michel (ULiège)
Mr. ARNST Maarten (ULiège)
Mr. EL KADI ABDERREZZAK Kamal (LNHE, EDF R&D)

Academic year 2020-2021

Abstract

Fluvial dike breaches are a recurrent and major worldwide issue. Indeed, many recent events have shown the disastrous impacts that can occur as a result of dike failure. Therefore, it is essential to be able to obtain information on the hydraulic variables related to this type of event. The emergence of numerical methods enables the creation and the use of different models allowing the prediction of these variables. Complex models (2D/3D) already exist in literature. However, the need for simpler models is increasing. These provide a higher number of simulations because the computation time is very low. This is one of the advantages of this kind of model. The present work has enabled the development of two simpler numerical models (0D/1D) based exclusively on hydraulic principles. The numerical models used allow obtaining hydraulic variables such as lateral discharge. However, the first steps in the development of the models were focused on obtaining lateral discharge coefficients. For this purpose, formulations of the lateral discharge coefficient had to be sought. Some empirical formulae coming from literature were used.

The models development was first based on simpler hydraulic configuration cases. The configurations used are characterized by a fixed breach geometry with zero or non-zero lateral crest height. These basic cases enabled the comparison of the results obtained with the different models and the experimental results. In addition to the creation of numerical models, this work allowed the different empirical formulae for the discharge coefficient to be tested. For each test performed, the results obtained with these formulae were analyzed in order to identify relevant and irrelevant formulations. Once the base cases were analyzed, the models were redeveloped to suit dynamic breach evolutions. The results obtained in these more complex configurations were analyzed according to the model used and the formulation employed.

A sensitivity analysis was also conducted to identify how uncertainties in the input parameters influence the results. This analysis was conducted on the dynamic breach tests. It was found that the uncertainties do not significantly influence the results. This conclusion is only valid in the experimental context.

The overall synthesis of the empirical formulae accuracy was not straightforward to obtain. Formulations which work for one specific test do not necessarily correspond to those which work best for the other tests. Nevertheless, this work has highlighted the most effective formulations for each test performed. Subramanya and Awasthy (1972) formula provides the best breach discharge results for fixed lateral opening with zero crest height. Singh et al. (1994) expression must be used with non-zero crest height configuration. For dynamic breach opening cases, Hager (1987) formulation gives the most accurate results.

In addition, a comparison of the results from the two models was also conducted. This enabled the identification of the appropriate use of one model rather than the other. The lumped model combined with the accurate formulations gives better breach discharge results than the spatially-discretized model for experiments with fixed breach geometry. For this type of tests, the water depths are more accurately estimated by the 1D model. For the dynamic breach opening, the 0D model provides an accurate average water depth. However, the spatially-discretized provides the most accurate peak breach discharges.

Résumé

Les ruptures de digues fluviales sont un problème récurrent et majeur à l'échelle mondiale. En effet, de nombreux événements récents ont montré les impacts désastreux que peut avoir une rupture de digue. Il est donc essentiel de pouvoir obtenir des indications sur les variables hydrauliques liées à ce type d'événement. L'émergence des méthodes numériques permet la création et l'utilisation de différents modèles permettant la prédiction de ces variables. Des modèles complexes (2D/3D) existent déjà dans la littérature. Cependant, le besoin de modèles plus simples est croissant. Un des avantages de ces modèles simples est la possibilité de réaliser un plus grand nombre de simulations étant donné le faible temps de calcul nécessaire. Le présent travail a permis le développement de deux modèles numériques plus simples (0D/1D) basés exclusivement sur des principes hydrauliques. Les modèles numériques utilisés permettent l'obtention de variables hydrauliques telles que le débit de brèche. Les premières étapes du développement de ce genre de modèles se sont focalisées sur l'obtention de coefficients de débit latéral. Pour ce faire, des formulations empiriques issues de la littérature ont été utilisées.

Le développement de ces modèles s'est d'abord basé sur des configurations hydrauliques plus simples caractérisées par une géométrie de brèche fixe avec ou sans crête latérale. Ces cas de base ont permis de comparer les résultats obtenus avec les différents modèles avec les résultats expérimentaux. En plus de la création de modèles numériques, ce travail a permis de tester les différentes formules empiriques de coefficient de débit. Pour chaque test effectué, les résultats obtenus avec ces formules ont été analysés afin d'identifier la pertinence de ces formulations. Une fois les cas de base analysés, les modèles ont été redéveloppés pour s'adapter aux évolutions dynamiques de brèches. Les résultats obtenus dans ces configurations plus complexes ont également été analysés en fonction du modèle utilisé et de la formulation employée.

Une analyse de sensibilité a également été menée afin de caractériser l'influence des incertitudes des paramètres d'entrée sur les résultats. Cette analyse a été menée sur les essais de rupture dynamique. Il a été constaté que les incertitudes n'influencent pas significativement les résultats. Cette conclusion n'est valide que pour le contexte expérimental.

La synthèse générale de la pertinence des formules empiriques n'a pas été simple à obtenir. En effet, certaines formulations qui fonctionnent pour un test spécifique ne correspondent pas nécessairement à celles qui fonctionnent le mieux pour les autres tests. Néanmoins, ce travail a mis en évidence les formulations les plus efficaces pour chaque test effectué. La formule de Subramanya and Awasthy (1972) permet l'obtention de meilleurs résultats de débit de brèche pour une ouverture latérale fixe avec une hauteur de crête nulle. La formulation de Singh et al. (1994), quant à elle, peut être utilisée avec une configuration de hauteur de crête non nulle. Pour les cas d'ouverture de brèche dynamique, la formule de Hager (1987) doit être privilégiée. Un classement de performance des différentes formulations a également été établi afin de synthétiser les diverses analyses réalisées.

En outre, une comparaison des résultats provenant des deux modèles a également été effectuée. Cela a permis d'identifier l'utilisation appropriée d'un modèle plutôt que l'autre. Le modèle 0D combiné aux formulations efficaces permet d'obtenir de meilleurs résultats de débit de brèche que le modèle spatialement discrétisé pour les expériences avec une géométrie de brèche fixe. Pour ce type d'essais, les hauteurs d'eau sont estimées avec plus de précision par le modèle 1D. Concernant les essais avec ouverture dynamique de la brèche, le modèle 0D fournit une hauteur d'eau moyenne précise. Cependant, c'est le modèle spatialement discrétisé qui offre les meilleurs résultats en termes de débit de brèche.

Remerciments

Au travers de ces quelques lignes, je tiens à remercier chacune des personnes ayant contribué à l'élaboration de mon travail de fin d'études. Il me serait difficile de remercier individuellement celles et ceux qui sont intervenues de manière positive sur mon parcours universitaire tellement cette liste est étendue. Je vais donc me limiter aux personnes ayant participé de manière directe ou indirecte à la réalisation du présent travail.

Je voudrais tout d'abord remercier mon promoteur B. Dewals ainsi que son doctorant V. Schmitz pour l'engagement et le sérieux avec lequel ils m'ont encadré durant tout ce quadrimestre. Leurs précieux conseils m'ont permis de viser toujours plus haut. Je n'oublierai jamais leur bienveillance à mon égard. Je les remercie également pour la confiance qui m'a été accordée. Je tiens à remercier également le département d'hydraulique de m'avoir donné l'opportunité de réaliser ce travail au sein de leur service. Je remercie également E. Mignot et G. Michelazzo pour leur professionnalisme lors de nos échanges relatifs à leurs articles scientifiques respectifs.

Ensuite, je remercie toutes les personnes qui ont pris de leur temps pour relire et apporter des corrections à mon travail. Je tiens à souligner leur implication et leur dévouement sans faille.

Enfin, je remercie mes proches pour le soutien inconditionnel durant ces 5 années et plus particulièrement durant ce quadrimestre. Leurs encouragements presque quotidiens m'ont permis de rester focalisé sur mon objectif principal : la réalisation et finalisation de ce mémoire. Cela ne fût pas de tout repos (même pour eux!). Les mots me manquent pour leur dire combien leur présence fût capitale tout au long de mon parcours scolaire.

Je terminerai en réitérant mes remerciements à chacun des intervenants pour m'avoir encouragé et permis d'être fier du travail accompli lors de mon parcours universitaire au sein de l'Université de Liège.

Contents

1 Introduction **1**

1.1 Context . . . 1

1.2 Specific objectives . . . 4

2 Literature review **5**

2.1 Basic concepts of dikes . . . 5

2.2 Numerical models . . . 10

2.2.1 2D model (Rifai, 2018) . . . 10

2.2.2 Simple process-oriented model (Wu, 2013) . . . 11

3 Reference data **12**

3.1 Flow with fixed breach geometry . . . 13

3.1.1 Roger et al. (2009) . . . 13

3.1.2 Michelazzo et al. (2015) . . . 16

3.1.3 Mignot et al. (2020) . . . 20

3.2 Flow with dynamic breach geometry . . . 23

3.2.1 Rifai (2018) . . . 23

3.3 Side weir discharge coefficient formulations . . . 29

3.3.1 Comparison methodology . . . 32

4 Models development **34**

4.1 Lumped model: 0D model . . . 35

4.2 Spatially-distributed model: 1D model . . . 37

4.2.1 Rectangular cross-section . . . 38

4.2.2 Trapezoidal cross-section . . . 42

5 Results **46**

5.1 Flow with fixed breach geometry and zero lateral crest height . . . 47

5.1.1 Roger et al. (2009) . . . 47

5.1.2 Michelazzo et al. (2015) . . . 57

5.1.3 Mignot et al. (2020) . . . 68

5.1.4 Tests comparison . . . 77

5.2 Flow with fixed breach geometry and non-zero lateral crest height . . . 79

5.2.1 Mignot et al. (2020) . . . 79

5.2.2 Changes in the implementation of formulations . . . 87

5.3 Flow with dynamic breach geometry 89
5.3.1 Rifai (2018) 89
5.3.2 Sensitivity analysis 101
5.4 Overview of the results 116

6 Perspectives **119**

7 Conclusion **120**

References **122**

A Appendix **125**
A.1 Results comparison of the different rating curves for Michelazzo et al. (2015) tests 125
A.1.1 Lumped model 125
A.1.2 Spatially-distributed model 125
A.2 PDF used for sensitivity analyses 132

List of Figures

1.1 Surrounding New Orleans dikes failure (after Hurricane Katrina) caused severe flooding of the city (Hallissy, 2005). . . . 1

1.2 Examples of recent breach events around the world (non-exhaustive list): A (Gaddie et al., 2021); B (RTBF, 2010); C (RTBF, 2012); D (APNews, 2019). . . 2

1.3 St. Elizabeth's flood in the Netherlands (Rijksmuseum, 2021). . . . 3

2.1 Natural dikes formation (Rifai, 2018). . . . 5

2.2 Dike construction near a watercourse (TenCate, 2021). . . . 6

2.3 Failure mechanisms (Flóriàn et al., 1998). . . . 7

2.4 Number of dike failures according to the failure mode (Danka and Zhang, 2015). 8

2.5 Evolution of the relative frequency of failure mechanism (Danka and Zhang, 2015). 8

2.6 Identification of 3 main stages of breach expansion for different tests carried out by Rifai (2018): longitudinal dikes profiles for two different tests ((a) Test 23 and (b) Test 8) with z the profile elevation and x the spatial coordinate along the main flow axis; width breach (w_b) evolution (c). The red dotted lines represent the floodplain fixed water level (Rifai, 2018). . . . 9

2.7 Coupling of hydrodynamic and morphodynamic models (Rifai, 2018). . . . 10

2.8 Embankment breach by overtopping: (a) longitudinal profile and (b) cross-section (Wu, 2013). . . . 11

3.1 Overall work organization: case with fixed breach (left) and dynamic breach (right). . . . 12

3.2 Experimental set-up (Roger et al., 2009). . . . 13

3.3 Water depth profiles from the 2D FV model. . . . 15

3.4 Michelazzo tests experimental set-up: (a) plan view; (b) longitudinal section (cut A-A'); (c) cross-section (cut DD') (Michelazzo et al., 2015). . . . 16

3.5 Different possible rating curves from Michelazzo (2014) and experimental results regressions with Q_d the downstream discharge. . . . 18

3.6 Water depth profiles along the center line of the main channel (Michelazzo et al., 2015). . . . 19

3.7 Experimental set-up (Mignot et al., 2020). . . . 20

3.8 Set of openings with dimensions in mm (Mignot et al., 2020). . . . 21

3.9 Experimental set-up (ULiège model) of the Rifai (2018) experiments (Rifai et al., 2019). . . . 24

3.10 Laser profilometry technique used in the experiments to collect information on the evolution of the dike geometry (Rifai, 2018). . . . 25

3.11 Rating curves for different discharges injected upstream of the channel: z_w is the downstream water depth obtained after weighting the water depths at the 3 probes (Rifai, 2018). . . . 26

3.12 Evolution of the breach geometry for a given section ($y = 0.65$m) according to the tests selected. 27
3.13 Evolution of the different experimental discharges according to the tests selected. 27
3.14 Evolution of the different experimental water depths at positions G1, G2 and G3 according to the tests selected. 28
3.15 Ranges of parameters (Fr and L_s/W) used in authors formulae and tests configurations (Michelazzo et al., 2015; Mignot et al., 2020; Roger et al., 2009). . . . 31
3.16 Ranges of parameters (Fr and p/h) used in authors formulae and tests configurations (Michelazzo et al., 2015; Mignot et al., 2020; Roger et al., 2009). 31

4.1 Implemented models and experiments used for each model. 34
4.2 Schematic representation of the 0D model (Equation 4.1 on the left and Equation 4.2 on the right). 35
4.3 Comparison of experimental and calibrated drainage discharges. 36
4.4 Rectangular cross-section with side weir. 38
4.5 Two-step Runge-Kutta algorithm (predictor and corrector). 40
4.6 Trapezoidal cross-section as used in Rifai (2018) experiments. 42

5.1 Organization of the chapter presenting the results obtained. 46
5.2 Breach discharge (0D model) for Roger et al. (2009) tests. 48
5.3 Difference between numerical (0D model) and experimental breach discharge for Roger et al. (2009) tests. 48
5.4 Water depth results (0D model) for Roger et al. (2009) tests. 49
5.5 Difference between numerical water depth results (0D model and 2D model) for Roger et al. (2009) tests. 50
5.6 Breach discharge results (1D model) for Roger et al. (2009) tests. 51
5.7 Difference between numerical (1D model) and measurement breach discharge results for Roger et al. (2009) tests. 51
5.8 Discharge profiles along the channel axis (1D model) for Roger et al. (2009) tests. 52
5.9 Froude profiles along the channel axis (1D model) for Roger et al. (2009) tests. . 53
5.10 Water depth profiles along the channel axis (1D model) and water depth profiles from 2D FV model for Roger et al. (2009) tests. 53
5.11 Breach discharge non-normalized indicators for Roger et al. (2009) tests. 54
5.12 Water depth non-normalized indicators for Roger et al. (2009) tests. 55
5.13 Water depth and breach discharge normalized indicators for all models, tests and formulations (Roger et al. (2009) tests). 56
5.14 Breach discharges (0D model) for Michelazzo et al. (2015) tests. 58
5.15 Breach discharges difference (0D model) for Michelazzo et al. (2015) tests. . . . 59
5.16 Water depths (0D model) for Michelazzo et al. (2015) tests. 59
5.17 Difference water depth (0D model) for Michelazzo et al. (2015) tests. 60
5.18 Breach discharges (1D model) for Michelazzo et al. (2015) tests. 61

5.19 Breach discharges difference (1D model) for Michelazzo et al. (2015) tests. . . . 61
5.20 Water depth profiles for all tests using the series A & B rating curve for Michelazzo et al. (2015) tests. . . . 62
5.21 Froude profiles for all tests using the series A & B rating curve for Michelazzo et al. (2015) tests. . . . 63
5.22 Discharge profiles for all tests using the series A & B rating curve for Michelazzo et al. (2015) tests. . . . 64
5.23 Breach discharge non-normalized indicators for Michelazzo et al. (2015) tests. . . 65
5.24 Water depth non-normalized indicators for Michelazzo et al. (2015) tests. 66
5.25 Water depth and breach discharge normalized indicators for the all tests, models and formulations (Michelazzo et al. (2015) tests). . . . 67
5.26 Breach discharge results (0D model) for Mignot et al. (2020) Op2 tests. 69
5.27 Breach discharge difference between numerical (0D model) and measurement for Mignot et al. (2020) Op2 tests. . . . 69
5.28 Water depth results (0D model) for Mignot et al. (2020) Op2 tests. 70
5.29 Water depth difference between numerical (0D model) and measurement for Mignot et al. (2020) Op2 tests. . . . 70
5.30 Breach discharge results (1D model) for Mignot et al. (2020) Op2 tests. 71
5.31 Breach discharge difference between numerical (1D model) and measurement for Mignot et al. (2020) Op2 tests. . . . 72
5.32 Water depth profiles (1D model) for Mignot et al. (2020) Op2 tests. 73
5.33 Discharge profiles (1D model) for Mignot et al. (2020) Op2 tests. 73
5.34 Froude profiles (1D model) for Mignot et al. (2020) Op2 tests. 74
5.35 Breach discharge non-normalized indicators for Mignot et al. (2020) Op2 tests. . 75
5.36 Water depth non-normalized indicators for Mignot et al. (2020) Op2 tests. . . . 75
5.37 Water depth and breach discharge normalized indicators for the all tests, models and formulations (Mignot et al. (2020) Op2 tests). . . . 76
5.38 Water depth and breach discharge normalized indicators for the all tests (Michelazzo, 2014; Mignot et al., 2020; Roger et al., 2009), models and formulations. 78
5.39 Breach discharge results 0D model for Mignot et al. (2020) Op1 tests. 80
5.40 Breach discharge difference (0D model) for Mignot et al. (2020) Op1 tests. . . . 80
5.41 Water depth results 0D model for Mignot et al. (2020) Op1 tests. 81
5.42 Water depth difference (0D model) for Mignot et al. (2020) Op1 tests. 81
5.43 Breach discharge results (1D model) for Mignot et al. (2020) Op1 tests. 82
5.44 Breach discharge difference between numerical (1D model) and measurement for Mignot et al. (2020) Op1 tests. . . . 83
5.45 Water depth profiles (1D model) for Mignot et al. (2020) Op1 tests. 84
5.46 Discharge profiles (1D model) for Mignot et al. (2020) Op1 tests. 84
5.47 Froude profiles (1D model) for Mignot et al. (2020) Op1 tests. 84
5.48 Breach discharge non-normalized indicators for Mignot et al. (2020) Op1 tests. . 85

5.49 Water depth non-normalized indicators for Mignot et al. (2020) Op1 tests. . . . 86
5.50 Water depth and breach discharge non-normalized indicators for all tests, models and formulations (Mignot et al. (2020) Op1 tests). 86
5.51 Impact of alternative formulations implementation on breach discharge non-normalized indicators. 88
5.52 Impact of alternative formulations implementation on water depth non-normalized indicators. 88
5.53 Methodology used to select the bottom depth for each numerical model. 89
5.54 Breach width and bottom depth evolution used in the 0D model. 90
5.55 Breach geometry evolution for Test 1 used in the 1D model. 91
5.56 Test 1 (0D model): evolution of breach and outlet discharges and water depth. . 93
5.57 Test 4 (0D model): evolution of breach and outlet discharges and water depth. . 93
5.58 Test 8 (0D model): evolution of breach and outlet discharges and water depth. . 94
5.59 Test 11 (0D model): evolution of breach and outlet discharges and water depth. 94
5.60 Test 1 numerical results (1D model): time evolution of breach discharge, outlet discharge and water depths at G1 and G3 positions; water depth profiles during specific time included in stage 1 and stage 2. 97
5.61 Test 4 numerical results (1D model): time evolution of breach discharge, outlet discharge and water depths at G1 and G3 positions; water depth profiles during specific time included in stage 1 and stage 2. 98
5.62 Test 8 numerical results (1D model): time evolution of breach discharge, outlet discharge and water depths at G1 and G3 positions; water depth profiles during specific time included in stage 1 and stage 2. 99
5.63 Test 11 numerical results (1D model): time evolution of breach discharge, outlet discharge and water depths at G1 and G3 positions; water depth profiles during specific time included in stage 1 and stage 2. 100
5.64 Main steps of the sensitivity analysis. 101
5.65 Example of the generated PDF (in orange) and the distribution of the thousand random draws made (blue bars), here for the inlet discharge. 103
5.66 Method used to transform random value y to normalized form parameter by using CDF^{-1}. 103
5.67 Calculation procedure where ν is the number of simulations only for 1 parameter change, n the number of considered parameters, ref refers to the reference parameters, *comp* refers to the computed parameters. 104
5.68 Convergence of the normalized form of the significant descriptor for the 3 selected output variables (0D model). 107
5.69 Convergence of the normalized form of the significant descriptor for the 3 selected output variables (0D model) with $\alpha = 10$. 109
5.70 Convergence of the normalized significant descriptor results for peak breach discharge and the time at which it occurs (1D model). 113
5.71 Convergence of the normalized significant descriptor results for water depth at different positions during stage 1 (1D model). 114

5.72 Convergence of the normalized significant descriptor results for water depth at different positions during stage 2 (1D model). 115

5.73 Identification of accurate (✓) or inaccurate (x) empirical formulae according to the numerical model used and the hydraulic variable considered for each experimental test. For each hydraulic variable of each test, a combination of the numerical model and the formulation giving the best results is also provided (bold shaded formula). The coloreds legend used for each formula throughout the thesis is also indicated. 117

5.74 Breach discharges ranking performance of the formulations according to the test and the hydrodynamic model considered. 118

A.1 Breach discharge results (0D model) for the 4 rating curves of Michelazzo et al. (2015) tests. 126

A.2 Difference between numerical (0D model) and measurement breach discharge results for the 4 rating curves of Michelazzo et al. (2015) tests. 127

A.3 Water depth results (0D model) for the 4 rating curves of Michelazzo et al. (2015) tests. 128

A.4 Water depth difference between numerical (0D model) and experimental average for the 4 rating curves of Michelazzo et al. (2015) tests. 129

A.5 Breach discharge results (1D model) for the 4 rating curves of Michelazzo et al. (2015) tests. 130

A.6 Breach discharge difference between numerical (1D model) and measurement for the 4 rating curves of Michelazzo et al. (2015) tests. 131

A.7 PDF for all input parameters (in orange) and the distribution of the thousand random draws made (blue bars) for 0D model with $\alpha = 4$. 132

A.8 PDF for all input parameters (in orange) and the distribution of the thousand random draws made (blue bars) for 0D model with $\alpha = 10$. 133

A.9 PDF for all input parameters (in orange) and the distribution of the five hundred random draws made (blue bars) for 1D model with $\alpha = 4$. 134

1 | Introduction

1.1 Context

Water management has become a global issue over the years. Humans have been trying for generations to control this complex element. Whether in shortage or excess, water management is a key parameter for the sustainability of human life. Therefore, the control of water is a major point of interest throughout the entire world.

Climate change has a major impact on the flow dynamics such as river flow for instance. The scientific community is even talking about the "rising water level" resulting from climate change, particularly in the melting of glaciers. The change in the behavior of water flows can have a strong impact on human civilization. Indeed, for decades, the rapid development of urbanization due to the constant demographic increase is observed. The emergence of these new urban areas considerably increases the risk of flooding in flood events. Indeed, as risk is defined as the combination of causes and consequences, the more potential assets that can be damaged, the more numerous and costly the consequences, the higher the level of risk. The causes are diverse, but climate change is increasing the frequency of flooding and therefore the level of risk.

It is essential to be able to predict the behavior of our rivers to prevent the risk of flooding. Flooding can occur as a consequence of many causes. A possible cause is, for instance, the breach of a fluvial dike. This kind of event can have disastrous consequences such as asset destruction or casualties. A concrete example is Hurricane Katrina (2005) which affected southern Louisiana. As a result of this hurricane, the city of New Orleans was almost completely flooded (Figure 1.1). Indeed, shortly after the hurricane hit, more than 80% of the city was underwater. The cause of the flooding was nothing less than the breach development in the dikes (by overtopping) surrounding the city (Knabb et al., 2005).

Figure 1.1: Surrounding New Orleans dikes failure (after Hurricane Katrina) caused severe flooding of the city (Hallissy, 2005).

The New Orleans dike failure is not an isolated case. There are many examples of dike breaches. The following list is a non-exhaustive selection of reported cases of dike breaches:

- 3 June 2004 (FIGURE 1.2A): dike breach (Sacramento-San Joaquin River) in Jones Track (Northern California, United States).
- 22 June 2010 (FIGURE 1.2B): river flooding caused the failure of the Changkai dike (Jiangxi province, China).
- 5 January 2012 (FIGURE 1.2C): heavy rainfall increased the discharge of the Muriaé River and caused the partial collapse of a dike protecting the town of Campos do Goytacazes (Rio de Janeiro state, Brazil).
- 3 June 2019 (FIGURE 1.2D): breach of Pin Oak dike (Mississippi River) in Winfield (Illinois, United States).

Figure 1.2: Examples of recent breach events around the world (non-exhaustive list): A (Gaddie et al., 2021); B (RTBF, 2010); C (RTBF, 2012); D (APNews, 2019).

During these breaching events, part of the population had to be relocated as the situation was considered unsafe. This was the case during the Brazilian levee failure (FIGURE 1.2C), which resulted in the relocation of fewer than 4000 people (RTBF, 2012). The dike breach in China (FIGURE 1.2B) resulted in the fatalities of more than 100 people and economic losses of millions of euros (RTBF, 2010).

As the examples show, the problem of dike breaches is still major nowadays. This problem exists for centuries. A case of flooding due to dike breaches has been recorded in 1421: the St. Elizabeth's flood (the Netherlands). The dike breach occurred after a strong storm in the region. The consequence of this failure was significant flooding of the land, with more than 25 villages submerged (FIGURE 1.3). This dramatic event was one of the most lethal floods in the world, with thousands of casualties (Weerts et al., 2012).

FIGURE 1.3 illustrates a historical painting of the St. Elizabeth's flood. In the top right-hand corner of the figure, the dike breach causing the flooding of the land is clearly identified.

Figure 1.3: St. Elizabeth's flood in the Netherlands (Rijksmuseum, 2021).

The number of dike breaches recorded shows the importance of this issue. The examples illustrated previously highlight the historical nature of this issue and its current occurrence. Thus, it is essential to develop methods to improve the understanding of the dike failure phenomenon by identifying the geotechnical and hydraulic parameters influencing this process. Understanding the dynamics of dike breaches is therefore a key element in the fight against flood risk.

1.2 Specific objectives

The main objective of this thesis is the development of simple numerical models that can be used to quickly obtain valuable information about the flow dynamics through dike breaches. To achieve this aim, the models were first tested on multiple cases. The purpose is to implement these models in a first step on simple cases. Then, in a second step, to improve them to get closer and closer to real cases of dike failures.

A parallel objective to the development of numerical models is to use weir discharge coefficient formulations for all tests. The test cases were used to analyze the performance of weir coefficient formulae proposed in literature (Mignot et al., 2020) for fixed lateral openings. These expressions have been tested for the simplest cases of flow corresponding to the very essence of their development. Then, for complex cases, these empirical expressions have been tested to validate or not their use even if they have not been developed in this context.

These different steps allow progressing from simple cases of lateral opening flows to more complex flows with dynamic breaching. Three different hydraulic configurations were covered, including 24 tests in total. The results are also analyzed step by step according to the hydraulic configurations tested.

For this thesis two numerical models were implemented: a lumped model (0D model) and a model with a spatial discretization in the main flow direction (1D model). Like all simple models, they do not take into account all physical phenomena and some are simplified. However, these models allow obtaining conclusive results fairly quickly. Nevertheless, it is important to be aware of the various approximations made in the models.

The models developed only consider flows and are therefore exclusively based on hydrodynamic concepts. Sediment and erosion concepts have not been implemented. One of the perspectives of a future work on this thesis would be to include the morphodynamic processes in the different models. This would allow getting closer to the processes regulating the breach opening and the dynamics related to these processes. Thus, there would be a combination of hydrodynamic and morphodynamic processes.

This work focuses exclusively on the development of breaches related to dike failure by external erosion and more specifically by overtopping. The overtopping of dikes was intensively studied by Rifai (2018) during his doctoral thesis. The experiments carried out by Rifai (2018) are used as test cases in this thesis.

2 | Literature review

2.1 Basic concepts of dikes

Dikes[1] are structures that are mainly located along watercourses or coastal zones. These structures form the watercourse banks or coastal defenses and protect the plains from possible flooding (watercourses minor bed or coastal overflows). The main purpose of fluvial dikes is to maintain the main flow in the minor river bed. The aim of coastal dikes is to separate the sea or ocean from the inland coastal zone. Both types of dikes have the same main concern: to prevent flooding (CIRIA, 2013). This purpose belongs in the context of flood risk management.

Dikes can be created naturally or artificially by human intervention (Rifai, 2018). Natural dikes can be formed by a succession of flooding cycles and return to the normal situation. Indeed, during a flood period, the water level rises in the minor bed and can sometimes exceed the bank level to reach the major bed. During these rises in water level, sediments can be carried away and deposited in the major river bed at the level of the floodplains. When the water recedes, the water returns to its minor bed but the sediment remains on the banks. After several cycles, thanks to the accumulation of sediments, the banks are higher than initially: dikes have been created naturally. This creation process is illustrated below in FIGURE 2.1. In stage 2 (FIGURE 2.1(b)), sediment deposition takes place in the major river bed. The thickest and coarsest sediments settle on the edges of the channel, closest to the minor bed. By contrast, thin and fine sediments settle on the outer parts of the floodplain, furthest from the minor bed (Hudson, 2005).

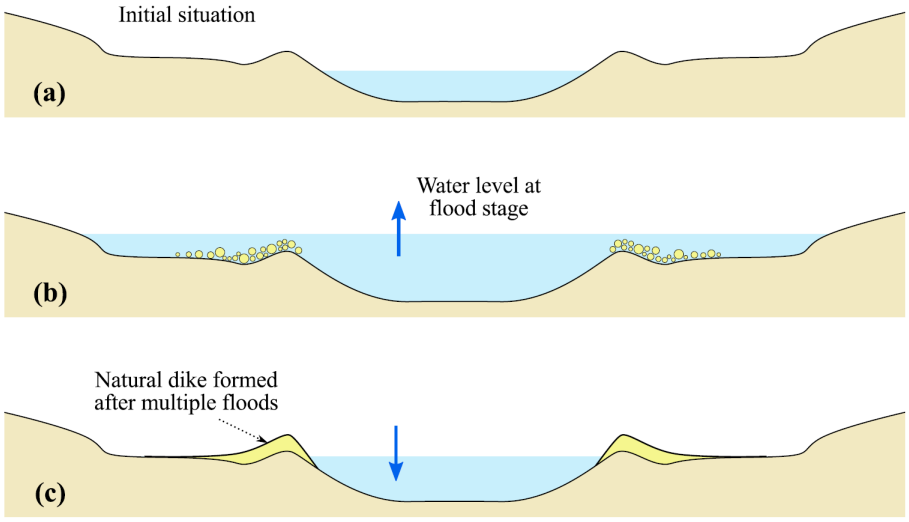

Figure 2.1: Natural dikes formation (Rifai, 2018).

The artificial dikes construction follows the same logic as the natural dikes formation. Coarse and fine materials such as rock or sand are piled up step by step to form the dike (Rifai, 2018). An example of an area that has been artificially reshaped by human is shown in FIGURE 2.2. This figure also shows the layout of the watercourse bed and banks, which are usually made up of coarser materials for rivers or coastal areas.

[1] Also called dykes or levees.

In contrast, the banks and bottoms of channels are made of smooth materials such as concrete (TenCate, 2021). On the left side of the figure, a protective dike is illustrated. These dikes can be made of simple granular materials such as natural dikes or more artificial materials like polymers (represented by the orange lines) such as man-made dikes.

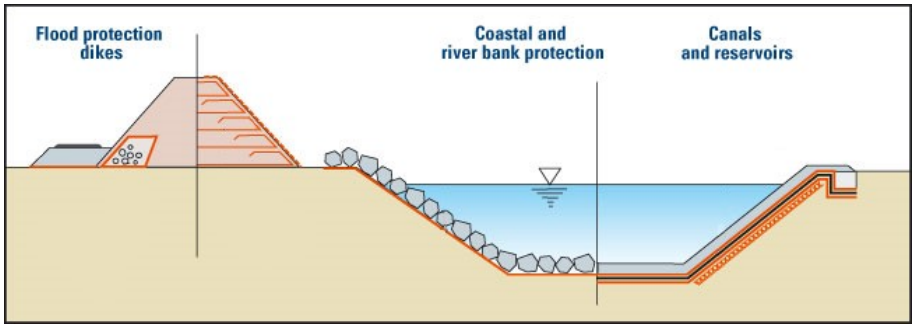

Figure 2.2: Dike construction near a watercourse (TenCate, 2021).

Dikes, regardless of their nature, are usually structures built with natural materials from the alluvial plains. As a result, dikes are often non-regular structures in their shape and/or construction. Therefore, special attention must be paid to these structures during their entire life cycle, from the design phase, through construction, maintenance, repair, etc., to an eventual replacement (Rifai, 2018). Indeed, a local weakness in dikes leads to a significant vulnerability of these structures: *"such systems should be considered as chains that are only as strong as the weakest link"* (CIRIA, 2013).

The consequences of a dike failure can be disastrous. Damages have different forms (direct or indirect) and are measured differently (tangible or non-tangible) (de Moel et al., 2015). Direct tangible damages include damages to buildings and their contents for instance. The following table (TABLE 2.1) illustrates the differences between damages based on their forms and measurements.

		Measurement	
		Tangible	Intangible
Form of the damage	Direct	Physical damage to assets: - buildings - contents - infrastructures	- Loss of life - Health effects - Loss of ecological goods
	Indirect	- Loss of industrial production - Traffic disruption - Emergency costs	- Inconvenience of post-flood recovery - Increased vulnerability of survivors

Table 2.1: Damage classification (Dewals, 2020).

Having identified the consequences of dike failure, there is now a need to understand the main mechanisms leading to the failure. There are two principal types of dike failure mechanisms identified:

- Instability: this failure mechanism depends essentially on the specific properties of the dike, such as its granular material composition and structure. Instability occurs when the external forces applied to the dike exceed its intrinsic resistance. This is the case when the forces of movement of the granular materials exceed the resisting forces of cohesion (Rifai, 2018).
- Erosion: this failure mechanism can be differentiated into two distinct mechanisms depending on the eroded area: the first being internal erosion and the second external erosion.
  - Internal erosion concerns, as its name indicates, the erosion inside the dike: erosion of the dike core. This type of erosion is the consequence of excessive infiltration within the dike. This seepage carries away particles from the dike structure and creates internal erosion (Rifai, 2018).
  - External erosion refers to the degradation of the outer dike surfaces by external actions such as waves, floods or wind. These actions carry away particles and deconsolidate the dike sides (FEMA, 2004).

The different dike failure modes are presented in Figure 2.3, which can be classified according to the failure mechanism considered. This classification is described in Table 2.2.

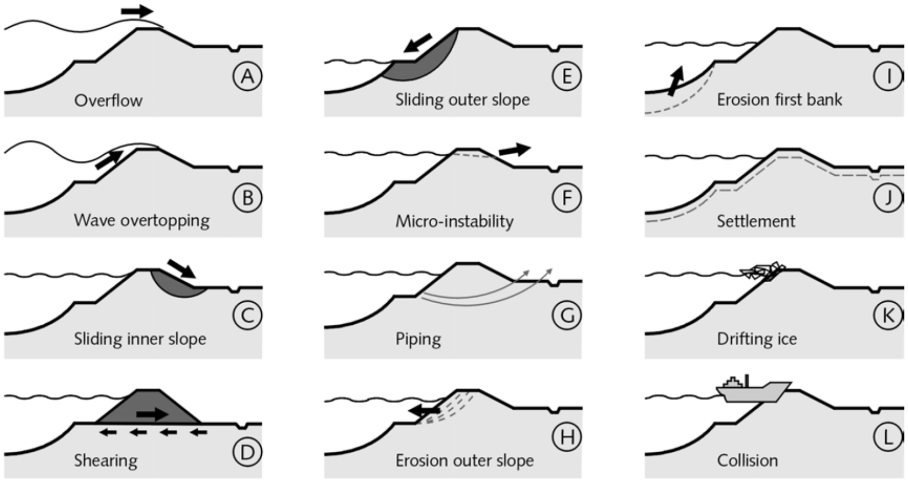

Figure 2.3: Failure mechanisms (Flóriàn et al., 1998).

Instability	Erosion	
	Internal	External
C D E F J	G	A B H

Table 2.2: Dike failure modes classification.

A study was carried out by Danka and Zhang (2015) on breaching cases has highlighted the most frequent failure mechanisms. Among all cases collected, 503 rupture mechanisms were identified. Here are the results obtained thanks to this study:

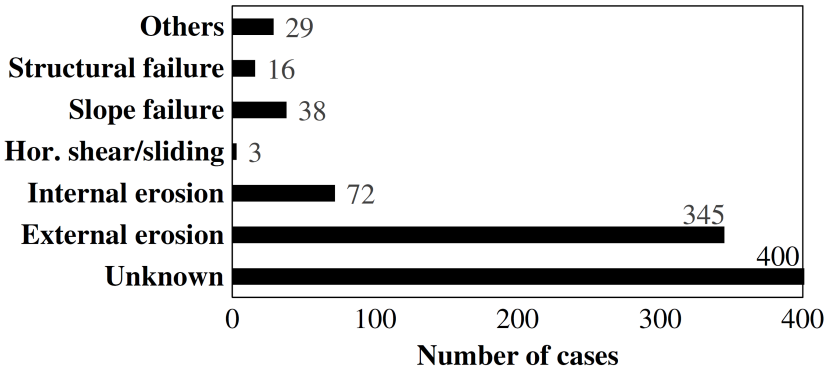

Figure 2.4: Number of dike failures according to the failure mode (Danka and Zhang, 2015).

The most frequent failure mode is therefore external erosion failure created mainly by overtopping (Danka and Zhang, 2015). The other mechanisms category includes human (FIGURE 2.3L) and animal damage as well as soil failure, ice drift (FIGURE 2.3K) and micro instabilities (FIGURE 2.3F).

Additionally, the authors described the temporal evolution of failure mechanism frequencies from 1850 to nowadays (FIGURE 2.5). On average, dike failure by external erosion exceeds 60% relative frequency, which makes it the most frequent failure mechanism.

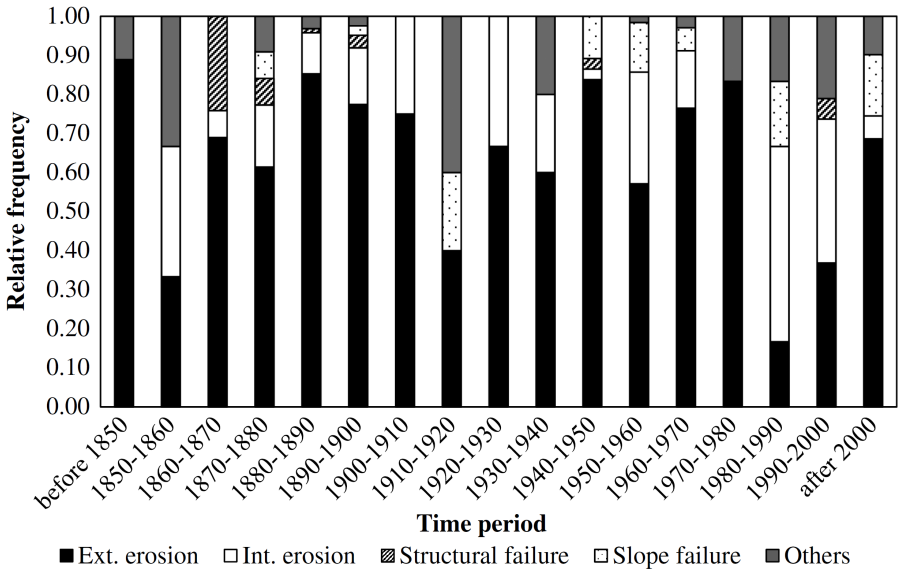

Figure 2.5: Evolution of the relative frequency of failure mechanism (Danka and Zhang, 2015).

To conclude the diverse explanations regarding the fundamental principles of dikes, a specific point concerning the development of dike openings by overtopping is described hereafter. It should be noted that the dynamics of dike opening can be described in 3 main stages (Rifai, 2018). These different stages are described below and are based on the explanations of Rifai (2018) and Schmitz et al. (2021):

- Stage 0: this stage corresponds to the beginning of the overflow at the weak point of the dike, which can be seen as a notch. This notch enables the flow to pass from its main

bed to the floodplain. This is an initial stage that will gradually lead to the erosion of the dike. At this stage, the erosion remains moderate.

- Stage 1: when stage 1 appears, things accelerate. There is a significant increase in erosion at the dike. This rapid erosion results in a major increase in the evolution of the breach geometry. The breach widens and deepens. This sudden change in geometry has an impact on the discharge through the breach. During this stage, the breach discharge increases rapidly until it reaches a peak: the peak breach discharge.

- Stage 2: the final stage of breach development is a stabilization stage after the rapid increase in breach geometry that occurred in stage 1. During this stage, the flow tends to stabilize. The water depth in the main flow bed is reduced. The breach geometry continues to evolve but less significantly than in stage 1. However, the width of the breach tends to widen downstream.

An illustration of the explanations is shown in FIGURE 2.6, which shows experimental results over 2 tests carried out by Rifai (2018). It illustrates the evolution of the breach geometry (FIGURES 2.6(a) and 2.6(b)) as well as the breach width (FIGURE 2.6(c)) in the different stages (Stage 0, Stage 1 and Stage 2). The floodplain water level was different for each test: 0 m for Test 8 and 0.15 m for Test 23.

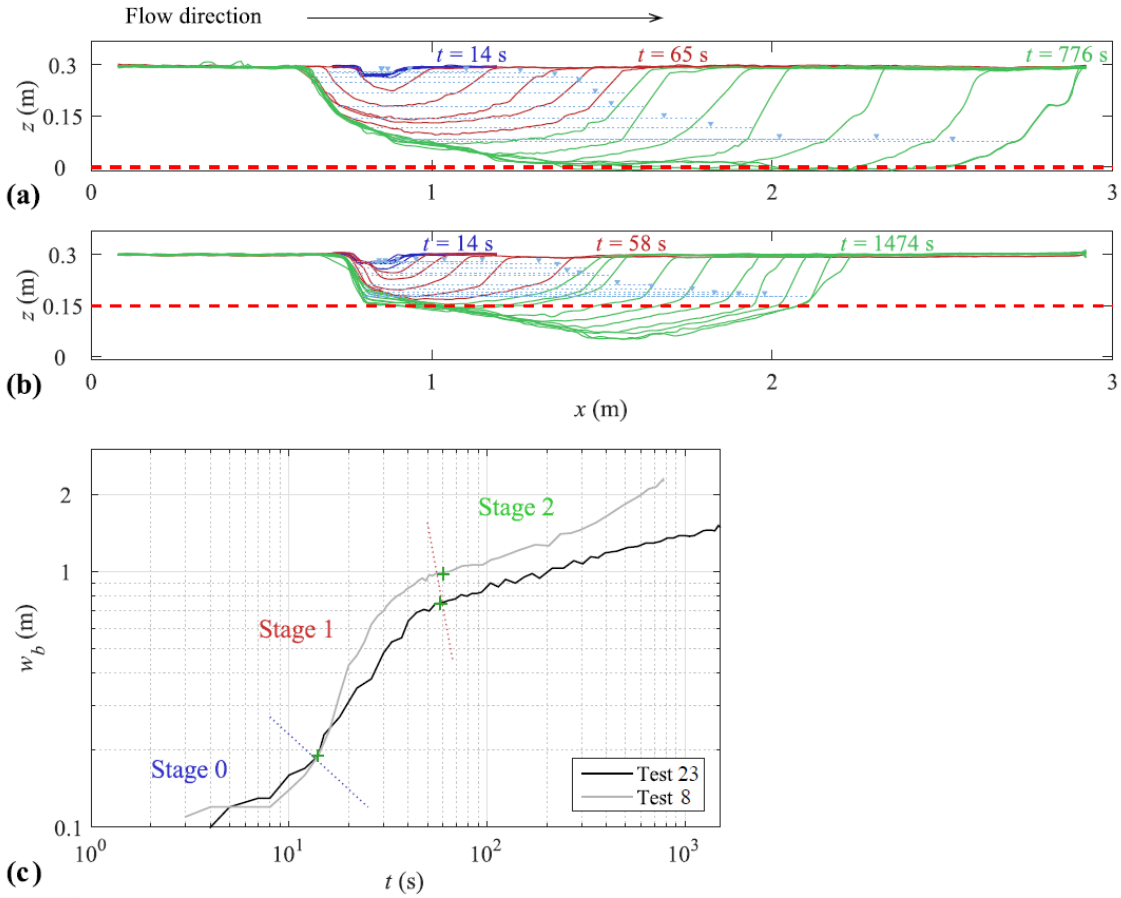

Figure 2.6: Identification of 3 main stages of breach expansion for different tests carried out by Rifai (2018): longitudinal dikes profiles for two different tests ((a) Test 23 and (b) Test 8) with z the profile elevation and x the spatial coordinate along the main flow axis; width breach (w_b) evolution (c). The red dotted lines represent the floodplain fixed water level (Rifai, 2018).

2.2 Numerical models

The development of numerical models to simulate the dynamics of flow through breaches is not a recent achievement. There are several models described in scientific literature. An analysis of the different existing models highlights the efforts made in the past to understand and study the breach failure and the breach flow through a fluvial dike. In the following sections, different studies using different numerical models are presented. This is a non-exhaustive list.

2.2.1 2D model (Rifai, 2018)

Rifai worked on the failure of fluvial dikes by overtopping. During this work, he set up numerous experiments in order to analyze the behavior of dikes subjected to flow. In particular, he took experimental measurements during the experiments. A description of the experiments is given in section 3.2. These experiments were used as reference data for this thesis. After measuring the experimental results, Rifai compared these results with two 2D numerical models. The first model is devoted to the purely hydrodynamic study. It is a model based on the 2D shallow water equations (TELEMAC-2D). The second model used enables the morphodynamic character to be taken into account (SISYPHE). It is a coupling of a hydrodynamic model and a morphodynamic model. The morphodynamic model makes it possible to take into account sediment transport.

The hydrodynamic model used by Rifai allows the 2D shallow water equations to be solved using the finite element method or the finite volume method. It allows knowing the water depth as well as the longitudinal and transverse velocities over the entire domain.

The coupling between the two numerical models is illustrated in FIGURE 2.7.

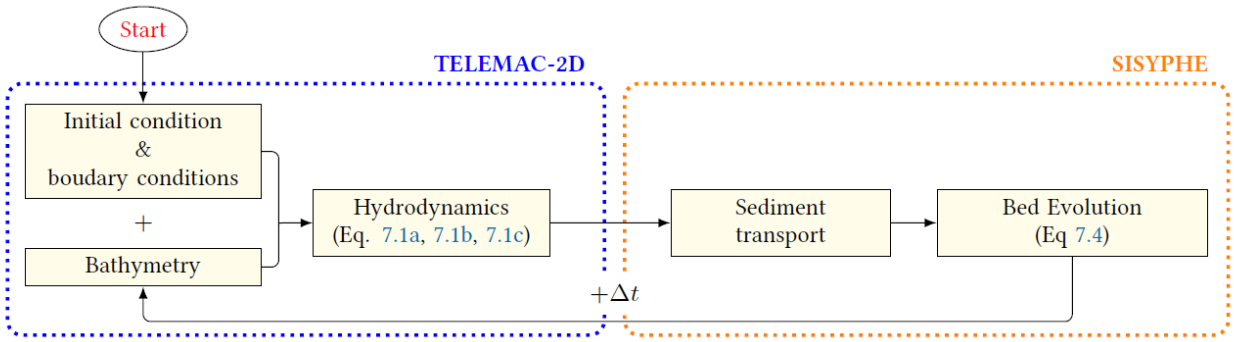

Figure 2.7: Coupling of hydrodynamic and morphodynamic models (Rifai, 2018).

The different models used by Rifai were studied by varying several parameters. Sensitivity analyses were carried out on various key parameters of hydrodynamic flows. These analyses were divided into two parts: (1) numerical parameters such as the Strickler coefficient or the turbulence model, for example; (2) experimental parameters affected by uncertainties such as the inlet discharge or the rating curves (Rifai, 2018).

The comparison between the experimental data and the numerical results showed the ability of the numerical model to reproduce the experimental results. In addition, *via* sensitivity analysis, the numerical model has been tested to see how it evolves with some changes.

Overall, the numerical model used was able to reproduce the experimental results fairly reliably. However, a more complex model such as the 2D model requires a rather long calculation time. One of the motivations to develop a simpler numerical model is to reduce the computation time.

2.2.2 Simple process-oriented model (Wu, 2013)

A simpler process-oriented model was developed by Wu (2013). This model is used to understand and analyze the development of breach by overtopping on earthen embankment. A mass conservation equation is applied to a control volume. This describes the distribution of the initial discharge over time to the output flows, which are the breach discharge and the spillway and sluice gates. Although very simple, this model also takes into account the morphodynamic processes associated with breach development. Different parameters allow considering these erosion effects at the dike. In this model, the evolution of the breach geometry is considered trapezoidal. The overtopping flow is idealized as a flat broad-crested weir.

A global illustration of breach development by overtopping is provided in FIGURE 2.8. It illustrates the geometrical view with which the model has been implemented.

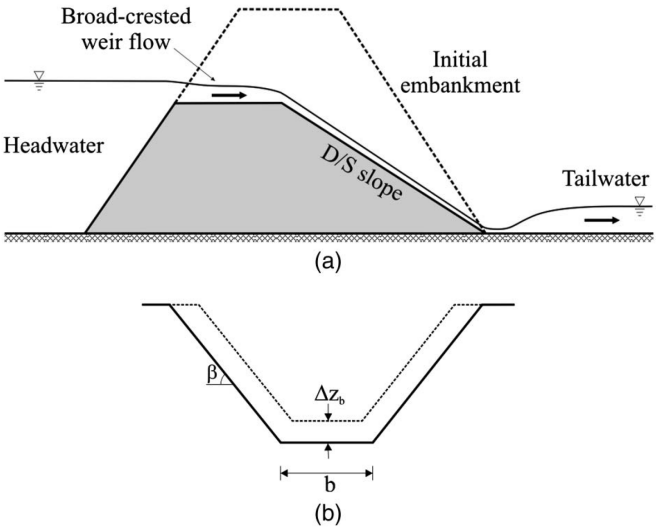

Figure 2.8: Embankment breach by overtopping: (a) longitudinal profile and (b) cross-section (Wu, 2013).

However, Wu (2013) model has some limitations. The first limitation is that this model is not spatially discretized. The spatial distribution of hydraulic variables of interest (e.g. water depth) is not possible with this kind of model. This model has been developed in a frontal context (e.g. dam failure). The latter is not suitable for dike failures by overtopping which constitutes a second important limitation. The implementation of a spatially distributed model adapted to lateral flows is then required. The various limitations of the mentioned models lead to the development of more suitable models. This is why the development of models is the core of this thesis.

3 | Reference data

In order to evaluate various numerical models developed in this research, it is first necessary to select reference experimental tests from the literature. By using the different test configurations, the numerical results obtained with the models may be compared with the experimental results. The comparison of the numerical and experimental results is essential to draw conclusions from the numerical results.

Two main categories of configurations have been tested. The first category concerns tests with fixed breach geometry. This means that there is no temporal or spatial change in the geometry of the lateral opening. Tests in this category are referred to as fixed breach geometry flows. The second category concerns evolving breach geometries. There is therefore a temporal as well as a spatial evolution of the breach geometry. This category of test is called flow with dynamic breach geometry.

All these explanations are illustrated in FIGURE 3.1. Each category of tests refers to one or more tests found in literature. The fixed breach geometry flows with zero lateral crest height are based on the tests of Roger et al. (2009), Michelazzo et al. (2015) and Mignot et al. (2020). Fixed geometry flows with a non-zero lateral crest height are based exclusively on Mignot et al. (2020) tests. Flow with dynamic breach geometry is based on the Rifai (2018) tests.

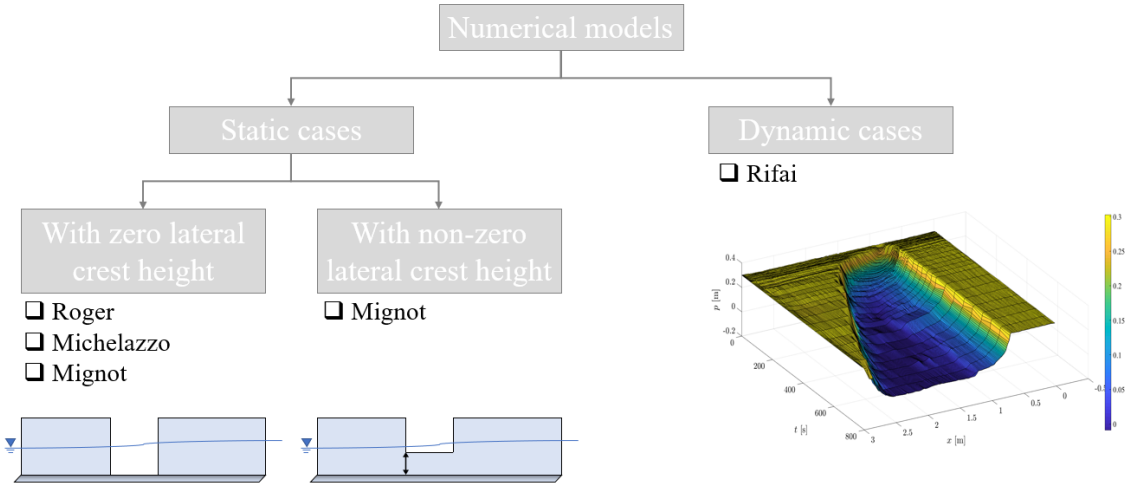

Figure 3.1: Overall work organization: case with fixed breach (left) and dynamic breach (right).

The following sections of this chapter describe the various tests selected from literature. The experimental set-up, the uncertainties in the measurements, the downstream boundary conditions as well as the experimental results are scrutinized in these sections. The description of the tests follows the order described above (i.e. first the flows with fixed breach geometry and then the flows with dynamic breach geometry).

The last section of this chapter (section 3.3) concerns the various discharge coefficient formulations proposed in literature. These have been tested and compared when analyzing the results of numerical models. A description of the comparison methodology used is also described in this section.

3.1 Flow with fixed breach geometry

3.1.1 Roger et al. (2009)

Experimental set-up

The tests conducted by Roger et al. (2009) were carried out in a horizontal channel 1 m wide and approximately 9 m long (FIGURE 3.2). The bed roughness is characterized by a Manning coefficient n of 0.015 s/m$^{1/3}$. The discharges injected in the upstream part of the channel are 0.2 and 0.3 m^3/s. The initial water levels in the channel are 0.4 and 0.5 m.

The breach width is fixed at 0.7 m. The side opening leads to a floodplain 3.5 m wide and 4 m long. It is this floodplain that collects the water passing through the breach. Downstream of the main channel, a weir with a variable crest depending on the test considered acts as a downstream boundary condition.

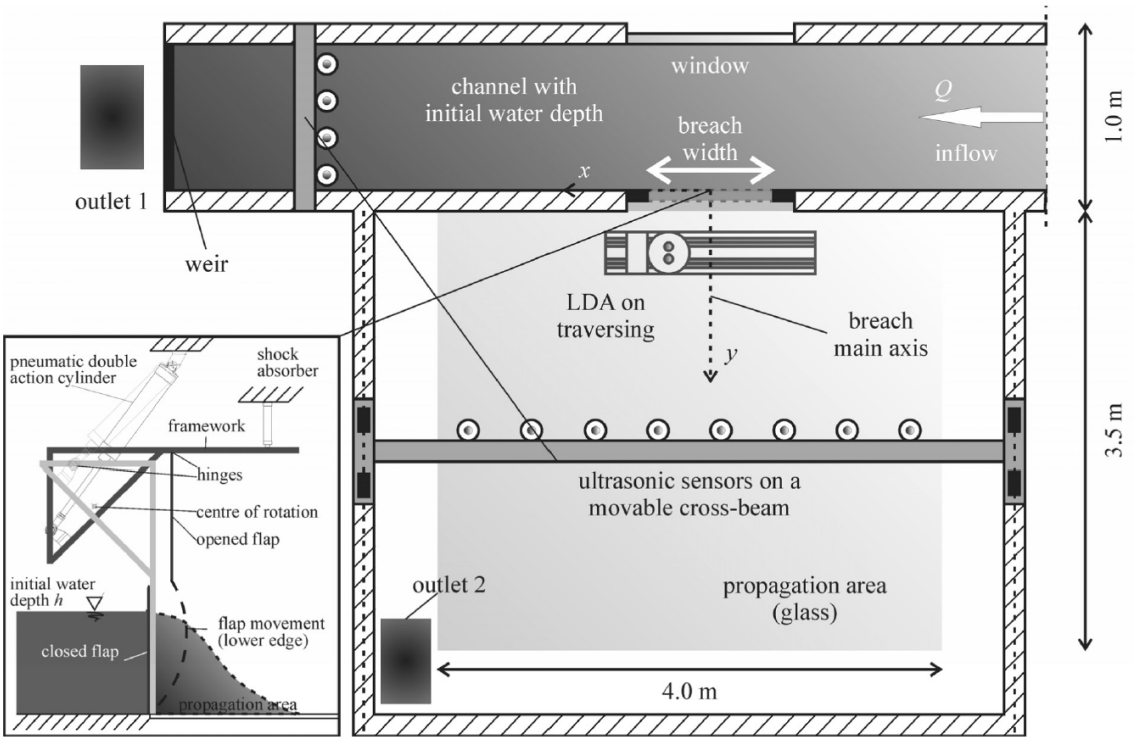

Figure 3.2: Experimental set-up (Roger et al., 2009).

Studied experiments

Four tests were conducted by Roger et al. (2009). All these tests were considered for the numerical model studies. Each test is characterized by a specific initial hydraulic configuration. The different configurations used in the tests are given in TABLE 3.1. As mentioned before, the tests differ in the discharge injected upstream of the main channel, the initial water depths in the channel and the height of the weir downstream to regulate the flows.

Test ID	Q_{in} [m^3/s]	h_0 [m]	h_w [m]
Q300-h50	0.3	0.5	0.241
Q300-h40	0.3	0.4	0.152
Q200-h50	0.2	0.5	0.297
Q200-h40	0.2	0.4	0.202

Table 3.1: Parameters of test configurations (Roger et al., 2009) with Q_{in} the upstream discharge, h_0, the initial water depth and h_w, the crest height of the downstream weir.

Measurement uncertainties

The inlet discharge, as well as the outlet discharge, were measured for each test undertaken. Each of the flow meters has a maximum measurement error of 1%.

The results of experimental measurements of water depths could not be obtained. The only water depths available are the numerical ones obtained with the 2D *WOLF* model. These were used for the comparison with the numerical water depths obtained with both numerical models.

Downstream boundary condition

As mentioned previously, the tests are controlled downstream by a weir. For each of the tests, the authors gave a water depth-discharge relation at the weir (Equation 3.1). This function is fundamental for numerical simulations. Indeed, it is used as the downstream boundary condition. This rating curve is defined by the authors as follows:

$$Q_{out} = \frac{2}{3}\mu b\sqrt{2g(h-h_w)^3} \tag{3.1}$$

with Q_{out} the downstream weir discharge [m^3/s], μ the discharge coefficient [-], b the weir width [m], g the gravity acceleration [m/s^2], h the water depth just upstream of the downstream weir [m] and h_w is the crest height of the downstream weir [m]. Based on experimental results, the authors were able to calibrate μ as a cubic polynomial form (Equation 3.2):

$$\mu = a_3 h_*^3 + a_2 h_*^2 + a_1 h_* + a_0 \tag{3.2}$$

where a_i is a coefficient of the cubic polynomial (Table 3.2) and h_* is the difference between h and h_w (i.e. $h - h_w$).

With this downstream relation, the implementation of the downstream boundary condition is really smooth and efficient.

Test ID	a_3	a_2	a_1	a_0	Range of validity
Q300-h50	–7.291	4.561	–0.554	0.752	$0.05 < Q < 0.3$
Q300-h40	–10.84	6.009	–0.359	0.738	$0.05 < Q < 0.3$
Q200-h50	–62.63	26.61	–3.508	0.887	$0.03 < Q < 0.2$
Q200-h40	–65.62	29.01	–3.665	0.877	$0.03 < Q < 0.2$

Table 3.2: Coefficients of cubic approximations (Roger et al., 2009).

Experimental results

The discharge through the lateral opening (Q_l) was measured for the various Roger et al. (2009) tests. In addition to these observed experimental results, the authors used two numerical models to represent the experimental tests. These are the following models: FE model and FV model (*WOLF*). The description of these models is given in TABLE 1 of the reference document. The results obtained are given in TABLE 3.3.

Test ID	Measured [m^3/s]	FE model [m^3/s]	FV model [m^3/s]
Q300-h50	0.218	0.200	0.198
Q300-h40	0.159	0.141	0.141
Q200-h50	0.194	0.183	0.182
Q200-h40	0.154	0.143	0.141

Table 3.3: Comparison between breach discharges (Q_l) observed and computed with second order accuracy by both models.

Regarding the water depth profile along the canal (h), unfortunately, no experimental results have been found. The only available data are the depth profiles from 2D numerical simulations using the FV model (FIGURE 3.3).

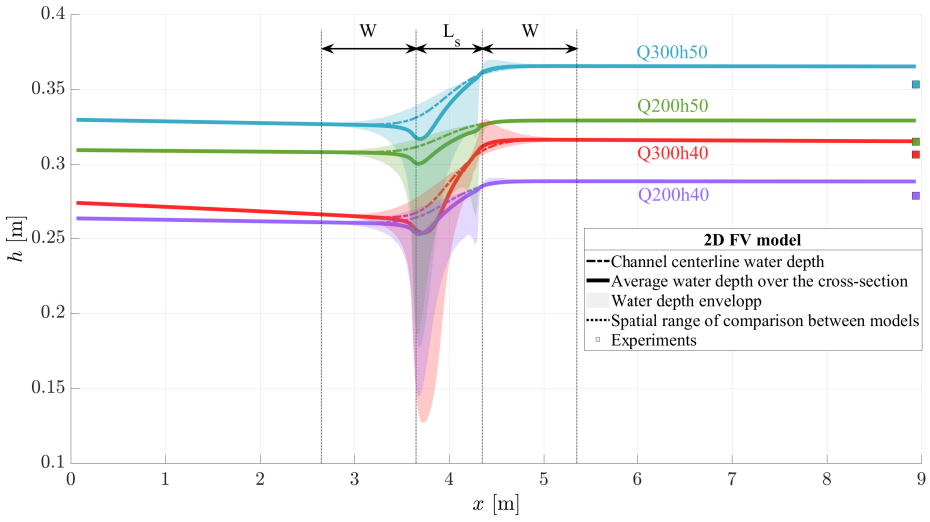

Figure 3.3: Water depth profiles from the 2D FV model.

3.1.2 Michelazzo et al. (2015)

Experimental set-up

The tests conducted by Michelazzo et al. (2015) were carried out in the laboratory in a 0.1% inclined channel 0.3 m wide and 5.1 m long (FIGURE 3.4). The bed roughness made up of gravels was characterized by a Manning coefficient n of 0.024 s/m$^{1/3}$ (Rifai et al., 2017).

Alongside the main channel was placed a 0.12 m wide lateral canal to collect the water discharge passing through the zero-height breach (Q_s). The discharge injected in the upstream part of the channel (Q_u) was set at 0.010 m^3/s. The width of the breach was set at a different value depending on the test performed (L_s). Downstream of the channel, a sluice gate with a variable opening was placed and acted as a downstream boundary condition.

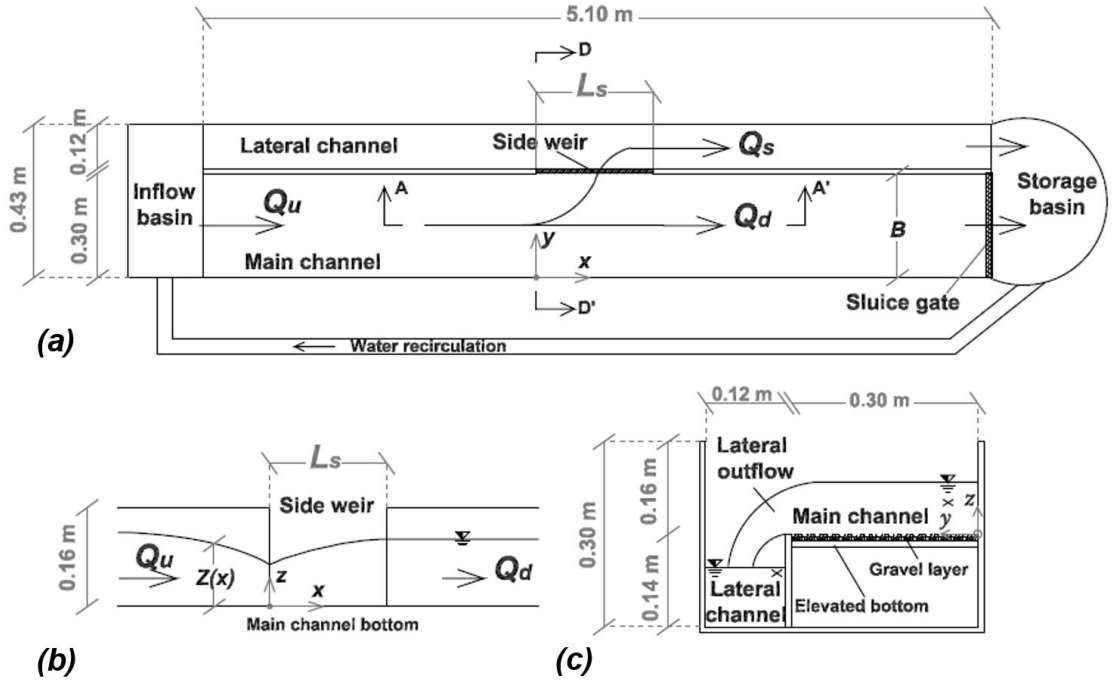

Figure 3.4: Michelazzo tests experimental set-up: (a) plan view; (b) longitudinal section (cut A-A'); (c) cross-section (cut DD') (Michelazzo et al., 2015).

Studied experiments

Multiple tests were carried out by Michelazzo (2014). Each of the tests is characterized by a lateral opening length. The inlet discharge for each of the series B tests is almost similar ($\approx$ 0.01 m^3/s). The different parameters used for each of the tests are listed in TABLE 3.4. Series A[1] tests were performed in a closed channel (i.e. zero breach width). The injected discharge was different for each test. Each series B test had a different breach width from 0.03 to 0.47 m (Michelazzo et al., 2015). For both sets of experiments, the downstream sluice gate opening (Y_g) was set at 2 cm.

[1]At the beginning of the numerical code implementation, the A-series tests were used as a reference (stationary flow in a closed channel). Nevertheless, the results will not be presented in this work as they finally illustrate a simple waterline calculation.

	Test ID	Q_{in} [m^3/s]	L_s [m]
B7	L03Q9.52Yg2.0	0.0095	0.03
B8	L08Q10.1Yg2.0	0.0101	0.08
B9	L13Q10.0Yg2.0	0.0100	0.13
B10	L18Q10.1Yg2.0	0.0101	0.18
B11	L23Q10.0Yg2.0	0.0100	0.23
B12	L28Q10.1Yg2.0	0.0101	0.28
B13	L33Q10.1Yg2.0	0.0101	0.33
B14	L38Q10.1Yg2.0	0.0101	0.38
B15	L43Q10.1Yg2.0	0.0101	0.43
B16	L47Q10.1Yg2.0	0.0101	0.47
A1	L00Q3.00Yg2.0	0.003	0
A2	L00Q4.50Yg2.0	0.0045	0
A3	L00Q6.50Yg2.0	0.0065	0

Table 3.4: Parameter of test configurations Michelazzo (2014) with a 2 cm sluice gate opening (Y_g).

Measurement uncertainties

The inlet discharge was measured using a flow meter with an accuracy of 0.1 l/s. The water depths along the channel were measured using ultrasonic sensors with an accuracy of 1mm.

The breach discharge was calculated using a rating curve placed at the end of the side channel. This rating curve was obtained by coupling the water depth and discharge measurements at the end of the side channel. From this side channel discharge, the main channel outlet discharge was calculated using the continuity principle. It was also calculated in a second way using a rating curve downstream of the main channel. The difference in outlet discharge between the two methods did not exceed 5% (Michelazzo, 2014).

Downstream boundary condition

In order to use numerical models, it is essential to provide two boundary conditions: an upstream boundary condition (i.e. the injected flow) and a downstream boundary condition (i.e. a downstream water depth or discharge). In the case of the Michelazzo experiments, the upstream discharge is known (Table 3.4).

Regarding the downstream boundary condition, Michelazzo (2014) gave a rating curve that can be used in the downstream part of the channel. However, the accuracy with which this curve has been reconstructed is not optimal. Indeed, after comparing the results obtained for the A series by Michelazzo (2014) and the values given by the rating curve, a divergence between the results was noticed. Figure 3.5 shows the differences in results between the rating curve reconstructed from the experimental results and the experimental results themselves.

For a certain input discharge, the difference in water depth between the Michelazzo rating curve and the one reconstructed with the experimental results can reach almost 2 cm, which is not negligible. Such a large error in the downstream boundary condition can lead to numerical results that are far from the experimental results, which should obviously be avoided. In the interest of accuracy, the rating curve used as the downstream boundary condition will be those reconstructed from the experimental results series A & B (in green in FIGURE 3.5) as used by Rifai et al. (2017)[2].

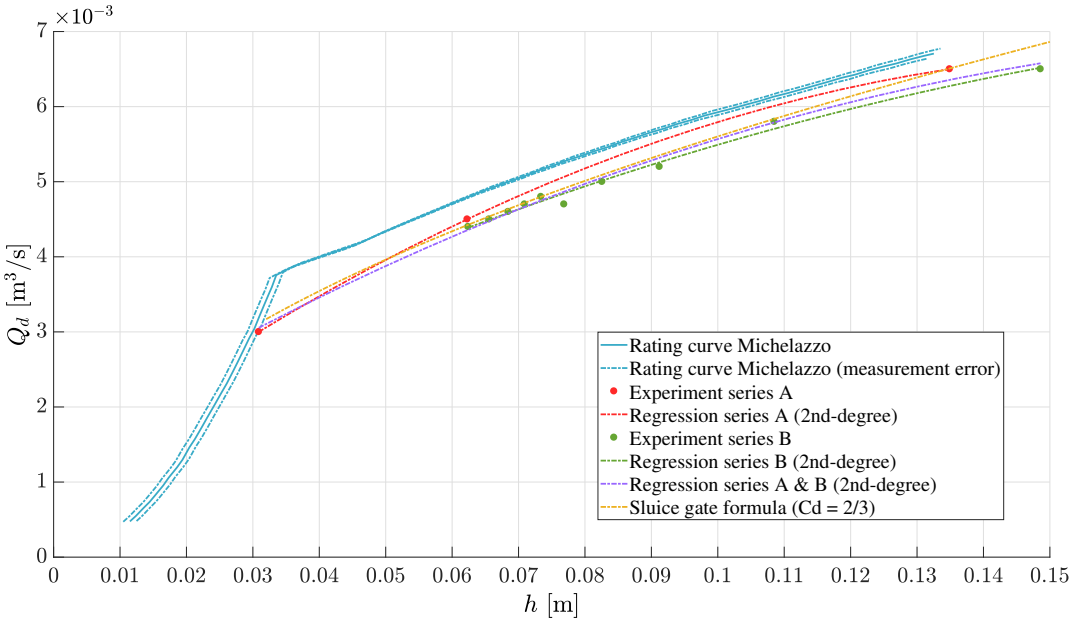

Figure 3.5: Different possible rating curves from Michelazzo (2014) and experimental results regressions with Q_d the downstream discharge.

Experimental results

The lateral discharge[3] (Q_l) and the water depth profiles were measured for the different Michelazzo et al. (2015) tests. The observed discharges are given as well as the output discharges (Q_o) in TABLE 3.5.

In this table, it can be observed that the breach discharge increases as the breach length increases. In fact, the breach discharge of test B7 ($L_s = 0.03$ cm) is lower than that of test B16 ($L_s = 0.47$ cm).

Test ID	B7	B8	B9	B10	B11	B12	B13	B14	B15	B16
Q_{out} [m^3/s]	0.0065	0.0058	0.0052	0.005	0.0047	0.0048	0.0047	0.0046	0.0045	0.0044
Q_l [m^3/s]	0.003	0.0043	0.0048	0.0051	0.0053	0.0053	0.0054	0.0055	0.0056	0.0057

Table 3.5: Lateral discharges (Q_l) observed for all Michelazzo et al. (2015) tests.

[2]Nevertheless, a comparison between the different rating curves was carried out.
[3]The use of breach or lateral discharge/opening is not important because both terms refer to the same idea.

The experimental water depth profiles (h) are illustrated in FIGURE 3.6. The length of the breach is also indicated[4]. The comparison range with the numerical models is used to compare the results obtained with the different formulations and/or models. The x-axis is the distance from the upstream end of the breach divided by the width of the main channel (i.e. $x^* = x/B$).

In this figure, it is clear that the lower the breach discharge (smaller breach length), the higher the water depth in the channel. This explains the reason why the water depth for test B7 is higher than the water depth for test B16. It can also be seen that the higher the breach length, the more pronounced the water depth profile is in the area of the breach.

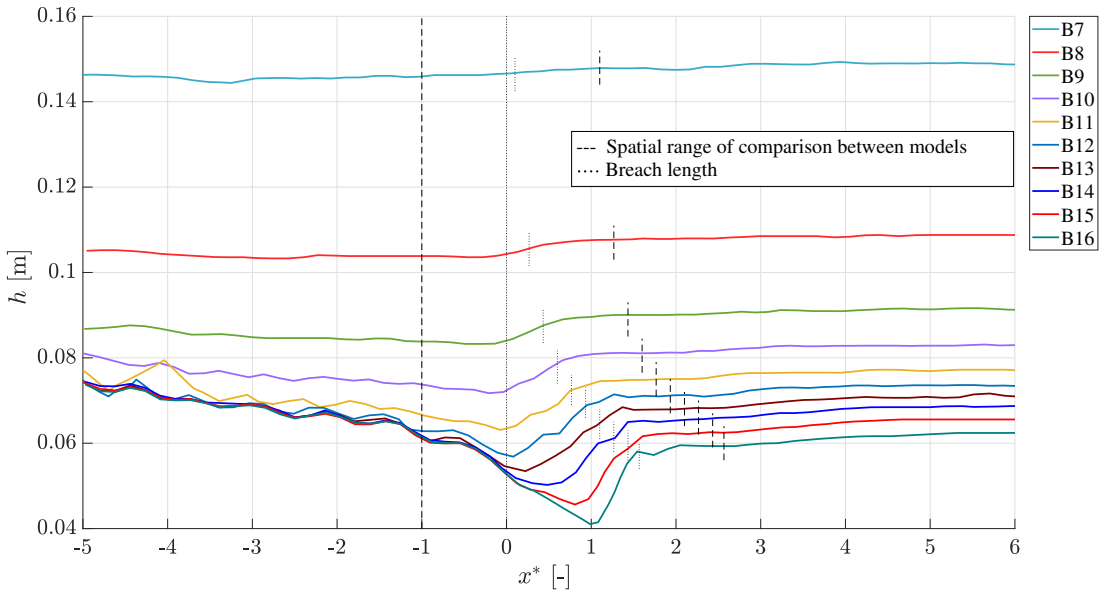

Figure 3.6: Water depth profiles along the center line of the main channel (Michelazzo et al., 2015).

[4]It is the distance between the light dotted line of abscissa 0 and the vertical bar of the same aspect.

3.1.3 Mignot et al. (2020)

Experimental set-up

The experimental set-up used by Mignot et al. (2020) (FIGURE 3.7) consists of a 8.35 m long and 0.79 m wide rectangular cross-section open channel with a slope of 0.0018. A secondary channel is placed parallel to the main channel to collect the water passing through the opening. A grid buffer and a small honeycomb mesh were used as an upstream main channel boundary condition. A sharp-crested tailgate was set at the channel end to control the water depth in front of the opening.

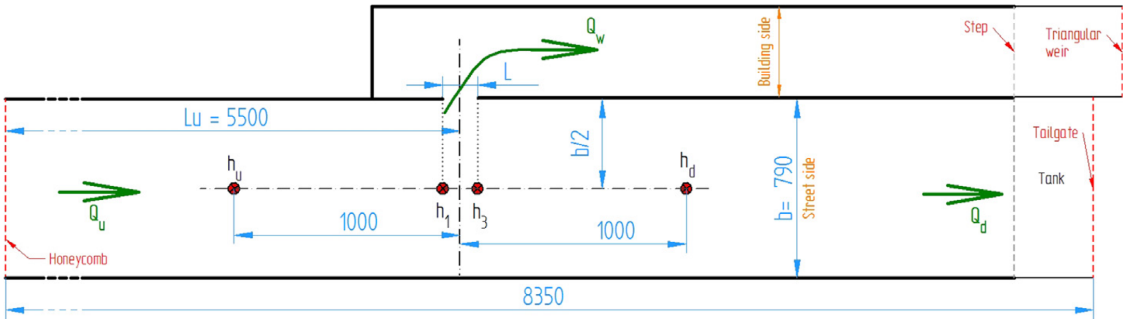

Figure 3.7: Experimental set-up (Mignot et al., 2020).

Five flow configurations with different flow parameters have been tested (Mignot et al., 2020). These flow configurations with their hydraulic parameters are listed in the table below (TABLE 3.6):

Test ID	h_1 [m]	Q_{in} [m^3/s]	Fr_1 [-]	Re_1 [-]
F1	0.025	0.002	0.2	9,524
F2	0.108	0.0176	0.2	69,980
F3	0.025	0.0054	0.55	25,714
F4	0.090	0.0367	0.55	151,340
F5	0.108	0.046	0.52	182,903

Table 3.6: Tested flow configurations (Mignot et al., 2020). The subscript indicates the position just upstream of the opening (see FIGURE 3.7).

A set of four different openings was considered (FIGURE 3.8). Among this set, there is a window opening (Op1), an open/damaged door (Op2), a wider window (Op3) and a grid of small openings (Op4) (Mignot et al., 2020). Here, the focus is set on openings Op1 (as a proxy of partially developed breaches) as well as opening Op2 (representing a breach extending down to the level of the main channel bottom).

Some of Mignot et al. (2020) experiments also involve obstacles in the flow. In this work, only tests without obstacles are considered.

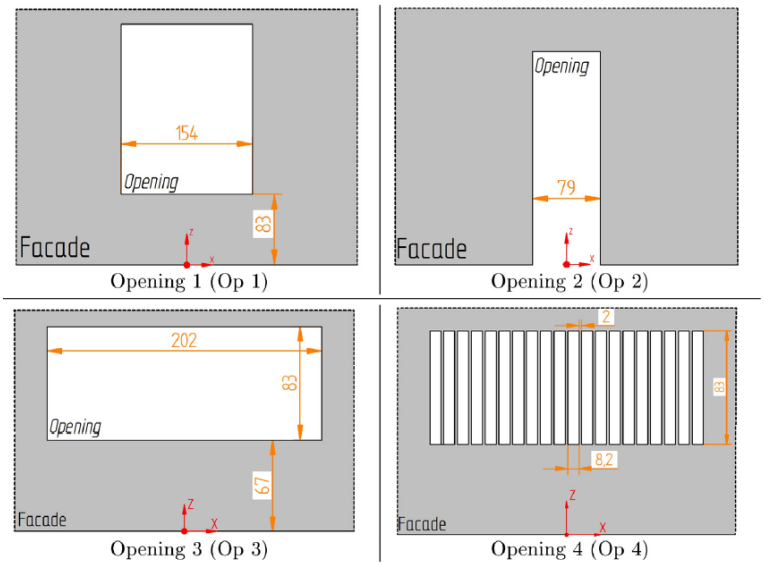

Figure 3.8: Set of openings with dimensions in mm (Mignot et al., 2020).

Studied experiments

A total of 6 configurations (hydraulic and opening) were selected from the tests conducted. These are the 6 tests without obstacles with openings corresponding to the cases treated. In these tests, 4 concern flows with a breach geometry fixed with zero lateral crest height (Op2) and 2 with non-zero lateral crest height (Op1). The different configurations used for these 6 tests are given in TABLE 3.7.

Test configuration					
With non-zero lateral crest height		With zero lateral crest height			
Op1F2	Op1F5	Op2F1	Op2F2	Op2F3	Op2F4

Table 3.7: Flow configurations for the selected Mignot et al. (2020) tests.

Measurement uncertainties

The discharge injected upstream of the channel has a certain level of uncertainty. This is monitored using two electromagnetic flow meters. The first flow meter has a range of use from 5 to 40 l/s while the second, more accurate, has a range of 0 to 5 l/s. The respective uncertainties of the two flow meters are 0.2 l/s and 0.05 l/s (Mignot et al., 2020).

Uncertainties related to the water depth measurements are different depending on the flow regime characterized by the Froude number. Nevertheless, these do not exceed 2% (the most critical case for high Froude number flow regimes). For low Froude number flow regimes, the uncertainties do not exceed 1.8% (Mignot et al., 2020).

Regarding the measured lateral discharge uncertainty, the latter does not exceed 3% (Mignot et al., 2020). This value should therefore be kept in mind when comparing numerical and experimental discharges.

Downstream boundary condition

For the different hydraulic configurations (F), rating curves have been calculated by X. Li (Ph.D. student from the University of Liege who worked on Mignot et al. (2020) tests). The expressions of these rating curves are given in TABLE 3.8. These expressions were obtained on the basis of the different hydraulic configurations (F) used by Mignot et al. (2020). These rating curves must be applied to the d point (1 m from the opening center, seeFIGURE 3.7).

Hydraulic configuration	Rating curves expression
F1	$h = 5.7837 \cdot Q + 21.055$
F2	$h = 2.6713 \cdot Q + 62.601$
F3	$h = 0.7251 \cdot Q + 23.214$
F4	$h = 1.4948 \cdot Q + 46.021$
F5	$h = 1.1744 \cdot Q + 54.155$

Table 3.8: Rating curves expression, for all hydraulic configurations, obtained from Mignot et al. (2020) tests (h in [mm] and Q in [l/s]).

Experimental results

The lateral discharge (Q_l) was measured for the different Mignot et al. (2020) tests. Water depths were measured at 4 fixed points h_u, h_1, h_2 and h_d (FIGURE 3.7). The observed discharges and water depths are given in TABLE 3.9.

Test ID	Q_l [m^3/s] $\cdot 10^{-3}$	h_u [m]	h_1 [m]	h_2 [m]	h_d [m]
Op1F2	1.273	0.106	0.109	0.108	0.107
Op1F5	1.142	0.108	0.108	0.107	0.107
Op2F1	0.673	0.026	0.029	0.028	0.028
Op2F2	4.19	0.096	0.099	0.098	0.098
Op2F3	0.578	0.025	0.027	0.026	0.027
Op2F4	3.37	0.089	0.096	0.093	0.094

Table 3.9: Lateral discharges (Q_l) and water depths at fixed points observed for Mignot et al. (2020) tests.

3.2 Flow with dynamic breach geometry

3.2.1 Rifai (2018)

Experimental set-up

Rifai (2018) experiments are characterized by two experimental set-ups. The first one is the model of the University of Liege carried out at the department of hydraulic structures of this institution. The second is the LNHE model, which was carried out at the National Laboratory for Hydraulics and the Environment of EDF. The following studies are exclusively based on the first model (ULiège model). This is the one presented in this section.

This experimental set-up (Figure 3.9) consists of a flat main channel of 10 m length and 1 m width. The channel has a lateral opening of 3 m long overlooking a floodplain of 4.3 m long and 2.5 m wide.

To represent the trapezoidal fluvial dike, the side opening was closed with sand. In its initial configuration, the dike has a base width of 1.3 m, a crest width of 0.1 m and a height of 0.3 m. The upstream and downstream slopes of the dike are 0.5 (V/H = 1/2). In order to initiate the development of the breach, a 0.02 m deep and 0.1 m wide opening was made in the dike at a distance of 0.85 m from the upstream end of the dike.

A drainage system, consisting of a 4 cm layer of drainage material wrapped in a geotextile, was also installed parallel to the dike. This drainage system was placed at the base of the dike to limit water seepage and ensure the global stability of the dike throughout the tests.

The upstream flow condition was regulated by a honeycomb placed upstream of the main channel. Several downstream boundary conditions were used depending on the tests considered. These include a perforated plate, a rectangular weir and a removable gate. The tests studied in this work were all carried out considering the perforated plate as the downstream limit condition.

For all tests and during the entire test period, the breach geometry was measured. This data acquisition was done using a Laser Profiling Technique (LPT). This method (Figure 3.10) consists in scanning the surface of the dike with a laser plane in order to collect information on the evolution of the dike geometry (Rifai et al., 2020). The images are then processed to transform the coordinates of the laser profiles (2D) into a set of points in a 3D coordinate system. Thanks to this technique, the spatial and temporal evolution of the dike geometry are known. This information enables the simulation of a dynamic breach.

Studied experiments

There are 30 different tests performed on the experimental set-up of the University of Liege. These experiments differ in the discharge injected upstream of the main channel, the type of regulation condition downstream of the main channel, the depth in the floodplain and the median particle size diameter.

Among these various tests, 4 were selected as reference cases for the numerical simulations. These are tests n°1, 4, 8 and 11. The parameters considered for these tests are listed in Table 3.10. Only the input discharge is different for each of the selected tests.

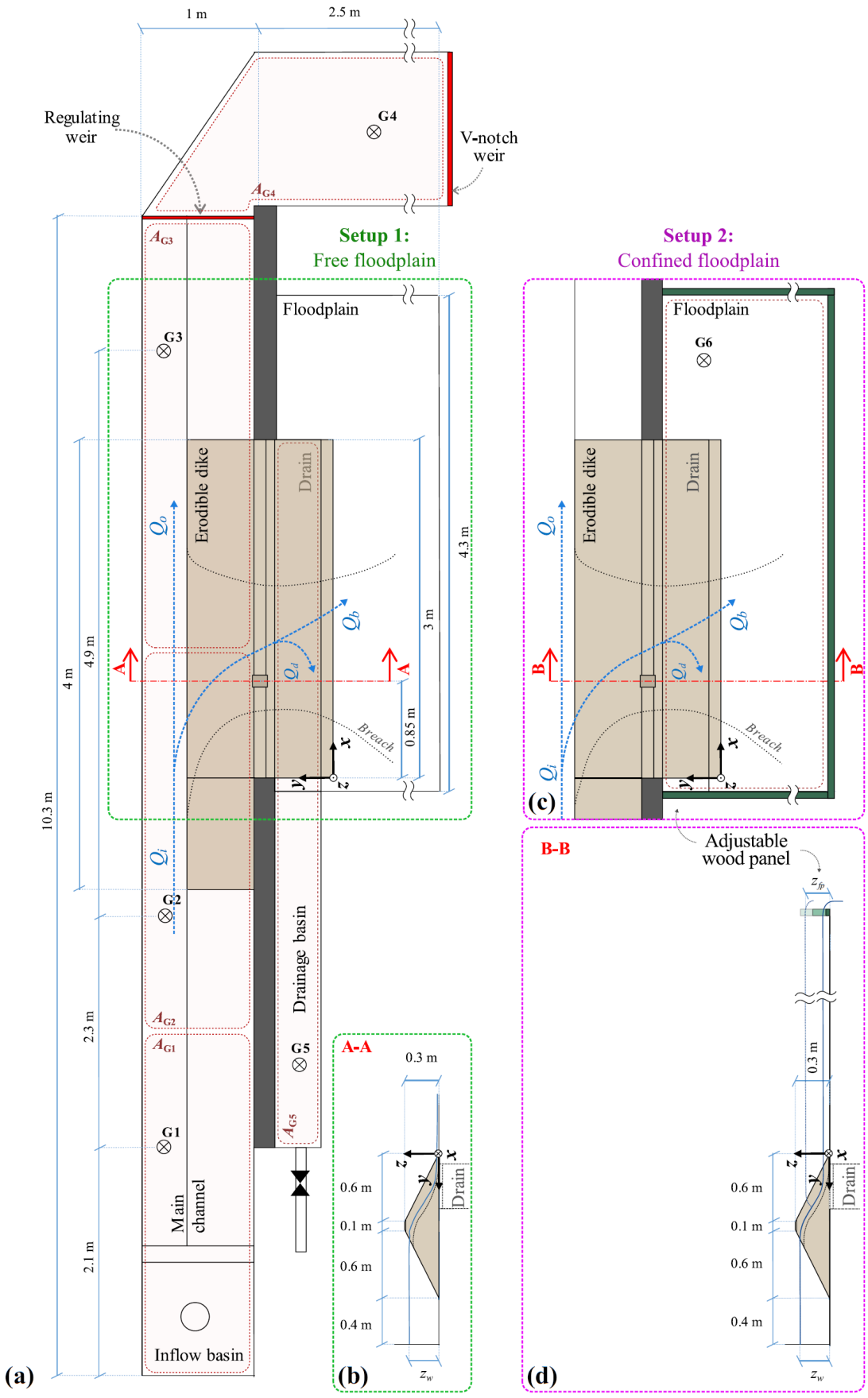

Figure 3.9: Experimental set-up (ULiège model) of the Rifai (2018) experiments (Rifai et al., 2019).

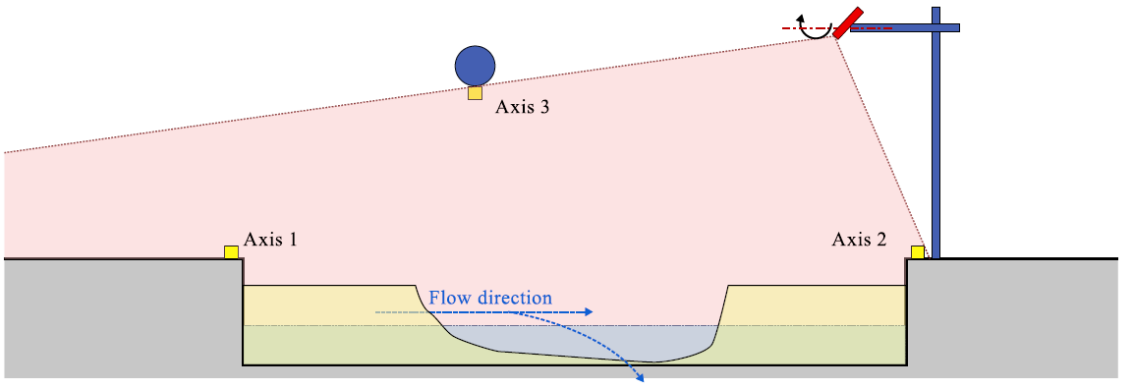

Figure 3.10: Laser profilometry technique used in the experiments to collect information on the evolution of the dike geometry (Rifai, 2018).

Test ID	Q_i [m^3/s]	Channel length [m]	Downstream condition	Floodplain water level [m]	d_{50} [mm]
1	0.020	8	Perforated plate	0	1
4	0.030				
8	0.040				
11	0.050				

Table 3.10: Configurations of the selected Rifai (2018) tests.

Measurement uncertainties

During the tests, the water depths were measured at several fixed locations. In the main channel, 3 measurements were performed using ultrasonic sensors represented by the symbol ⊗ in FIGURE 3.9 (G1, G2 and G3). The measurement accuracy of these devices was ±1%.

The inlet discharge into the main channel was measured by an electromagnetic flow meter with an accuracy of ±4%. The outlet discharge was deduced by taking into account the measurement of the water depth at the V-notch weir (sensor G4) and a mass balance on the volume present between the two weirs: regulating weir and V-notch weir.

Downstream boundary condition

As indicated in TABLE 3.10, the downstream boundary condition for the selected tests is a perforated plate. Rifai (2018) shows the rating curves obtained for the different tests shown (different inlet discharges). These curves are shown in FIGURE 3.11.

The use of these rating curves in the implemented numerical models requires first the acquisition of several points present on each curve (on average about fifty). Then, a linear interpolation was performed between these different points to reconstruct a full curve.

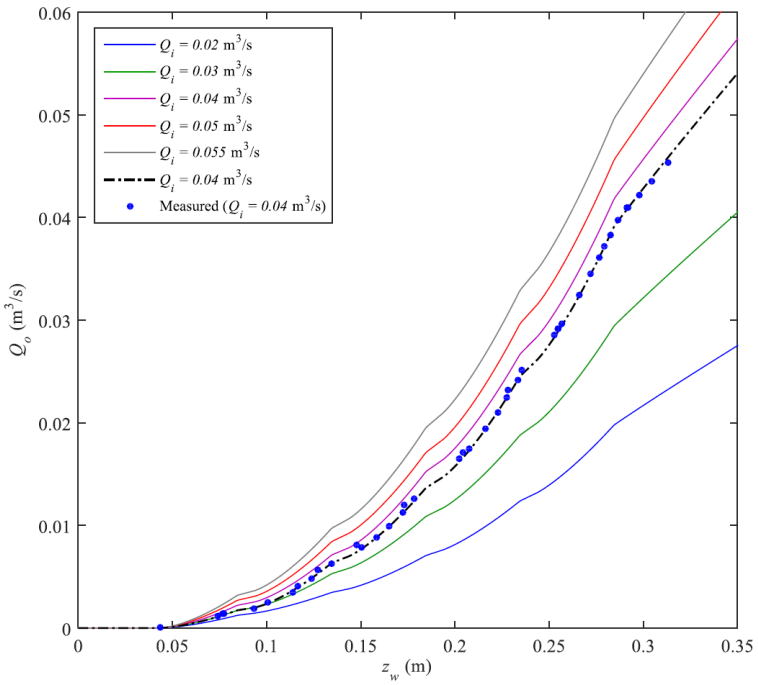

Figure 3.11: Rating curves for different discharges injected upstream of the channel: z_w is the downstream water depth obtained after weighting the water depths at the 3 probes (Rifai, 2018).

Experimental results

For the 4 tests considered, the spatial and temporal evolution of the dike geometry was recorded. FIGURE 3.12 represents the evolution of the dike geometry from a section in the center of the dike (in the middle of the crest: $y = 0.65$m, see FIGURE 3.9) for all tests. As the numerical models used have at most one spatial dimension, it was necessary to choose a longitudinal section of the dike where to focus on the evolution of the geometry. This was appropriately chosen in the center of the dike to represent the overall behavior of the breach evolution.

In FIGURE 3.12, x represents the main channel direction where the reference is taken from the upstream end of the dike, t the time and p the vertical depth of the dike evolving with time and space.

During the tests, as breach geometry, water levels and inlet discharge were measured. The water depths were measured with the G1, G2, G3 sensors. Using the water depth measurements and the continuity principle, the other discharges were determined. These are shown as blue dotted lines in FIGURE 3.9. These are:

- Q_i: the inlet discharge of the main channel.
- Q_d: the drain discharge.
- Q_l: the breach discharge. This discharge is defined as the overtopping dike discharge[5].
- Q_o: the outlet discharge of the main channel.

The evolution of breach discharges and water depths are shown in FIGURES 3.13 and 3.14 respectively.

[5]Note that the breach discharge is also called Q_b.

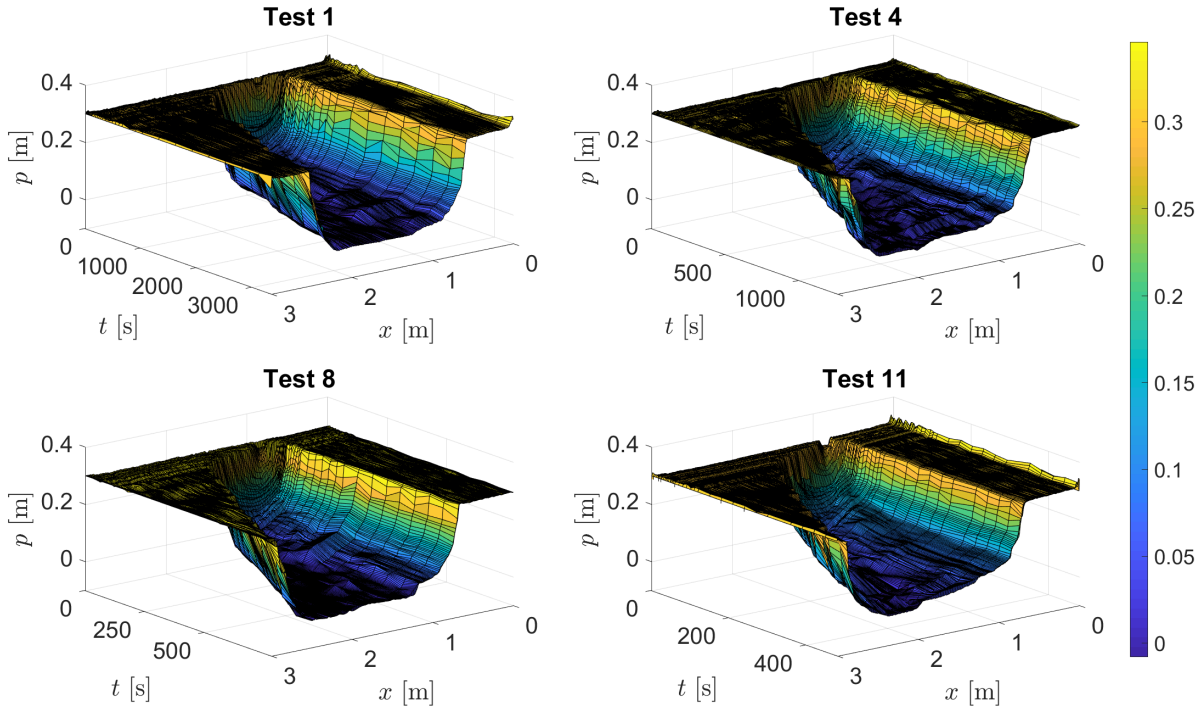

Figure 3.12: Evolution of the breach geometry for a given section ($y = 0.65$m) according to the tests selected.

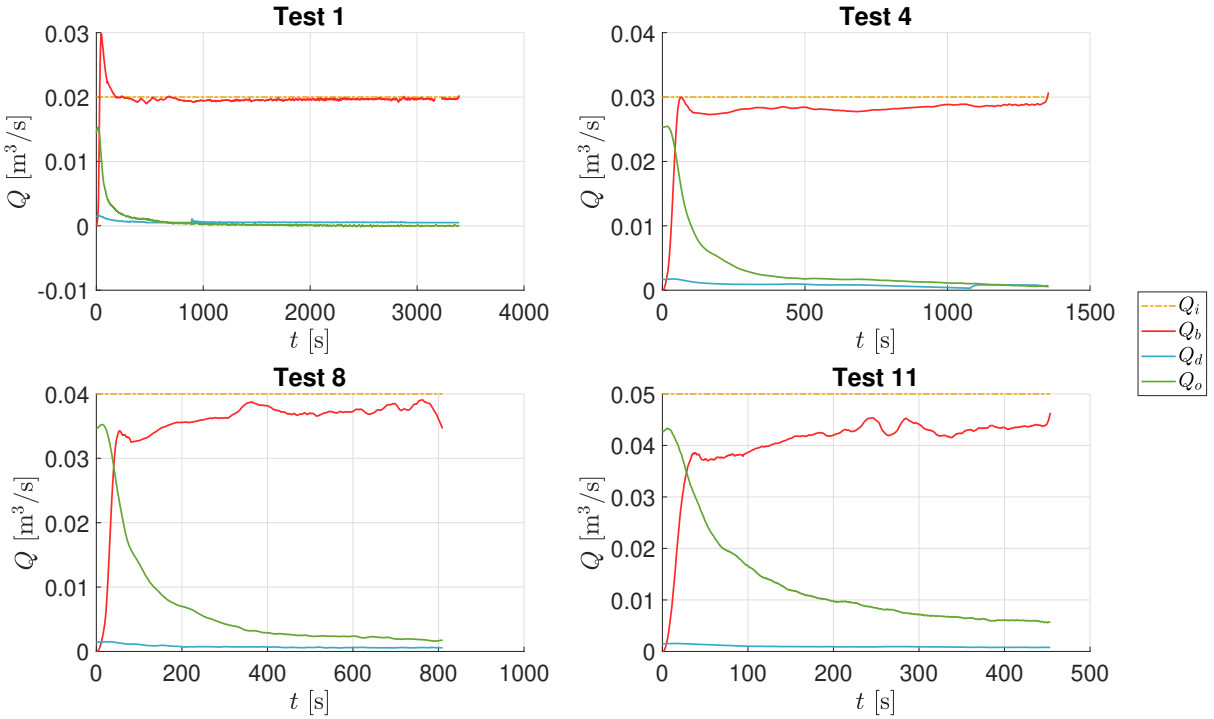

Figure 3.13: Evolution of the different experimental discharges according to the tests selected.

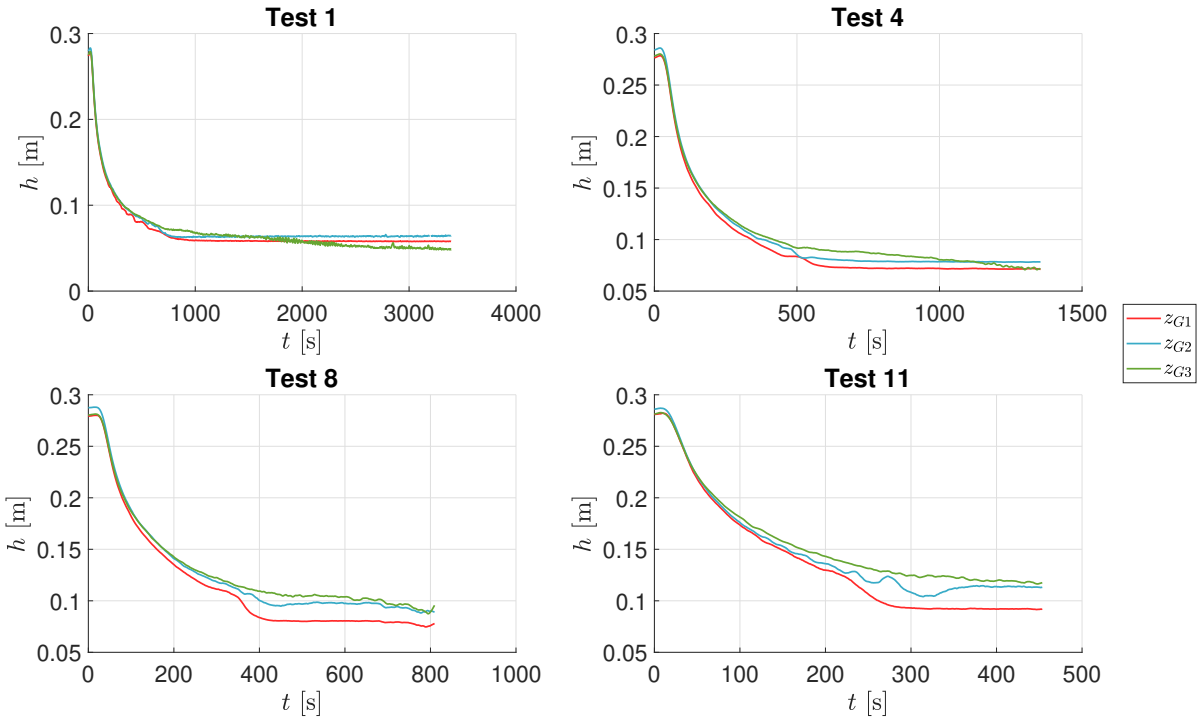

Figure 3.14: Evolution of the different experimental water depths at positions G1, G2 and G3 according to the tests selected.

3.3 Side weir discharge coefficient formulations

The side weir discharge coefficient is one of the fundamental unknowns in the process of numerical representation of the selected experimental results. One way to fix this unknown is to use various formulations that allow, with the use of hydraulic parameters such as the Froude number, obtaining a value of this coefficient. This technique was used by Mignot et al. (2020) in their publication. Many authors have described formulae for calculating the discharge coefficient of a rectangular fixed geometry side weir. The formulations tested will be those proposed by Mignot et al. (2020). These are listed in TABLE 3.11.

It is important to note that TABLE 3.11 has been slightly modified from TABLE 3 presented in Mignot et al. (2020) publication. Indeed, after discussion with E. Mignot and L. Camusson, it appeared that a proposed formulation (Swamee et al., 1994a) was not correct. The reference was wrong: it is a publication of Kandaswamy and Rouse (1957). However, this formulation concerns frontal weirs and not lateral weirs, which are the subject of the study. This formulation was therefore discarded.

Some modifications of the range of values (light gray in TABLE 3.11) compared with the reference publication Mignot et al. (2020), have also been made after a careful reading of the reference articles for each formulation.

The intrusion discharge through a rectangular side weir (Q_l) can be evaluated with De Marchi (1934) equation:

$$Q_l = \frac{2}{3} C_d \sqrt{2g} (h - p)^{3/2} L_s \tag{3.3}$$

with Q_l the lateral discharge [m^3/s], C_d the discharge coefficient [-], h the water depth at the upstream section of the opening [m], p the side weir crest height [m] and L_s the side weir length [m].

The discharge coefficient (C_d) is estimated from semi-empirical formulae proposed by various authors (TABLE 3.11). These formulae were each developed for a specific range of non-dimensional parameters (Fr, p/h and L_s/W), as detailed in the last three columns of TABLE 3.11. The range of validity of the semi-empirical formulae is summarized in FIGURE 3.15, together with the characteristic values of Fr and L_s/W corresponding to the experiments considered here (Michelazzo et al., 2015; Mignot et al., 2020; Roger et al., 2009). FIGURE 3.16 illustrates the range of validity in terms of Fr and p/h. Note that, outside these ranges of validity, the formulations are not guaranteed to be effective.

In these figures, it can be seen that some formulae have smaller ranges of validity than others. For example, in FIGURE 3.15, the formula proposed by Emiroglu et al. (2011) covers most of the tests. By contrast, the formulations of Ranga Raju et al. (1979) and Singh et al. (1994) cover only one test. Hager (1987) formulation was only tested for one value of L_s/W and therefore does not have an extended validity range along the L_s/W axis.

Roger et al. (2009) and Michelazzo et al. (2015) tests are characterized by zero lateral crest height (i.e. $p = 0$ m) as can be seen in FIGURE 3.16. Among Mignot et al. (2020) tests, two have a non-zero lateral crest height (Op1).

Bagheri et al. (2013) formula (n°11 in TABLE 3.11) is not suitable for tests with zero lateral crest height because of its mathematical expression (p in the denominator). This formulation can therefore only be used for the two Mignot et al. (2020) tests with Op1.

Rifai (2018) tests have not been included in FIGURES 3.15 and 3.16 because the geometry of the lateral opening is dynamic and therefore changes over time.

N°	Source	Discharge coefficient formula (C_d [-])	Fr [-]	p/h [-]	L_s/W [-]
1	Nandesamoorthy and Thomson (1972)	$0.432\left(\frac{2+Fr^2}{1+2Fr^2}\right)^{0.5}$	0.02-4.3	0-0.96	0.2-1.0
2	Subramanya and Awasthy (1972)	$0.611\left(1-\frac{3Fr^2}{2+Fr^2}\right)^{0.5}$	0.02-4.3	0-0.96	0.2-1.0
3	Yu-Tech (1972)	$0.622-0.222Fr$	0.02-4.3	0-0.96	0.2-1.0
4	Ranga Raju et al. (1979)	$0.81-0.6Fr$	0.1-0.5	n/a	0.33-0.5
5	Hager (1987)	$0.485\left(\frac{2+Fr^2}{2+3Fr^2}\right)^{0.5}$	0.3-2	0-0.75	3.33
6	Singh et al. (1994)	$0.33-0.18Fr+0.49\frac{p}{h}$	0.22-0.42	0.45-0.85	0.4-0.8
7	Swamee et al. (1994b)	$0.447\left[\left(\frac{44.7p}{49p+h}\right)^{6.67}+\left(\frac{h-p}{h}\right)^{6.67}\right]^{-0.15}$	0.1-0.93	0-0.31	0.4-1
8	Jalili and Borghei (1996)	$0.71-0.41Fr-0.22\frac{p}{h}$	0.1-2	0.05-0.87	0.67-2.5
9	Borghei et al. (1999)	$0.7-0.48Fr-0.3\frac{p}{h}+0.06\frac{L_s}{W}$	0.1-0.9	0.02-0.87	0.3-2.33
10	Emiroglu et al. (2011)	$\left[0.836+\left(-0.035+0.39\left(\frac{p}{h}\right)^{12.69}+0.158\left(\frac{L_s}{W}\right)^{0.59}+0.049\left(\frac{L_s}{h}\right)^{0.42}+0.244Fr^{2.125}\right)^{3.018}\right]^{5.36}$	0.08-0.92	0.34-0.91	0.3-3
11	Bagheri et al. (2013)	$-1.423Fr^{0.138}+0.744\left(\frac{h-p}{L_s}\right)^{-0.083}+0.723\left(\frac{h-p}{p}\right)^{0.088}+0.182\left(\frac{L_s}{W}\right)^{-0.241}$	0.08-0.91	0.22-0.9	0.33-1.5

Table 3.11: Side weir discharge coefficient C_d [-] formulae where Fr is the Froude number just upstream of the side opening [-], p is the side weir crest height [m], h is the water depth just upstream the side opening [m], L_s is the side weir length [m], W is the channel width [m] (inspired by Mignot et al., 2020).

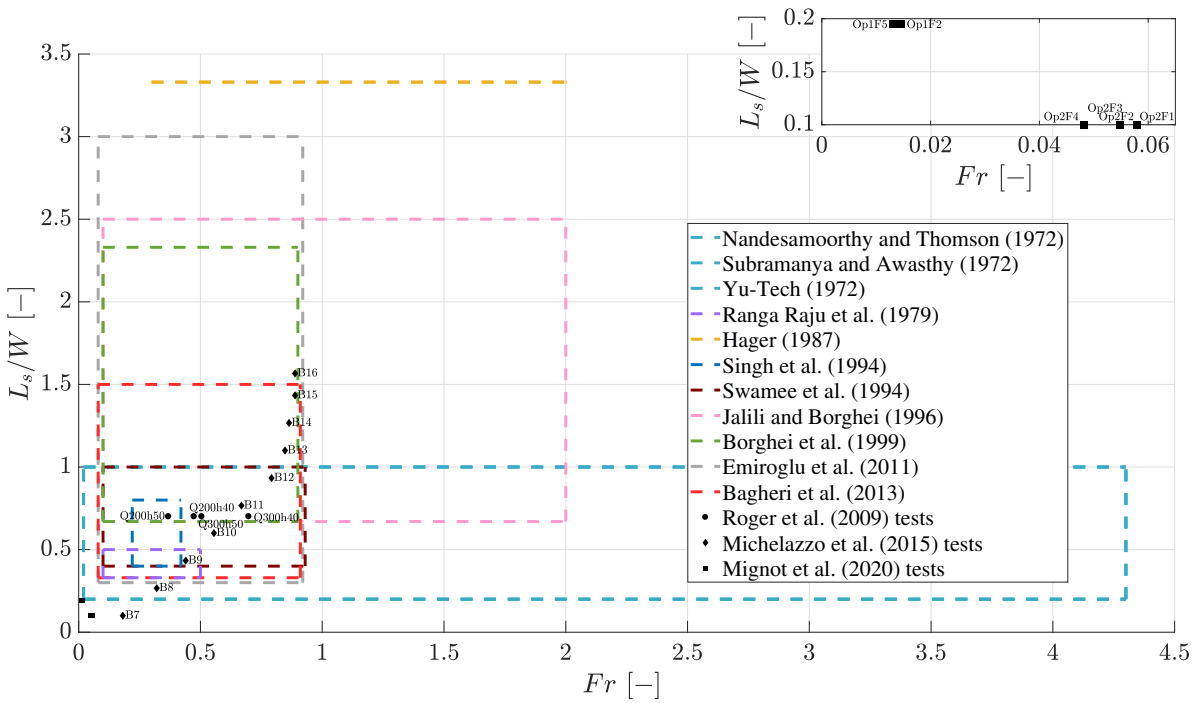

Figure 3.15: Ranges of parameters (Fr and L_s/W) used in authors formulae and tests configurations (Michelazzo et al., 2015; Mignot et al., 2020; Roger et al., 2009).

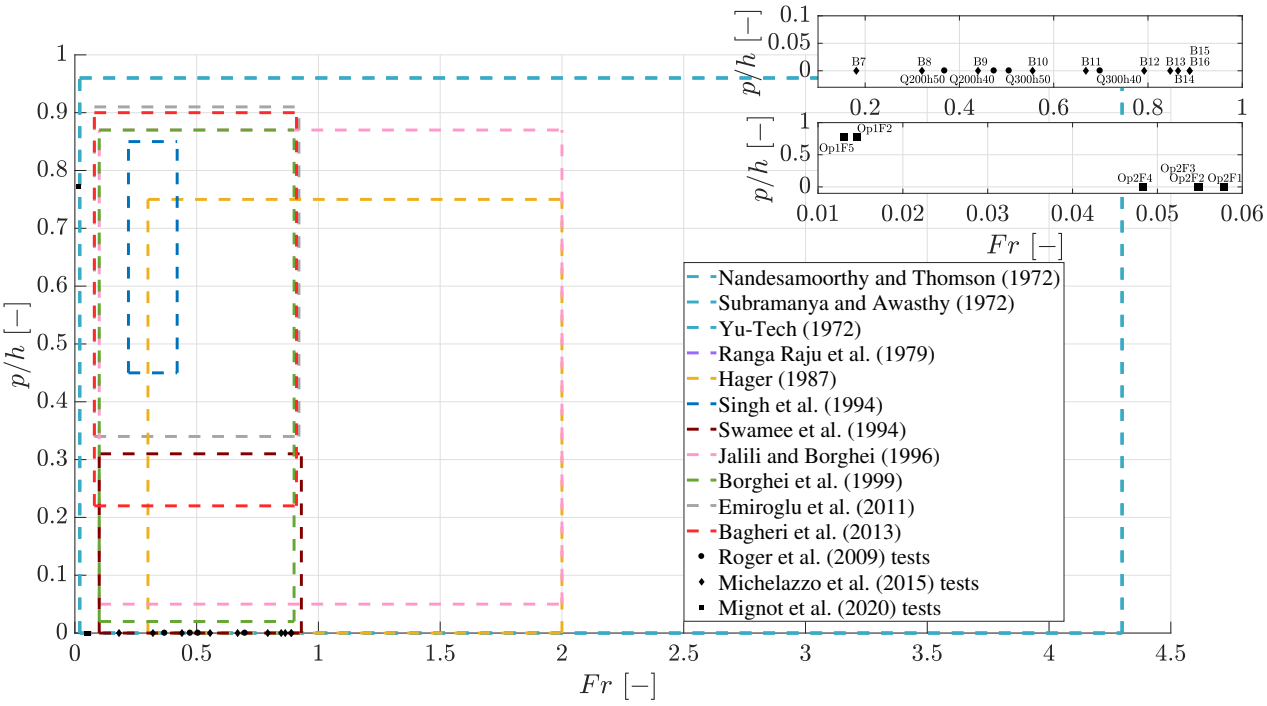

Figure 3.16: Ranges of parameters (Fr and p/h) used in authors formulae and tests configurations (Michelazzo et al., 2015; Mignot et al., 2020; Roger et al., 2009).

3.3.1 Comparison methodology

As stated at the beginning of this chapter, the formulations used have to be compared for different test cases. A methodology must therefore be established to compare these formulations.

The two variables of interest in these comparisons are the breach discharge and the water depth. One way to compare the formulations is to use indicators. In total, 5 indicators were used, of which three are normalized indicators. Depending on the variable of interest, the mathematical formulation of the indicators is different. Indeed, for the breach discharge, only one value is obtained for each formulation/test. For the water depth, it varies spatially, which leads to a revision of the mathematical definition of the indicators. The following formulae express how these indicators have been computed for each formulation.

Lateral breach discharge

Two different indicators have been used: the root mean square error ($RMSE$) and the bias ($Bias$). These indicators are expressed mathematically as follows:

$$\begin{cases} RMSE = \sqrt{\dfrac{1}{N}\sum_{i}^{N}\left(Q_{l,num,i} - Q_{l,meas,i}\right)^2} \\ Bias = \dfrac{1}{N}\sum_{i}^{N}\left(Q_{l,num,i} - Q_{l,meas,i}\right) \end{cases} \tag{3.4}$$

with N the number of tests, Q_l the variable of interest, $Q_{l,num}$ the computed value, $Q_{l,meas}$ the observed value.

In order to facilitate the interpretation of these indicators, three normalized indicator forms were also introduced in the analyses: the Nash-Sutcliffe model efficiency coefficient (NSE), the normalized root mean square error ($NRMSE$) and the normalized ($NBias$). These normalized indicators are expressed mathematically as follows:

$$\begin{cases} NSE = 1 - \dfrac{\dfrac{1}{N}\sum_{i}^{N}\left(Q_{l,num,i} - Q_{l,meas,i}\right)^2}{\dfrac{1}{N}\sum_{i}^{N}\left(\overline{Q_{l,meas}} - Q_{l,meas,i}\right)^2} = 1 - \dfrac{\sum_{i}^{N}\left(Q_{l,num,i} - Q_{l,meas,i}\right)^2}{\sum_{i}^{N}\left(\overline{Q_{l,meas}} - Q_{l,meas,i}\right)^2} \\ NRMSE = \dfrac{1}{\overline{Q_{l,meas}}}\sqrt{\dfrac{1}{N}\sum_{i}^{N}\left(Q_{l,num,i} - Q_{l,meas,i}\right)^2} \\ NBias = \dfrac{1}{\overline{Q_{l,meas}}}\dfrac{1}{N}\sum_{i}^{N}\left(Q_{l,num,i} - Q_{l,meas,i}\right) \end{cases} \tag{3.5}$$

with $\overline{Q_{l,meas}}$ the average observed values over the tests.

The NSE is a very standard non-dimensional indicator, which is commonly used to determine the predictive ability of hydrological models (Nash and Sutcliffe, 1970). Here are some of the features of this indicator:

- Range of variation: $]-\infty; 1]$.
- Typical range of variation: $[0.5; 1]$ (but NSE can be lower).
- If $NSE = 1$: the model used is perfect.
- If $NSE = 0$: the model used has the same error as simply using the average of the measurements.

- If $NSE < 0$: the model used performs worse than simply taking the mean of all measurements.

Water depth

This indicators analysis is a bit more complex in this case because the water depth is not a fixed value but is spatially distributed. A new strategy for calculating the indicators must therefore be considered. For each formulation, an indicator will be calculated as follows:

- For the 0D model: the water depth obtained by the numerical model was considered constant over the whole domain. Then, a sum of differences between the water depth of the 0D model and the experimental results was carried out for a series of points, in the comparison range, and averaged over the number of points considered. Finally, the indicator was averaged over the four tests.
- For the 1D model: the same method as for the 0D model was used except that in this case the model water depth is not constant but varies according to the water profile found by the 1D model.

This methodology is expressed mathematically by the following equations: Equation 3.6 (non-normalized forms) and Equation 3.7 (normalized forms).

$$\begin{cases} RMSE_i = \sqrt{\dfrac{1}{M}\sum_j^M \left(h_{num,j} - h_{meas,j}\right)^2} & \longrightarrow RMSE = \dfrac{1}{N}\sum_i^N RMSE_i \\ Bias_i = \dfrac{1}{M}\sum_j^M \left(h_{num,j} - h_{meas,j}\right) & \longrightarrow Bias = \dfrac{1}{N}\sum_i^N Bias_i \end{cases} \tag{3.6}$$

$$\begin{cases} NSE_i = 1 - \dfrac{\sum_j^M \left(h_{num,j} - h_{meas,j}\right)^2}{\sum_i^M \left(\overline{h_{meas}} - h_{meas,j}\right)^2} & \longrightarrow NSE = \dfrac{1}{N}\sum_i^N NSE_i \\ NRMSE_i = \dfrac{1}{\overline{h_{meas}}}\sqrt{\dfrac{1}{M}\sum_j^M \left(h_{num,j} - h_{meas,j}\right)^2} & \longrightarrow NRMSE = \dfrac{1}{N}\sum_i^N NRMSE_i \\ NBias_i = \dfrac{1}{\overline{h_{meas}}}\dfrac{1}{M}\sum_j^M \left(h_{num,j} - h_{meas,j}\right) & \longrightarrow NBias = \dfrac{1}{N}\sum_i^N NBias_i \end{cases} \tag{3.7}$$

with i the index of the considered test, j the index of the point considered, M the number of points considered to compute the difference, N the number of tests, h the water depth [m].

In the next part of this chapter, for each test (Michelazzo et al., 2015; Mignot et al., 2020; Roger et al., 2009), the results of four indicators obtained for each formulation are detailed. After consideration, the NSE indicator was not used because it has a major drawback for water depths. Indeed, if the measured depth is close to the average depth, the denominator of this indicator tends towards zero. Consequently, the value of this indicator tends towards infinity. The use of this indicator has therefore been discarded.

4 | Models development

The main objective of this thesis is the development of numerical models to simulate the dynamics of fluvial dike failure. As previously stated, the models developed are simple models allowing to obtain important hydraulic variables such as water depth and breach discharge. Therefore, it is a question of implementing models that are simple and efficient enough to obtain these variables quickly with sufficient accuracy of the results obtained.

The different models implemented were tested on the experiments described in Chapter 3. In order to be able to implement these models, it is first necessary to know the boundary conditions to be prescribed. These have been presented in the description of the different tests. In addition to the boundary conditions, as well as the configuration parameters of the tests (length of the channel, size of the breach, etc.), it is also essential to evaluate the breach discharge coefficient to determine the breach discharge. As there is no prescribed value of the discharge coefficient for the various tests, another solution has to be found. It is for this reason that formulations found in literature are used. Indeed, several formulations have been found that allow, depending on the hydraulic variables, computing a discharge coefficient. Therefore, an analysis of these formulations through the results obtained is interesting to carry out in order to test the relevance as well as the performance of these formulae.

Two numerical models were implemented in this thesis. The first one is the simplest model available: a lumped model. The mathematical equation governing this model is a mass balance at the control volume under consideration. The second model is a spatially-distributed model along the main flow direction. The system of equations governing this model is the 1D system of Saint-Venant equations based on a mass balance equation and a momentum balance equation. For the 1D model, the Saint-Venant equations are adapted to the cross-section of the channel (i.e. rectangular section for Roger et al. (2009), Michelazzo (2014) and Mignot et al. (2020) experiments and trapezoidal section for Rifai (2018) experiments). This information is synthesized in Figure 4.1.

The following sections of this chapter are dedicated to the presentation of the 0D and 1D models used to simulate the various experimental tests.

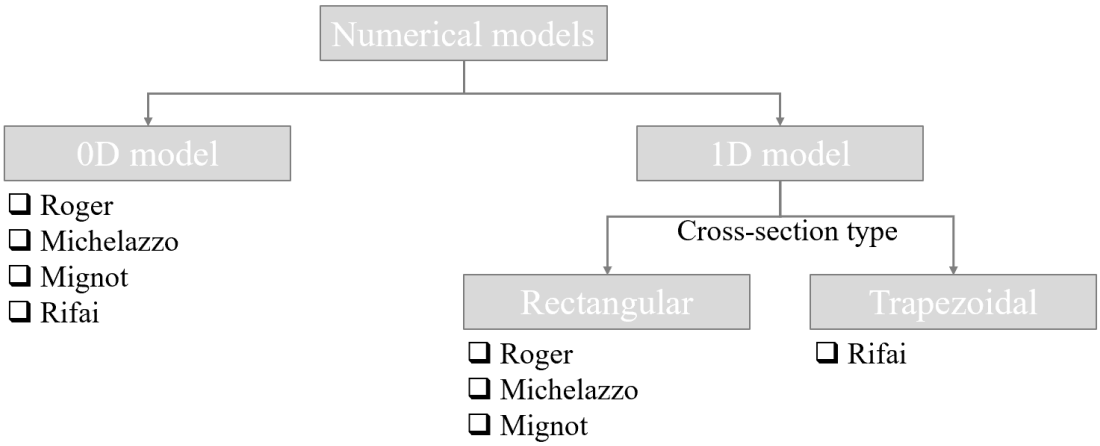

Figure 4.1: Implemented models and experiments used for each model.

4.1 Lumped model: 0D model

This numerical model is a simple model that does not use spatial discretization. The model can be seen as a box (control volume) to which an equilibrium equation is imposed. In the context of the experiments to be simulated, the balance equation imposed is that of conservation of mass (EQUATION 4.1). This equation can be written as follows:

$$A \cdot \frac{dh}{dt} = Q_{in} - Q_l - Q_{out} \tag{4.1}$$

with A the horizontal area of the main channel [m^2], h the water depth [m], t the time [s], Q_{in} the upstream input discharge [m^3/s], Q_l the lateral discharge [m^3/s] and Q_{out} the downstream output discharge [m^3/s].

EQUATION 4.1 is valid for all the experiments shown except for Rifai (2018) tests. In these experiments, a drain discharge was extracted along the dike. Therefore, a drain discharge term must be added to the right-hand side of the equation. The mass balance equation used to numerically simulate the Rifai (2018) experiments is therefore written:

$$A \cdot \frac{dh}{dt} = Q_{in} - Q_l - Q_d - Q_{out} \tag{4.2}$$

where Q_d is the drained discharge along the dike [m^3/s].

EQUATIONS 4.1 and 4.2 are illustrated at the control volume level as follows (FIGURE 4.2):

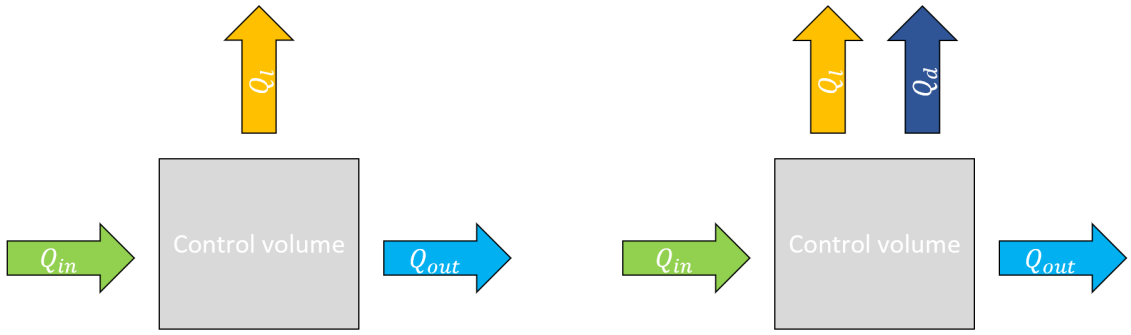

Figure 4.2: Schematic representation of the 0D model (EQUATION 4.1 on the left and EQUATION 4.2 on the right).

The upstream discharge (Q_{in}) is given for each test. Regarding the outflows, the downstream discharge is directly related to the imposed downstream boundary condition (rating curve[1]). For each series of tests, an upstream boundary condition (inflow) and a downstream boundary condition (outflow) are used. The lateral outflow is directly related to the lateral weir flow coefficient formula used in the De Marchi (1934) equation (EQUATION 3.3). For Rifai (2018) experiments, the drain discharge was calibrated using an empirical formula[2]:

$$Q_d = Q_{d,max} \cdot \left(\frac{h}{h_{crest}} \right)^k, \tag{4.3}$$

[1]The rating curves used were described in the presentation of the reference data.
[2]This formulation was introduced by Schmitz (2021) when the author described the hydrodynamic model.

where $Q_{d,max}$ is the maximum drain discharge [m^3/s], h the water depth [m], h_{crest} the initial dike crest depth [m] and k a calibrated parameter [-].

EQUATION 4.3 is calibrated with the parameter k to fit the experimental drain discharge as closely as possible. An example of the numerically drainage discharge for Rifai (2018) Test 1 is shown in FIGURE 4.3 ($k = 0.7$ and $Q_{d,max} = 1.5 \cdot 10^{-3}$ m^3/s). The largest oscillations visible in this figure illustrate the periods of emptying of the drainage basin.

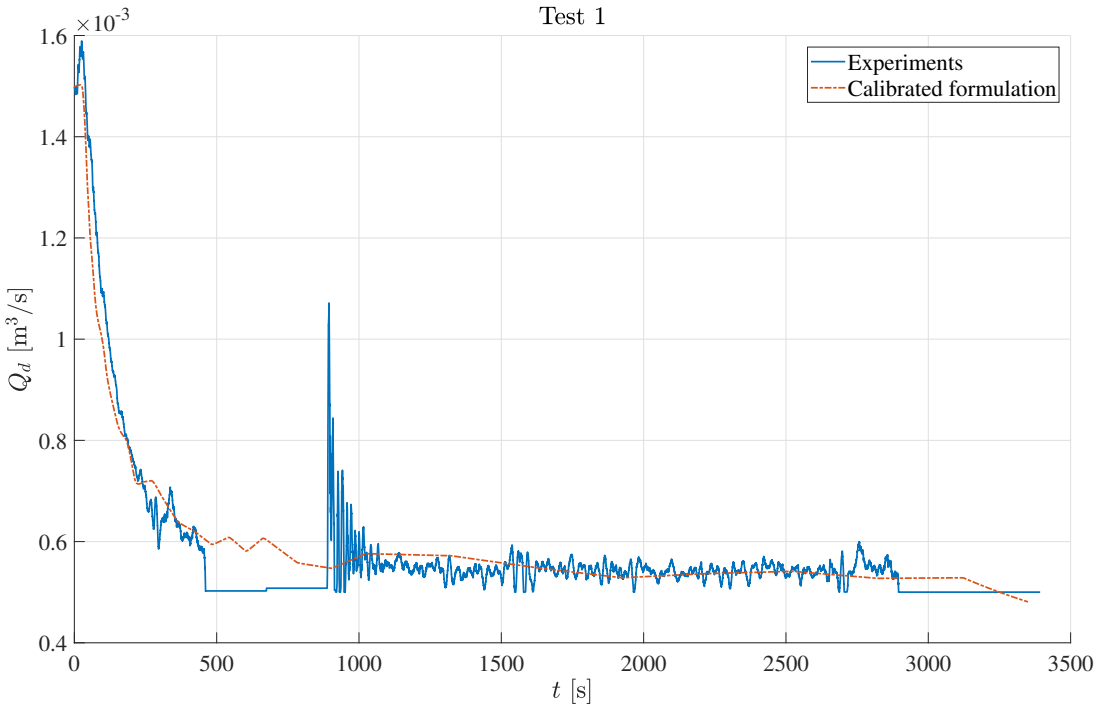

Figure 4.3: Comparison of experimental and calibrated drainage discharges.

The hydraulic variables of interest are the water depth (h) and the lateral discharge (Q_l), which will be compared between the two models. Nevertheless, it is necessary to be careful with the water depth obtained by the 0D model because it represents a water depth over a control volume. This value can be considered as the "average" water depth along the channel since the 0D model is a lumped model.

4.2 Spatially-distributed model: 1D model

The 1D model is a more complex model using a spatial discretization. This model is based on the 1D Saint-Venant equations:

$$\begin{cases} \dfrac{\partial A}{\partial t} + \dfrac{\partial Q}{\partial x} = 0 \\ \dfrac{\partial Q}{\partial t} + \dfrac{\partial}{\partial x}\left(QV + gA\overline{y}\right) = gA\left(S_0 - S_f\right) \end{cases} \tag{4.4}$$

where A is the cross-section [m^2], Q the channel discharge [m^3/s], V the velocity [m/s], g the gravity acceleration [m/s^2], $\overline{y}$ the average water depth [m], S_0 the bed slope [-] and S_f the friction slope [-].

The first equation of the system expresses the conservation of mass while the second expresses the conservation of momentum. These equations are written for a configuration without lateral discharge.

This form of the Saint-Venant equations is achieved by making a number of assumptions:

Assumptions to make mathematical derivations more tractable:

- Water density is considered constant.
- The main channel bottom slope is small. This means that the water depths measured normal to the bottom channel or simply vertically are similar.
- The velocity is uniform over the channel cross-section.
- The channel is prismatic: the cross-section of the channel and the channel bottom slope are constant.

Assumptions intrinsically related to the use of Saint-Venant equations:

- Water is considered incompressible.
- The pressure distribution is assumed hydrostatic. This is only valid if the streamlines do not have sharp curvatures.
- The velocity distribution over the channel cross-section is known *a priori* (as it cannot be predicted by the Saint-Venant equations).
- The head losses in unsteady flow may be simulated using the steady state resistance formulae (e.g. Manning).

The following sections describe the modifications made by considering first a rectangular section and then a trapezoidal section. The discretization schemes are also detailed.

4.2.1 Rectangular cross-section

For a rectangular cross-section, the system of equations (EQUATION 4.4) is expressed in terms of two hydraulic variables: h and q. Rewriting the conservation of mass and conservation of momentum equations, representing the flow in a channel without lateral flow, finally leads to:

$$\begin{cases} \frac{\partial h}{\partial t} + \frac{\partial q}{\partial x} = 0 \\ \frac{\partial q}{\partial t} + \frac{\partial}{\partial x}\left(\frac{q^2}{h} + \frac{gh^2}{2}\right) + gh\frac{\partial z_b}{\partial x} + ghJ = 0 \end{cases} \tag{4.5}$$

with h the water depth [m], t the time [s], q the specific discharge [m^2/s], x the position [m], g the gravity acceleration [m/s^2], z_b the channel bottom elevation [m], J the head loss [-].

These equations (EQUATION 4.5) consist of 3 different terms: inertial terms, convective terms and source terms.

Taking into account the lateral discharge *via* the lateral opening (breach), two terms have to be added to EQUATION 4.5. These are two source terms to be introduced on the right-hand side of each equation as follows:

$$\begin{cases} \frac{\partial h}{\partial t} + \frac{\partial q}{\partial x} = -\frac{q_L}{W} \\ \frac{\partial q}{\partial t} + \frac{\partial}{\partial x}\left(\frac{q^2}{h} + \frac{gh^2}{2}\right) + gh\frac{\partial z_b}{\partial x} + ghJ = -\frac{q}{h}\frac{q_L}{W} \end{cases} \tag{4.6}$$

with W the channel width [m] and q_L the specific lateral discharge [m^2/s].

The specific lateral discharge (q_L) can be expressed as a function of the water depth:

$$q_L = C_d\sqrt{2g\left|h + z_b - h_{FP} - z_{FP}\right|^3} \tag{4.7}$$

with C_d the side weir discharge coefficient[3] [-], h_{FP} the flood plain water depth [m] and z_{FP} the flood plain elevation [m]. The variables used in this equation are illustrated in FIGURE 4.4.

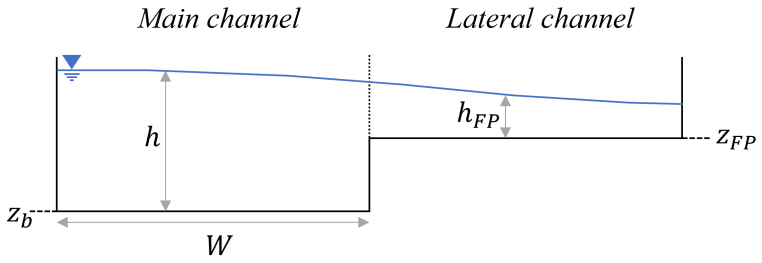

Figure 4.4: Rectangular cross-section with side weir.

The implemented 1D numerical model allows solving the equations EQUATION 4.6 and to find the unknowns h, q and q_l. The advantage of this model compared with the 0D model is that it enables the spatial variation along the channel of the variables h and q.

[3]The side weir discharge coefficient used in EQUATION 4.7 can be expressed by various formulations (see section 3.3).

Discretization schemes

The 1D code is a finite volume numerical code using two types of discretization schemes: a spatial discretization scheme and a temporal discretization scheme.

For the spatial discretization scheme, an integration of EQUATION 4.6 was performed on a finite volume defined from $x_{i-1/2}$ to $x_{i+1/2}$, where i is the current finite volume number and $i \pm 1/2$ are the edges of the finite volume i. Below are these integrated equations:

$$\begin{cases} \displaystyle\int_{x_{i-1/2}}^{x_{i+1/2}} \frac{\partial h}{\partial t}\,\mathrm{d}x + \int_{x_{i-1/2}}^{x_{i+1/2}} \frac{\partial q}{\partial x}\,\mathrm{d}x = \int_{x_{i-1/2}}^{x_{i+1/2}} -\frac{q_L}{W}\,\mathrm{d}x \\ \displaystyle\int_{x_{i-1/2}}^{x_{i+1/2}} \frac{\partial q}{\partial t}\,\mathrm{d}x + \int_{x_{i-1/2}}^{x_{i+1/2}} \frac{\partial}{\partial x}\left(\frac{q^2}{h} + \frac{gh^2}{2}\right)\mathrm{d}x + \int_{x_{i-1/2}}^{x_{i+1/2}} gh\frac{\partial z_b}{\partial x}\,\mathrm{d}x + \int_{x_{i-1/2}}^{x_{i+1/2}} ghJ\,\mathrm{d}x = \int_{x_{i-1/2}}^{x_{i+1/2}} -\frac{q}{h}\frac{q_L}{W}\,\mathrm{d}x \end{cases} \tag{4.8}$$

The integration of the convective terms results in a flux balance:

$$\begin{aligned} &\int_{x_{i-1/2}}^{x_{i+1/2}} \frac{\partial q}{\partial x}\,\mathrm{d}x = q_{i+1/2} - q_{i-1/2} \\ &\int_{x_{i-1/2}}^{x_{i+1/2}} \frac{\partial}{\partial x}\left(\frac{q^2}{h} + \frac{gh^2}{2}\right)\mathrm{d}x = \left.\frac{q^2}{h}\right|_{i+1/2} - \left.\frac{q^2}{h}\right|_{i-1/2} + \left.\frac{gh^2}{2}\right|_{i+1/2} - \left.\frac{gh^2}{2}\right|_{i-1/2} \end{aligned} \tag{4.9}$$

The other terms (inertial and source terms) are obtained by approximations based on the nodal values (EQUATION 4.10). In these equations, the spatial step Δx is defined as: $\Delta x = x_{i+1/2} - x_{i-1/2}$.

$$\begin{aligned} &\int_{x_{i-1/2}}^{x_{i+1/2}} \frac{\partial h}{\partial t}\,\mathrm{d}x \approx \left.\frac{\partial h}{\partial t}\right|_i \Delta x \qquad \int_{x_{i-1/2}}^{x_{i+1/2}} gh\frac{\partial z_b}{\partial x}\,\mathrm{d}x \approx gh_i \left.\frac{\partial z_b}{\partial x}\right|_i \Delta x \qquad \int_{x_{i-1/2}}^{x_{i+1/2}} -\frac{q_L}{W}\,\mathrm{d}x \approx -\frac{q_{L_i}}{W}\Delta x \\ &\int_{x_{i-1/2}}^{x_{i+1/2}} \frac{\partial q}{\partial t}\,\mathrm{d}x \approx \left.\frac{\partial q}{\partial t}\right|_i \Delta x \qquad \int_{x_{i-1/2}}^{x_{i+1/2}} ghJ\,\mathrm{d}x \approx gh_iJ_i\Delta x \qquad \int_{x_{i-1/2}}^{x_{i+1/2}} -\frac{q}{h}\frac{q_L}{W}\,\mathrm{d}x \approx -\frac{q_i}{h_i}\frac{q_{L_i}}{W}\Delta x \end{aligned} \tag{4.10}$$

The spatially discretized conservation of mass and conservation of momentum equations can be therefore written as follow:

$$\begin{cases} \left.\dfrac{\partial h}{\partial t}\right|_i \Delta x = -\left(q_{i+1/2} - q_{i-1/2}\right) - \dfrac{q_{L_i}}{W}\Delta x \\ \left.\dfrac{\partial q}{\partial t}\right|_i \Delta x = -\left(\left.\dfrac{q^2}{h}\right|_{i+1/2} - \left.\dfrac{q^2}{h}\right|_{i-1/2} + \left.\dfrac{gh^2}{2}\right|_{i+1/2} - \left.\dfrac{gh^2}{2}\right|_{i-1/2}\right) - gh_i\left.\dfrac{\partial z_b}{\partial x}\right|_i \Delta x - gh_iJ_i\Delta x \\ \qquad\qquad - \dfrac{q_i}{h_i}\dfrac{q_{L_i}}{W}\Delta x \end{cases} \tag{4.11}$$

Finally, it is possible to summarize the equations to be solved in the following forms:

$$\left.\frac{\partial f}{\partial t}\right|_i = RHS_i \tag{4.12}$$

with:

$$RHS_i = \frac{-1}{\Delta x} \cdot \left[\left(F_{i+1/2} - F_{i-1/2}\right) + S_i \Delta x\right] \tag{4.13}$$

where the new functions are expressed in terms of the former functions (TABLE 4.1):

New functions	Continuity equation	Momentum conservation equation
f	h	q
F	q	$\frac{q^2}{h} + \frac{gh^2}{2}$
S	$\frac{q_L}{W}$	$gh\frac{\partial z_b}{\partial x} + ghJ + \frac{q}{h}\frac{q_L}{W}$

Table 4.1: Expressions of the new functions in terms of the former functions.

To solve EQUATION 4.12, a time discretization must be implemented. The time discretization scheme is based on the two-step Runge-Kutta algorithm. This discretization requires the use of what is called a predictor (f^*) and a corrector (f^{**}):

$$\begin{cases} f_i^* = f_i^t + \Delta t \cdot RHS_i^t \\ f_i^{**} = f_i^t + \Delta t \cdot RHS_i^* \end{cases} \tag{4.14}$$

The value of the function at the next time step ($f^{t+\Delta t}$) can therefore be seen as a linear combination of the predictor and the corrector:

$$f_i^{t+\Delta t} = (1 - a_1) \cdot f_i^* + a_1 \cdot f_i^{**} \tag{4.15}$$

A graphical representation of this algorithm is given below in FIGURE 4.5.

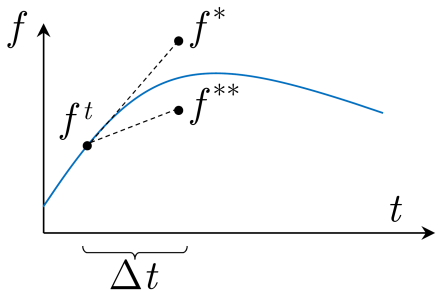

Figure 4.5: Two-step Runge-Kutta algorithm (predictor and corrector).

Two schemes have been introduced depending on the parameter value a_1. The characteristics of these two schemes are shown in table (TABLE 4.2):

Name	a_1 [-]	Specificity	Application
RK21	1	Maximum dissipation	Steady process
RK22	0.5	Maximum accuracy	Unsteady process

Table 4.2: Particularities of the temporal schemes implemented for the 1D model.

4.2.2 Trapezoidal cross-section

As already mentioned, Rifai (2018) experiments are carried out in a trapezoidal channel section, unlike the other experiments which are carried out in a rectangular channel section. Therefore, the Saint-Venant equations have to be adapted to find a numerically solvable system of equations. This section aims to illustrate the different changes made to construct the 1D model with trapezoidal section.

The main hydraulic variables used are different in the case of the 1D trapezoidal model. Indeed, in the rectangular section, the model used h and q (EQUATION 4.6). Now the variables are A and Q (EQUATION 4.16). The system of Saint-Venant equations is expressed as:

$$\begin{cases} \dfrac{\partial A}{\partial t} + \dfrac{\partial Q}{\partial x} = -q_L \\ \dfrac{\partial Q}{\partial t} + \dfrac{\partial}{\partial x}\left(QV + gA\overline{y}\right) + gA\left(S_f - S_0\right) = -V_x q_L \end{cases} \tag{4.16}$$

where A is the cross-section [m^2], Q the channel discharge [m^3/s], q_L the specific lateral discharge [m^2/s], V the velocity [m/s], g the gravity acceleration [m/s^2], $\overline{y}$ the average water depth [m], S_0 the bed slope [-] and S_f the friction slope [-].

There is obviously a link between the cross-sectional area and the water depth. This link allows switching from one variable to another at any time. These explanations are illustrated in FIGURE 4.6 showing the cross-section of a trapezoidal cross-section channel.

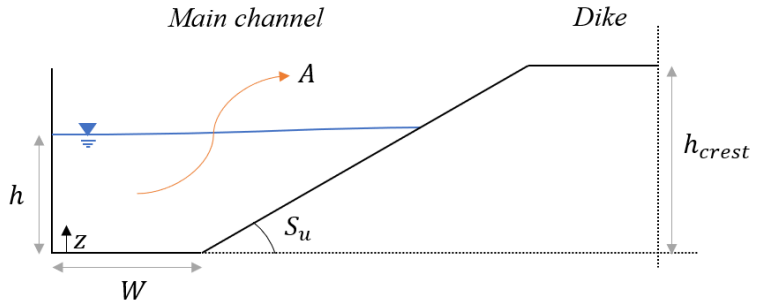

Figure 4.6: Trapezoidal cross-section as used in Rifai (2018) experiments.

The cross-section can be expressed as a function of the water depth and other geometric constants:

$$A = h \cdot W + \frac{h^2}{2S_u} \tag{4.17}$$

Alternatively, the water depth is expressed as:

$$h = \frac{-W + \sqrt{W^2 + \dfrac{4A}{2S_u}}}{\dfrac{1}{S_u}} \tag{4.18}$$

where the second root of EQUATION 4.17 is not considered because this is physically impossible (i.e. $h < 0$).

The convective term in the momentum conservation equation (EQUATION 4.16) can be written in another terms by expressing V (EQUATION 4.19) and $A\overline{y}$ (EQUATION 4.20).

$$V = \frac{Q}{A} \tag{4.19}$$

$$A\overline{y} = \int_0^h (h - z) \cdot \left(W + \frac{z}{S_u} \right) dz = \frac{h^2 \cdot (3S_u W + h)}{6S_u} \tag{4.20}$$

To solve the system only by considering the variables A and Q, it is necessary to rewrite EQUATION 4.20 in terms of A (EQUATION 4.21).

$$A\overline{y} = \frac{\left(\frac{-W + \sqrt{W^2 + \frac{4A}{2S_u}}}{\frac{1}{S_u}} \right)^2 \cdot \left(3S_u W + \left(\frac{-W + \sqrt{W^2 + \frac{4A}{2S_u}}}{\frac{1}{S_u}} \right) \right)}{6S_u} = A\overline{y}_* \tag{4.21}$$

The last major change to the system of equations concerns the friction slope, also called head losses. This is calculated using a friction law. In this case, the Manning law (EQUATION 4.22) has been chosen (for both rectangular and trapezoidal sections).

$$S_f = \Delta H = \frac{n^2 V^2}{R_h^{4/3}} = \frac{n^2 \left(\frac{Q}{A} \right)^2}{R_h^{4/3}} \tag{4.22}$$

where n is the Manning coefficient [s/m$^{1/3}$] and R_h the hydraulic radius [m].

The hydraulic radius is calculated as the cross-sectional area divided by the wetted perimeter. For a rectangular cross-section, the hydraulic radius is:

$$R_h = \frac{hW}{2h + W} \tag{4.23}$$

For a trapezoidal cross-section, the hydraulic radius is:

$$R_h = \frac{h \cdot W + \frac{h^2}{2S_u}}{h + W + \sqrt{h^2 + \left(\frac{h}{S_u} \right)^2}} \tag{4.24}$$

Note: the channel width W is not the same for the channel in rectangular section and the channel in trapezoidal section. For the trapezoidal cross-section, this value indicates the bottom width of the channel (FIGURE 4.6).

Discretization schemes

Knowing all the modifications mentioned in this section, the equation system can be discretized in the same way as for the 1D rectangular cross-section model except that the hydraulic variables of interest are different. The integrated system equations are expressed:

$$\begin{cases} \displaystyle\int_{x_{i-1/2}}^{x_{i+1/2}} \frac{\partial A}{\partial t}\,\mathrm{d}x + \int_{x_{i-1/2}}^{x_{i+1/2}} \frac{\partial Q}{\partial x}\,\mathrm{d}x = \int_{x_{i-1/2}}^{x_{i+1/2}} -q_L\,\mathrm{d}x \\ \displaystyle\int_{x_{i-1/2}}^{x_{i+1/2}} \frac{\partial Q}{\partial t}\,\mathrm{d}x + \int_{x_{i-1/2}}^{x_{i+1/2}} \frac{\partial}{\partial x}\left(\frac{Q^2}{A} + gA\overline{y}_*\right)\mathrm{d}x + \int_{x_{i-1/2}}^{x_{i+1/2}} gAS_f\,\mathrm{d}x - \int_{x_{i-1/2}}^{x_{i+1/2}} gAS_0\,\mathrm{d}x = \int_{x_{i-1/2}}^{x_{i+1/2}} -\frac{Q}{A}q_L\,\mathrm{d}x \end{cases} \tag{4.25}$$

The integration of the convective terms results in a flux balance:

$$\begin{aligned} &\int_{x_{i-1/2}}^{x_{i+1/2}} \frac{\partial Q}{\partial x}\,\mathrm{d}x = Q_{i+1/2} - Q_{i-1/2} \\ &\int_{x_{i-1/2}}^{x_{i+1/2}} \frac{\partial}{\partial x}\left(\frac{Q^2}{A} + gA\overline{y}_*\right)\mathrm{d}x = \left.\frac{Q^2}{A}\right|_{i+1/2} - \left.\frac{Q^2}{A}\right|_{i-1/2} + A\overline{y}_*|_{i+1/2} - A\overline{y}_*|_{i-1/2} \end{aligned} \tag{4.26}$$

The other terms (inertial and source terms) are obtained by approximations based on the nodal values (Equation 4.27). In these equations, the spatial step Δx is defined as: $\Delta x = x_{i+1/2} - x_{i-1/2}$.

$$\begin{aligned} &\int_{x_{i-1/2}}^{x_{i+1/2}} \frac{\partial A}{\partial t}\,\mathrm{d}x \approx \left.\frac{\partial A}{\partial t}\right|_i \Delta x \quad \int_{x_{i-1/2}}^{x_{i+1/2}} gAS_0\,\mathrm{d}x \approx gA_iS_{0i}\Delta x \quad \int_{x_{i-1/2}}^{x_{i+1/2}} -q_L\,\mathrm{d}x \approx -q_{L_i}\Delta x \\ &\int_{x_{i-1/2}}^{x_{i+1/2}} \frac{\partial Q}{\partial t}\,\mathrm{d}x \approx \left.\frac{\partial Q}{\partial t}\right|_i \Delta x \quad \int_{x_{i-1/2}}^{x_{i+1/2}} gAS_f\,\mathrm{d}x \approx gA_iS_{fi}\Delta x \quad \int_{x_{i-1/2}}^{x_{i+1/2}} -\frac{Q}{A}q_L\,\mathrm{d}x \approx -\frac{Q_i}{A_i}q_{Li}\Delta x \end{aligned} \tag{4.27}$$

The spatially discretized conservation of mass and conservation of momentum equations can be written as follow:

$$\begin{cases} \left.\dfrac{\partial A}{\partial t}\right|_i \Delta x = -\left(Q_{i+1/2} - Q_{i-1/2}\right) - q_{Li}\Delta x \\ \left.\dfrac{\partial Q}{\partial t}\right|_i \Delta x = -\left(\left.\dfrac{Q^2}{A}\right|_{i+1/2} - \left.\dfrac{Q^2}{A}\right|_{i-1/2} + gA\overline{y}_*|_{i+1/2} - gA\overline{y}_*|_{i-1/2}\right) - gA_iS_{0i}\Delta x - gA_iS_{fi}\Delta x \\ \qquad\qquad - \dfrac{Q_i}{A_i}q_{Li}\Delta x \end{cases} \tag{4.28}$$

Finally, it is possible to summarize the equations to be solved in the following forms:

$$\left.\frac{\partial f}{\partial t}\right|_i = RHS_i \tag{4.29}$$

with:

$$RHS_i = \frac{-1}{\Delta x} \cdot \left[\left(F_{i+1/2} - F_{i-1/2}\right) + S_i \Delta x\right] \tag{4.30}$$

where the new functions are expressed in terms of the former functions (TABLE 4.3):

New functions	Continuity equation	Momentum conservation equation
f	A	Q
F	Q	$\frac{Q^2}{A} + A\overline{y}_*$
S	q_L	$gAS_0 + gAS_f + \frac{Q}{A}q_L$

Table 4.3: Expressions of the new functions in terms of the former functions.

5 | Results

This chapter discusses the numerical results obtained with the different models depending on the type of experiments considered. The latter is divided into 3 main sections that highlight the hydraulic configurations tested. The first section is dedicated to the flow experiments with a fixed breach geometry with zero lateral crest height. The results obtained for Roger et al. (2009), Michelazzo et al. (2015) and Mignot et al. (2020) experiments are detailed in this section. The second section concerns the flow experiments with a fixed breach geometry with non-zero lateral crest height. The results of the two Mignot et al. (2020) experiments considered are also presented. Finally, the third section of this chapter covers the flow experiments with dynamic breach geometry. Rifai (2018) experiments are described in detail.

Each section exhibits the results obtained for both numerical models (0D and 1D). The different discharge coefficient formulations have been tested and form an integral part of the analysis of the results. Once the numerical results are detailed for each model and formulation, a comparison between the results obtained with the different models and formulations is presented.

An explicit diagram describing the organization of this chapter is given in FIGURE 5.1.

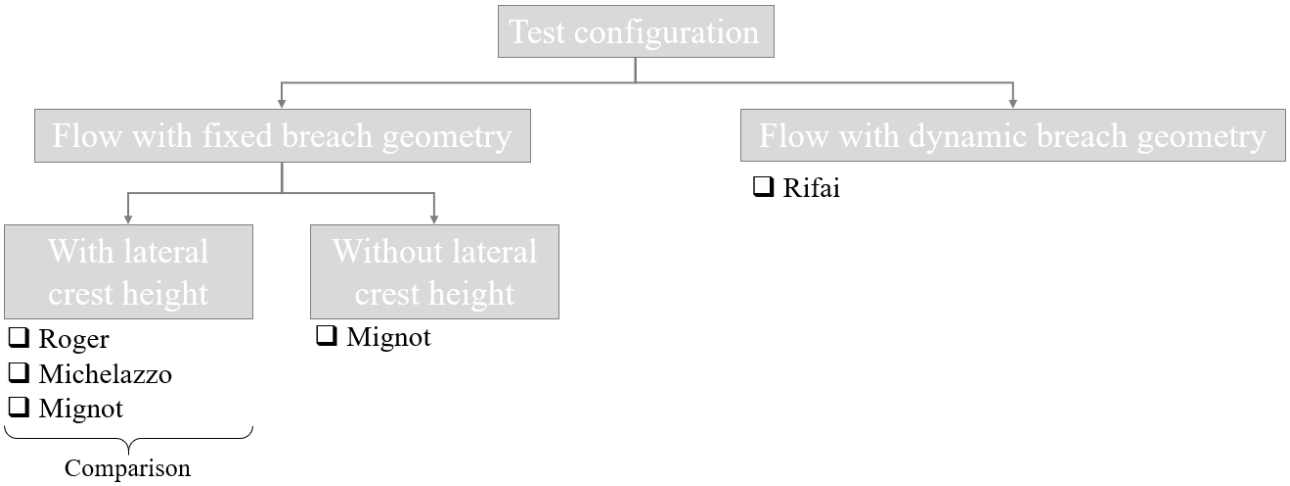

Figure 5.1: Organization of the chapter presenting the results obtained.

5.1 Flow with fixed breach geometry and zero lateral crest height

5.1.1 Roger et al. (2009)

Lumped model

The first analysis carried out was the determination of the breach discharge and the water depth calculated by the lumped model. For this purpose, in EQUATION 4.1, the expression of the breach discharge Q_l used is the one proposed by De Marchi (EQUATION 3.3) with the breach discharge coefficient C_d varying according to the adopted formulation (TABLE 3.11). The downstream discharge (Q_{out}) was directly computed with the rating curve determined by Roger et al. (2009) (EQUATION 3.1). Thus, the new form of EQUATION 4.1 now depends only on the water depth[1].

The breach discharges obtained for each discharge coefficient formulation are shown in FIGURE 5.2. In this figure, the black dotted line represents the breach discharge measured during Roger et al. (2009) experiments. The blue dotted lines represent the breach discharge obtained by 2D models (FE and FV). Some results must be taken with caution as some formulations have not been tested for the parameter ranges (Fr, L_s/W and p/h) illustrated in FIGURES 3.15 and 3.16. Although these formulations have not been tested for these ranges, they could be suitable. If not, the results should speak for themselves.

It can be observed in FIGURE 5.2 that several formulae give results close to the experimental data. In order to interpret this figure, an illustration of the difference between the numerically obtained and observed breach discharge is given in FIGURE 5.3. This figure shows clearly the formulations giving the closest results to the experimental results. Furthermore, the sign of the difference indicates whether the formulae tend to overestimate the breach discharge or underestimate the breach discharge.

Except for two empirical expressions (Emiroglu et al., 2011; Singh et al., 1994), the results obtained with the lumped model have a difference with the experimental results well under 10%. Actually, these results are more around the 5% difference. It is not surprising that these two formulations give results that are further away from the experimental results (respectively a lateral discharge difference of more than 25% and 10%). These were tested for lateral openings with a non-zero crest height. However, Roger et al. (2009) experiments do not involve a non-zero crest height at the side opening (i.e. zero crest height). This could explain the divergence in results.

The 0D model exhibits an error of less than 7% for most empirical expressions. The results obtained on the breach discharge with this basic model are better than those obtained with the more complex 2D models.

Regarding the proposed formulations, it has to be mentioned that four of them (Emiroglu et al., 2011; Hager, 1987; Singh et al., 1994; Swamee et al., 1994a) underestimate the breach discharge for all tests. This can be seen in FIGURE 5.2 as the bars are below the black dotted lines. In FIGURE 5.3, the difference between numerical and observed discharges is negative, which corresponds to an underestimation of the discharge by the numerical model. The 2D models always underestimate the breach discharge.

[1]Some formulations use the Froude number to compute the discharge coefficient C_d. For the 0D model, Fr is computed as follow: $\frac{Q_{in}}{WH\sqrt{gh}}$.

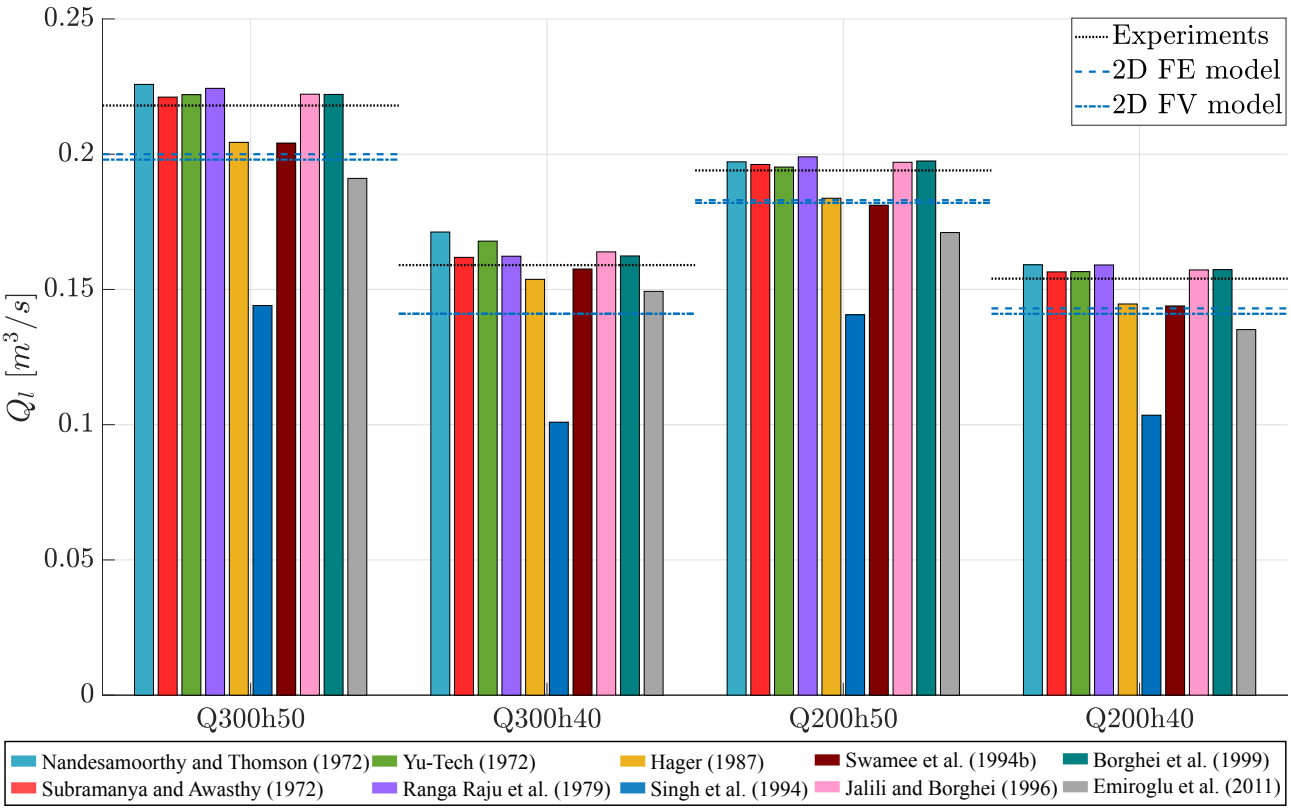

Figure 5.2: Breach discharge (0D model) for Roger et al. (2009) tests.

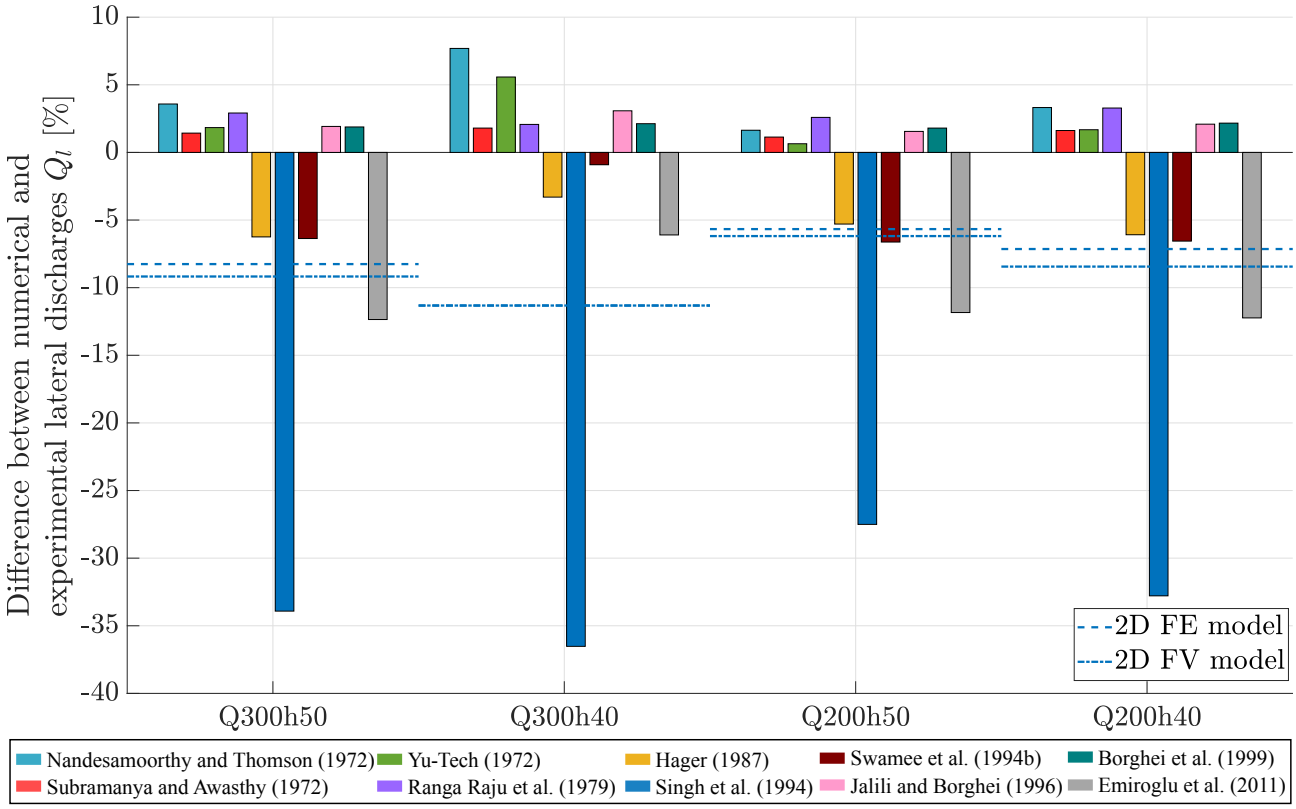

Figure 5.3: Difference between numerical (0D model) and experimental breach discharge for Roger et al. (2009) tests.

The same analysis as for the breach discharge has been carried out for the water depth. However, as the 0D model is non-discretized, the computed water depth is a single value and not a water depth profile along the channel. This water depth is equivalent to the averaged water depth in the two main directions (main flow axis and perpendicular to this axis).

FIGURE 5.4 illustrates the numerical water depths. The blue dotted lines represent the extremum water depths obtained by the 2D FV model (*WOLF*). Actually, these are the minimum and maximum water depths of the envelopes shown in FIGURE 3.3. The water depth averaged along the two main directions has also been plotted in this figure. As previously stated, experimental depth profiles could not be obtained. Therefore, the compared water profile is the one obtained numerically by Roger et al. (2009). In FIGURE 5.4, most of the water depths are within the range of the minimum and maximum water depths (except for the two formulations identified earlier). This last observation is not surprising due to the fact that the breach discharge is underestimated by the numerical model. This means that the discharge through the breach is lower than the observed discharge. Therefore, the downstream discharge as well as the water depth in the channel are higher.

Finally, the water depths obtained are quite close to those obtained by averaging the depths along the two axes. It seems relevant that the numerical results are close to the average obtained with *WOLF* given the signification of the water depth calculated by the 0D model.

FIGURE 5.5 illustrates the difference between the water depths obtained in the lumped model and those averaged from the 2D model. For the formulations that predict most accurately the breach discharge, the difference in water depth is less than 5%. It should be remembered that the comparison of the depths is based on the 2D numerical results and not on the experimental results. This analysis already provides some indication of the results obtained but does not enable a comparison with the real experimental data.

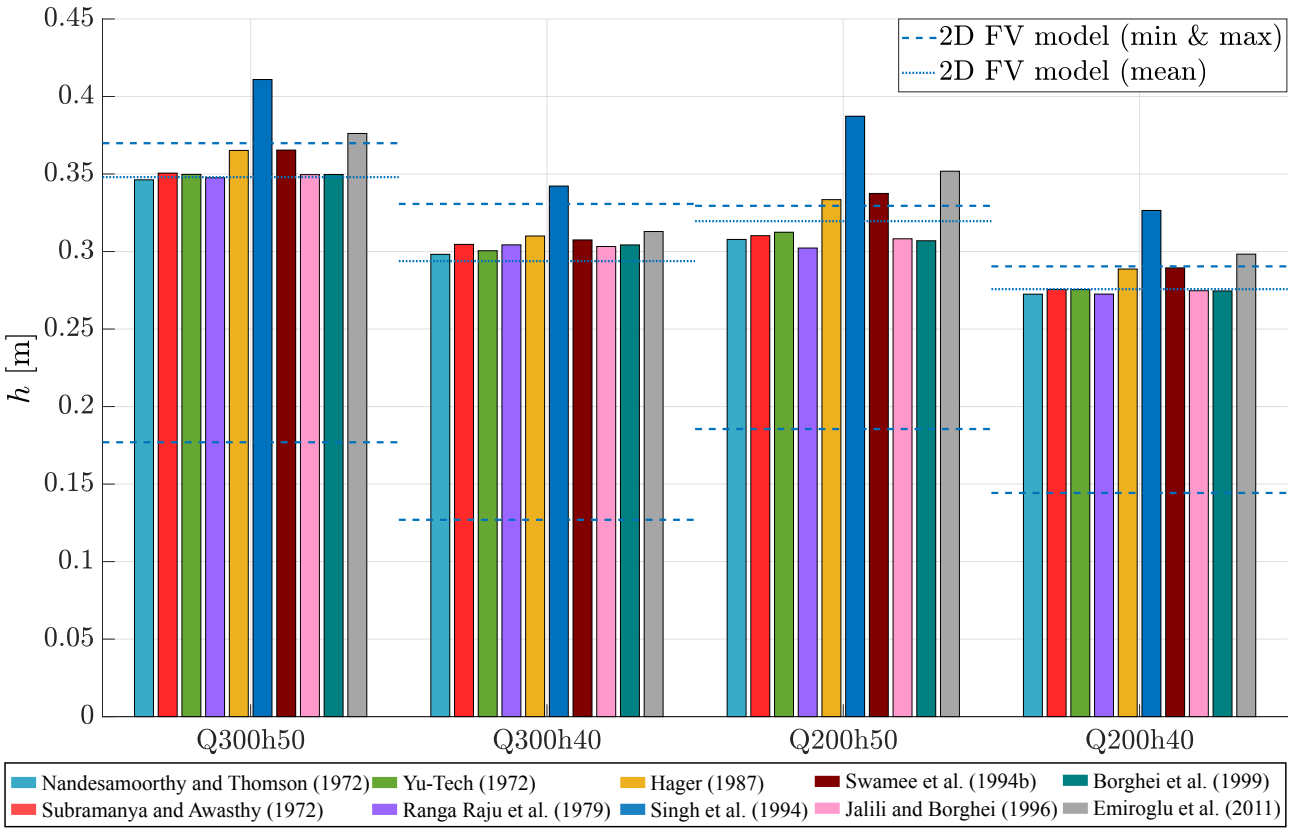

Figure 5.4: Water depth results (0D model) for Roger et al. (2009) tests.

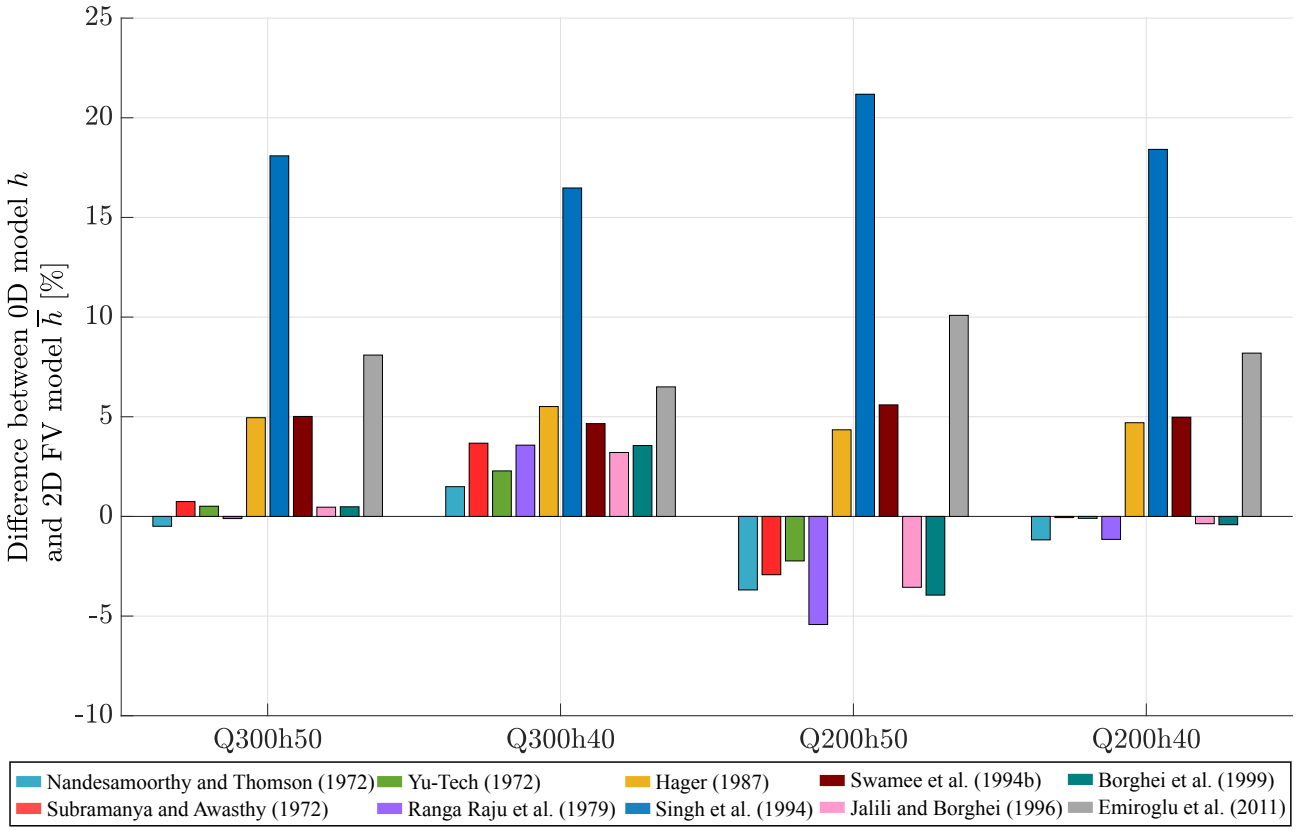

Figure 5.5: Difference between numerical water depth results (0D model and 2D model) for Roger et al. (2009) tests.

Spatially-distributed model

The same analyses as for the lumped model have been done for the spatially-distributed model. In FIGURE 5.6, it can be seen that no matter the discharge coefficient formulation used, the breach discharge is always underestimated (except for test Q200h50 with Ranga Raju et al. (1979) formula). The same analysis is shown in FIGURE 5.7, which represents the difference between numerical and observed discharges. Singh et al. (1994) formula remains the least effective empirical formulation with differences of more than 25%. For the other formulations, the differences are less than 15%. Overall the most accurate formulae for the 0D model remain accurate for the 1D model.

6 formulations seem to stand out: Nandesamoorthy and Thomson (1972), Subramanya and Awasthy (1972), Yu-Tech (1972), Ranga Raju et al. (1979), Jalili and Borghei (1996) and Borghei et al. (1999) expressions. Indeed, they provide good results with both numerical models. These numerical results are even better than the 2D models results which is quite outstanding.

In addition to obtaining a value for the breach discharge, the spatially-distributed model provides information on the hydraulic variables along the main flow axis. Thus, this model adds new information about the spatial evolution of the discharge as well as the water depth. It has to be mentioned that these results could not be obtained with the lumped model.

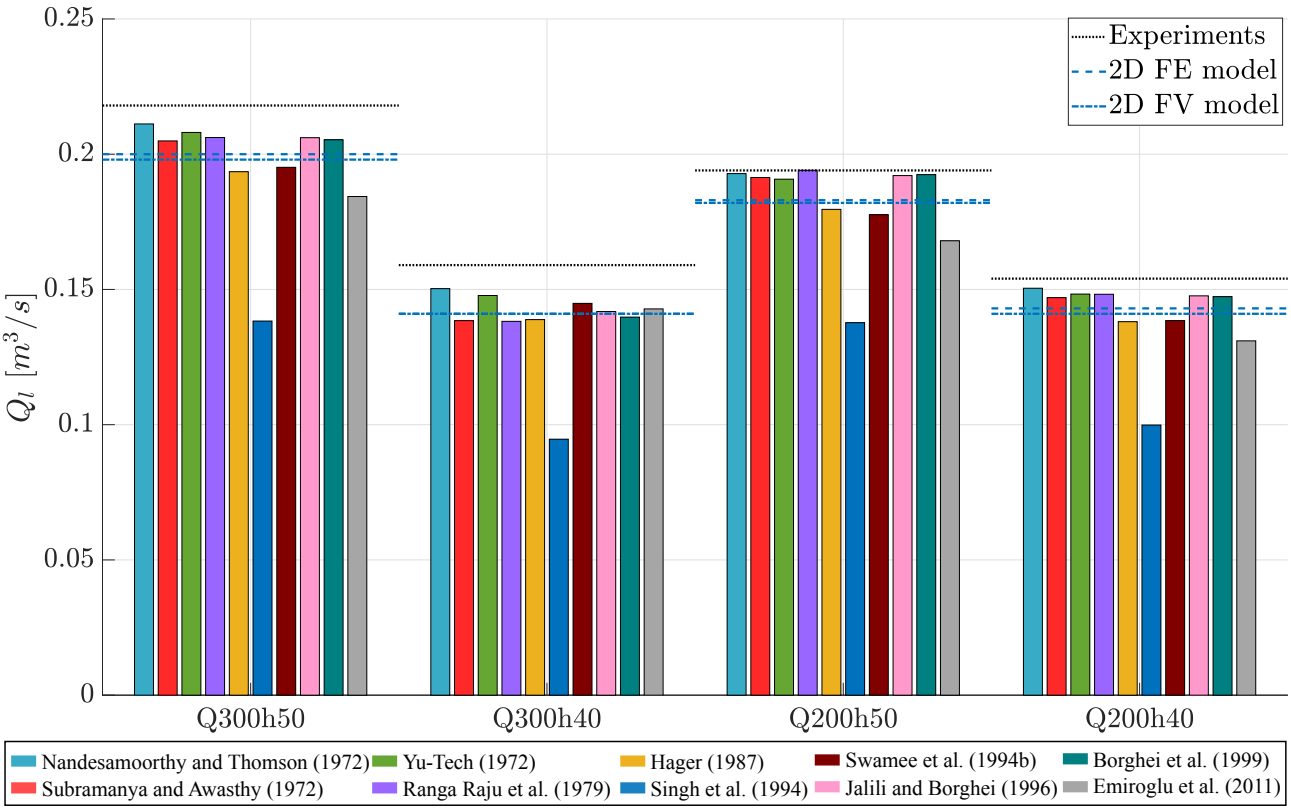

Figure 5.6: Breach discharge results (1D model) for Roger et al. (2009) tests.

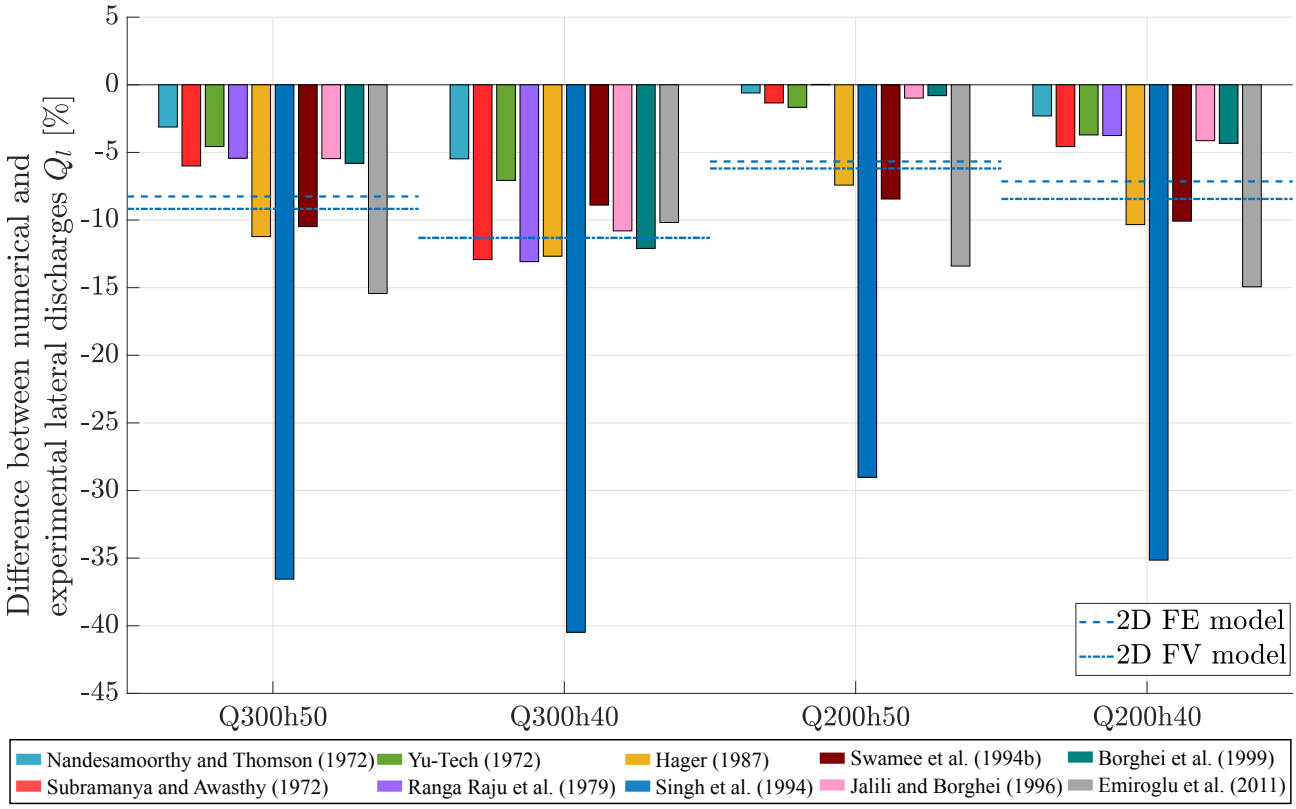

Figure 5.7: Difference between numerical (1D model) and measurement breach discharge results for Roger et al. (2009) tests.

The discharge profiles are illustrated in FIGURE 5.8. Before the upstream end of the breach ($x \approx 3.6$ m), the discharge in the channel equals the injected discharge (Q_{in}). Once the upstream end of the breach is crossed, the channel discharge decreases as part of the channel flow passes through the breach. The discharge obtained downstream of the breach is the difference between the injected discharge and the discharge through the breach (by continuity) and considering also the water depth variation of the free surface.

It is quite simple to link FIGURES 5.6 and 5.8, as the lower the breach discharge (FIGURE 5.6), the higher the discharge observed downstream of the breach (FIGURE 5.8). Singh et al. (1994) formula has the lowest breach discharge and therefore the highest downstream discharge. The opposite is true for Nandesamoorthy and Thomson (1972) formulation.

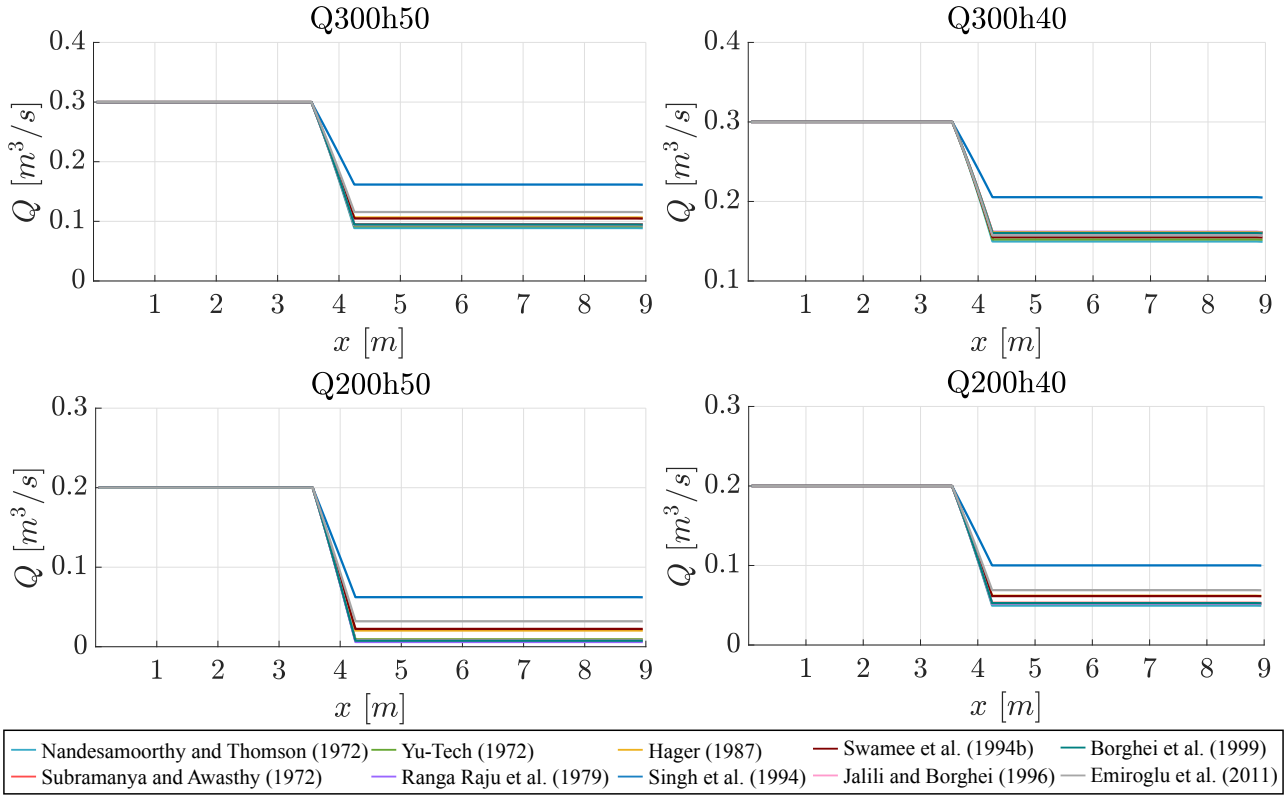

Figure 5.8: Discharge profiles along the channel axis (1D model) for Roger et al. (2009) tests.

The spatial evolution of the Froude number is shown in FIGURE 5.9. For all tests, over the entire length of the channel, the observed flow regime is a subcritical regime (i.e. $Fr < 1$).

For each formula/test, there is a more or less important increase in the Froude number upstream of the breach. This increase is particularly visible for the Q300h40 test (FIGURE 5.9). The higher the discharge and the lower the depth, the higher the Froude number. This is why Fr is higher for Nandesamoorthy and Thomson (1972) formulation and lower for Singh et al. (1994) formulation.

Regarding water depth profiles (FIGURE 5.10), these can be compared with the 2D FV model. The water depth profiles obtained with the 1D model fit quite well the water depth profiles obtained with the 2D FV model, which is convincing. According to the breach discharge coefficient formula used, the profiles are translated vertically. Only one water depth data was available for each experiment. These are shown in FIGURE 5.10. The experimental water depth appears to be lower than the water depth obtained with the different numerical models (0D, 1D and 2D).

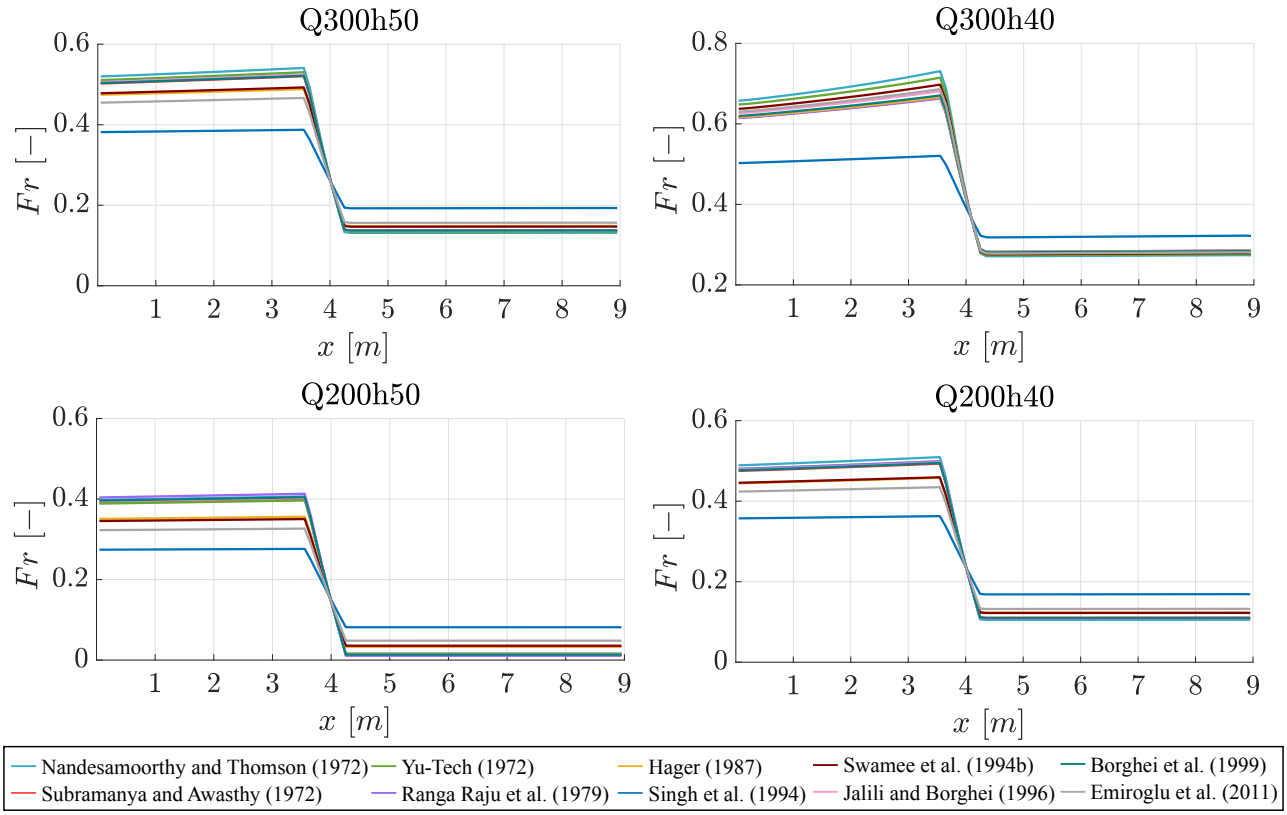

Figure 5.9: Froude profiles along the channel axis (1D model) for Roger et al. (2009) tests.

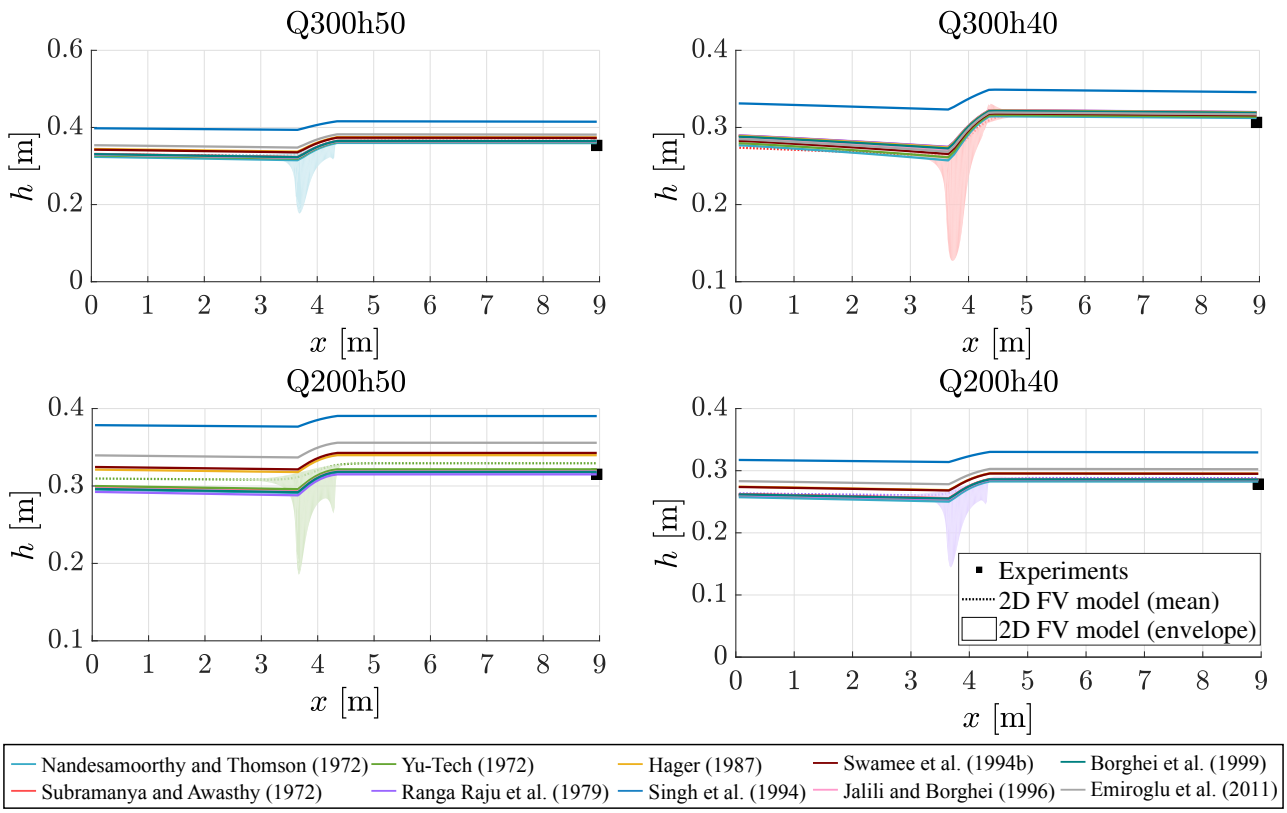

Figure 5.10: Water depth profiles along the channel axis (1D model) and water depth profiles from 2D FV model for Roger et al. (2009) tests.

Numerical models and formulations comparisons

As previously mentioned, a comparison of the formulations as well as the numerical models was carried out based on the indicators presented in section 3.3.1.

The breach discharge analysis can be performed by using these indicators. FIGURE 5.11 allows comparing the formulations as well as the numerical models using the first two non-normalized indicators namely *RMSE* and *Bias*.

In this figure, bars represent *RMSE* and read on the left blue y-axis while the diamonds represent *Bias* and read on the right orange y-axis. The lighter color (light blue and yellow) corresponds to the lumped model while the darker color (dark blue and orange) corresponds to the spatially-distributed model. A first important analysis is that the lumped model gives better results than the spatially-distributed model for all formulations (except Nandesamoorthy and Thomson (1972) formula). Indeed, *RMSE* of the 0D model is always lower than the 1D model one. This means that the breach discharge computed by the lumped model is closer to the experimental results than the one computed with the other model. As already observed in the previous analyses, Singh et al. (1994) formulation is the worst formulation (for both models).

Regarding the *Bias* indicator, for the 1D model, it is always negative. This observation is in good agreement with the previous findings that the 1D model underestimated the breach discharge for all tests. For the 0D model, four formulations underestimated the breach discharge (Emiroglu et al., 2011; Hager, 1987; Singh et al., 1994; Swamee et al., 1994a). The remaining formulations overestimated the breach discharge.

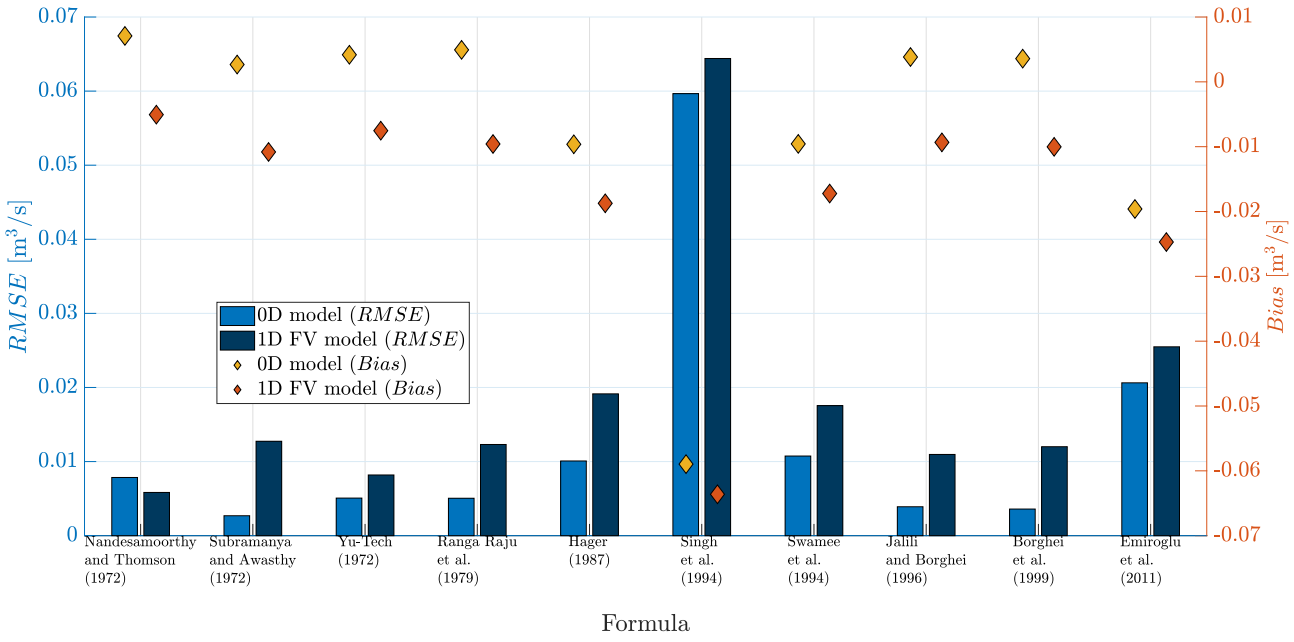

Figure 5.11: Breach discharge non-normalized indicators for Roger et al. (2009) tests.

FIGURE 5.12 illustrates the water depth comparison. It seems clear that the 0D model cannot provide an accurate solution for the water depth. For the most accurate formulations, the 1D model deviates by less than 1 cm from the ones found with the *WOLF* model (FIGURE 5.12). However, this is a comparison with the 2D model and not the experimental results. The analysis of water depths is consequently less relevant.

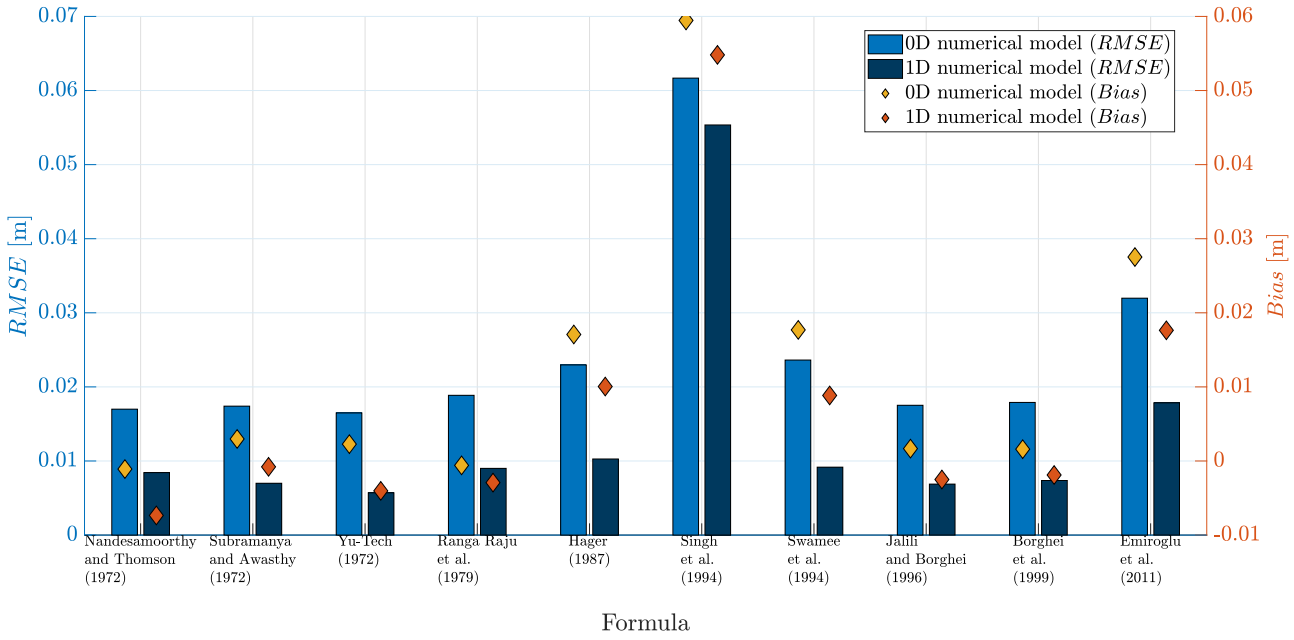

Figure 5.12: Water depth non-normalized indicators for Roger et al. (2009) tests.

Finally, a last figure (FIGURE 5.13) summarizes all the results obtained in terms of normalized indicators for lateral discharge and water depths, but also for the two implemented models and the discharge coefficient formulations.

In this figure, 5-pointed stars represent the $NRMSE$ indicator with the corresponding axes in blue and 6-pointed stars represent the $NBias$ indicator with the corresponding axes in orange. The darker colors represent the 1D model while the lighter colors represent the 0D model. The graph in the upper right-hand corner of the figure shows more precisely the distribution of $NRMSE$ for the most accurate formulations.

By analyzing the results of the $NRMSE$, two formulations are less accurate than the others (i.e. results further away from zero) whatever the numerical model used: formulations of Singh et al. (1994) and Emiroglu et al. (2011). These observations have already been established earlier through the analysis of lateral discharge and water depth for each numerical model. It will be necessary to see if the same tendency emerges from the numerical results of Michelazzo et al. (2015) and Mignot et al. (2020) tests in order to discard these formulations.

By doing the comparison of results according to the numerical models, it seems that the 0D model allows obtaining discharges closer to the observations than the 1D model as well as the 2D models (5-pointed star marker dotted lines). Apart from a few formulations, the spatially-distributed model is able to predict a more accurate breach discharge than the 2D models. For the water depths, the 1D model results come closer to the results obtained by *WOLF* than the 0D model results.

Regarding the $NBias$ indicator, this indicator is always better for the lumped model than for the 1D model (up and right shift for each formulation). For the $NBias\ Q_l$ indicator, the spatially-distributed model underestimates the breach discharge regardless of the formulation. The 0D model, for the best formulations, overestimates the breach discharge. These observations have already been discussed above. The 2D models are generally worse for this indicator (except for the worst formulations of both models). Concerning the $NBias\ h$ indicator, the results of the lumped model and the spatially-distributed model are close to zero for the best formulations.

For Roger et al. (2009) tests, a conclusion would be the use of the 0D model which is faster and more precise for the breach discharge. Once spatially varying information is required, a spatially-distributed model (1D or 2D model) must be chosen. It should be remembered that in simplified models many physical phenomena are not taken into account (or simplified). Therefore, cautiousness should be exercised during the analysis.

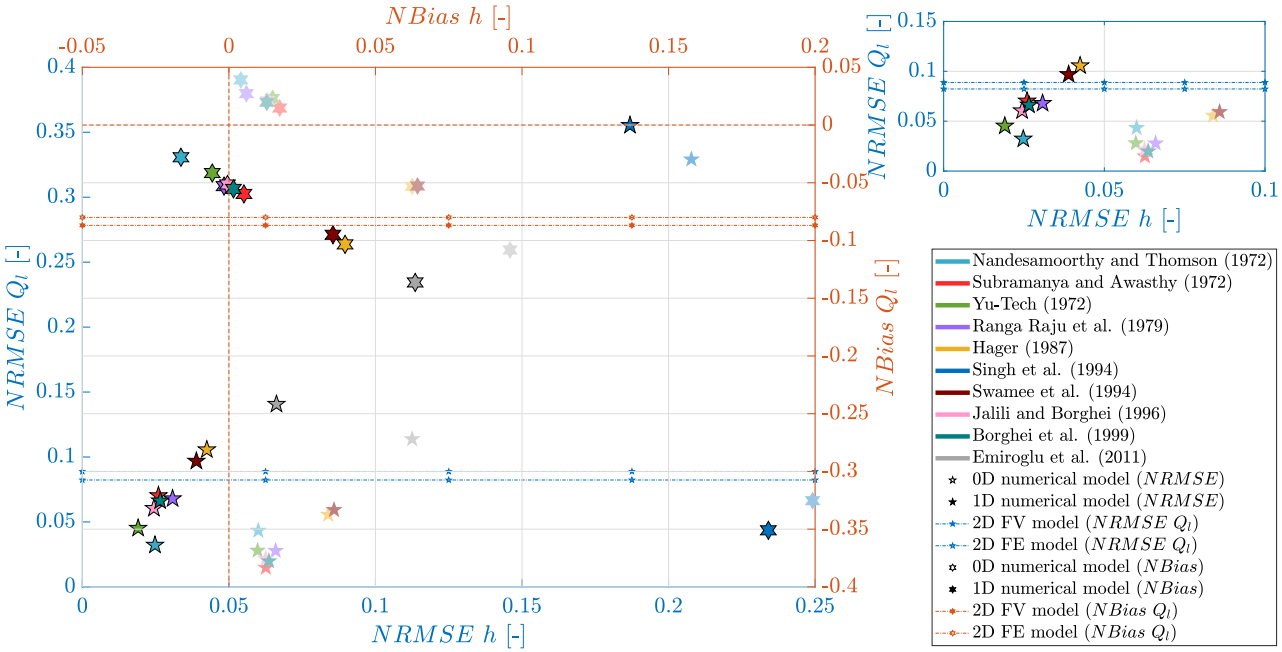

Figure 5.13: Water depth and breach discharge normalized indicators for all models, tests and formulations (Roger et al. (2009) tests).

5.1.2 Michelazzo et al. (2015)

The analyses carried out for Roger et al. (2009) tests were also conducted for Michelazzo et al. (2015) experiments. The difference between the two experiments is that Michelazzo et al. (2015) tests have different breach widths for each test, whereas Roger et al. (2009) tests have a fixed breach width for all tests. In contrast to Roger et al. (2009), all the Michelazzo et al. (2015) tests use the same hydraulic configurations (inlet discharge).

As shown earlier (section 3.1.2), there are several potential rating curves for the Michelazzo et al. (2015) tests. The models analysis takes into consideration 4 rating curves: the rating curve proposed by Michelazzo et al. (2015), the rating curve based on series A & B results, the rating curve based on series B results and the rating curve based on the sluice gate formula (with a discharge coefficient of 2/3).

In the following presentation of the results, the rating curve used is the one reconstructed from the experimental data of series A and B (series A & B regression). This choice is motivated because the rating curves give approximately the same results (Appendix A.1). In an analysis conducted by Rifai et al. (2017), the authors used the rating curve reconstructed by regression. This motivates this choice even more. After discussion with Michelazzo, the latter pointed out that some errors may have been made in establishing the rating curve (Michelazzo rating curve). Therefore, the use of a rating curve reconstructed from the experimental data appeared to be the best solution.

Lumped model

The breach discharges obtained for each test using the various formulations[2] are shown in Figure 5.14. In order to better compare the obtained breach discharges, Figure 5.15 shows the difference between the numerical breach discharges and the experimental breach discharges.

In general, the breach discharges obtained are close to the experimental results up to test B11. For tests B12 to B16, they are increasingly different from the experimental results. By analyzing Figure 5.15, it appears that the difference in results between the 0D model and the experiments is less than 10% in most cases, with the exception of Singh et al. (1994) formulation, which for tests from B7 to B11 shows a larger difference. As a reminder, this formulation was not suitable for Roger et al. (2009) tests. Nevertheless, Singh et al. (1994) formulation appears to be effective for tests from B12 to B16. The most effective formulations for Roger et al. (2009) experiments give good results for the first tests. Once the breach opening becomes significant (i.e. the hydraulic conditions tend towards supercritical configurations), these formulations are less effective.

Based on these observations, it seems difficult to conclude which formulations over- or underestimate the breach discharge in this case because it depends on the test as well as the empirical formula considered. Nevertheless, Singh et al. (1994) expression always underestimates the breach discharge. The so-called accurate formulations tend to overestimate the breach discharge.

The numerical water depths range between the maximum and minimum Michelazzo et al. (2015) experimental ones for most formulae (Figure 5.16). Figure 5.17 shows a general trend: the formulations tend to underestimate the water depth except for the Singh et al. (1994) formulation.

[2]For tests B13 to B16, the results obtained with Emiroglu et al. (2011) formula diverge completely. These have therefore not been represented.

Overall, the larger the breach width, the further the water depths calculated with the 0D model are from the experimental mean. Indeed, for the tests from B7 to B10, the results remain below the 10% difference with the experimental results. Beyond test B10, the numerical depths are far from the experimental depths (i.e. the difference increases). The 15% difference is reached for some of the formulations giving good results for Roger et al. (2009) experiments. A general trend can be observed from the obtained results: the more the breach discharge is overestimated, the more the water depth is underestimated.

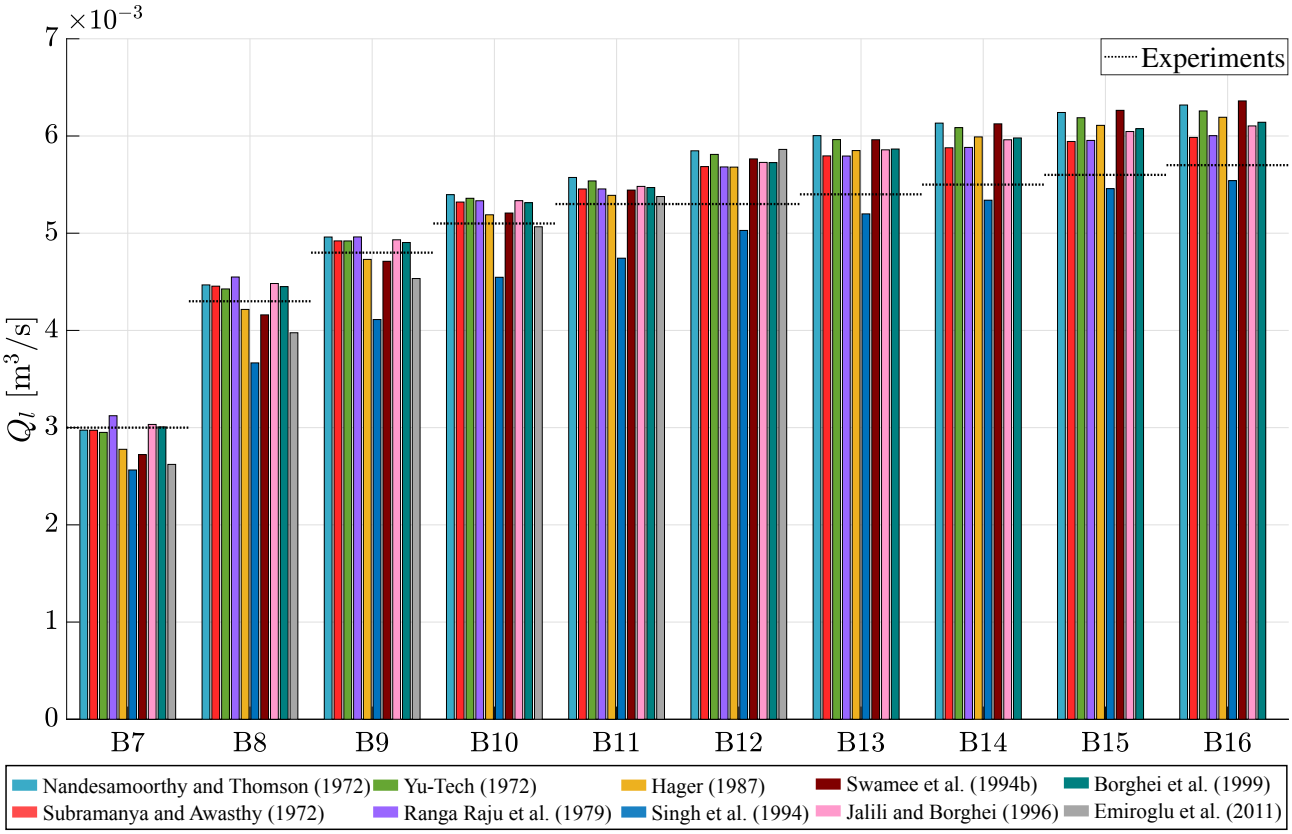

Figure 5.14: Breach discharges (0D model) for Michelazzo et al. (2015) tests.

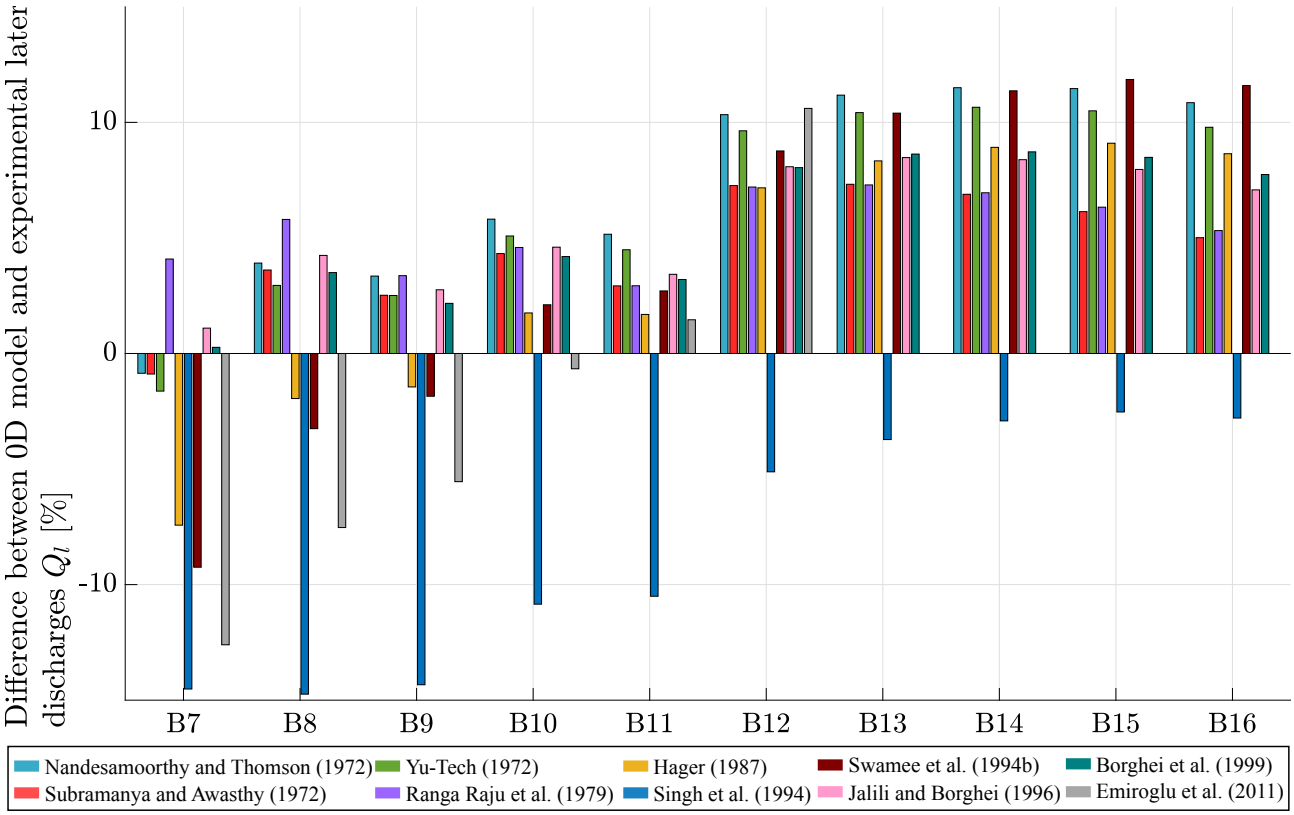

Figure 5.15: Breach discharges difference (0D model) for Michelazzo et al. (2015) tests.

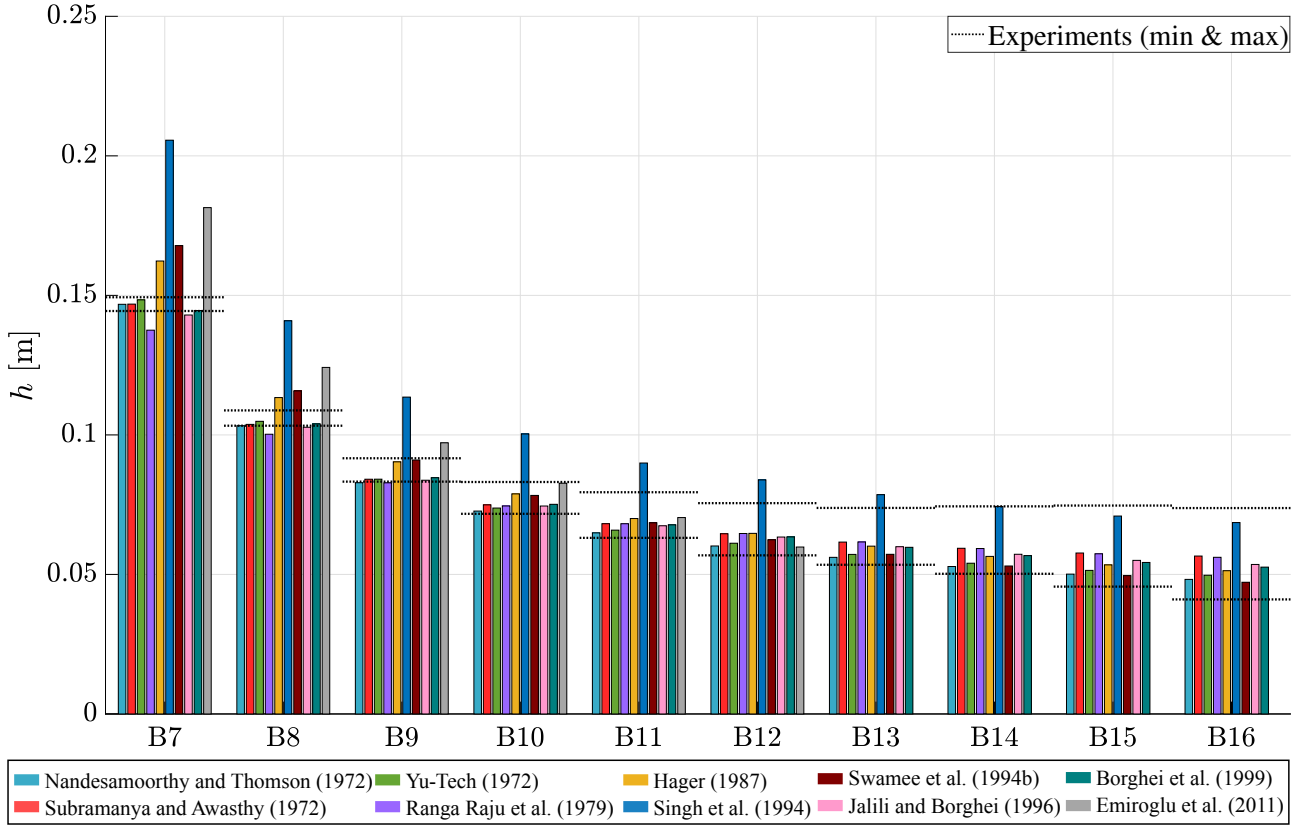

Figure 5.16: Water depths (0D model) for Michelazzo et al. (2015) tests.

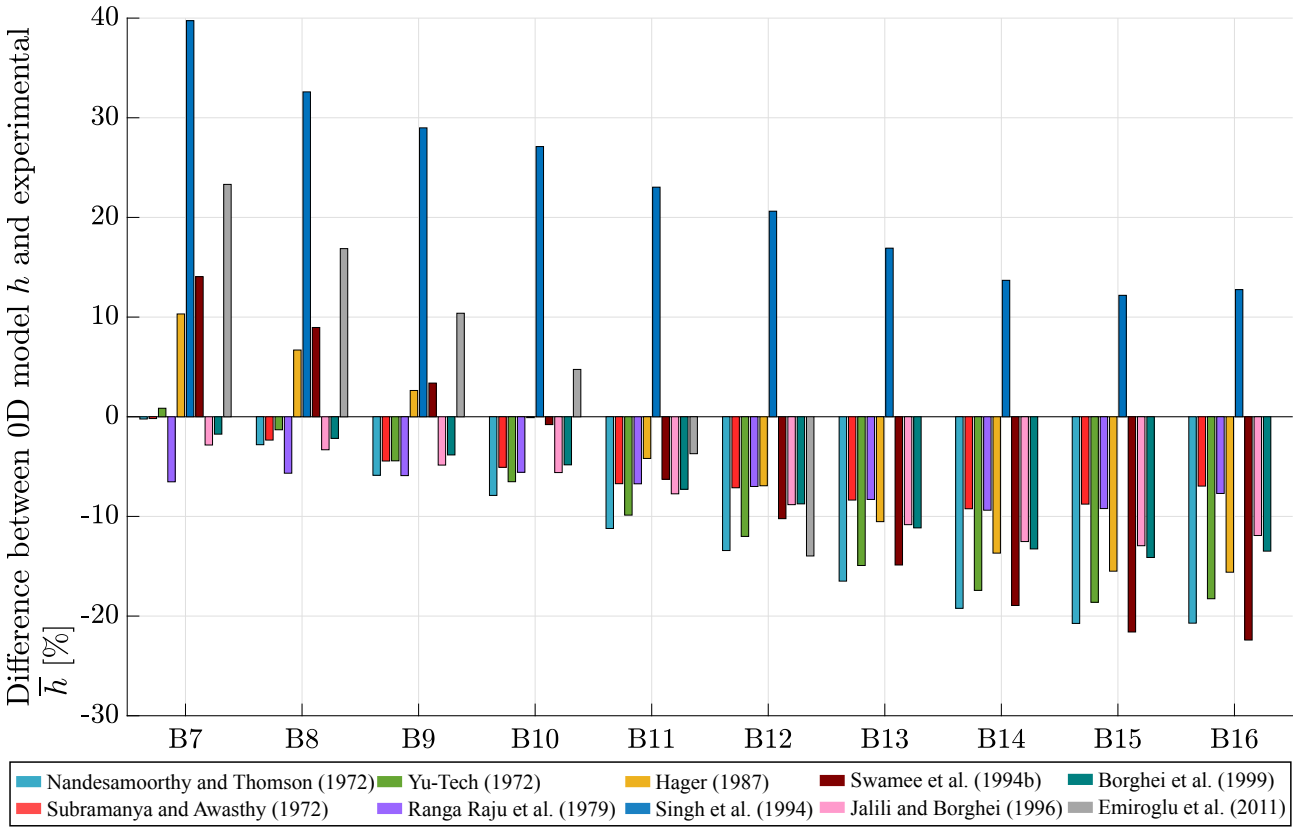

Figure 5.17: Difference water depth (0D model) for Michelazzo et al. (2015) tests.

Spatially-distributed model

The breach discharge obtained with this model is close to the experimental breach discharge (FIGURE 5.18). For the effective formulations, the difference between results is less than 5% (FIGURE 5.19). As with the lumped model, the results obtained with the Singh et al. (1994) formula are better when the breach opening is larger. The difference is almost divided by three between tests B7 and B16. Emiroglu et al. (2011) formulation gives particular results. This expression is better for the B10 and B11 tests than for the other tests. For configurations with larger breaches, this formula becomes the least effective with more than 15% difference for test B16.

The profiles of the different hydraulic variables are given in the following figures. The x-axis is as used in the Michelazzo experiments. As a reminder, x^* is defined as the distance from the breach discharge divided by the channel width.

The water depth profiles (FIGURE 5.20) have the same shape as the experimental profiles at least until test B12. For test B13 to test B16, the numerical water profiles are more influenced by the breach than the experimental profiles. These profiles tend to deepen further upstream and then rise sharply. This is reminiscent of the hydraulic jump phenomenon. The Froude number profiles (FIGURE 5.21) for these tests show a change in flow regime at the breach area. The flow suddenly changes from a subcritical to a supercritical flow regime. Once the breach zone is exceeded, the flow suddenly becomes subcritical again. Thus the flow is affected by a rapid change in the flow regime at the breach zone.

The discharge profiles are shown in FIGURE 5.22, which complete the analysis of the results from the 1D model. A decrease in discharge into the channel is well observed along the breach. The shorter the breach, the faster the decrease in discharge.

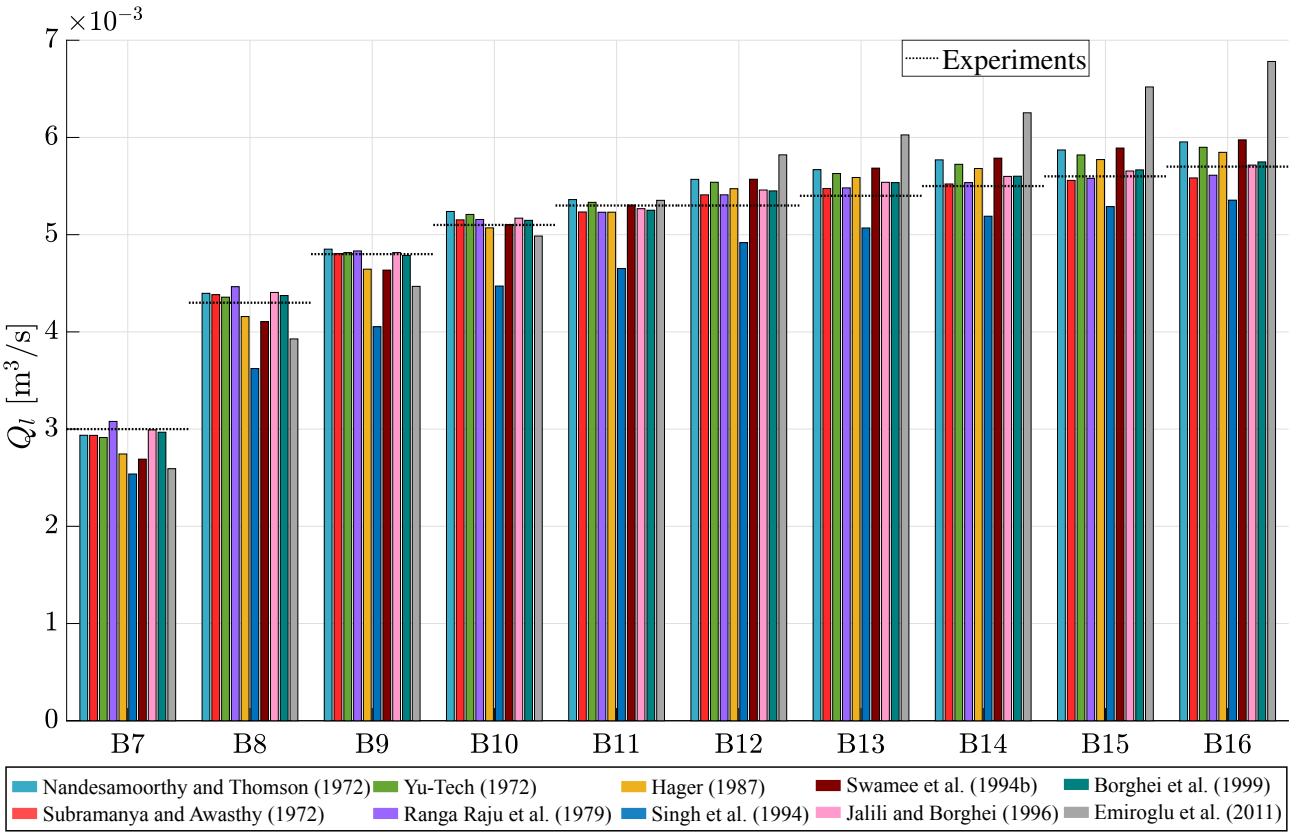

Figure 5.18: Breach discharges (1D model) for Michelazzo et al. (2015) tests.

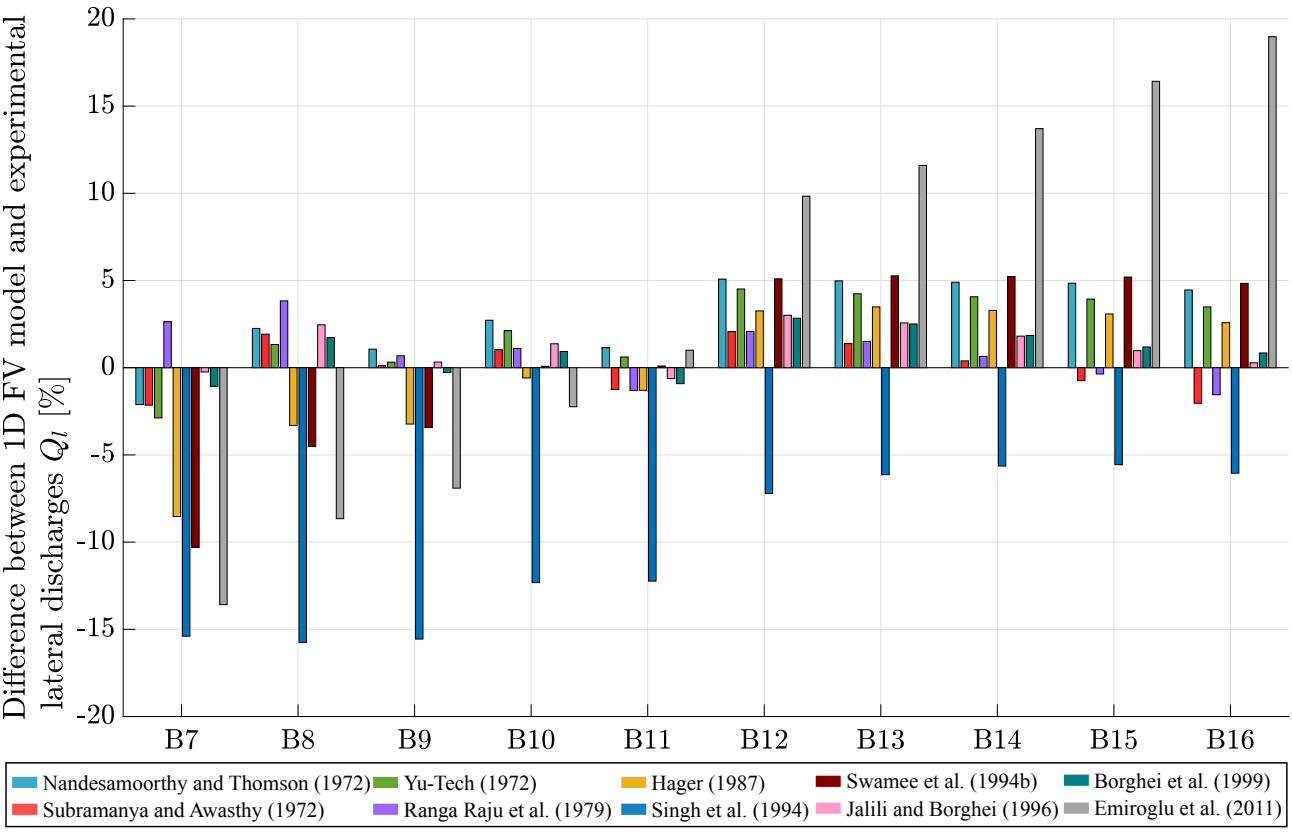

Figure 5.19: Breach discharges difference (1D model) for Michelazzo et al. (2015) tests.

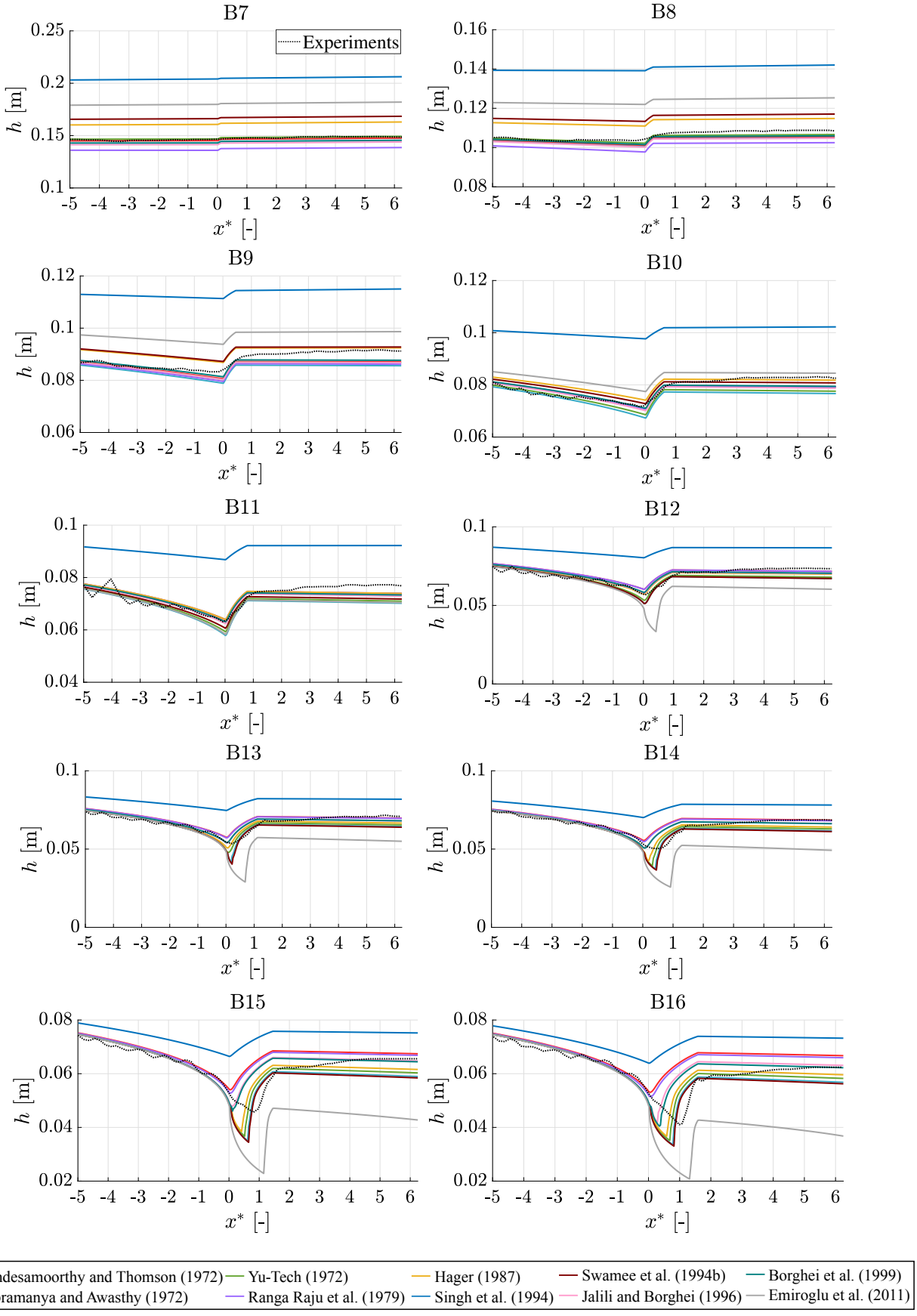

Figure 5.20: Water depth profiles for all tests using the series A & B rating curve for Michelazzo et al. (2015) tests.

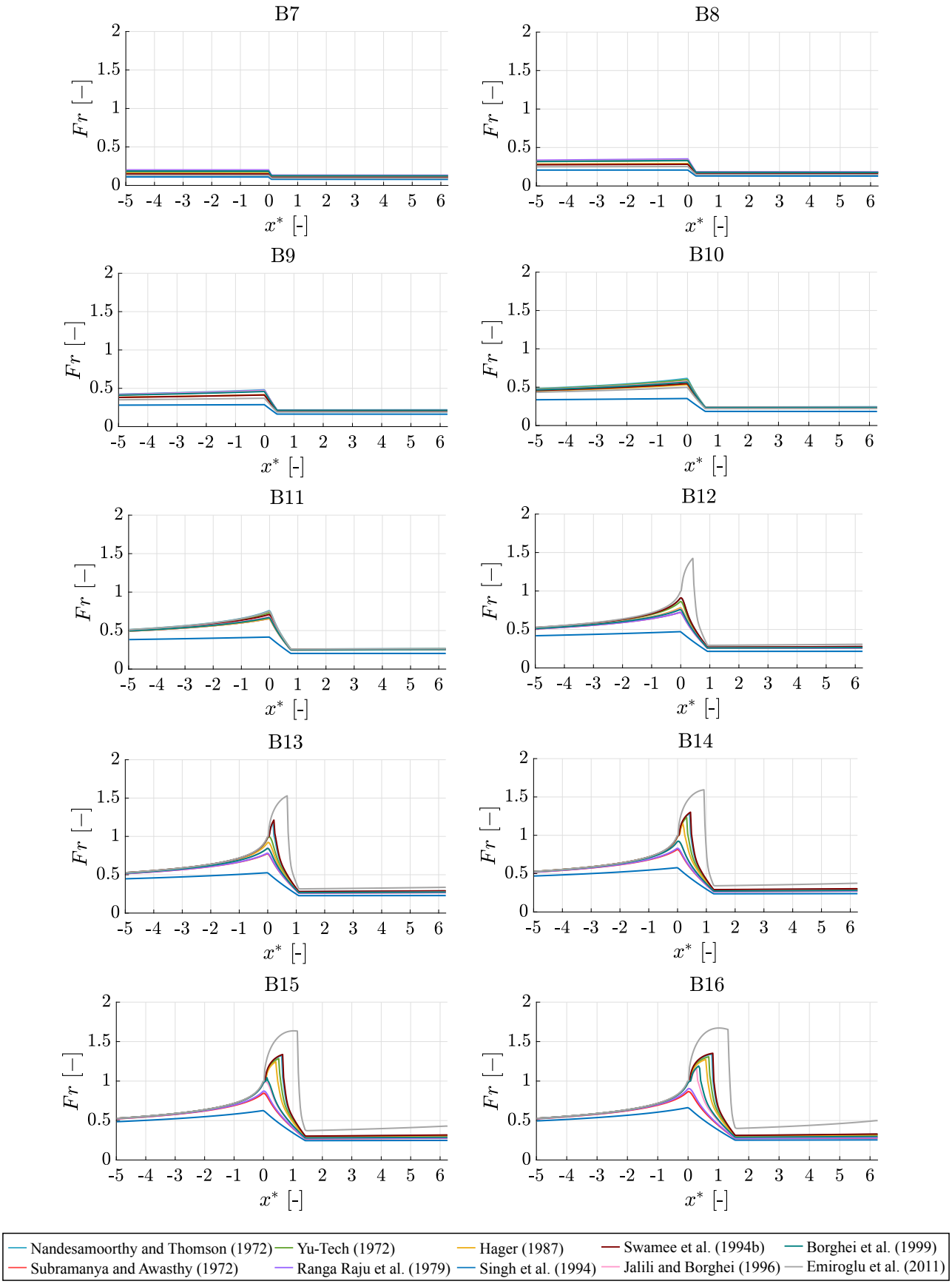

Figure 5.21: Froude profiles for all tests using the series A & B rating curve for Michelazzo et al. (2015) tests.

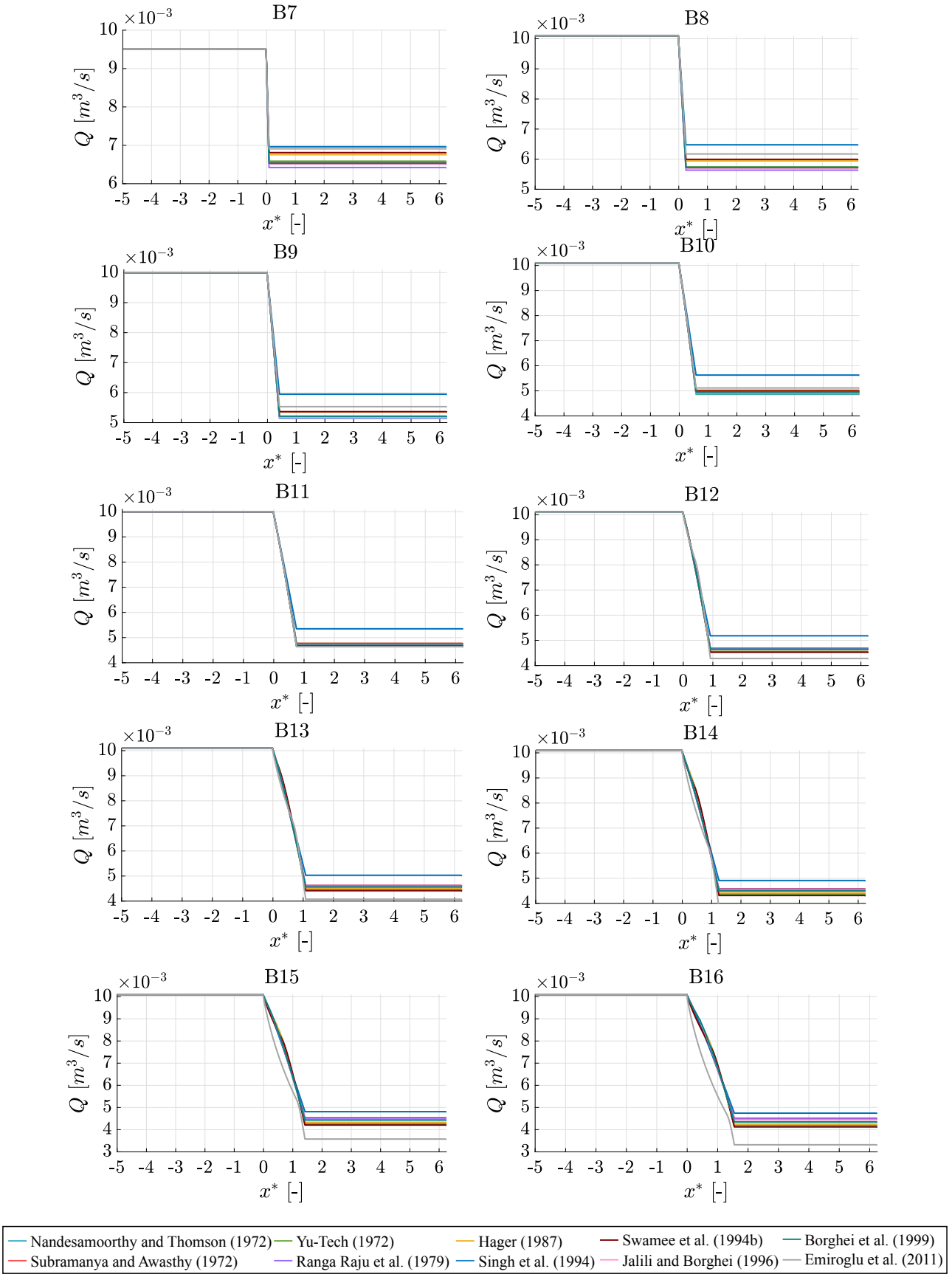

Figure 5.22: Discharge profiles for all tests using the series A & B rating curve for Michelazzo et al. (2015) tests.

Numerical models and formulations comparisons

Having highlighted the different obtained results, it is also essential to synthesize them. To do this, the non-normalized indicators allow determining the efficiency of the formulations as well as the numerical models implemented. FIGURES 5.23 and 5.24 illustrate the indicators $RMSE$ and $Bias$ respectively for the breach discharge and the water depth.

The 1D model gives results closer to the experimental results than the 0D model (for both hydraulic variables). The formulations that work best for Roger et al. (2009) tests are also those that give the best results for Michelazzo et al. (2015) experiments. The bias is globally positive for the breach discharge. This means that the latter is overestimated by the numerical models for almost all formulations (except Singh et al. (1994) formulation). The bias analysis for the water depth is more difficult to generalize. Depending on the formulation and the numerical model used, the bias can be positive or negative. For the majority of the formulations, the bias is less than 1 cm, which is rather acceptable.

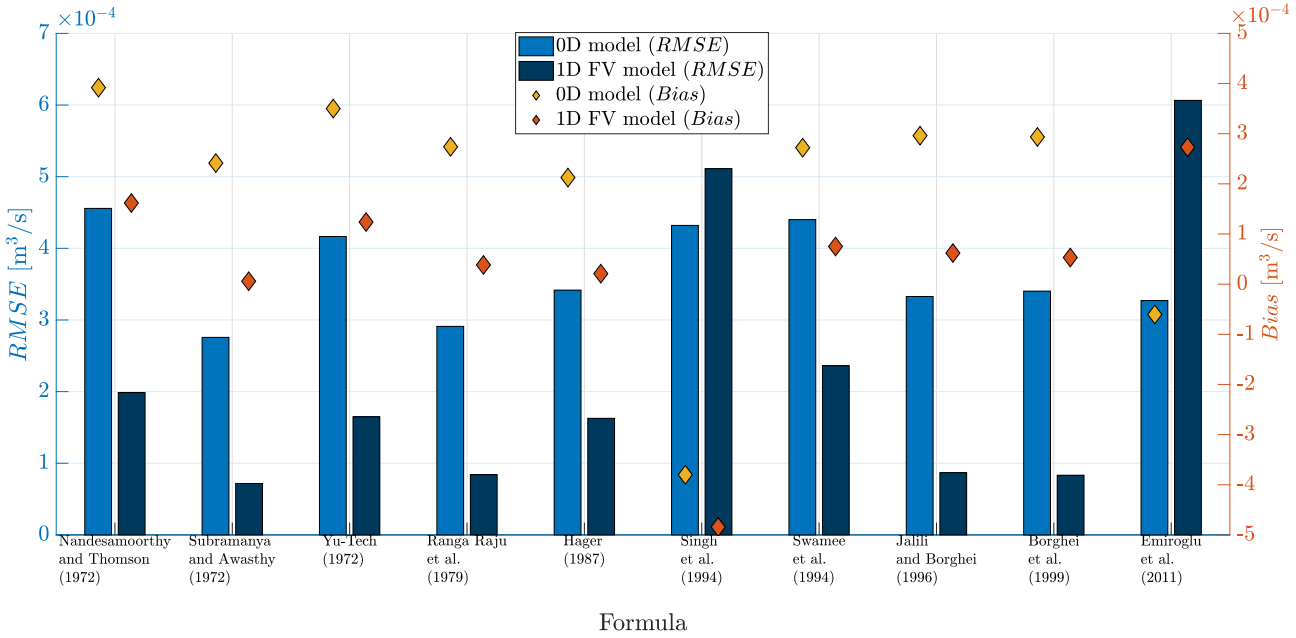

Figure 5.23: Breach discharge non-normalized indicators for Michelazzo et al. (2015) tests.

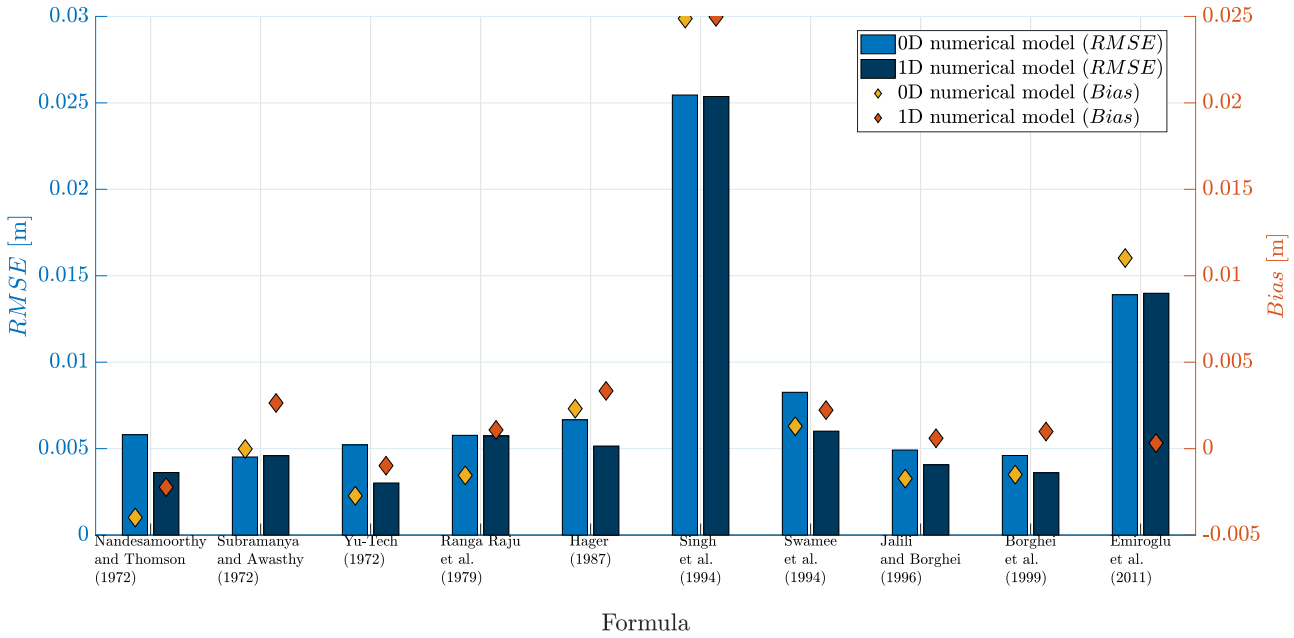

Figure 5.24: Water depth non-normalized indicators for Michelazzo et al. (2015) tests.

The following figure shows the results in terms of normalized indicators (FIGURE 5.25). This diagram enables an easier comparison between the formulations and models.

As already mentioned, for the most efficient formulations, the spatially-distributed model predicts the breach discharge more accurately than the lumped model. For this hydraulic variable, the $NRMSE\,Q_l$ as well as $Nbias\,Q_l$ are closer to zero. Note that both models overestimate the breach discharge (i.e. $Nbias\,Q_l > 0$).

The same analysis is applicable to the water depth. The water depth predicted by the 1D model is closer to the experiments than that predicted by the 0D model ($NRMSE\,h$ closer to zero). The analysis of the normalized bias is less direct than that for the breach discharge. One part of the results gives a positive $Nbias\,h$ while for the other part this indicator is negative. Nevertheless, the results are scattered around the zero bias (i.e. $Nbias\,h = 0$).

A graphical analysis of the $NRMSE$ indicator for both models shows that the indicator for the spatially-distributed model is always lower and shifted to the left compared to the $NRMSE$ of the lumped model, regardless of the formulation. This observation illustrates that the 1D model has a better $NRMSE\,Q_l$ and $NRMSE\,h$ than the other model. Indeed, these two indicators tend to be closer to zero for this model.

Analyzing the bias for both models, it appears that the bias of the spatially-distributed model is always lower and shifted to the right compared to the bias of the lumped model regardless of the formulation. This observation illustrates the fact this model has a lower bias on the breach discharge than the other one. However, for the bias on the water depth, no generalization can be made. Comparing the two models (0D to 1D), for some formulations the $Nbias\,h$ indicator decreases (e.g. Nandesamoorthy and Thomson, 1972) while for others it increases (e.g. Subramanya and Awasthy, 1972).

It should be noted that in the analyses mentioned above, the worst formulations (Emiroglu et al., 2011; Singh et al., 1994) were not taken into account given the poor results obtained with these formulations.

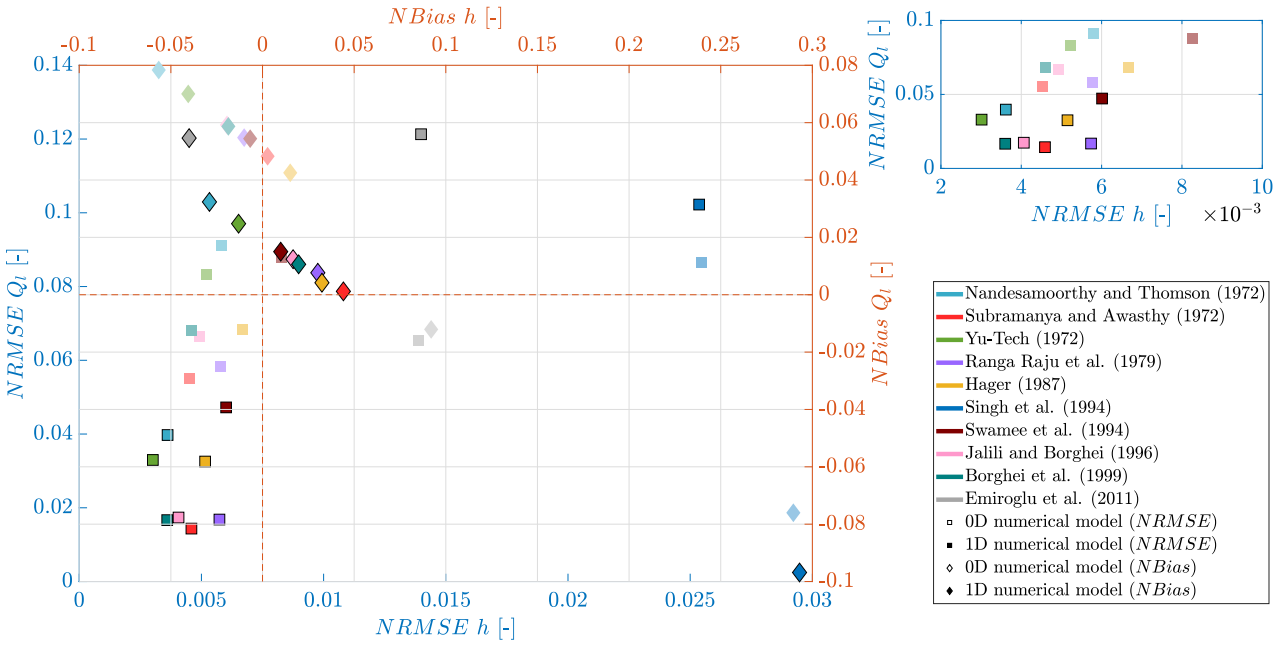

Figure 5.25: Water depth and breach discharge normalized indicators for the all tests, models and formulations (Michelazzo et al. (2015) tests).

5.1.3 Mignot et al. (2020)

The last tests analyzed for flows with fixed breach with zero lateral crest height are the experiments conducted by Mignot et al. (2020). The breach width and hydraulic configurations used in these experiments are different from those used in Roger et al. (2009) and Michelazzo et al. (2015) tests. A third type of test is used to confirm or not the analyses established earlier.

Lumped model

The results for the breach discharge are shown in FIGURES 5.26 and 5.27. FIGURE 5.26 shows that the majority of the formulations gives numerical results close to the experimental results. Indeed, in FIGURE 5.27, it can be seen that the differences between numerical models and experimental results are less than 10% for the formulations identified as effective during the analysis of Roger et al. (2009) test results. The non-accurate formulations remain non-accurate.

The Op2F3 test has numerical results that are furthest from the experimental results. Compared to the Op2F1 test, the injected discharge is almost 3 times higher for the Op2F3 test for similar water depths (0.025 m). The flow regime of the Op2F3 test is characterized by a higher Froude number. Compared to the Op2F4 test, the injected discharge of the Op2F3 test is 6 times lower for the same Froude number upstream of the breach. The water depth is about 0.1 m for the Op2F4 test, which is much higher than the water depth of the Op2F3 test. The high flow regime combined with the low water depth measurements could explain why the numerical results are further away from the experimental results. Nevertheless, the most accurate formulations do not exceed a 10% difference between the numerical and experimental results, which is still quite acceptable. Depending on the test and the formulation, the breach discharge is underestimated or overestimated. Only the least effective formulations (Emiroglu et al., 2011; Singh et al., 1994) and also, Hager (1987) and Swamee et al. (1994b) formulations, always underestimate the breach discharge.

Regarding the water depths, the results are equally convincing (FIGURES 5.28 and 5.29). All formulations give water depths very close to the experimental mean water depth (FIGURE 5.28). Indeed, the differences between the numerical and experimental results are less than 10% for all tests (FIGURE 5.29). The difference even falls under 3% for effective formulations. This figure also illustrates the fact that the water depth obtained overestimates the mean water depth for most of the formulations (except for Ranga Raju et al. (1979) formula). Singh et al. (1994) and Emiroglu et al. (2011) remain the two less effective expressions.

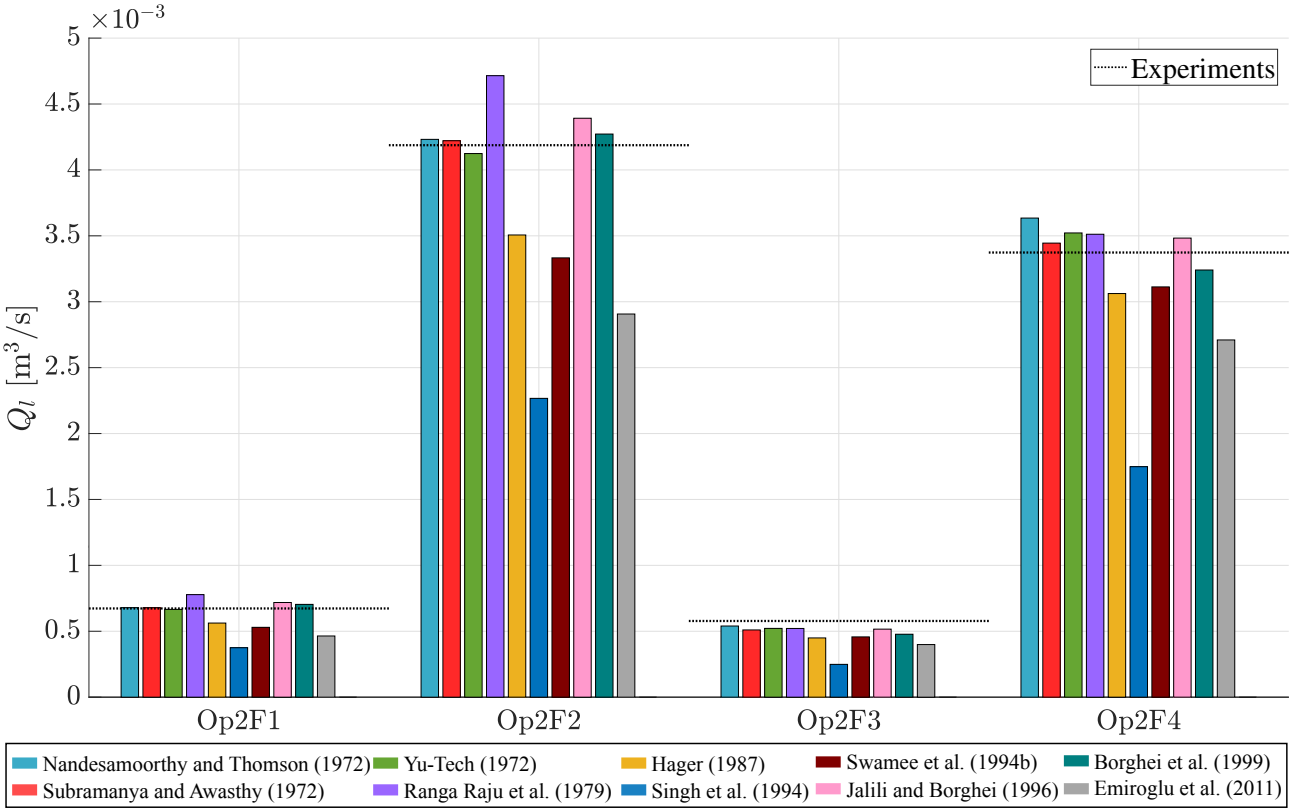

Figure 5.26: Breach discharge results (0D model) for Mignot et al. (2020) Op2 tests.

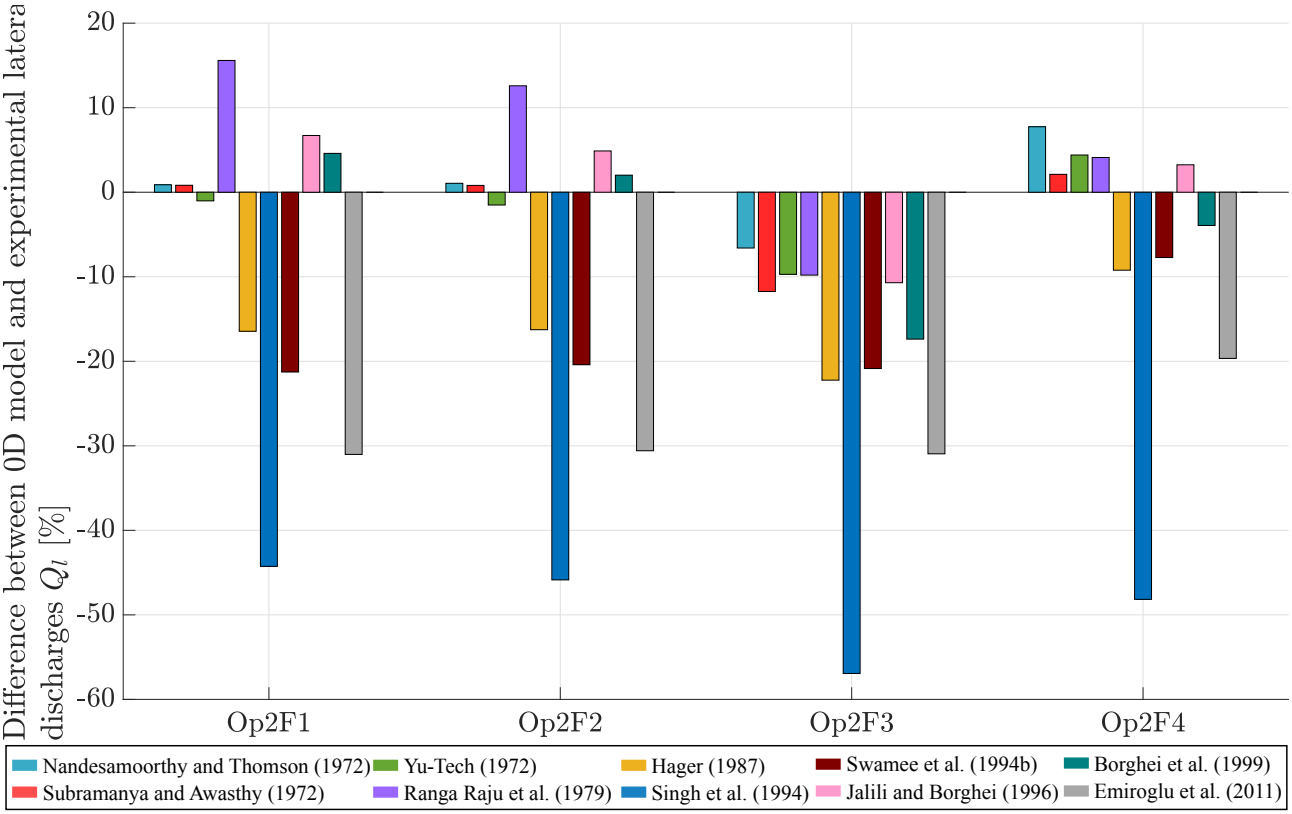

Figure 5.27: Breach discharge difference between numerical (0D model) and measurement for Mignot et al. (2020) Op2 tests.

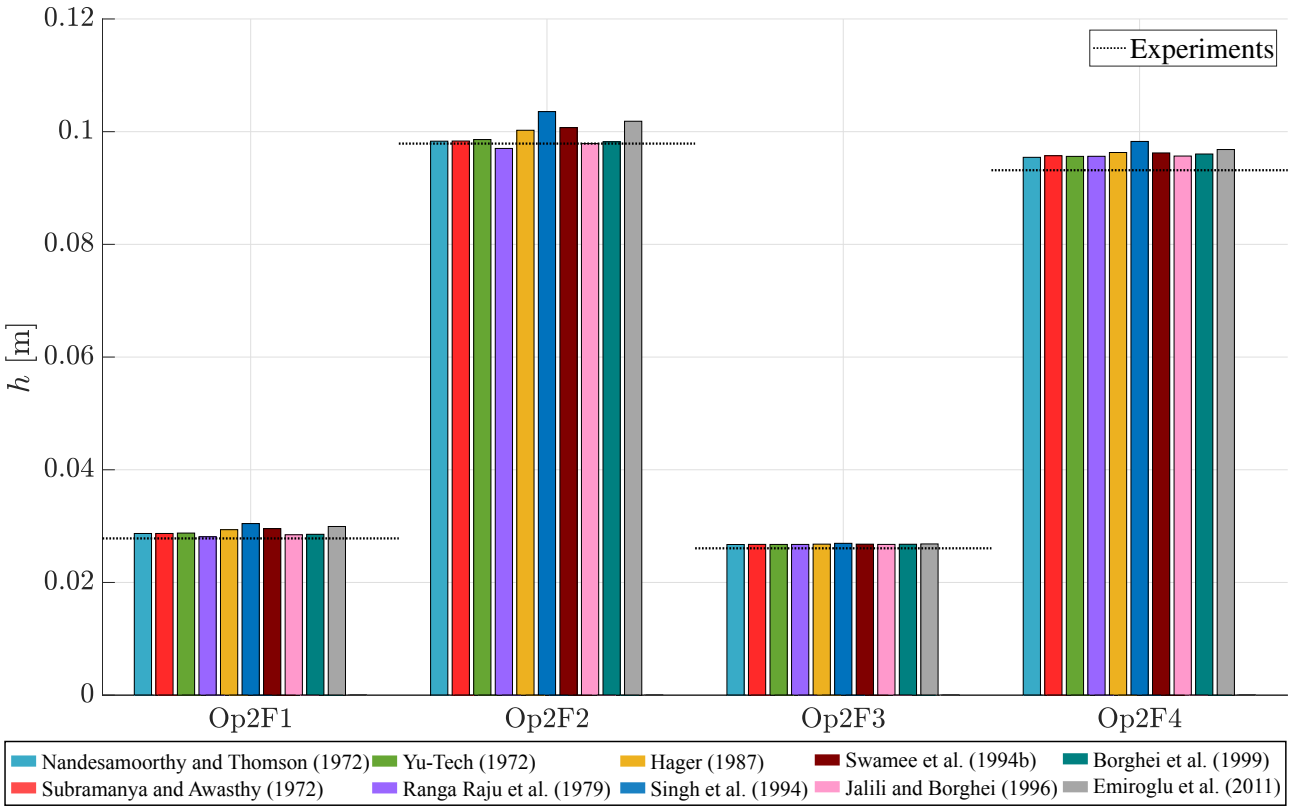

Figure 5.28: Water depth results (0D model) for Mignot et al. (2020) Op2 tests.

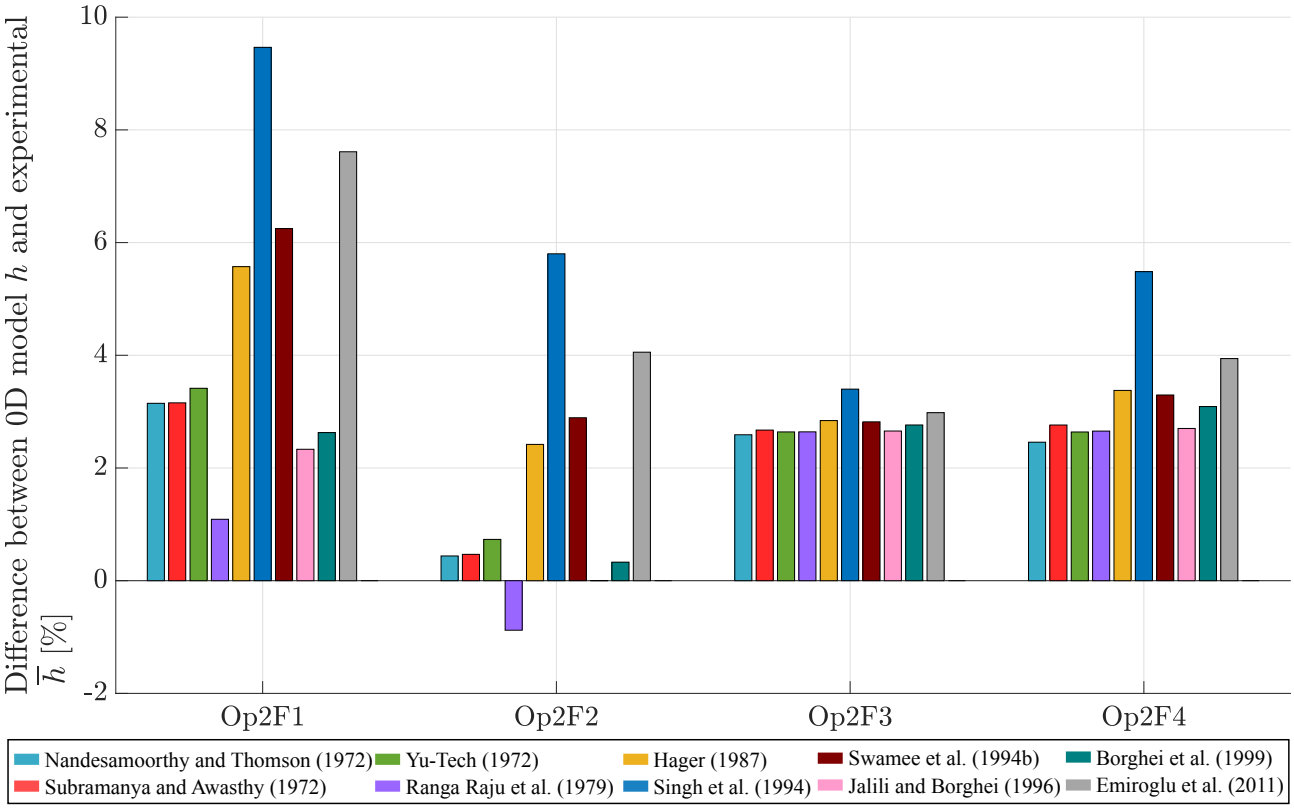

Figure 5.29: Water depth difference between numerical (0D model) and measurement for Mignot et al. (2020) Op2 tests.

Spatially-distributed model

The breaching discharges obtained with the 1D model mostly underestimate the experimental breaching discharges (FIGURE 5.30). The results from the most accurate formulations show differences of less than 10% except for the Op2F3 test, which shows less convincing results (FIGURE 5.31). The reasons for these differences have already been discussed in the analysis of the lumped model.

A comparison between the results obtained with the two numerical models shows that the breach discharges computed with the lumped model (FIGURE 5.27) are globally closer to the experimental results than those obtained with the spatially-distributed model (FIGURE 5.31), which leads to a lower difference between the results.

Nevertheless, the 1D model offers a spatial discretization of the variables h, Q and Fr, which is not the case with the 0D model. Thus, it is interesting to illustrate these results.

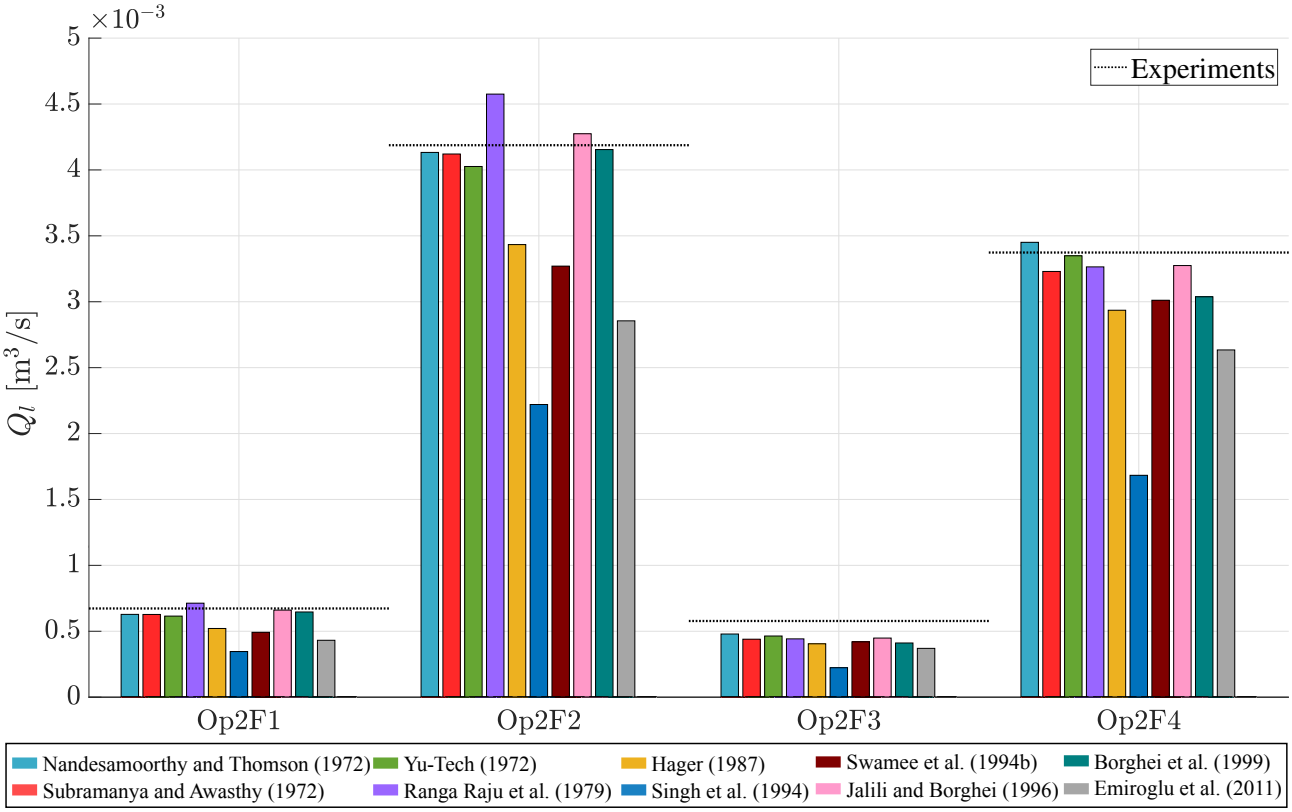

Figure 5.30: Breach discharge results (1D model) for Mignot et al. (2020) Op2 tests.

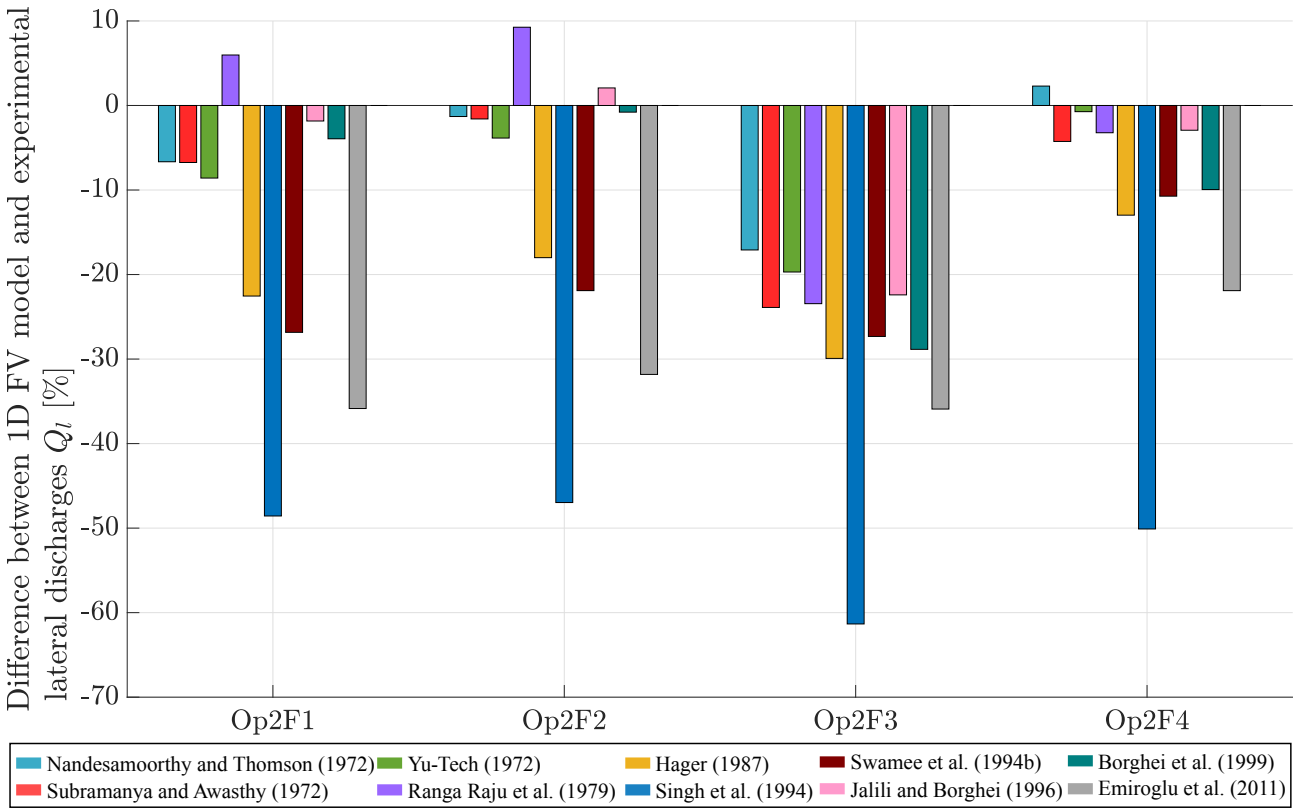

Figure 5.31: Breach discharge difference between numerical (1D model) and measurement for Mignot et al. (2020) Op2 tests.

The water depths obtained for the various tests are shown in FIGURE 5.32. For sake of clarity, the experimental water depths have also been plotted in this figure. Except for the Op2F3 test, the numerical water depths fit the experimental water depths quite well (depending on the formulation considered). Uncertainties in water depth measurements (error bars in FIGURE 5.32) could also explain why they are so far from the numerical results (the other explanations stated remain valid).

The discharge profiles are illustrated in FIGURE 5.33. This figure does not provide any new information as the injected and breach discharges are known. In fact, the upstream discharge corresponds to the experimentally injected discharge. As mentioned in the analysis of the previous tests, the downstream discharge is determined by calculating the difference between the upstream and breach discharges taking into account the variation of the free surface. This figure only illustrates that the numerical results respect the continuity principle.

For the sake of completeness, all that is missing is the spatial evolution of the Froude number (FIGURE 5.34). Tests Op2F3 and Op2F4 are the tests with a higher flow regime, which results in a higher Froude number than tests Op2F1 and Op2F2. For each test, the water depth increases from upstream to downstream. An increase in water depth results in a decrease in Froude number (for the same discharge). This analysis can be seen in FIGURE 5.34. The Froude number profiles decrease from upstream to downstream.

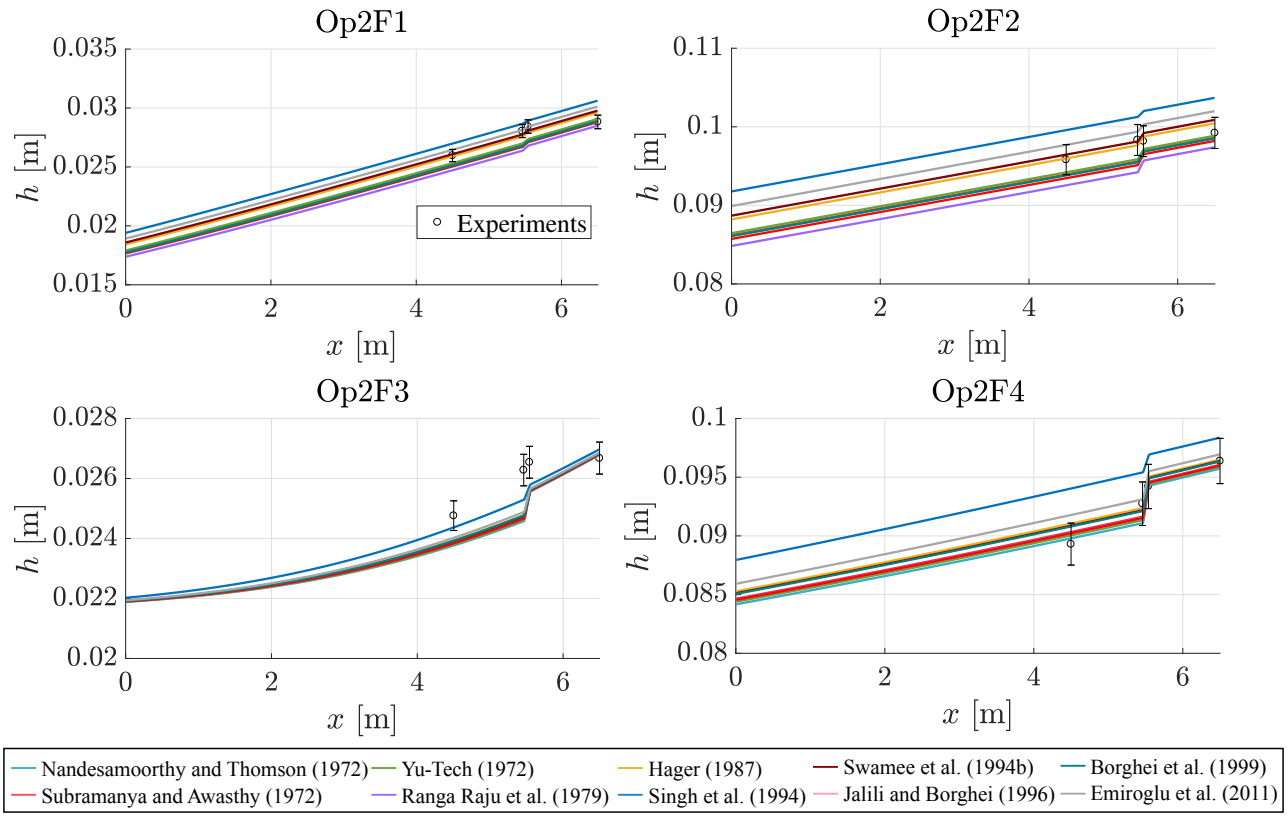

Figure 5.32: Water depth profiles (1D model) for Mignot et al. (2020) Op2 tests.

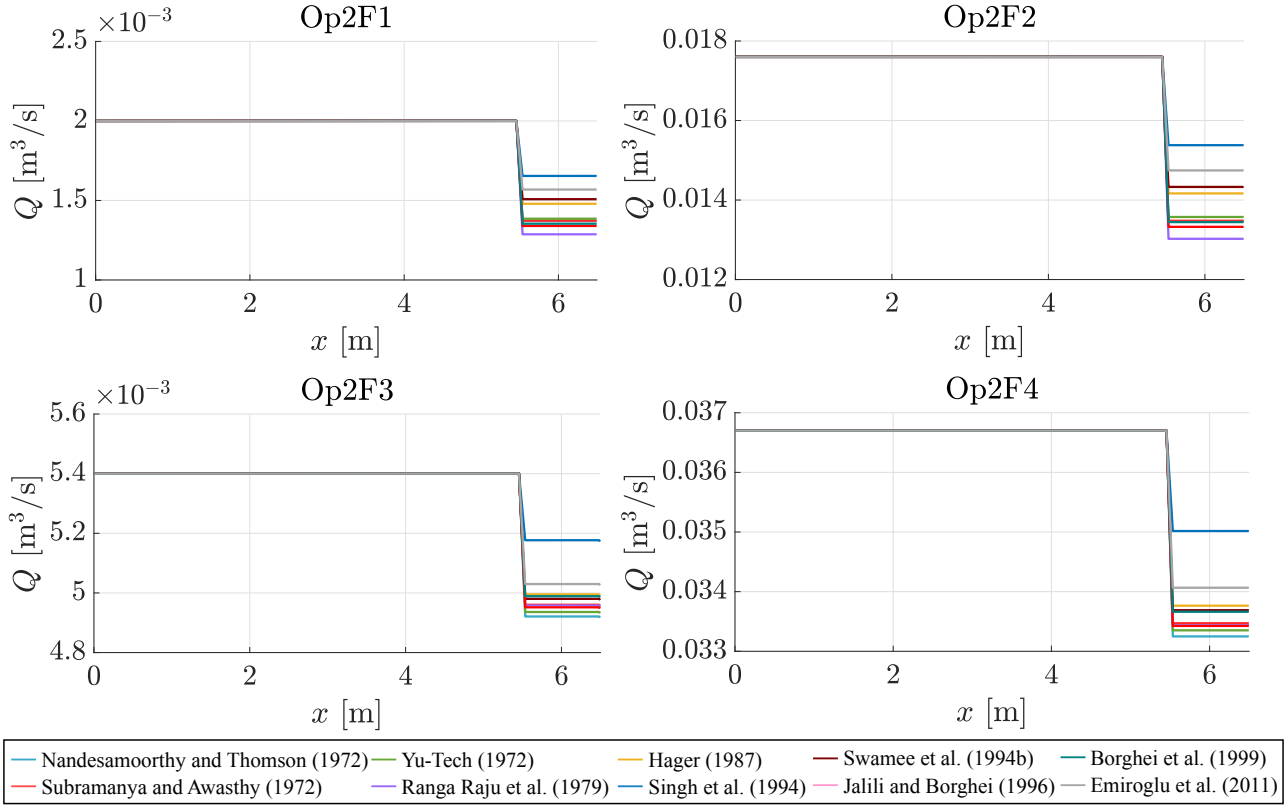

Figure 5.33: Discharge profiles (1D model) for Mignot et al. (2020) Op2 tests.

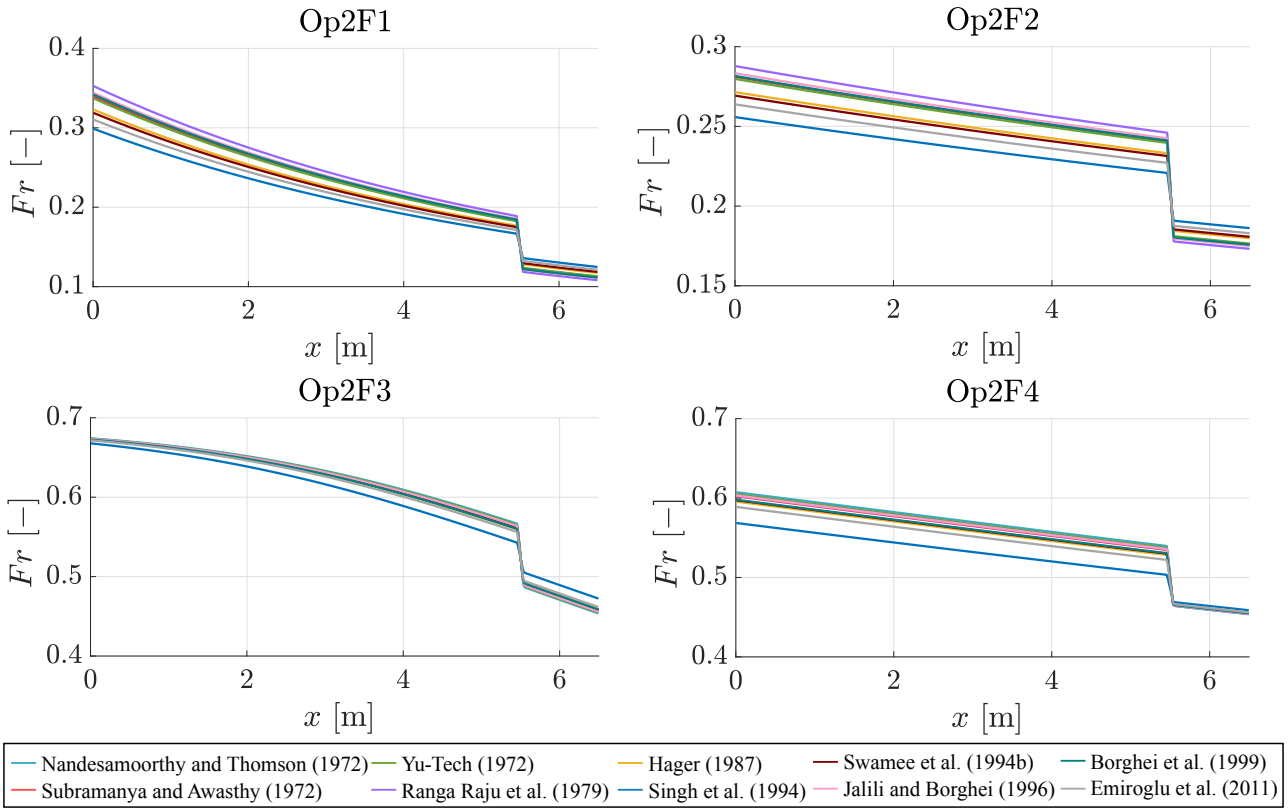

Figure 5.34: Froude profiles (1D model) for Mignot et al. (2020) Op2 tests.

Numerical models and formulations comparisons

The breach discharge indicators analysis reveals several important elements (FIGURE 5.35). Most of the formulations appear to be more effective (except Singh et al. (1994) and Emiroglu et al. (2011) formulae). For these formulae, the bias is close to zero which indicates that the numerical results are close to the experimental results.

The bias is positive for most of these formulations with the 0D model while it is negative with the 1D model. This clearly indicates the tendency of the lumped model to overestimate the breach discharge (only for the most accurate empirical expressions). In contrast, the spatially-distributed model tends to underestimate the breach discharge even for the least effective formulae.

Other indicator ($RMSE$), which are called error indicator, are not able to express whether the models and/or formulae tend to overestimate or underestimate the breach discharge, since these indicators are signless (always positive). This indicator measures the accuracy of the numerical results in relation to the experimental results. The 6 formulations identified with bias indicators are those with the best error indicator ($RMSE$ close to 0). Depending on the formulation used, one model gives better results than another.

The analysis of the water depth indicators is quite similar to that carried out for the breach discharge indicators (FIGURE 5.36). However, it should be noted that the number of points taken to calculate the differences between numerical and experimental results is limited: there are 4 of them as can be seen in FIGURE 5.32. The analyses carried out must be taken with caution.

The formulations identified as effective for the prediction of the breach discharge also turned out to be the ones that provide the best results for the water depth (for both numerical models)[3]. The 0D model always overestimates the water depth (see *Bias* indicator). The water depth is underestimated in the case of the 1D model for most of the formulae. However, the bias for the 1D model is of the order of a mm, which is not considerable.

In contrast to the conclusions drawn on the breach discharge, the water depth error indicator clearly shows that the 0D model is less effective than the 1D model (FIGURES 5.36).

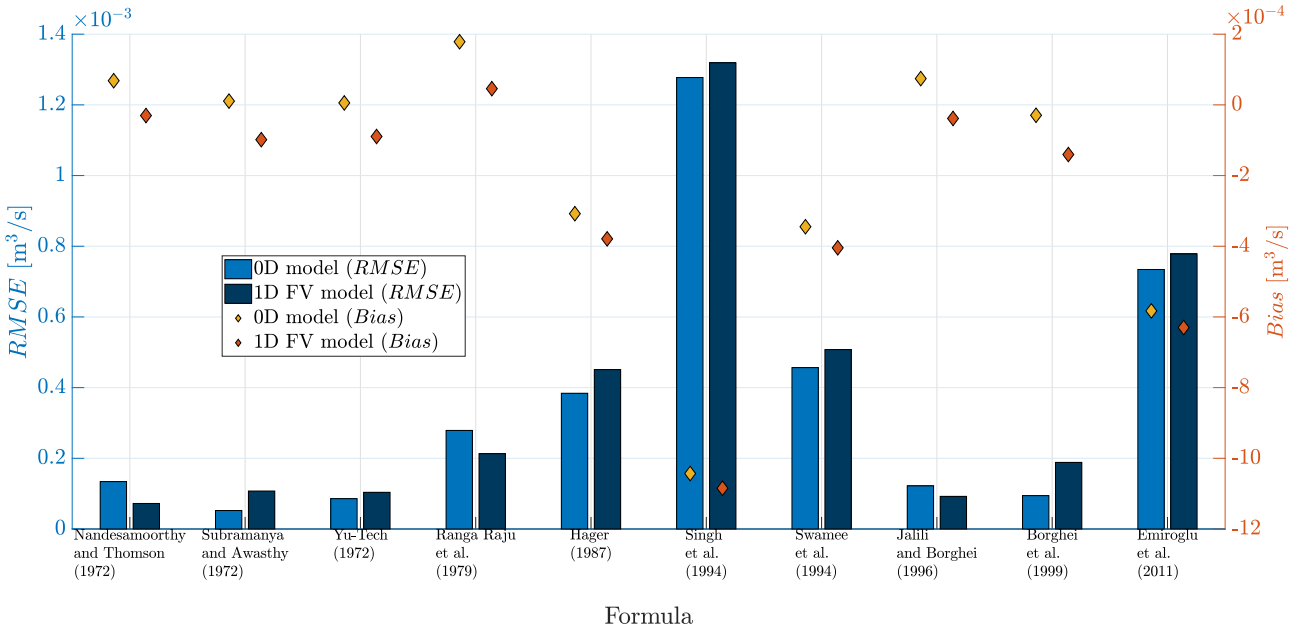

Figure 5.35: Breach discharge non-normalized indicators for Mignot et al. (2020) Op2 tests.

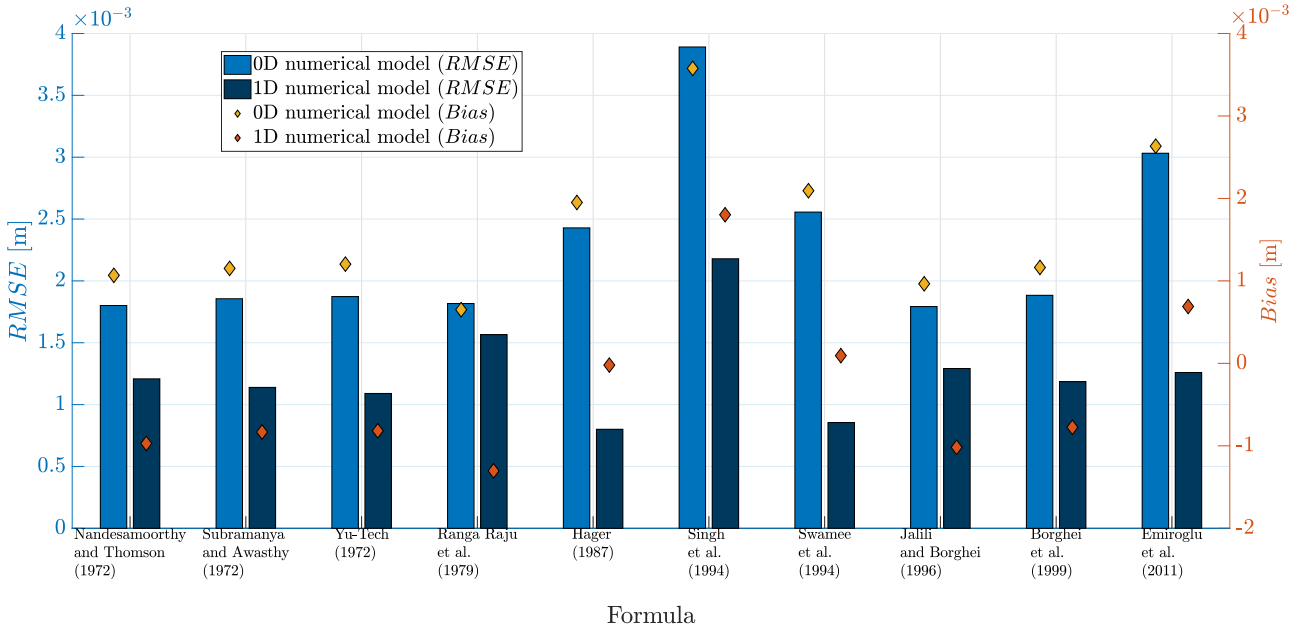

Figure 5.36: Water depth non-normalized indicators for Mignot et al. (2020) Op2 tests.

[3]However, Emiroglu et al. (2011) formulation seems to perform well for the prediction of water depths.

To conclude Mignot et al. (2020) tests analysis, FIGURE 5.37 shows the comparison of results from the different formulations and models.

The formulae identified as effective appear to be those that are closest to the origin of the error indicator axis system, regardless of the numerical model used. There are two formulations with a higher breach discharge error than the effective expressions but a lower water depth error (1D model): Hager (1987) and Swamee et al. (1994b) formulae.

Regarding the bias, the results obtained with both numerical models have to severe. In the 0D model case, the normalized bias on the water depth is always higher than zero. That means that this model overestimates the water depth. By contrast, the 1D model underestimates the water depth (except for two formulations: Emiroglu et al. (2011) and Singh et al. (1994)). This model also under-estimates the breach discharge (except for Ranga Raju et al. (1979) formulation). The 0D model normalized bias results analysis on the breach discharge is less straightforward. The effective formulae have a normalized bias on the breach discharge higher than zero. In this case, the 0D model overestimates the breach discharge. On the other hand, other formulations underestimate the breach discharge (i.e. normalized bias less than zero).

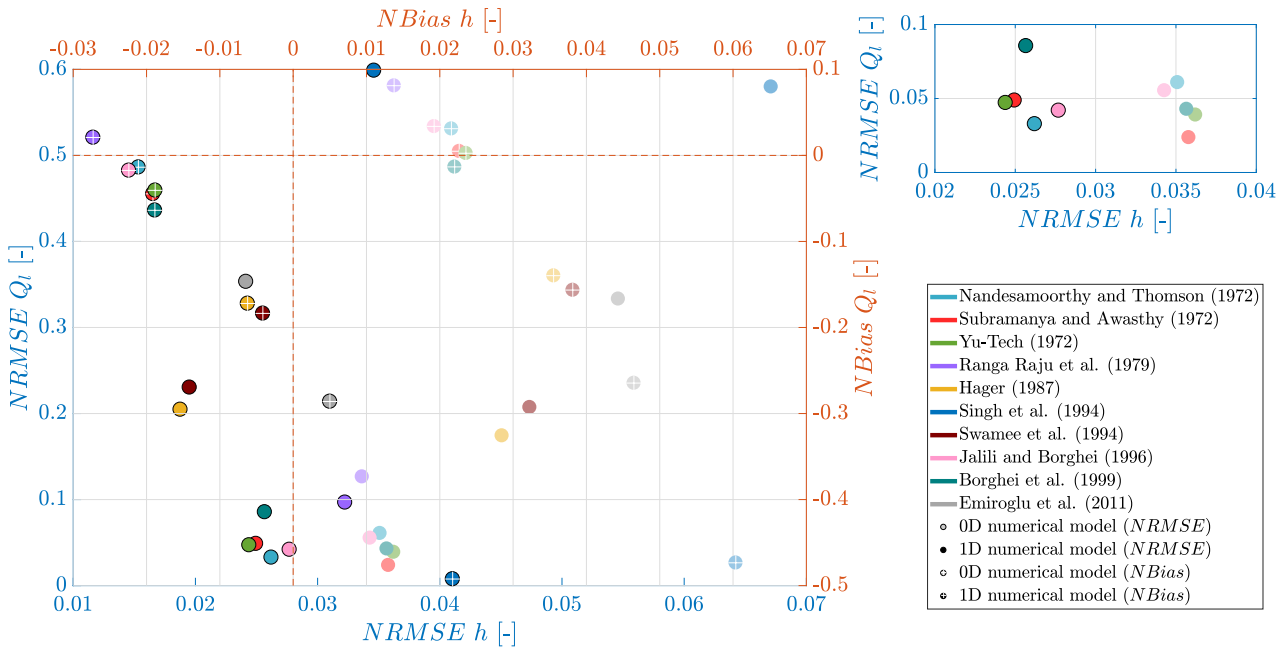

Figure 5.37: Water depth and breach discharge normalized indicators for the all tests, models and formulations (Mignot et al. (2020) Op2 tests).

5.1.4 Tests comparison

In order to complete the analysis of the flow experiments for a fixed breach with zero lateral crest height, a comparison of the tests of Roger et al. (2009), Michelazzo et al. (2015) and Mignot et al. (2020) was carried out (FIGURE 5.38). This figure shows all the results presented previously and highlights the similarities and differences between the experiments, models and formulations.

For the formulations:

The first remark is that the two formulations identified as not effective (Emiroglu et al., 2011; Singh et al., 1994) are not effective for the 3 experiments. Indeed, the $NRMSE$ indicator is the farthest from the origin of the reference system. For this type of configuration (fixed breach with zero lateral crest height), these two formulae can be discarded because the results obtained are not satisfactory.

The empirical expressions identified as effective are for all three types of experiments. These include Nandesamoorthy and Thomson (1972), Subramanya and Awasthy (1972), Yu-Tech (1972), Borghei et al. (1999), Ranga Raju et al. (1979), Swamee et al. (1994a) and Hager (1987). However, the effectiveness order of these formulations depends on the type of test considered.

The bias results, either for the breach discharge or the water depths, are close to zero for the different formulae of the 3 tests.

For the models:

The results obtained with the spatially-distributed model are generally better than those obtained with the lumped model. It appears that the 0D model tends to give worse results in terms of water depth than the 1D model (the points relative to the $NRMSE\,h$ are more shifted to the right). This is not surprising given that the 0D model is a lumped model able to predict a mean water depth. For Roger et al. (2009) experiments, the error on the water depth with the 0D model is much larger. Again, it is important to remember that for this experiment the water depths were compared to water depths from a 2D numerical model and not to experimental results. It is also good to remember that the depths for Mignot et al. (2020) experiments were evaluated at 4 points and not over the whole domain.

The biases on the 1D model breach discharge are negative for the Roger et al. (2009) and Mignot et al. (2020) experiments and positive for the Michelazzo et al. (2015) experiments. Those obtained with the 0D model are all positive. For this model, the formulations give an overestimation of the breach discharge. The water depths are overestimated by the lumped model for Roger et al. (2009) and Mignot et al. (2020) experiments. The 1D model mainly gives an underestimation of the water depths for these two tests.

As a conclusion, the diverse formulae (except the two rejected ones) as well as the models used give quite remarkable results. The hydraulic variables are fairly well estimated. Depending on the needs, one or the other model combined with accurate formulations enables to quickly obtain reliable results. However, one must be aware of what one wants to obtain and the desired precision. The lumped model gives almost instantaneous breach discharges but these are overestimated. The water depth results obtained by this model are further away from the experimental results but give an indication of the average depth on the canal. The 1D model also provides breach discharge results but gives additional information as the water depths are discretized along the main axis of the channel. Therefore, water depth information at the breach area is available.

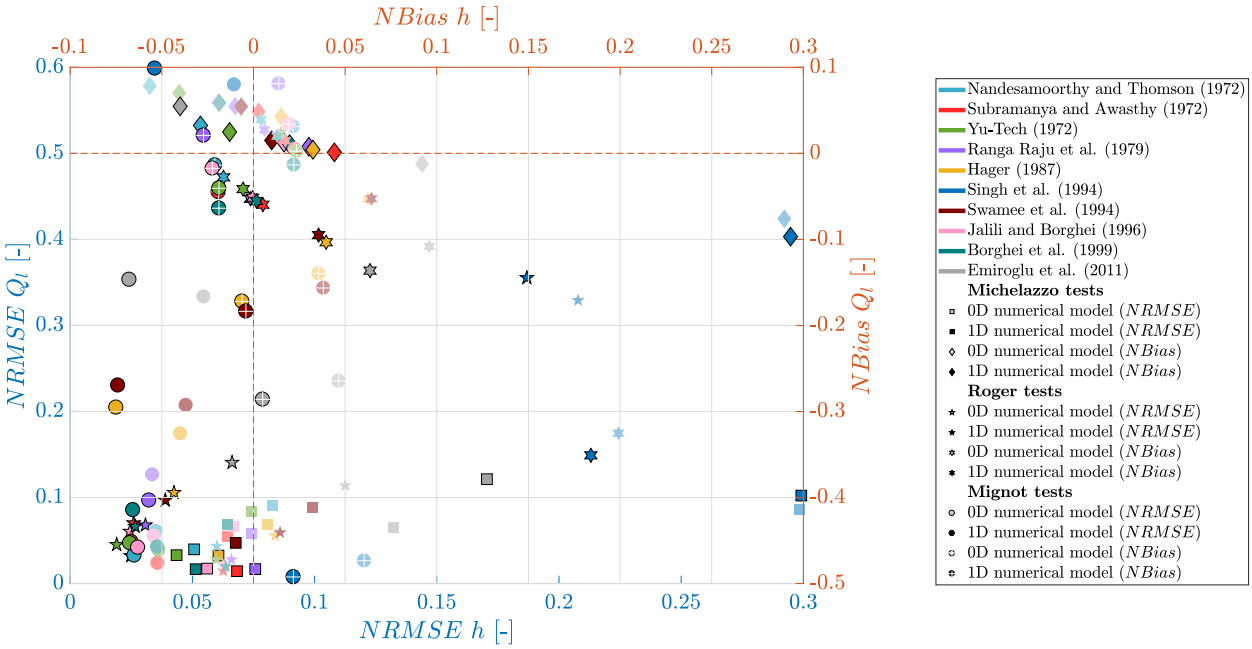

Figure 5.38: Water depth and breach discharge normalized indicators for the all tests (Michelazzo, 2014; Mignot et al., 2020; Roger et al., 2009), models and formulations.

5.2 Flow with fixed breach geometry and non-zero lateral crest height

In addition to testing the different numerical models and formulations of the discharge coefficient on multiple test cases with zero lateral crest height, it seems appropriate to test these elements on test cases with non-zero lateral crest height before moving on to the dynamic test cases. These tests correspond to Mignot et al. (2020) tests with Op1 (i.e. Op1F2 and Op1F5) shown in FIGURE 3.8. These results are analyzed in this section.

Given the number of tests (only 2), caution must be taken in analyzing the results obtained. Several similar tests would be necessary to confirm or not the analyses. A similar analysis of the results is presented in the next section to describe the results obtained with these new configurations.

5.2.1 Mignot et al. (2020)

Lumped model

The results in terms of breach discharge and water depth are shown respectively in FIGURES 5.39 and 5.41. FIGURES 5.40 and 5.42 illustrate the difference between the numerical and experimental results for both hydraulic variables.

The numerical breach discharges are quite far from the experimental discharges compared to the tests with zero lateral crest height. Indeed, the difference reaches more than 20% for the formulations considered previously as the most accurate. The breach discharge is always underestimated, regardless of the formula used. An important result is that Singh et al. (1994) formula, being one of the least accurate formulae for the configurations with zero lateral crest height, becomes an accurate formulation. This can be explained by the fact that this formula is originally intended for side weirs with non-zero lateral crest height.

Another formula was added to the analysis. This is Bagheri et al. (2013) formula. This could not be considered for the previous experiments due to the nature of the formulation (crest depth in the denominator). This formula gives more satisfactory results than the effective formulations identified previously.

Finally, Borghei et al. (1999), Jalili and Borghei (1996) and Emiroglu et al. (2011) expressions show differences of more than 35% with the experimental experiments. The difference even exceeds 50% in the Op1F5 test for Jalili and Borghei (1996) and Borghei et al. (1999) formulations. Such differences are obviously not tolerated.

The water depth results are quite surprising. While the breach discharges from the lumped model are quite far from the experimental results, it is completely the opposite for the water depths. The accuracy of the results is remarkable: less than 1% difference with the average depth for all empirical expressions. Therefore, the 0D model gives almost exact average water depth results.

It should be noted that no link is possible with the validity intervals of the formulae because Op1 Mignot et al. (2020) experiments are not included in any formulation intervals. The proposed formulae have not been validated for the configurations used by Mignot et al. (2020) experiments.

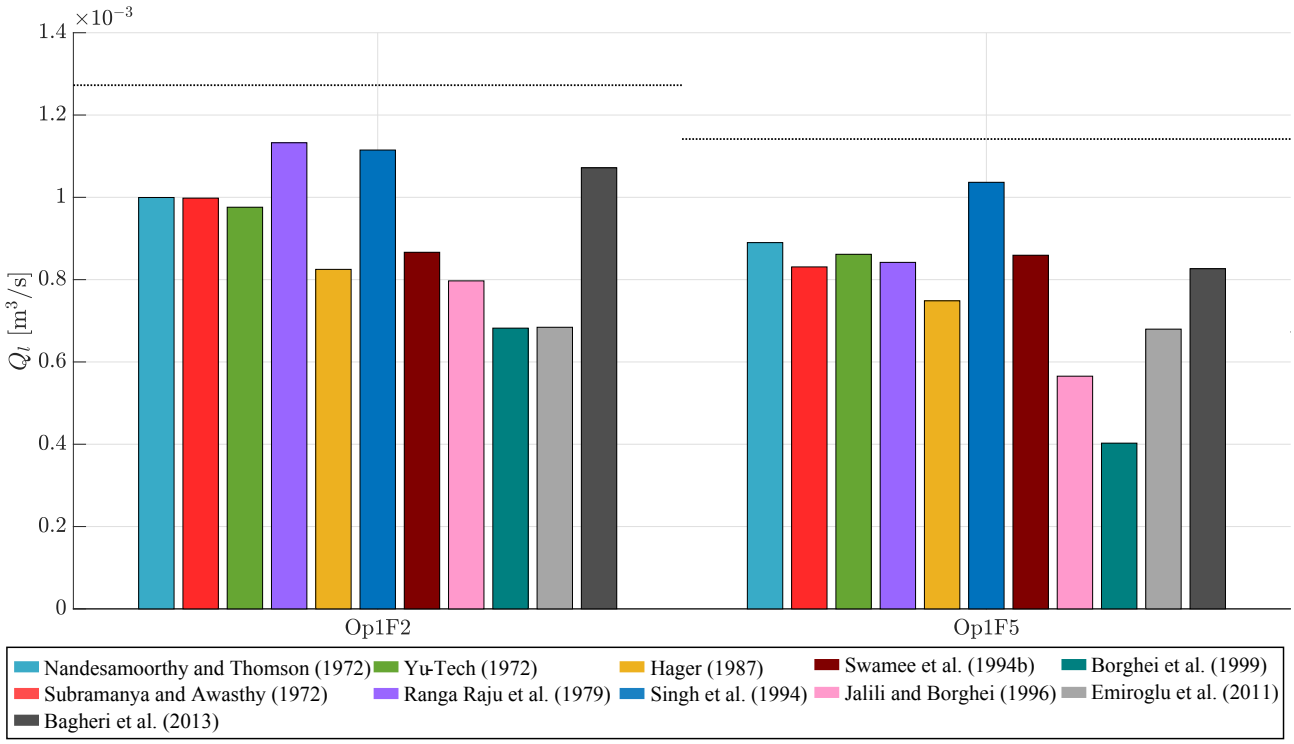

Figure 5.39: Breach discharge results 0D model for Mignot et al. (2020) Op1 tests.

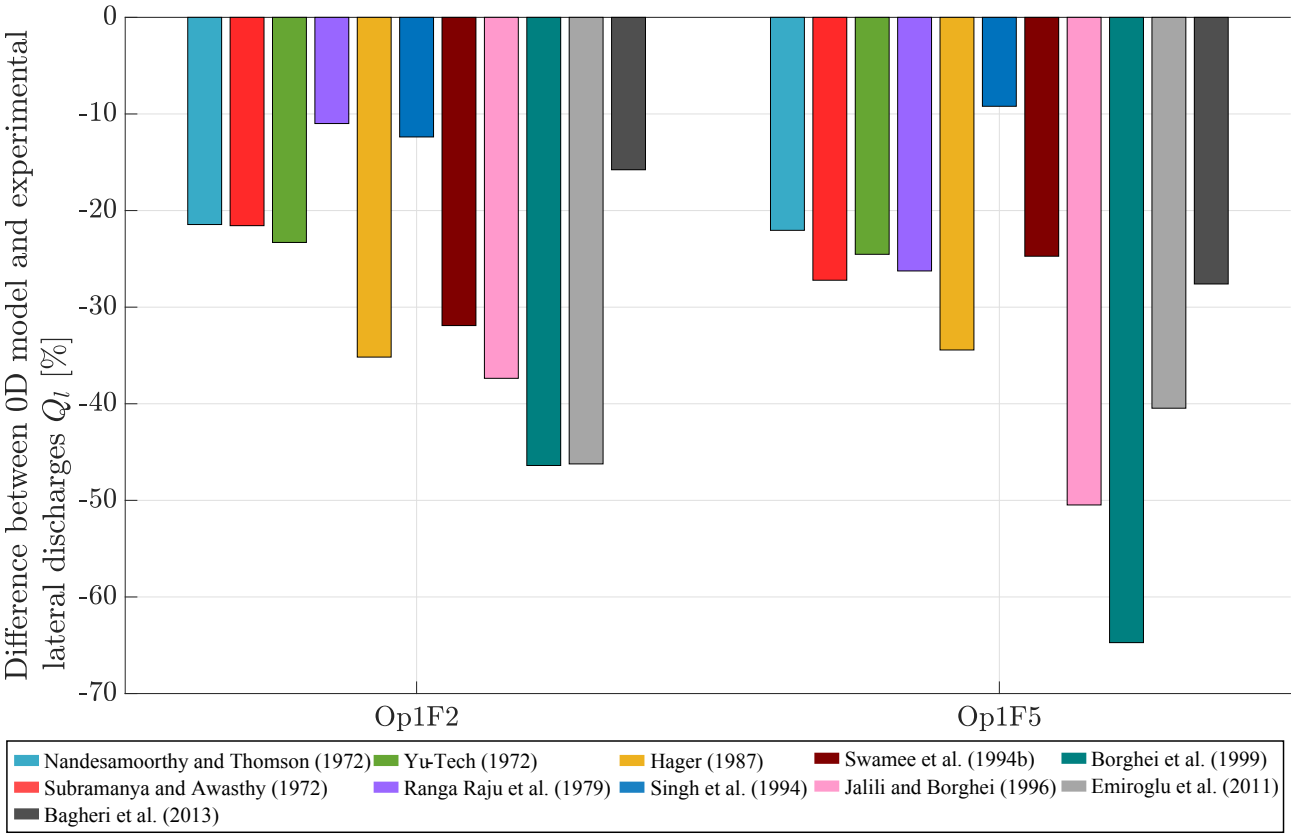

Figure 5.40: Breach discharge difference (0D model) for Mignot et al. (2020) Op1 tests.

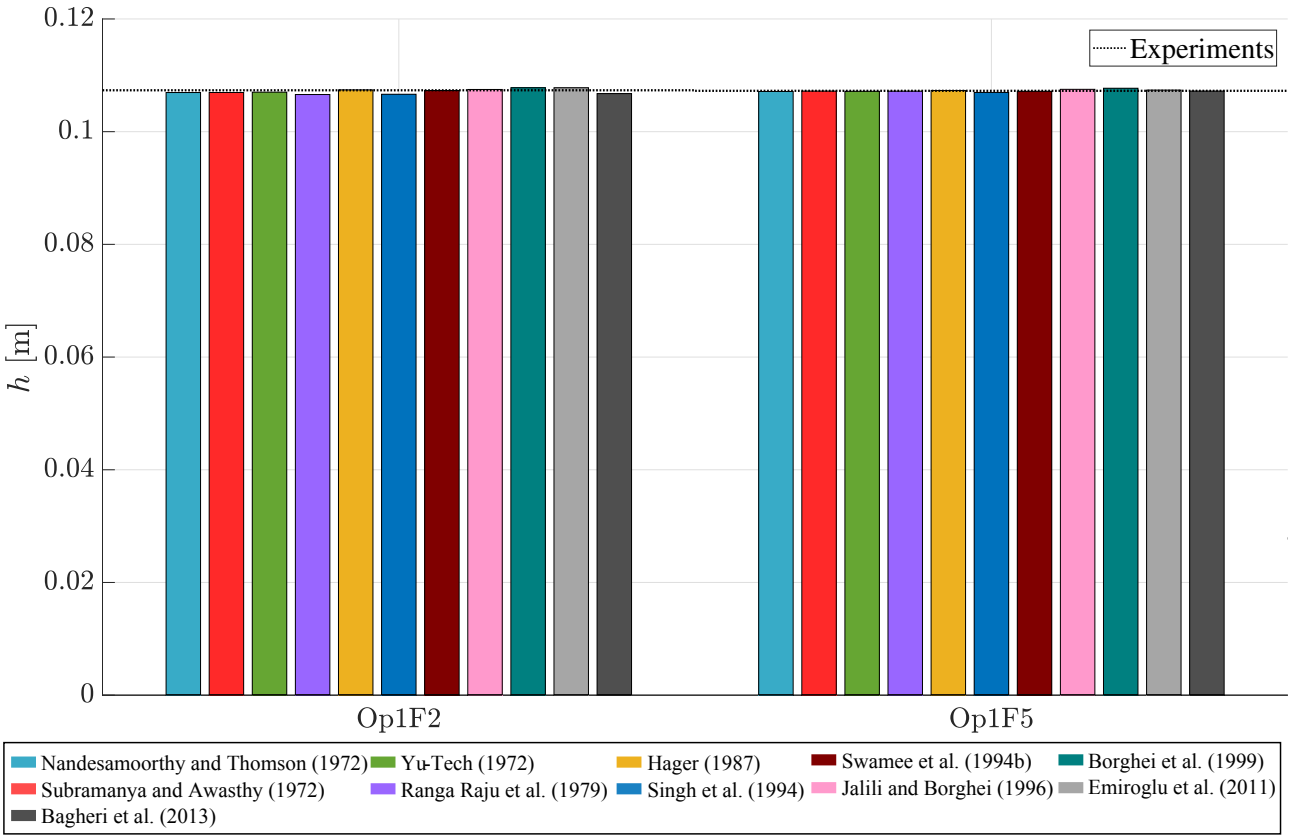

Figure 5.41: Water depth results 0D model for Mignot et al. (2020) Op1 tests.

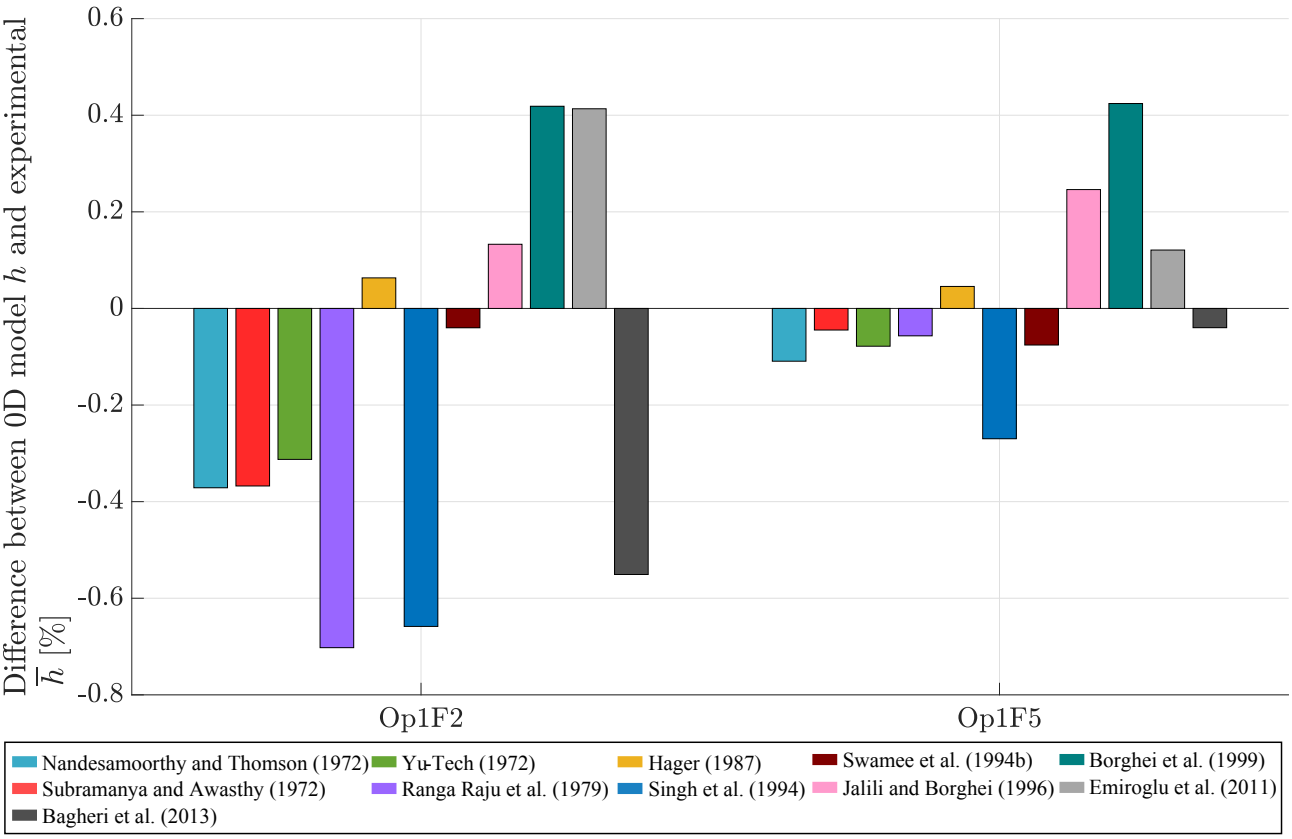

Figure 5.42: Water depth difference (0D model) for Mignot et al. (2020) Op1 tests.

Spatially-distributed model

The same conclusions as for the breach discharge obtained with the lumped model can be drawn. The results are shown in FIGURES 5.43 and 5.44.

A difference of the same order as that obtained for the lumped model can be seen. The results are even slightly worse with this spatially-distributed model. Any formulation does not differ from the experimental results by less than 15%. This observation is a radical change from experiments with zero lateral crest height. The so-called effective formulations are no longer effective for these hydraulic configurations. Singh et al. (1994) formula appears to be the best empirical expression in this case.

The formulae of Jalili and Borghei (1996), Borghei et al. (1999) and Emiroglu et al. (2011) give a difference in breach discharge with the experimental results of more than 40%. These expressions had already been identified as inaccurate for the lumped model. It can be concluded that these formulations should be discarded for Mignot et al. (2020) experiments with a non-zero lateral crest height.

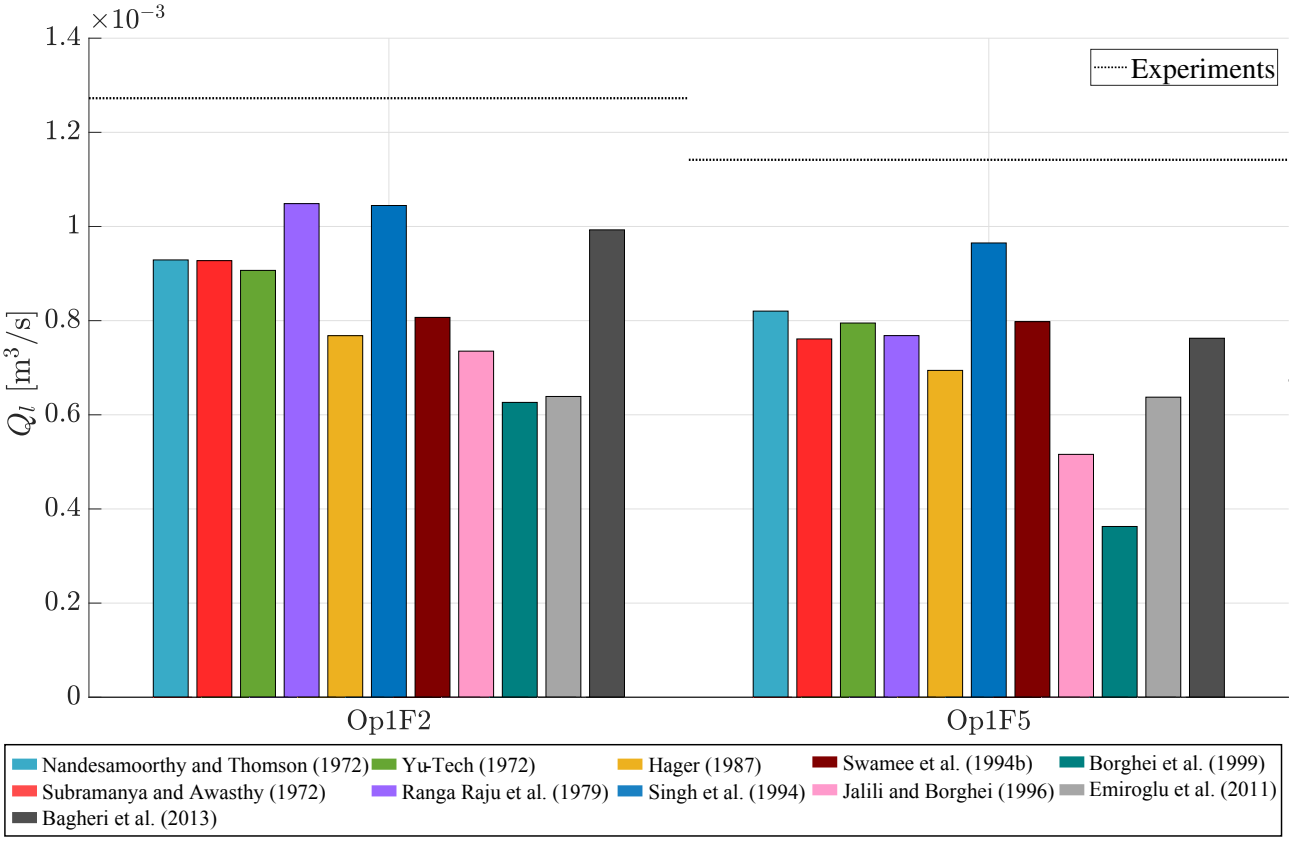

Figure 5.43: Breach discharge results (1D model) for Mignot et al. (2020) Op1 tests.

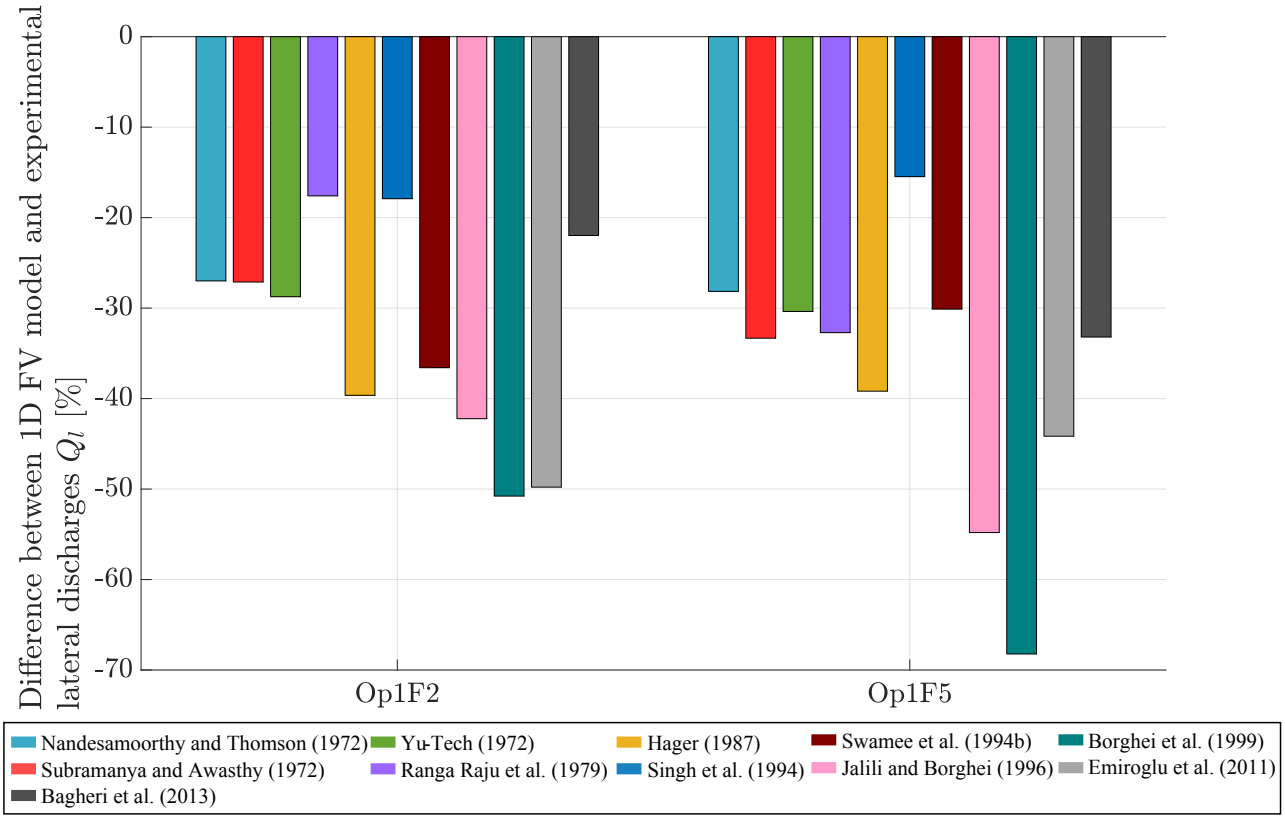

Figure 5.44: Breach discharge difference between numerical (1D model) and measurement for Mignot et al. (2020) Op1 tests.

The water depth, discharge and Froude profiles are shown in FIGURES 5.45, 5.46 and 5.46 respectively.

The same waterline shape can be seen in FIGURE 5.45 for all the formulations used. These water depth profiles differ only in their vertical position. The more the breach discharge is underestimated, the higher the water line. Borghei et al. (1999) formula has the highest water depth profile. Conversely, Singh et al. (1994) expression has the lowest water depth profile.

The same logic can be applied to the discharge profiles (FIGURE 5.46). Upstream of the breach, the discharge is the same for all formulations and is equal to the inlet discharge. Downstream of the breach, the maximum discharge is observed for Borghei et al. (1999) formulation and the minimum discharge is observed for the Singh et al. (1994) formula.

The hydraulic conditions of these experiments are subcritical ($Fr < 1$). The Froude number decreases along the main axis of the channel (FIGURE 5.47). For a constant discharge upstream of the breach, the water depth increases. This results in a decrease of the Froude number on the upstream part of the channel. When the upstream end of the breach is reached, the discharge in the channel decreases considerably, which results in a decrease of the Froude number since the water depth does not increase significantly. Downstream of the breach, the discharge remains constant. As the water depth increases, the Froude number decreases.

In FIGURE 5.45, at first sight, the water profiles seem different from the experimental points. However, this is misleading because the y-axis is focused on depths of about 10cm. In reality, the water depth in the channel is almost flat since there is a difference of ± 1cm between the upstream and downstream ends.

Finally, the water depths obtained with the 1D model only differ by a few mm from the experimental results, which represents a difference of a few % at most. Knowing that the uncertainty on the experimental measurements is ± 2%, the results obtained are very encouraging. The measurements uncertainties are represented by the error bars in FIGURE 5.45.

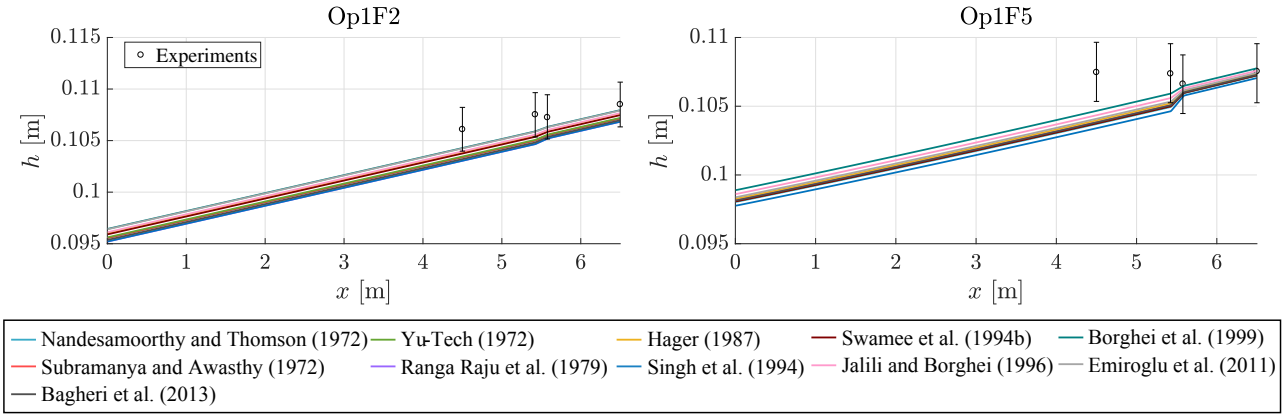

Figure 5.45: Water depth profiles (1D model) for Mignot et al. (2020) Op1 tests.

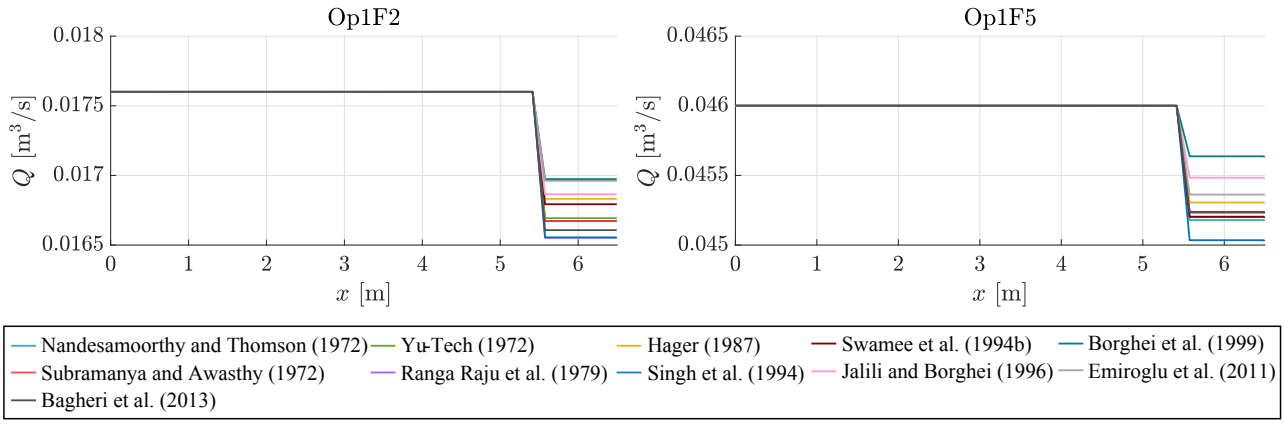

Figure 5.46: Discharge profiles (1D model) for Mignot et al. (2020) Op1 tests.

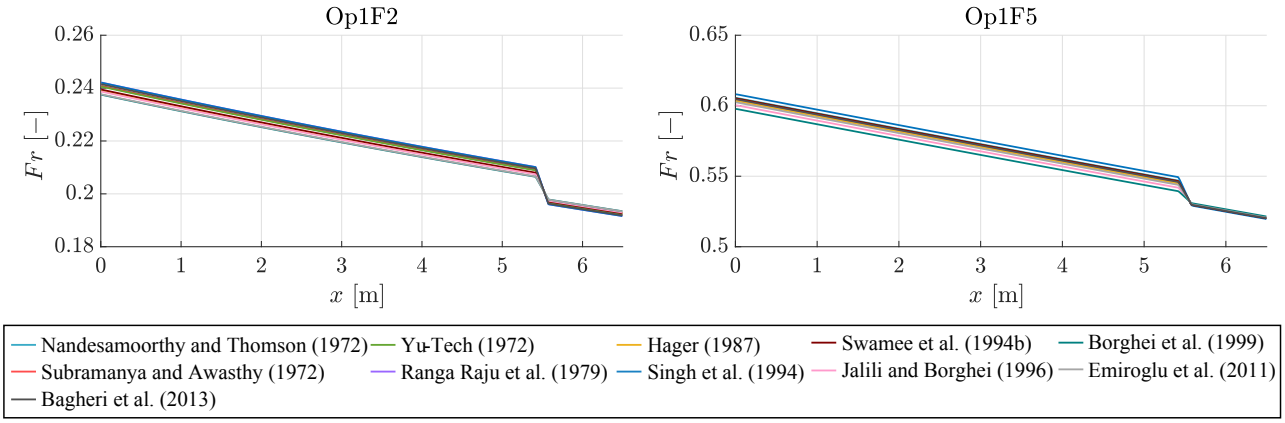

Figure 5.47: Froude profiles (1D model) for Mignot et al. (2020) Op1 tests.

Numerical models and formulations comparisons

Given the limited number of tests conducted, the comparison of results is a bit less relevant. However, this analysis highlights the results for configurations with non-zero lateral crest height. These configurations are closer to real dike conditions, but still far from it.

For all formulations, the breach discharge calculated with the lumped model is closer to the experimental results than the one calculated with the other model (FIGURE 5.48). However, the differences in terms of error between the models remain small. By analyzing the bias indicator, it appears that the breach discharge is underestimated for both numerical models. Indeed, the bias value is negative. Moreover, the 0D model bias results are lower than the bias calculated from the 1D model results. The two indicators lead to the conclusion that the lumped model provides better results for the breach discharge.

The analyses of water depths lead to the same conclusions (FIGURE 5.49). The lumped model gives results close to the average experimental depth (in terms of error and bias). The spatially-distributed model then has an error of the order of 2 mm on the water depths. The bias obtained is in a similar order of magnitude.

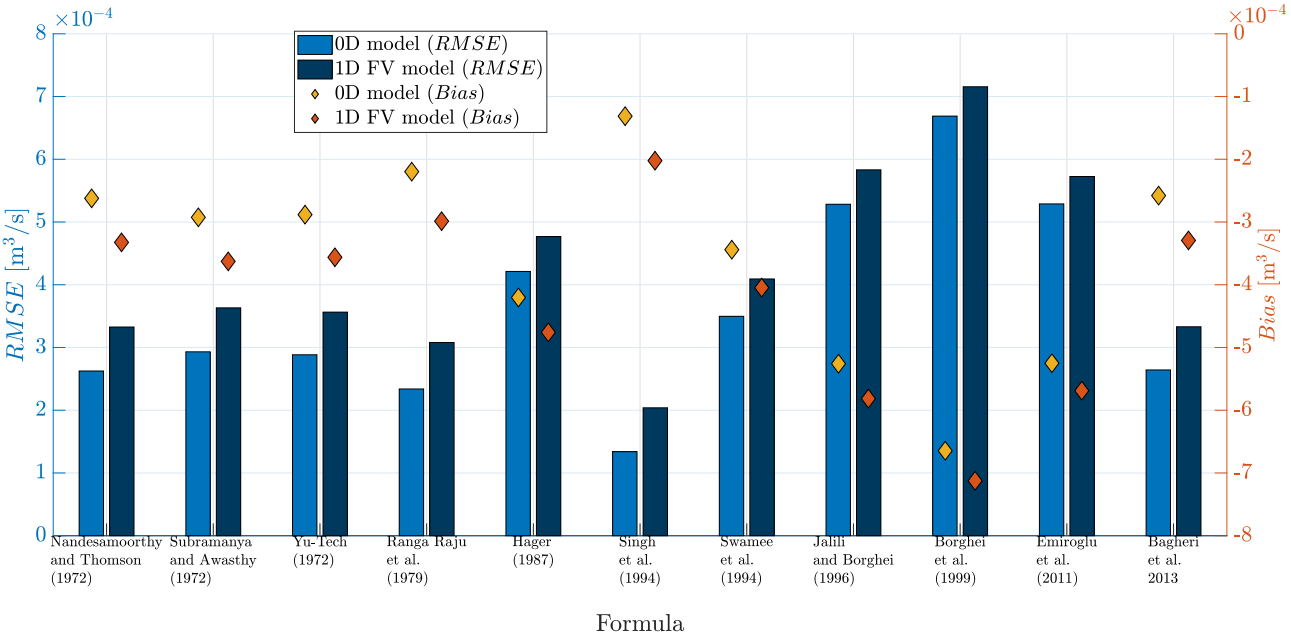

Figure 5.48: Breach discharge non-normalized indicators for Mignot et al. (2020) Op1 tests.

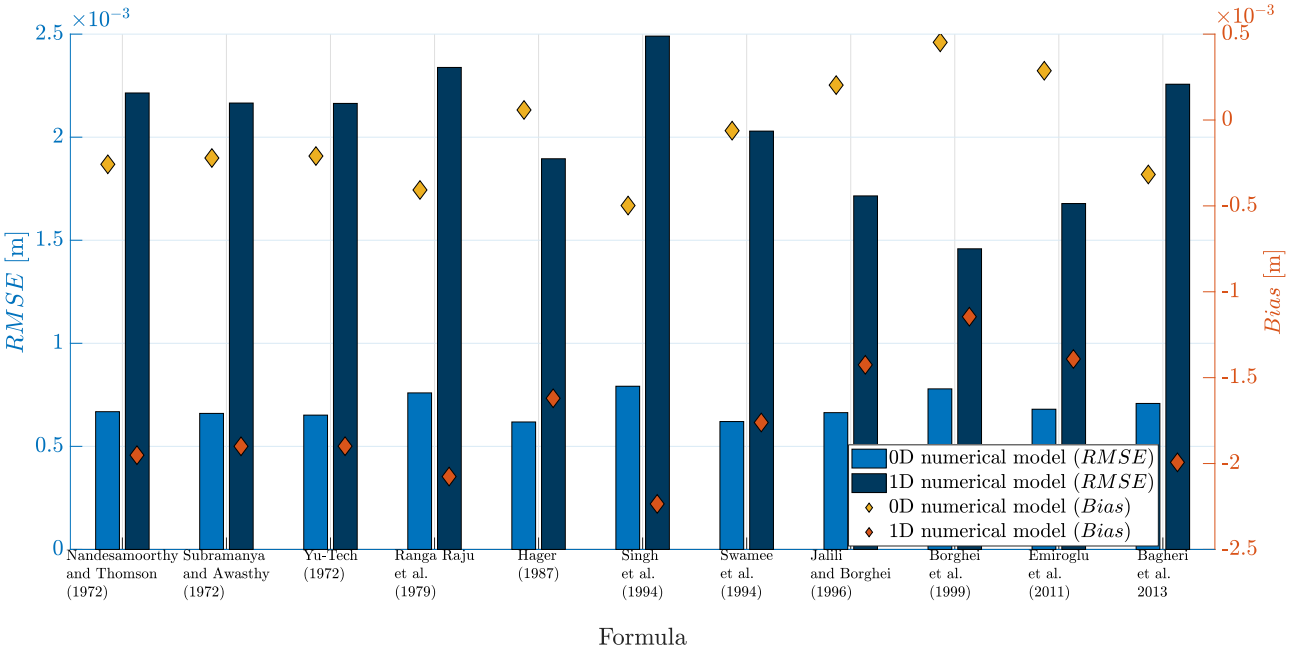

Figure 5.49: Water depth non-normalized indicators for Mignot et al. (2020) Op1 tests.

Finally, FIGURE 5.50 provides an overview of all the above findings in terms of the normalized indicator. It shows the dispersion of the results for each formulation according to the numerical model used. It is clear that the results of the 0D model are closer to the experimental ones (i.e. $NRMSE$ close to the origin axes and $Bias$ close to zero).

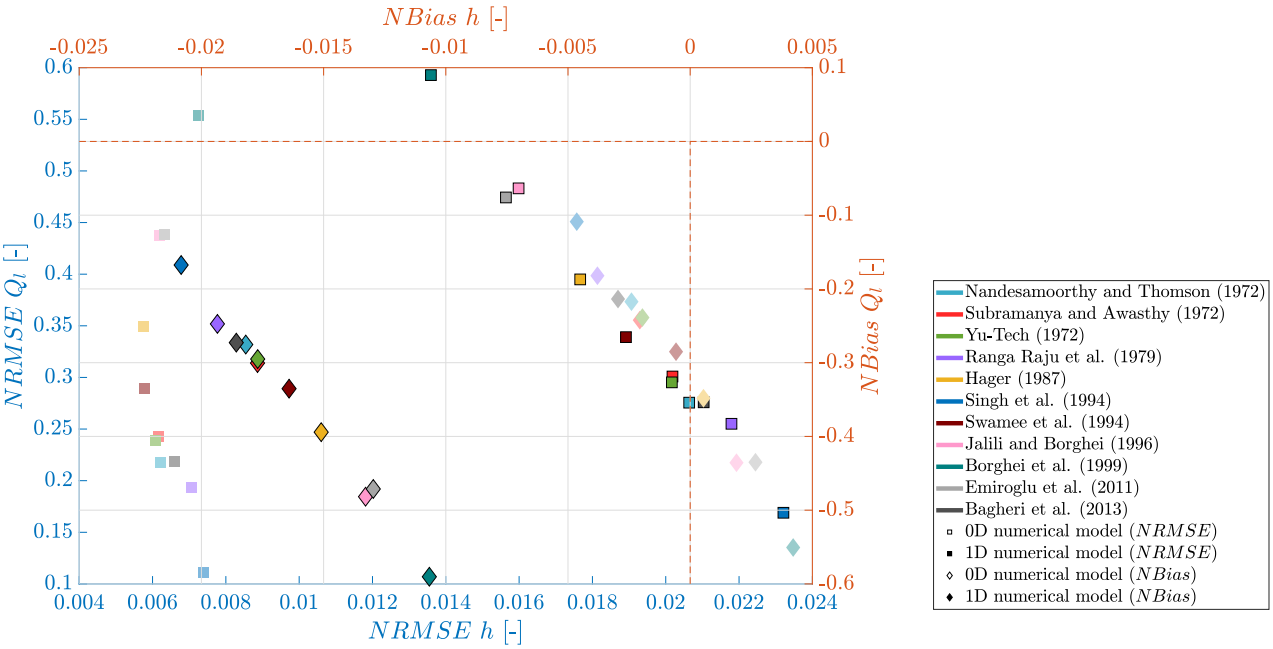

Figure 5.50: Water depth and breach discharge non-normalized indicators for all tests, models and formulations (Mignot et al. (2020) Op1 tests).

5.2.2 Changes in the implementation of formulations

The main challenge of this thesis is to be able to analyze the effectiveness of the various discharge coefficient formulations proposed in the Mignot et al. (2020) publication. These expressions are based on the geometric parameters of the breach as well as the hydraulic variables. Therefore, there are different parameters involved in the calculation of the discharge coefficient. So far, the numerical results have been obtained by strictly following the guidelines of the formulae. It was necessary to consider the different geometrical parameters such as the crest depth of the lateral weir (p), the length of the weir (L_s) or the width of the channel (W). These parameters come from the experimental set-up and cannot be modified. The hydraulic variables used in these formulae are the Froude number (Fr) and the water depth (h). The formulae were designed to consider both variables upstream of the breach. But what would happen if the place where these variables are considered changes?

For this purpose, two other formulation implementations (alternatives 1 and 2) in addition to the classical one have been examined. TABLE 5.1 illustrating the different ways (positions) of considering the hydraulic variables only for the 1D model.

	Hydraulic variables	
Implementation	Fr	h
Classical	Upstream	Upstream
Alternative 1	Upstream	Locally
Alternative 2	Locally	Locally

Table 5.1: Hydraulic variable positions in the use of discharge coefficient formulae.

The remainder of this section is dedicated to the comparison of the results for Mignot et al. (2020) tests (Op1) described previously. For this purpose, non-normalized indicators in terms of lateral discharge and water depth were used.

The results are quite clear: the alternatives proposed have no influence at all. Indeed, the comparison of the results shows that there is only a small change between the classical approach and the two alternatives (FIGURES 5.51 and 5.52).

The difference observed between the results obtained with alternative 2 and the classical approach is slightly larger than the difference between the results obtained with alternative 1 and the classical approach. This seems normal as most formulae are expressed in terms of Froude numbers. Therefore, if the latter remains unchanged (alternative 1), the results are identical to the classical approach. On the contrary, if the Froude number changes (alternative 2), the results must also change. However, the difference in results is not significant. The breach discharge indicator decreases very slightly while the water depth indicator slightly increases. The same is true for the bias.

Both alternatives were also tested in the Mignot et al. (2020) (Op2), Roger et al. (2009) and Michelazzo (2014) experiments. The changes are also not very significant.

In conclusion, the modification of the discharge coefficient formulations implementation has no impact on the results. The use of these alternatives can be considered irrelevant. Furthermore, the physical meaning of the discharge coefficient equations is lost. These were established for an upstream Froude number and an upstream water depth. Therefore, the classical approach is conserved for the following tests.

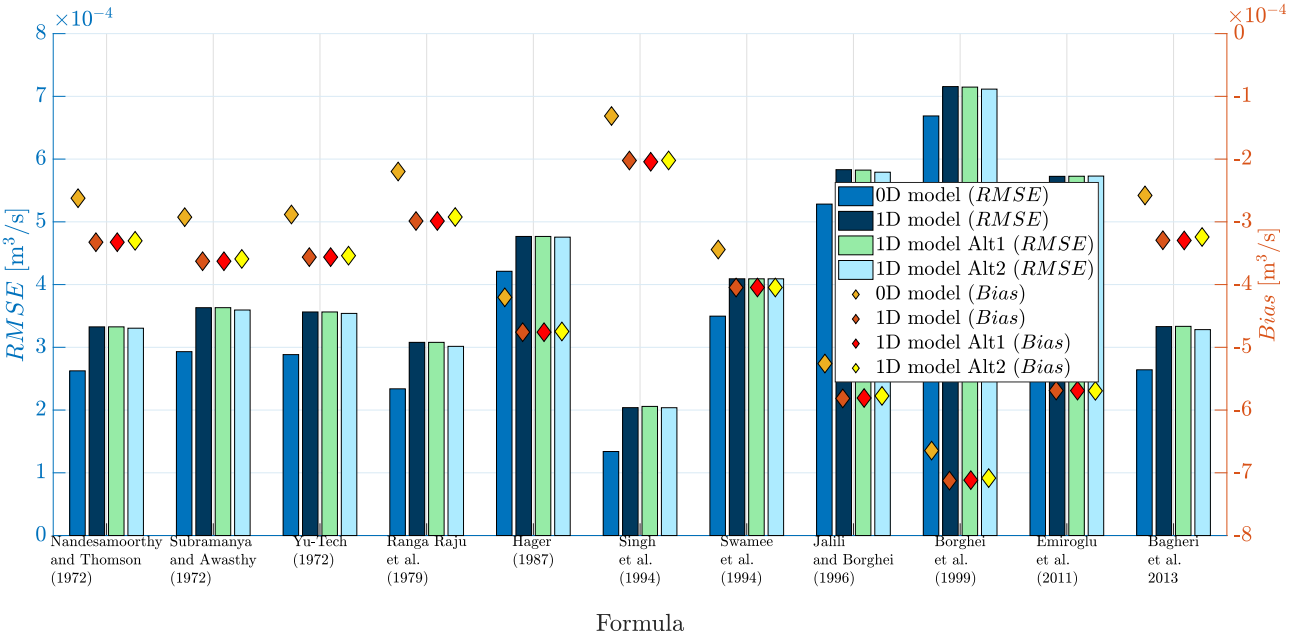

Figure 5.51: Impact of alternative formulations implementation on breach discharge non-normalized indicators.

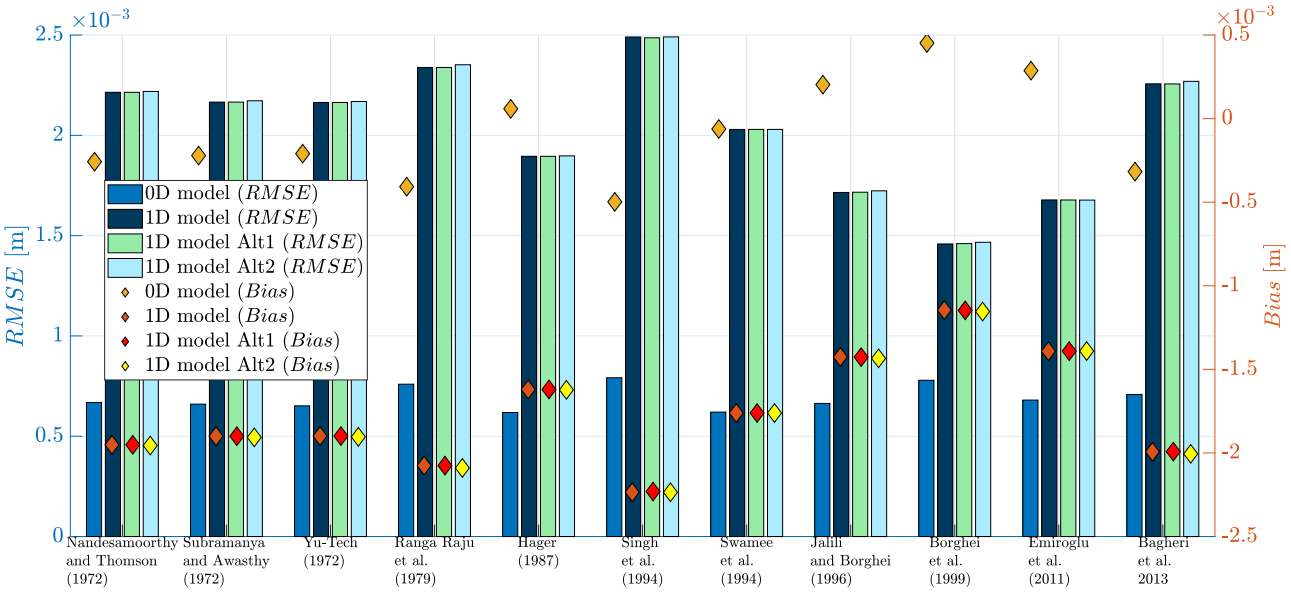

Figure 5.52: Impact of alternative formulations implementation on water depth non-normalized indicators.

5.3 Flow with dynamic breach geometry

5.3.1 Rifai (2018)

The purpose of this section is to analyze the results obtained from the Rifai (2018) experiments. These experiments are flow tests with dynamic breach geometry.

First, it is necessary to clarify how the dynamic opening is taken into account. During the Rifai (2018) experiments, measurements of the dike were made using laser profilometry. A database containing the evolution of the dike's geometry was thus created. This database contains all the depth profiles of the dike according to the two main axes x and y (main flow axis and transverse axis). Thanks to these data, the evolutionary geometry of the dike could be implemented.

For both models, the longitudinal profile in the center of the dike was considered (FIGURE 3.9). This is actually the "average" profile of the breach.

For the 1D model, the depth at the bottom of the breach is directly deduced from the data as a function of x and time. This means that each finite volume has the depth corresponding to its position.

For the 0D model, a unique bottom depth had to be found for each time step. For each time step, a breach width was computed. This width is the distance between two points located on the dike crest where the points in between have a varying breach depth that is lower than the crest depth. Then, by considering all the bottom heights along this width, a fixed depth was calculated. This is computed as the 15^{th} percentile (15% of the bottom heights are lower than the value calculated *via* the percentile principle). It is obvious that this 15% value was set arbitrarily. Indeed, this value is low enough to approach the minimum value of the bottom while remaining high enough to take into account the fact that the breach is not rectangular. In order to evaluate the influence of this choice, a sensitivity analysis was performed taking into account the value of the percentile and other parameters.

All these explanations are illustrated in FIGURE 5.53.

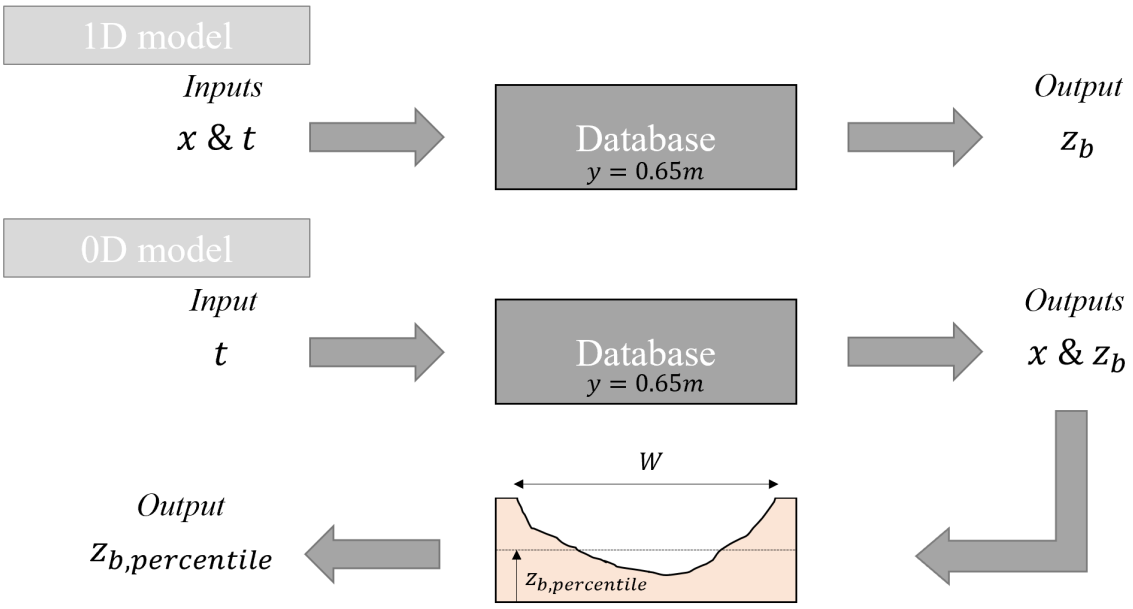

Figure 5.53: Methodology used to select the bottom depth for each numerical model.

FIGURE 5.54 shows the evolution of the breach width as well as the breach bottom depth over time used for the 0D model. The saw tooth shape of both variables is clearly visible in this figure. This can be explained by the small number of points available.

In addition, the measurements during the Rifai (2018) experiments were not taken at constant time intervals. There were more measurements at the beginning of the experiments than at the end. These saw tooth shapes clearly have an impact on the shapes of the hydraulic variables of interest (0D model: FIGURES 5.56, 5.57, 5.58 and 5.59; 1D model: FIGURES 5.60, 5.61, 5.62 and 5.63), such as the water depth or the breach discharge. The shape of these variables is therefore directly related to the lack of data collection. The impact of this lack of data on the results is minimal. It only influences the shape of the results.

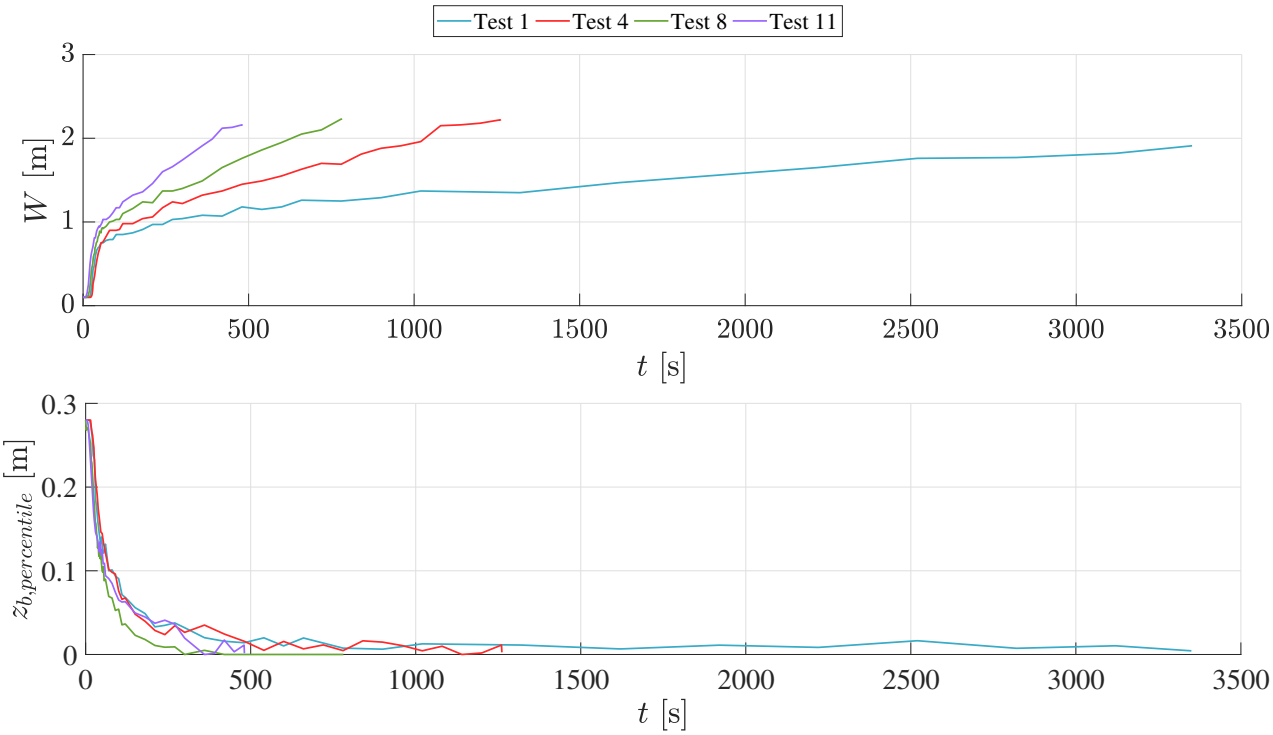

Figure 5.54: Breach width and bottom depth evolution used in the 0D model.

As the configurations of the tests are different, the duration of the test is also different. For Test 1, which corresponds to the lowest inlet discharge, the test duration is longer than for the other tests. On the contrary, for Test 11, which corresponds to the highest injected discharge, the test duration is shorter. This is directly related to the dynamics of the dike failure, which is more impacted by higher upstream discharges.

The temporal breach profiles used in the spatially-distributed model correspond to time cuts of the 3D curves shown in FIGURE 3.12. An example of a breach opening evolution is illustrated in FIGURE 5.55 (Test 1).

As it can be seen in FIGURES 5.54 and 5.55, the breach widens and deepens over time. The vertical deepening of the breach leads to a reduction in the bottom depth. This is why $z_{b,percentile}$ is decreasing over time.

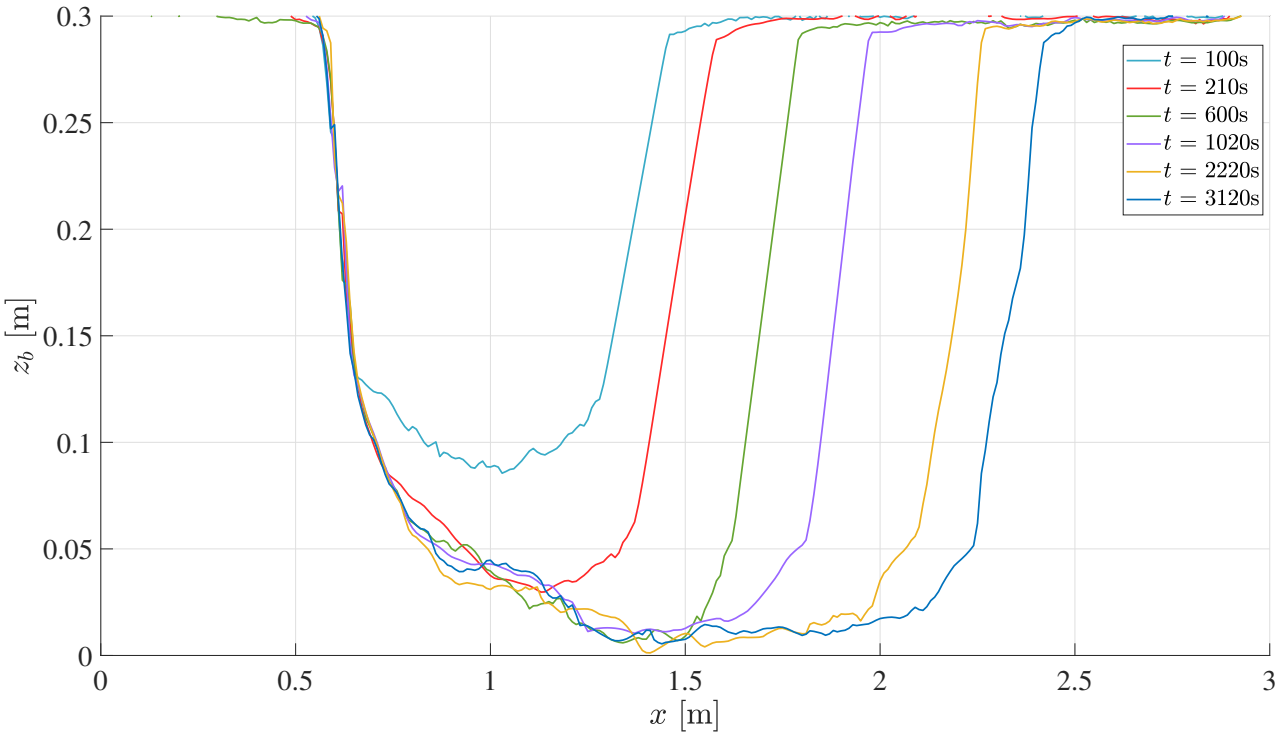

Figure 5.55: Breach geometry evolution for Test 1 used in the 1D model.

Lumped model

The results obtained with the lumped model are shown in FIGURES 5.56, 5.57, 5.58 and 5.59. Different hydraulic variables are represented such as the temporal evolution of the breach discharge, the outlet discharge and the water depth. The peak breach discharge[4] is also compared between the empirical expressions.

A general trend emerges from the results. The lumped model provides results that are close to the experimental results. The formulations give very similar results. It should be noted that Emiroglu et al. (2011) and Bagheri et al. (2013) formulae could not be obtained for certain tests. Emiroglu et al. (2011) formulation was already identified earlier as being less effective. For zero bottom depth (Tests 8 and 11; FIGURE 5.54), Bagheri et al. (2013) formulation cannot work.

The peak breach discharge analysis shows that the numerical breach discharge always overestimates the experimental breach discharge (for all tests). Further analysis of these results shows that the difference between the numerical and experimental breach discharge is not negligible. TABLE 5.2 shows the minimal and maximal difference between the numerical and experimental results for the peak breach discharge. This table also shows the best as well as the worst formulation for estimating the peak breach discharge.

Test	Difference [%]	Best formulation	Worst formulation
1	3 - 20	Hager (1987)	Ranga Raju et al. (1979)
4	6 - 14	Hager (1987)	Ranga Raju et al. (1979)
8	24 - 37	Singh et al. (1994)	Ranga Raju et al. (1979)
11	12 - 18	Singh et al. (1994)	Nandesamoorthy and Thomson (1972)

Table 5.2: Range of difference in peak breach discharge between numerical and experimental results (0D model).

Except for Test 8, the peak breach discharge is estimated at the maximum with a 20% overestimation. For Test 8, in the best case, the peak breach discharge is overestimated by about 24%. It is clear that for this test, the difference between the experimental peak breach discharge and the numerical breach discharge is too significant.

In terms of water depth, the results are quite similar for short as well as for long times. Between these two periods, the numerical water depth is always lower than the experimental one. The water depth obtained by the 0D model is an average water depth over a control volume. The variation of this water depth depends on the influenced breach discharge, which in turn depends on the breach bottom depth.

Initially, the breach is not large enough for the water to pass through. The breach discharge is then zero. Once the water is able to seep through the breach, the breach discharge increases quite rapidly (stage 1) to reach its peak (end of stage 1). The water depth and discharge decrease until a steady state is reached (stage 2). The breach discharge, the outlet discharge and the water depth stabilize. The drainage discharge has not been shown in the various figures. This one has been calibrated to correspond to the experimental drainage discharge.

[4]The peak breach discharge is defined as the maximum value of breach discharge between stage 1 and stage 2.

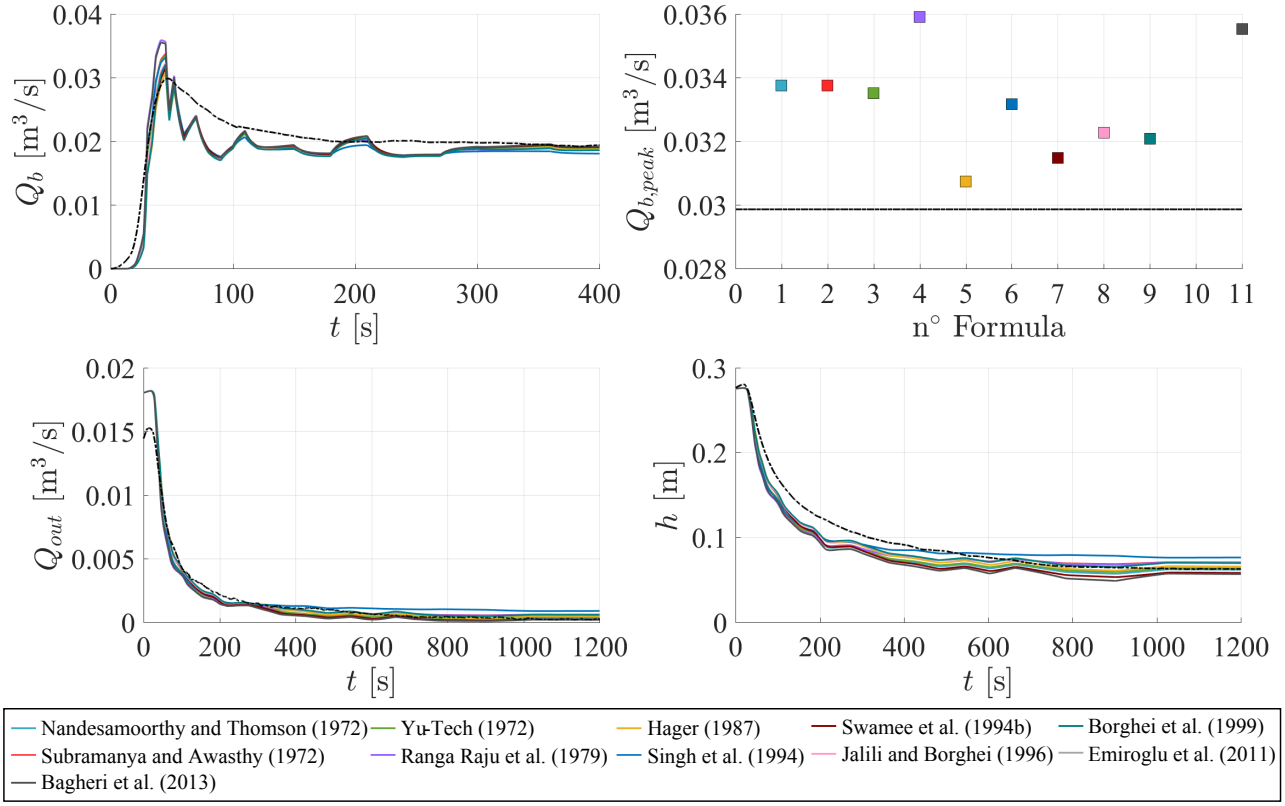

Figure 5.56: Test 1 (0D model): evolution of breach and outlet discharges and water depth.

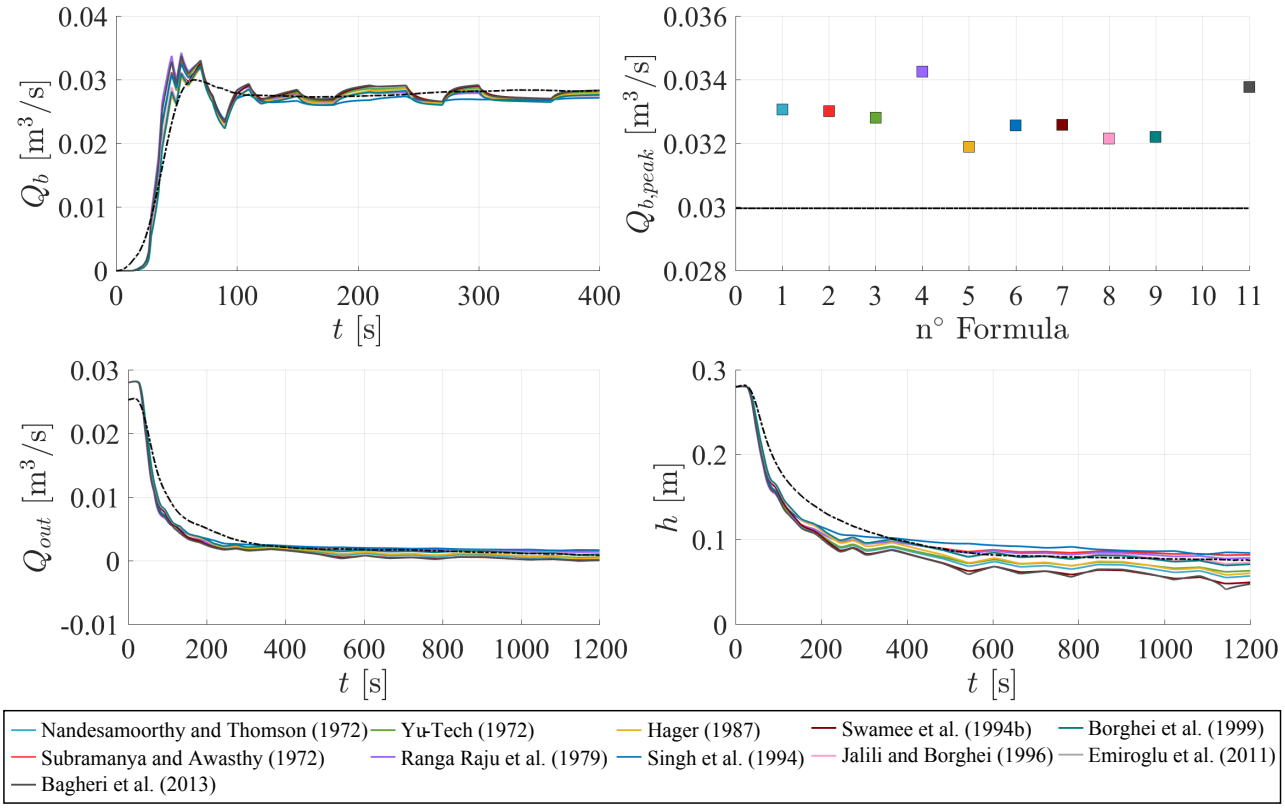

Figure 5.57: Test 4 (0D model): evolution of breach and outlet discharges and water depth.

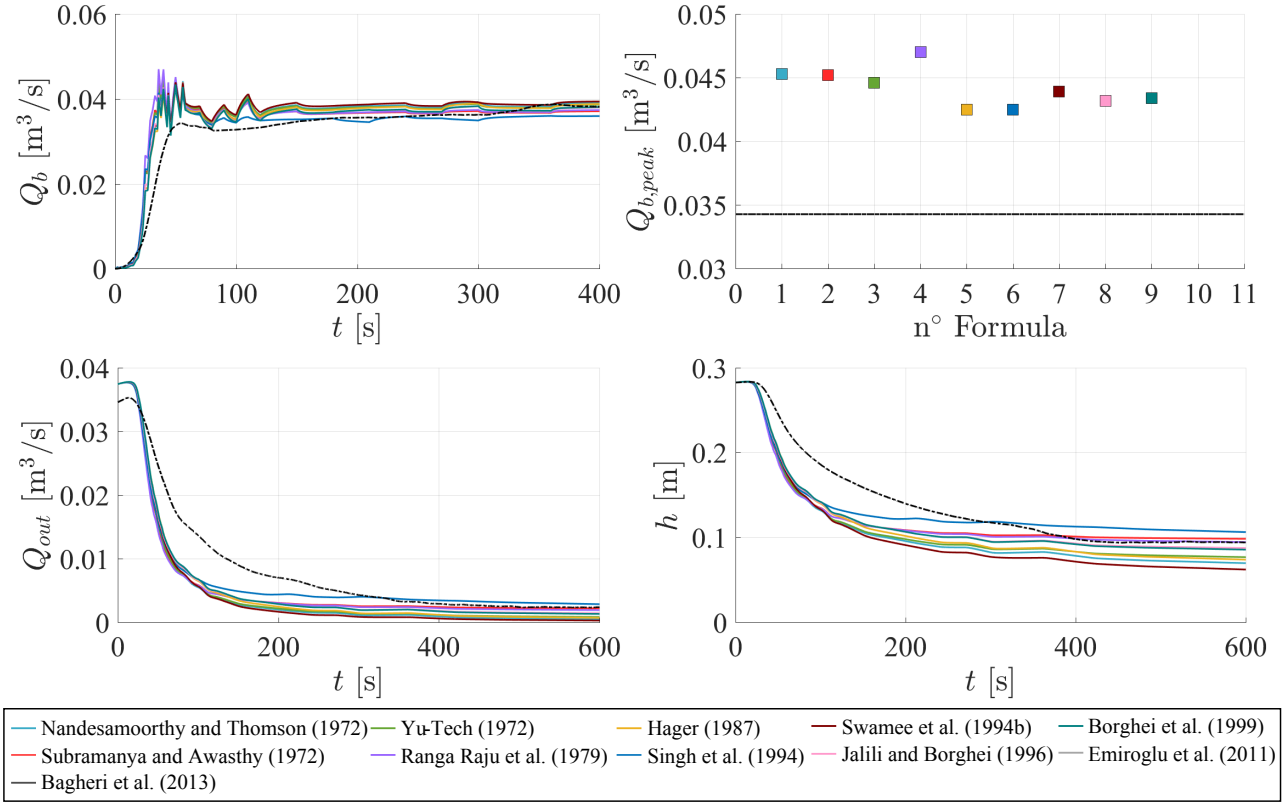

Figure 5.58: Test 8 (0D model): evolution of breach and outlet discharges and water depth.

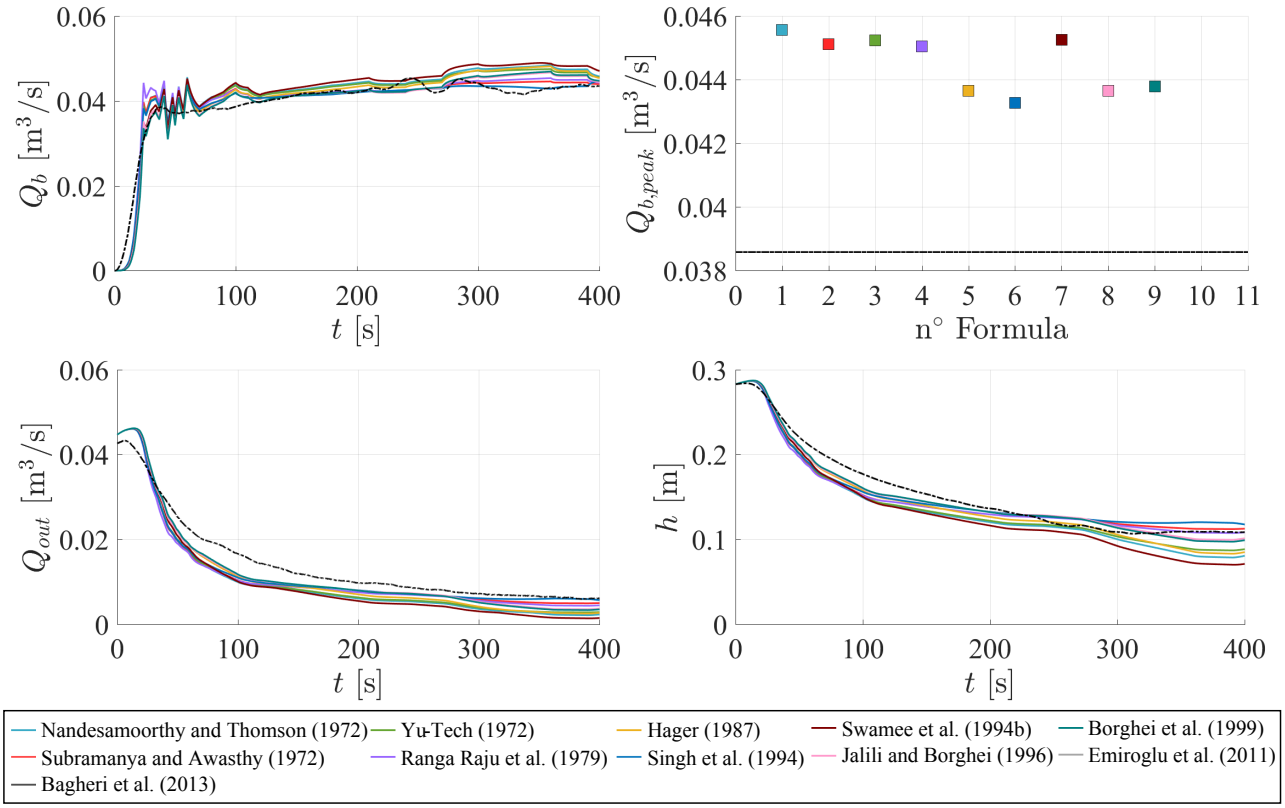

Figure 5.59: Test 11 (0D model): evolution of breach and outlet discharges and water depth.

Spatially-distributed model

The results in terms of breach discharge and water depth are given in FIGURES 5.60, 5.61, 5.62 and 5.63. These figures include the evolution of the breach discharge during stages 1 and 2, the different peaks of breach discharge obtained, the evolution of the outlet discharge as well as the water depths during stages 1 and 2 over the whole domain and the evolution of the water depths at certain upstream and downstream positions (respectively G1 and G3).

As for the lumped model, the results seem to be close to the experimental results at least until the end of stage 1. Indeed, the breach discharge as well as the water depths before the end of stage 1 are very close to the experimental results, which is encouraging. It was not guaranteed that the formulations used would yield such relevant results. Nevertheless, the stationary phase of the breach development is not well represented by the spatially-distributed model. The results deviate from the experimental results. These deviations are quite visible in the figures representing the evolution of the water depths at positions G1 and G3.

One of the important parameters during a dike breach is the evolution of the breach discharge and more specifically the peak of the breach discharge, which gives an idea of the intensity of the flow dynamics. The results obtained for this numerical model are quite close to the experimental results. The four corresponding figures illustrate these statements. In addition to these figures, TABLE 5.3 highlights the maximum and minimum differences between the numerical and experimental results as well as the best and worst formulations. The general tendency of the 0D model to overestimate the peak breach discharge is not transferable to the 1D model. Indeed, some results obtained with various formulae underestimate the peak. Thus, it is not possible to make a general conclusion as for the lumped model.

Test	Difference [%]	Best formulation	Worst formulation
1	-11 - 7	Borghei et al. (1999)	Ranga Raju et al. (1979)
4	0.5 - 11	Hager (1987)	Ranga Raju et al. (1979)
8	10 - 19	Hager (1987)	Ranga Raju et al. (1979)
11	-5 - 5	Swamee et al. (1994a)	Ranga Raju et al. (1979)

Table 5.3: Range of difference in peak breach discharge between numerical and experimental results (1D model).

Overall, the results obtained for the peak breach discharge with the 1D model show a smaller difference with the experimental results than the 0D model. Comparing TABLES 5.2 and 5.3, tables containing the peak breach discharge results for each model, it can be quickly seen that the maximum difference observed is smaller for the spatially-distributed model. At this point, it could be concluded that the use of the 1D model results in a lower maximum error.

Regarding the water depth, as mentioned above, the results obtained are similar to the experimental results before the end of step 1. This is not surprising because during this period all hydraulic variables overlap with the experimental results. However, the output discharge in stage 0 is different. This is due to the fact that the numerical model does not observe any flow through the breach for some time. The output discharge is larger than the experimental discharge during this period. After this period, the breach discharge gradually increases and the output discharge gradually decreases.

Once the end of stage 1 is reached, the numerical breach discharge is lower than the experimental breach discharge: a difference of less than 10% is observed. This means that less water is passing through the breach than during the experiments. Consequently, the observed downstream discharge as well as the water depth in the channel are more important than the experimental results. A difference of more than 60% (30%) between the numerical and experimental water depths is observed upstream (downstream) of the breach. This difference cannot be tolerated.

A relevant question that arises is why water depths are fairly well estimated during stage 1 and not during stage 2?

This conclusion is rather surprising. Indeed, the formulations were developed under stationary conditions (simple channel flow with a lateral opening) and not under unsteady conditions. It would have been logical to reach the opposite conclusions. This is not the case, however.

A first answer hypothesis could be found in the formulations used. As already mentioned, these formulations were not designed to be used in this experimental context. Therefore, it is likely that these formulations do not allow delivering sufficiently high output to ensure that the results tend to match the experimental ones.

The empirical discharge coefficient formulae have been calibrated for lateral openings with sharp-crested weir. The configuration of a dike is not at all similar to this. Indeed, the dike has a certain cross-sectional width. Therefore, the formulae used for sharp-crested weirs are not necessarily suitable for this type of configuration. Dike configurations are closer to broad-crested weir.

Another element of the answer could come from the different hypotheses considered. It should also be mentioned that certain assumptions were made in the model elaboration, such as taking the breach geometry from a longitudinal section in the middle of the dike. Thus, the 1D geometry used for the breach is an average estimation of the breach geometry observed. The complexity of the flows through the breaches may question the validity of these formulations in experiments with dynamic breach openings.

A final element of the answer could concern the physical principles of flow through breaches. The different models used approximate some principles of breach flows. The complexity of this type of flow is perhaps oversimplified by the use of very basic models that take into consideration empirical formulations of the breach discharge coefficient.

Finally, many elements could explain the results obtained by the spatially-distributed model. Some preliminary answers allow initiating a discussion on the results obtained.

There is no impact of the implementation of the formulations on the results. In other words, the alternatives tested on Mignot et al. (2020) experiments (Op1) do not change the results obtained on Rifai (2018) experiments.

The relevance of the hydraulic variables knowledge during the stationary phase is not negligible. The lumped model provides good information concerning this phase. On the other hand, the spatially-distributed model underestimates the discharge through the breach during this phase and considerably overestimates the water depths. In reality, the underestimation of this discharge can be dangerous (even if it remains moderate). Indeed, if the 1D model was used to estimate the volume passing through the breach and entering the floodplain, it turns out that the estimations would be underestimated. This may not be a problem in a sparsely populated area such as a field area. However, if the dike breach occurs in an urbanized area, the lack of knowledge of the breach discharge in the stationary phase can have much more dramatic consequences. An underestimation of the discharge would suggest a lower level of risk when in fact it is potentially higher.

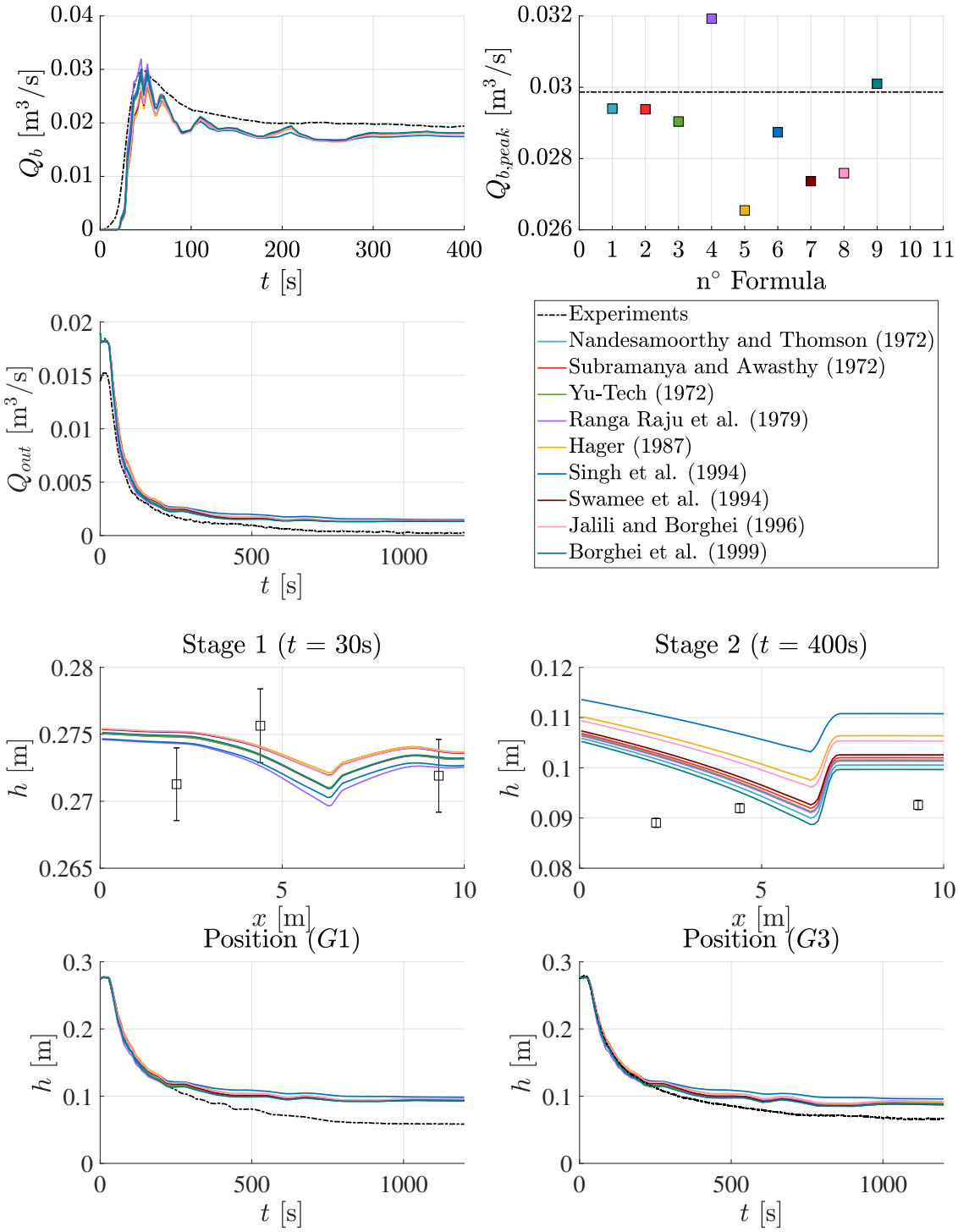

Figure 5.60: Test 1 numerical results (1D model): time evolution of breach discharge, outlet discharge and water depths at G1 and G3 positions; water depth profiles during specific time included in stage 1 and stage 2.

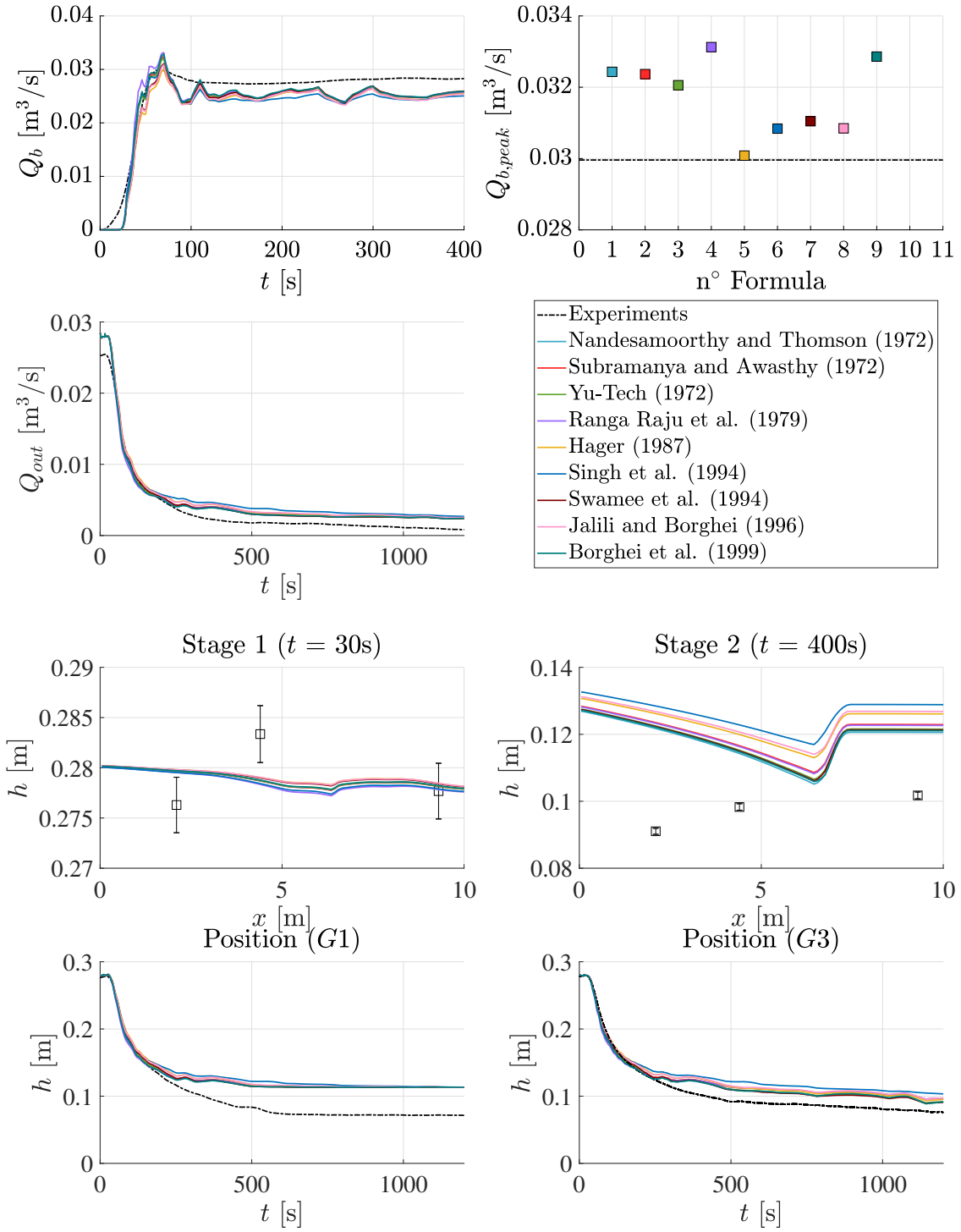

Figure 5.61: Test 4 numerical results (1D model): time evolution of breach discharge, outlet discharge and water depths at G1 and G3 positions; water depth profiles during specific time included in stage 1 and stage 2.

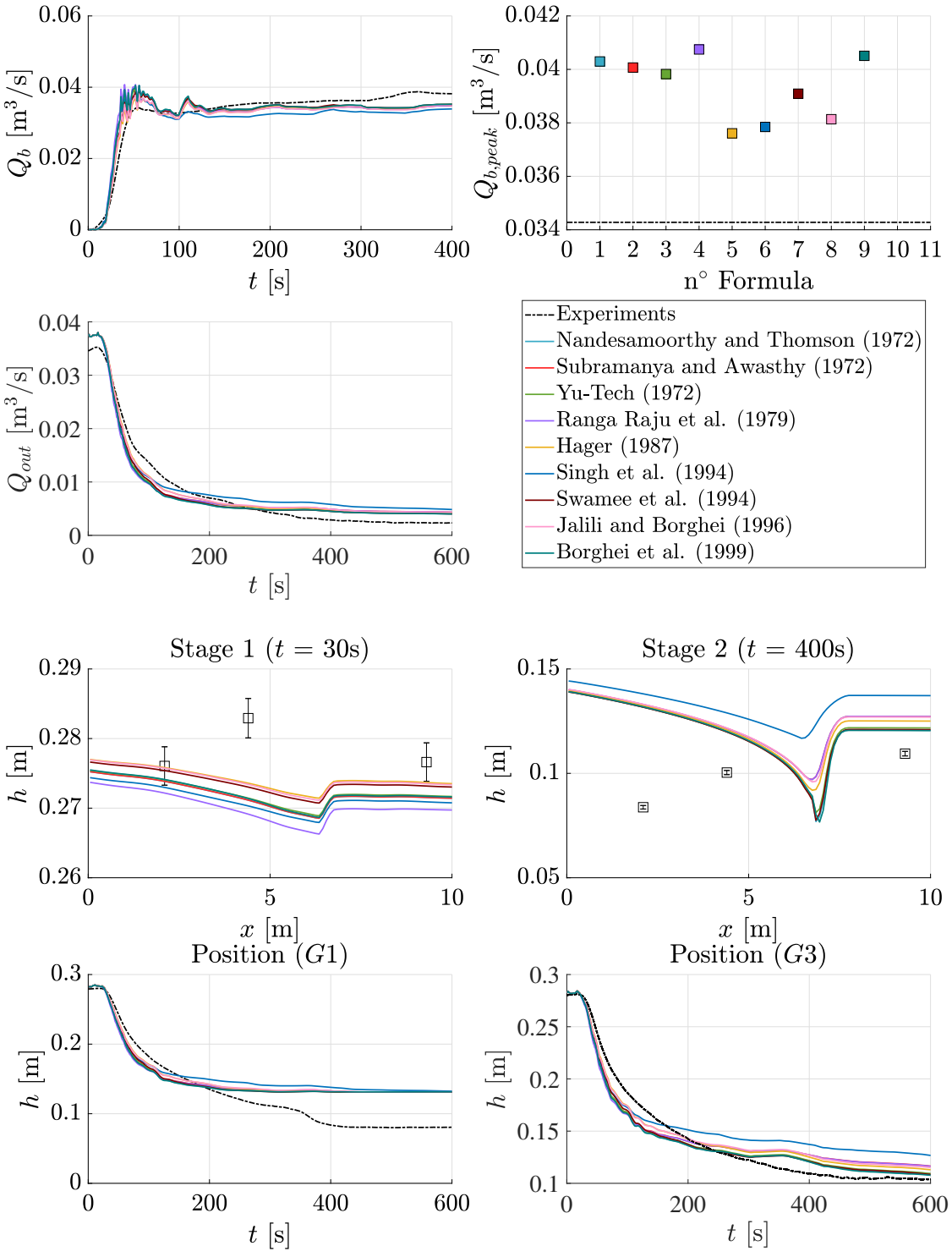

Figure 5.62: Test 8 numerical results (1D model): time evolution of breach discharge, outlet discharge and water depths at G1 and G3 positions; water depth profiles during specific time included in stage 1 and stage 2.

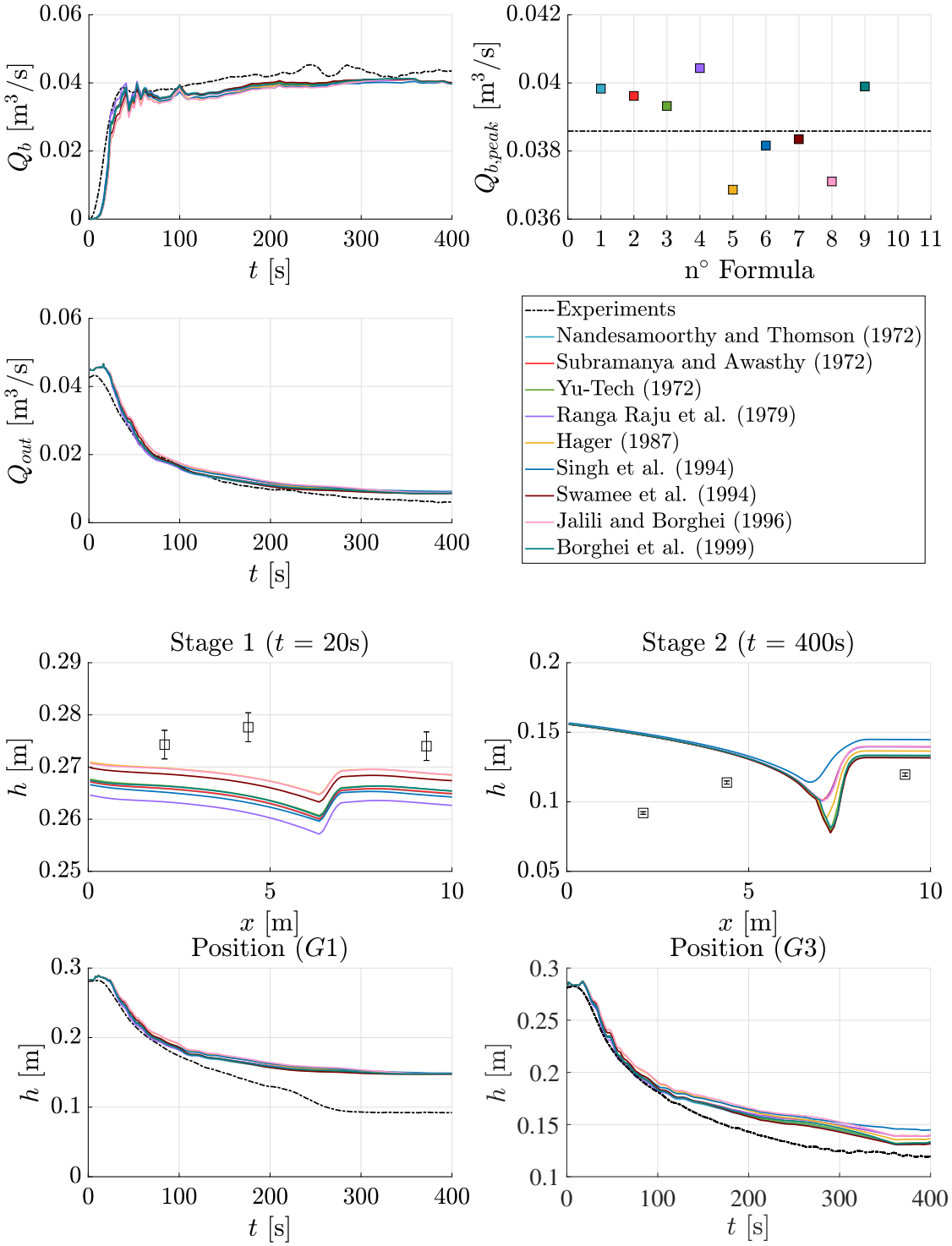

Figure 5.63: Test 11 numerical results (1D model): time evolution of breach discharge, outlet discharge and water depths at G1 and G3 positions; water depth profiles during specific time included in stage 1 and stage 2.

5.3.2 Sensitivity analysis

In any model, different parameters are not accurately known. Therefore, these parameters are considered to be subject to a certain degree of uncertainty. In the chapter detailing the different reference data, the level of uncertainties in different experimental measurements such as the water depth or the breach discharge was already outlined. In addition to the uncertainties in experimental measurements, other parameters of the numerical models can be also subject to uncertainties.

Through this section, uncertainties and their influence on the model results are examined. In other words, attention is focused on how do models react if the value of certain input parameters changes slightly.

This approach is called sensitivity analysis. This analysis is used to check whether differences between numerical and experimental results can be explained by the presence of these uncertainties in the input parameters.

Methodology

The methodology used to conduct the sensitivity analysis can be divided into 3 main steps. This is illustrated in FIGURE 5.64.

Firstly, the parameters to be varied must be determined. This step makes it possible to target the various parameters that may have an influence on the results. A concrete example is the channel inlet discharge. This is characterized by a known degree of uncertainty. In fact, the probes used to take measurements have a known level of uncertainty. Once the various parameters have been selected, a probability distribution must be assigned to each of them.

Secondly, knowing the probability distribution for each of the input parameters (or variables) considered, a very large number of random draws must be made on each of the parameters: this is the Monte Carlo method. This method consists of carrying out a large number of simulations on each of the parameters (law of large numbers theory).

Finally, the last step is to use a method to highlight the importance of uncertain input parameters. This method, based on the variance, is characterized by the significance descriptor (Arnst and Ponthot, 2014).

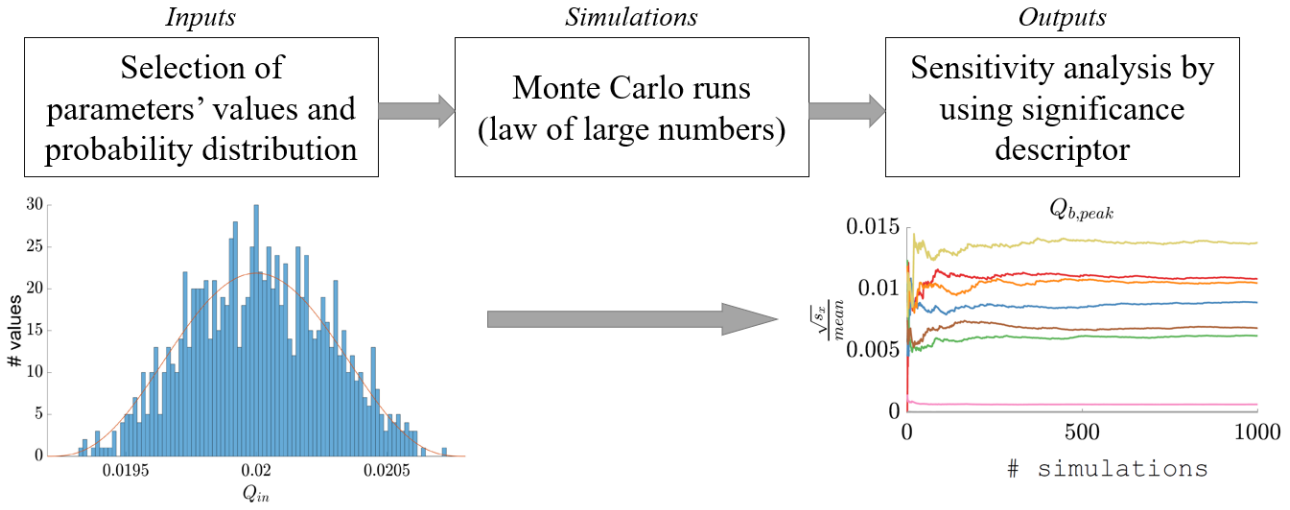

Figure 5.64: Main steps of the sensitivity analysis.

Probability distribution

Each variable is characterized by a most likely value. Once this reference value is known, it is necessary to fix the limits of the value interval in which the variable can vary, also called variation range. For example, if the input discharge is 0.02 m^3/s with an uncertainty of $\pm$ 4%, the reference value is 0.02 and the variation range is [0.0192;0.0208].

In addition to the reference value and the range of variation, the parameter α of the Beta law must also be provided. With all these terms, it is then possible to generate a probability density function (PDF). All PDF are based on a Beta distribution function. This choice can be motivated by the fact that the value taken by an input variable is considered independent of the values taken by the other variables. In this context, the generated PDF is also independent. Moreover, the Beta law is a law commonly used in the statistical field and allows having a closed support. Mathematically, the generated PDF is expressed as:

$$PDF(x,\alpha,\beta) = \frac{x^{\alpha-1}(1-x)^{\beta-1}}{B(\alpha,\beta)} \quad \text{with} \quad x = \frac{z-z_1}{z_2-z_1} \tag{5.1}$$

where x is the normalized form of the variable of interest, α and β, the positive real parameters (fixed), B the Beta function, z the non-normalized variable of interest, z_1 the minimal limit of the variation range and z_2 the maximal limit of the variation range[5].

The Beta function is expressed as:

$$B(\alpha,\beta) = \frac{\Gamma(\alpha)\Gamma(\beta)}{\Gamma(\alpha+\beta)} \quad \text{with} \quad \Gamma(w) = \int_0^\infty t^{w-1}e^{-t}dt \tag{5.2}$$

with $Re(w) > 0$.

The value of the parameter β is obtained simply by taking into account that the reference value must be the one with the maximum probability of occurrence. Therefore, to find β, the following equation must be solved:

$$\left.\frac{dPDF(x,\alpha,\beta)}{dx}\right|_{x_{ref}\in]0;1[} = 0 \tag{5.3}$$

An example of the resulting probability density function is given in FIGURE 5.65 ($z = 0.02$, $z_1 = 0.0192$, $z_2 = 0.0208$, $\alpha = 4$). This is the variable representing the inlet discharge. In this figure, the blue bars are the histogram of draws based on the Beta distribution constructed. The orange continuous curve represents the PDF constructed based on the Beta law. In the figure, the limits of the range of variations calculated previously are clearly visible. Moreover, the reference value is well located at the center of the distribution (i.e. the probability to obtain this value is maximum).

[5]The variation range is defined as: $[z_1; z_2]$.

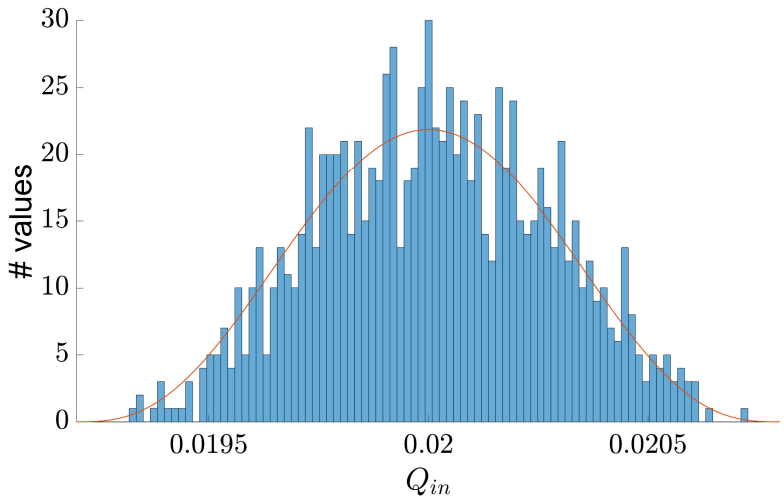

Figure 5.65: Example of the generated PDF (in orange) and the distribution of the thousand random draws made (blue bars), here for the inlet discharge.

Parameter's value selection

Once all PDF have been generated for each of the variables considered, it is necessary to be able to select a variable value at random (see blue bars in FIGURE 5.65). To do this, the cumulative density function (CDF) is used. A random value is then generated (corresponding to the probability of the variable). Then, *via* the CDF, it is quite easy to find the normalized form of the variable. In reality, the inverse of the CDF must be used. An illustration of this process is shown in FIGURE 5.66. After that, knowing the normalized form of the variable, the value of the non-normalized parameter can be found. Mathematically, these operations are written as follows:

$$x = CDF^{-1}(y) \quad \text{with} \quad y \in [0;1], u.d. \tag{5.4}$$

$$z = x \cdot (z_2 - z_1) + z_1 \tag{5.5}$$

where y is a generated random value corresponding to the parameter probability and CDF^{-1} the inverse CDF function.

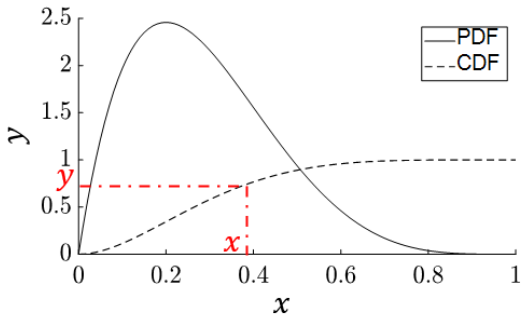

Figure 5.66: Method used to transform random value y to normalized form parameter by using CDF^{-1}.

Details of the calculation procedure

Knowing the number of simulations performed as well as the number of parameters subject to uncertainties, it is possible to generate ν sets of parameter values. These are the reference sets. For each parameter, a vector of length equal to the number of simulations thus contains the various possible values of the parameter. Then, for each variable, the generation of ν new sets of parameter values, for which only the value of the parameter of interest is modified, is proceeded. These are the comparative sets. These explanations are illustrated in FIGURE 5.67. Over the course of the various parameters and the number of simulations, the output parameter(s) are calculated with the chosen input parameter values (1 modification at a time).

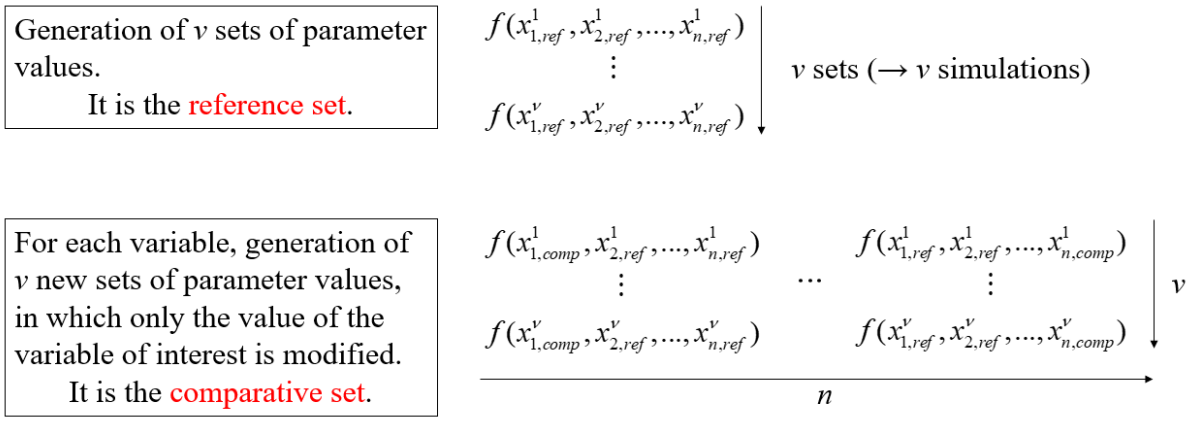

Figure 5.67: Calculation procedure where ν is the number of simulations only for 1 parameter change, n the number of considered parameters, ref refers to the reference parameters, *comp* refers to the computed parameters.

Significance descriptor

The final step of the sensitivity analysis is the computation of the significance descriptor (s_X). The significance descriptor is defined as the tool for gauging the importance of the input variables on the output variables (Arnst and Ponthot, 2014). This indicator enables the relative importance of inputs to be assessed. In other words, the larger the indicator, the larger the variability of the outputs relative to the uncertainties of the corresponding input variables.

The general expression of the importance descriptor is given in the Arnst and Ponthot (2014) publication. However, the numerical integration of such an equation requires excessive computational cost. The variance-based methods, however, avoid this problem by using a total variance law (Arnst and Ponthot, 2014). Therefore, the simplified expression of the performance descriptor can be expressed as:

$$s_{X^j} \approx s^\nu_{X^j} = \frac{1}{2\nu} \sum_{l=1}^{\nu} \left(f\left(x^l_{j,\,\text{comp}}, x^l_{[1,\ldots,j-1,j+1,\ldots,n],ref}\right) - f\left(x^l_{[1,\ldots,n],ref}\right)\right)^2 \tag{5.6}$$

where j is the parameter considered or a set of parameters, ν the number of simulations only for one parameter change[6].

[6]The total number of simulations is equal to $(1+n)\cdot\nu$.

Results

The sensitivity analysis was conducted on the two numerical models implemented. For each of them, the methodology described above was applied.

For each analysis, a detailed description of the parameters tested is provided. This description summarizes the parameters, as well as their signification and their reference value.

An illustration of the probability density function for each parameter is also provided to give a detailed graphical representation of each input parameter. In addition to the PDF, a distribution of random draws based on the Beta law (histogram) is also presented.

Finally, a figure illustrating the convergence of the significant descriptor of the considered output variable is provided and analyzed in relation to the input parameters.

Lumped model

In the sensitivity analysis, only one discharge coefficient formulation and one test were considered. A reference formulation and a test had to be taken for this analysis. Nandesamoorthy and Thomson (1972) formulation and Test 1 were chosen as references. Another formulation or test could have been chosen. This is an arbitrary choice.

A total of 8 input parameters have been selected, which can be divided into two categories: parameters related to hydraulic variables and parameters related to the test geometry. A description of each parameter and the values associated with these parameters is given in Table 5.4. The probability density functions are also given in Figure A.7 (Appendix A.2). These values have been chosen in a reasonable way to have the most realistic range possible. For each input parameter, the alpha parameter used in the beta law is identical and equals 4 (i.e. $\alpha = 4$). A certain amount of subjectivity is involved in these choices. Therefore, these choices can be discussed and/or challenged. Nevertheless, it seems that the ranges and distribution of values remain acceptable. As there are 8 input parameters and the number of simulations considered for each parameter is 1000, a total of $(1 + 8) \cdot 1000 = 9000$ simulations were carried out.

Figure 5.68 shows the results after simulations. These corresponding graphs show the convergence of the output variables given the large number of simulations[7]. To better interpret the results, a normalized version of the significant descriptor was used. This new form expresses in fact the observed standard deviation normalized by the mean value of the variable ($\sqrt{s_x}/mean$).

Three output variables were considered: the peak breach discharge, the time at which this discharge occurs and finally the average water depth computed by this numerical model. The exact values of the normalized significant descriptor are provided in Table 5.5. Based on Figure 5.68 and Table 5.5, the results were analyzed.

[7]The significant descriptor for the time at which the peak breach discharge occurs is not converged for any of the input parameters. These results are consequently not usable. The reason for this non-convergence is that two breach discharge peaks are quite close. When some parameters change, the maximum peak can be shifted between the two peak positions. The result is an alternating shift between the two peaks, which explains why convergence is not achieved.

		Symbol	Units	Description	Reference value	Variation range
Parameters	Hydraulic	y_0	m	Initial water depth	0.275	$[0.95 \cdot 0.275; 1.05 \cdot 0.275]$
		Q_{in}	m^3/s	Inlet discharge	0.020	$[0.96 \cdot 0.020; 1.04 \cdot 0.020]$
		Q^*_{out}	-	Coefficient applied on the outlet discharge coefficient	1	$[0.96 \cdot 1; 1.04 \cdot 1]$
		$Q_{d,max}$	-	Coefficient applied on the maximum drainage discharge	1	$[0.96 \cdot 1; 1.04 \cdot 1]$
		k	-	Coefficient applied on the calibrated parameter to compute drainage discharge	1	$[0.95 \cdot 1; 1.05 \cdot 1]$
	Geometrical	L^*_{breach}	-	Coefficient applied on the breach length	1	$[0.95 \cdot 1; 1.05 \cdot 1]$
		z^*_{breach}	-	Coefficient applied on the breach height	1	$[0.95 \cdot 1; 1.05 \cdot 1]$
		P	-	Percentile parameter used to define the breach height	25	$[15; 35]$

Table 5.4: Description of the different input parameters used in the 0D model sensitivity analysis. The reference value of the maximum drainage discharge ($Q_{d,max}$) was set at $1.5 \cdot 10^{-3}$ m^3/s and the calibrated parameter (k) at 0.7. The corresponding coefficients mentioned in the table are applied to these reference values.

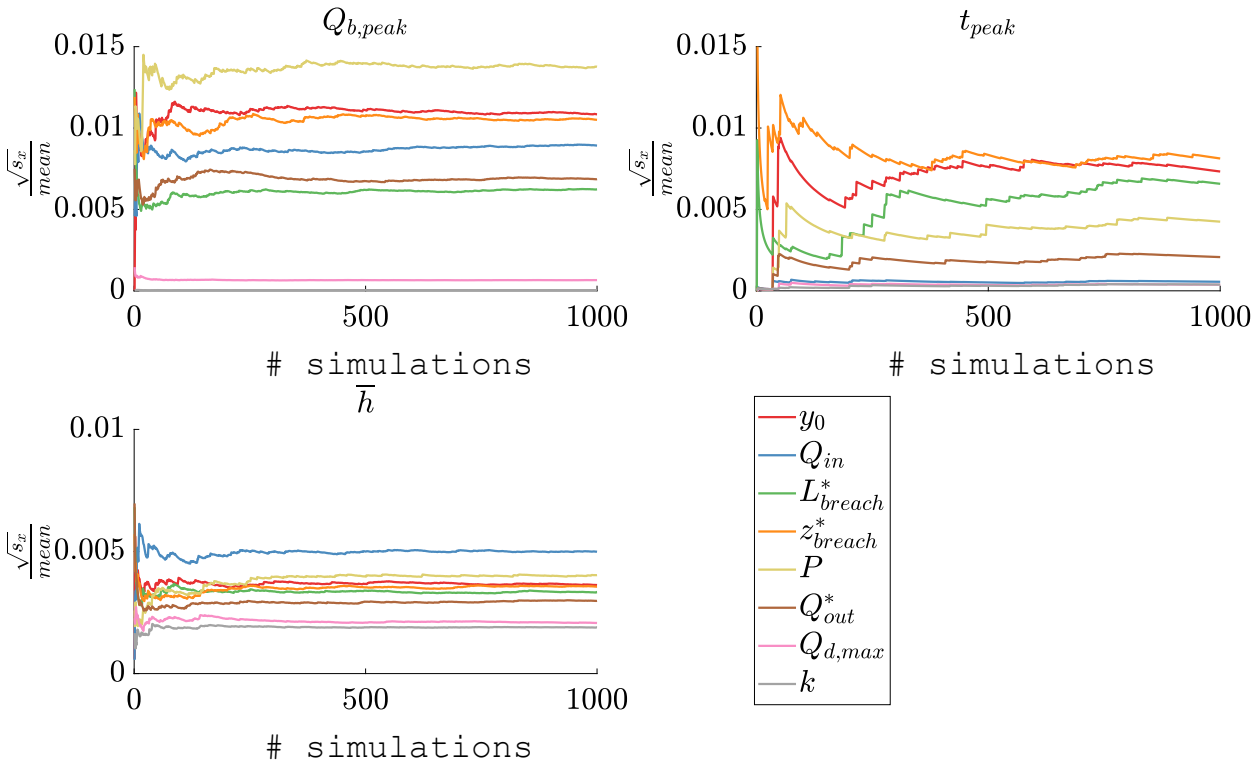

Figure 5.68: Convergence of the normalized form of the significant descriptor for the 3 selected output variables (0D model).

$Q_{b,peak}$ [%]		t_{peak} [%]		$\overline{h}$ [%]	
P	1.38	z^*_{breach}	0.81	Q_{in}	0.50
y_0	1.09	y_0	0.73	P	0.40
z^*_{breach}	1.05	L^*_{breach}	0.66	y_0	0.36
Q_{in}	0.89	P	0.43	z^*_{breach}	0.36
Q^*_{out}	0.69	Q^*_{out}	0.21	L^*_{breach}	0.33
L^*_{breach}	0.62	Q_{in}	0.056	Q^*_{out}	0.30
$Q_{d,max}$	0.066	k	0.039	$Q_{d,max}$	0.21
k	0.0041	$Q_{d,max}$	0.038	k	0.19

Table 5.5: Normalized significant descriptor results for the 3 selected output variables (0D model).

The analysis of the results shows quite different things. TABLE 5.5 shows the parameters influencing the results in order of importance. This order is also visible in the convergence graph (FIGURE 5.68).

The uncertainties in drainage parameters do not affect the investigated variables. Indeed, these parameters have the lowest normalized significant descriptor values. Physically, the impact of the drainage as such is low because the drainage discharge are very low compared to the inflow and outflow.

For each variable, the results of the sensitivity analysis are detailed individually below:

- Peak breach discharge: uncertainty in peak breach discharge is mainly influenced by the percentile uncertainties (1.38%). Uncertainties in water depth are the second most important parameter influencing the breach discharge (1.09%). The uncertainties in breach depth parameter influence similarly the results (1.05%). Then come the parameters influencing the discharges (inlet and outlet) and the parameter related to the breach width. The uncertainties on these parameters influence the peak breach discharge less than the 1%.

- Time of peak breach discharge: as previously mentioned, the results obtained are not converged and are therefore unusable.

- Average water depth: the uncertainties in inlet discharge influence the most the results (0.5%). Uncertainties in the percentile parameter, initial water depth, geometrical breach parameters similarly influence the normalized significant descriptor ($\approx 0.4\%$). Next is the outlet discharge parameter (0.3%).

Overall, the hydraulic variables of interest (i.e. peak breach discharge and average water depth) respectively have a maximum difference of 1.38 and 0.5% compared to the mean values. These differences are quite low (i.e. of the order of 1%). These results are quite encouraging. Even if the parameters of the model are not known with precision, the results obtained do not vary significantly. This shows that the lumped model is not very sensitive to uncertainties in the input data. However, the results described are only valid for the experimental context. These conclusions are also based on the assumptions made regarding the reference values and the validity ranges of the input parameters (TABLE 5.4). In practice, other ranges of values should be used. Thus, the assumptions used are quite different which can lead to completely opposite conclusions.

In order to confirm the results obtained, the sensitivity analysis was repeated by changing the alpha parameter characterizing the Beta law from 4 to 10. By taking this parameter to a larger value, the PDF tends to re-center its peak around the most probable value and to decrease the width of the curve. This means that there are no randomly drawn values near the extremity bounds. The general consequence of this change in alpha parameter is a decrease in the range of randomly drawn values. The probability density functions are given in FIGURE A.8 (Appendix A.2).

The results are presented in FIGURE 5.69, which shows the same tendency of the uncertainties of the input parameters on the uncertainties of the output variables as in the sensitivity analysis with a lower alpha. Indeed, the order of importance of the parameters is quite identical in both cases (with high or low alpha). The change in the alpha parameter therefore has no significant influence on the order of the influencing parameters. Another conclusion drawn from this new analysis is that the normalized significant descriptor is lower for high alpha. This is quite logical as the range of values taken by the input parameters is reduced in this case. If the range of values is smaller, the variation of these parameters is also smaller, which can explain the lower normalized form of the significant descriptor.

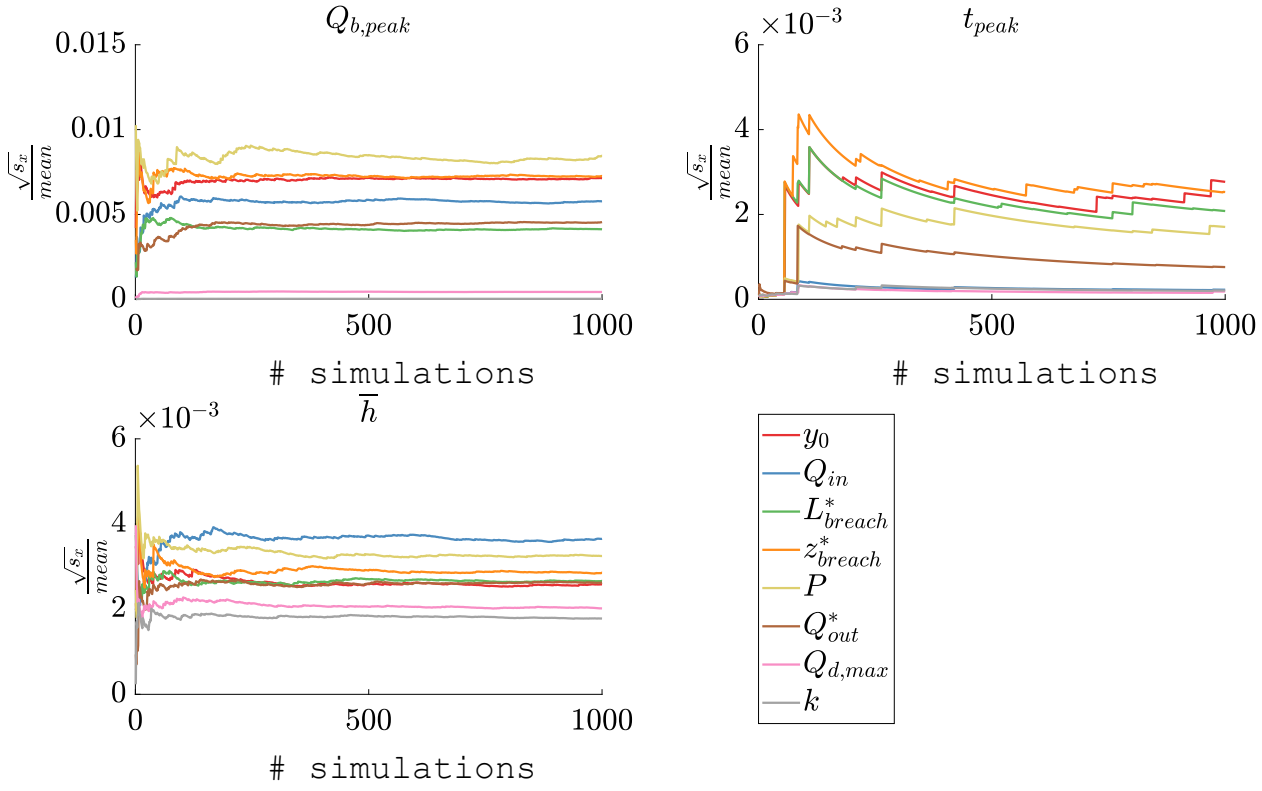

Figure 5.69: Convergence of the normalized form of the significant descriptor for the 3 selected output variables (0D model) with $\alpha = 10$.

Spatially-distributed model

As for the lumped model, only one discharge coefficient formulation and one test were considered. For the sake of consistency, the same formulation and the same test have been chosen for this new sensitivity analysis on the spatially-distributed model.

The same number of input parameters is used in this sensitivity analysis (8 input parameters). The parameters used are mainly those used in the analysis of the lumped model. However, two parameters are different. Indeed, the spatially-distributed model does not use the breach width or the percentile parameter. Two other parameters were used to replace these. These new parameters are respectively the Manning coefficient and the channel width. TABLE 5.7 shows the parameters used, their description and the values used for them. As the input parameters are close to the 0D model, the alpha parameter of the Beta law used was considered identical to that used in the lumped model (i.e. $\alpha = 4$). The probability density functions associated with the input parameters are given in FIGURE A.9 (Appendix A.2).

In total, 8 output variables were considered: the peak breach discharge, the time at which this peak occurs[8], the water depths at the different positions during a time in stage 1 on the one hand and stage 2 on the other hand.

As the 1D model takes longer to run than the 0D model and the results of the sensitivity analysis of the lumped model stabilize with 500 simulations, the number of simulations was reduced. The number of simulations considered for each parameter is 500, which gives a total of $(1 + 8) \cdot 500 = 4500$ simulations.

FIGURES 5.70, 5.71 and 5.72 illustrate the results obtained on the output variables in terms of normalized significant descriptor according to the uncertainties of the input variables. These graphs are convergence graphs which allow highlighting the relevance of the results.

The order of importance of the influence of the output variables according to the uncertainties in the input parameters is directly visible in the corresponding figures. TABLES 5.70, 5.71 and 5.72 also provide this information and also give the exact values of the normalized significant descriptor.

Before detailing the influence of the uncertainties of the input parameters on each output variable individually, a general conclusion can be drawn. The uncertainties in the parameters related to the drainage discharge are, as for the lumped model, barely influential.

A detailed description of the sensitivity analysis for each output variable considered is given below:

- Peak breach discharge: the uncertainty in the peak breach discharge is more related to the uncertainties in the height of the breach bottom as well as in the initial water depth ($\approx 1.3\%$). The uncertainties in the inflow and outflow are less influential than the previous parameters ($\approx 0.8\%$). The uncertainties in the width of the channel bottom is even less influential ($\approx 0.3\%$). Uncertainties in the Manning coefficient influence the peak breach discharge in the same way as the drainage flow parameters ($< 0.1\%$).
- Time of peak breach discharge: as previously stated, the results obtained are not converged and are therefore unusable. Nevertheless, it seems that the most influential parameters are the same as for the peak breach discharge.

[8]The same comment regarding the convergence of the results described for the lumped model is valid for the spatially-distributed model. The results are then unusable.

- Water depth at stage 1: the water depth at stage 1 is mainly influenced by uncertainties in the initial water depth ($\approx 0.85\%$). Uncertainties in the inlet and outlet discharges and in the depth at the bottom of the breach are for times less influential than the uncertainties in the initial depth ($\approx 0.2\%$). The uncertainties in the other input parameters have almost no influence on the water depth at stage 1 ($< 0.025\%$).

- Water depth at stage 2: the uncertainties in the bottom depth of the breach are the uncertainties giving the largest variation in water depth at stage 2 ($\approx 0.65\%$). The uncertainties in the inlet discharge and the Manning coefficient are, respectively, the second and third most influential parameters. Uncertainties in the other input parameters have only a limited influence on the water depth at stage 2 ($< 0.1\%$).

The analyses made on the results of the sensitivity analysis show that the selected output variables are influenced differently by the uncertainties of the input parameters. Indeed, each of the variables has a precise order on the influence of the uncertainties in the input parameters. The maximum uncertainties in the output variables are presented in Table 5.6.

	Stage 1	Stage 2
$Q_{b,peak}$ [%]	h_{Gi} [%]	h_{Gi} [%]
1.33	0.99	0.70

Table 5.6: Maximum value of the normalized significant descriptor for the different output variables (1D model).

The order of magnitude of the significant descriptor is similar to the one derived from the sensitivity analysis of the 0D model (i.e. $\approx 1\%$). Therefore, the uncertainties in the peak breach discharge ($< 1.33\%$) are smaller than the uncertainties in the inlet discharge ($\pm 4\%$). The maximum uncertainties in the water depths are of the same order of magnitude as the corresponding measurement uncertainties ($\pm 1\%$).

The conclusions drawn for the lumped model are transferable to the spatially-distributed model: in the experimental context and given the assumptions made, the uncertainties in the input parameters have a limited influence on the output variables. This means that even if one of the input parameters is not known accurately, the output variables considered are known with a correct accuracy (as long as the assumptions made are satisfied and the model is used in the experimental context considered).

It is clear that the other parameters could have been tested in this sensitivity analysis. Other output variables could also have been tested. Nevertheless, this analysis enabled for the consideration of a number of interesting input parameters as well as many output variables. This analysis gives an idea of the influence of the uncertainties in the input parameters on the output variables.

		Symbol	Units	Description	Reference value	Variation range
Parameters	Hydraulic	y_0	-	Coefficient applied on the initial water depth	1	$[0.95 \cdot 1; 1.05 \cdot 1]$
		Q_{in}	-	Coefficient applied on the inlet discharge	1	$[0.96 \cdot 1; 1.04 \cdot 1]$
		Q^*_{out}	-	Coefficient applied on outlet discharge coefficient	1	$[0.96 \cdot 1; 1.04 \cdot 1]$
		$Q_{d,max}$	-	Coefficient applied on the maximum drainage discharge	1	$[0.96 \cdot 1; 1.04 \cdot 1]$
		k	-	Coefficient applied on the calibrated parameter to compute drainage discharge	1	$[0.95 \cdot 1; 1.05 \cdot 1]$
		n	-	Coefficient applied on the Manning coefficient	1	$[0.8 \cdot 1; 1.15 \cdot 1]$
	Geom.	z^*_{breach}	-	Coefficient applied on the breach height	1	$[0.95 \cdot 1; 1.05 \cdot 1]$
		l^*_{bed}	-	Coefficient applied on the channel bottom width	1	$[0.95 \cdot 1; 1.05 \cdot 1]$

Table 5.7: Description of the different input parameters used in the 1D model sensitivity analysis. The reference value of initial water depth (y_0) was set at 0.275 m, the inlet discharge (Q_{in}) at 0.020 m^3/s, the maximum drainage discharge ($Q_{d,max}$) at $1.5 \cdot 10^{-3}$ m^3/s, the calibrated parameter (k) at 0.7 and the Manning coefficient at 0.018 $s/m^{1/3}$. The corresponding coefficients mentioned in the table are applied to these reference values.

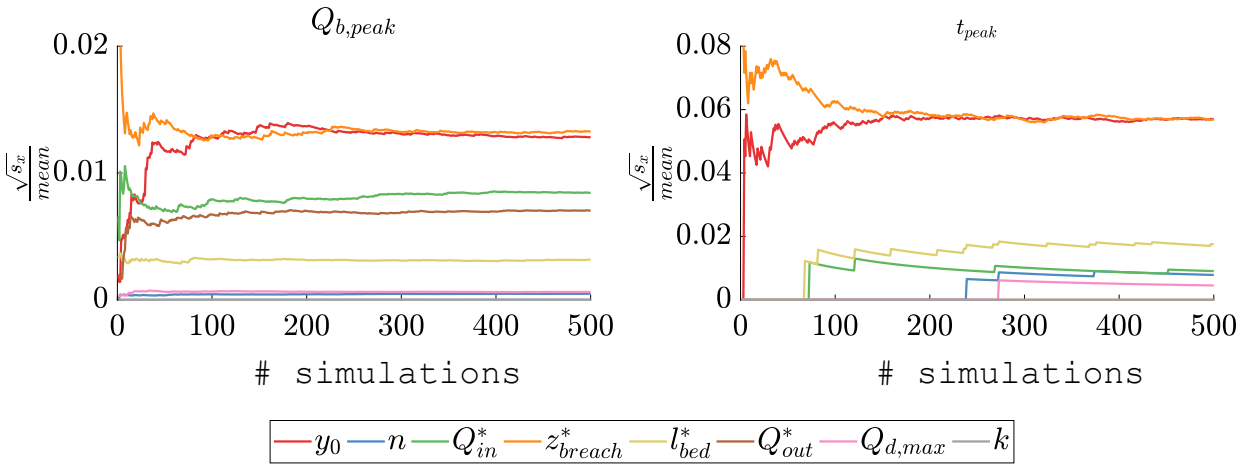

Figure 5.70: Convergence of the normalized significant descriptor results for peak breach discharge and the time at which it occurs (1D model).

$Q_{b,peak}$ [%]		t_{peak} [%]	
z^*_{breach}	1.33	y_0	5.71
y_0	1.28	z^*_{breach}	5.68
Q_{in}	0.84	l^*_{bed}	1.75
Q^*_{out}	0.71	Q_{in}	0.91
l^*_{bed}	0.32	n	0.79
$Q_{d,max}$	0.062	$Q_{d,max}$	0.45
n	0.048	Q^*_{out}	0
k	0.0032	k	0

Table 5.8: Normalized significant descriptor results for the peak output variable (1D model).

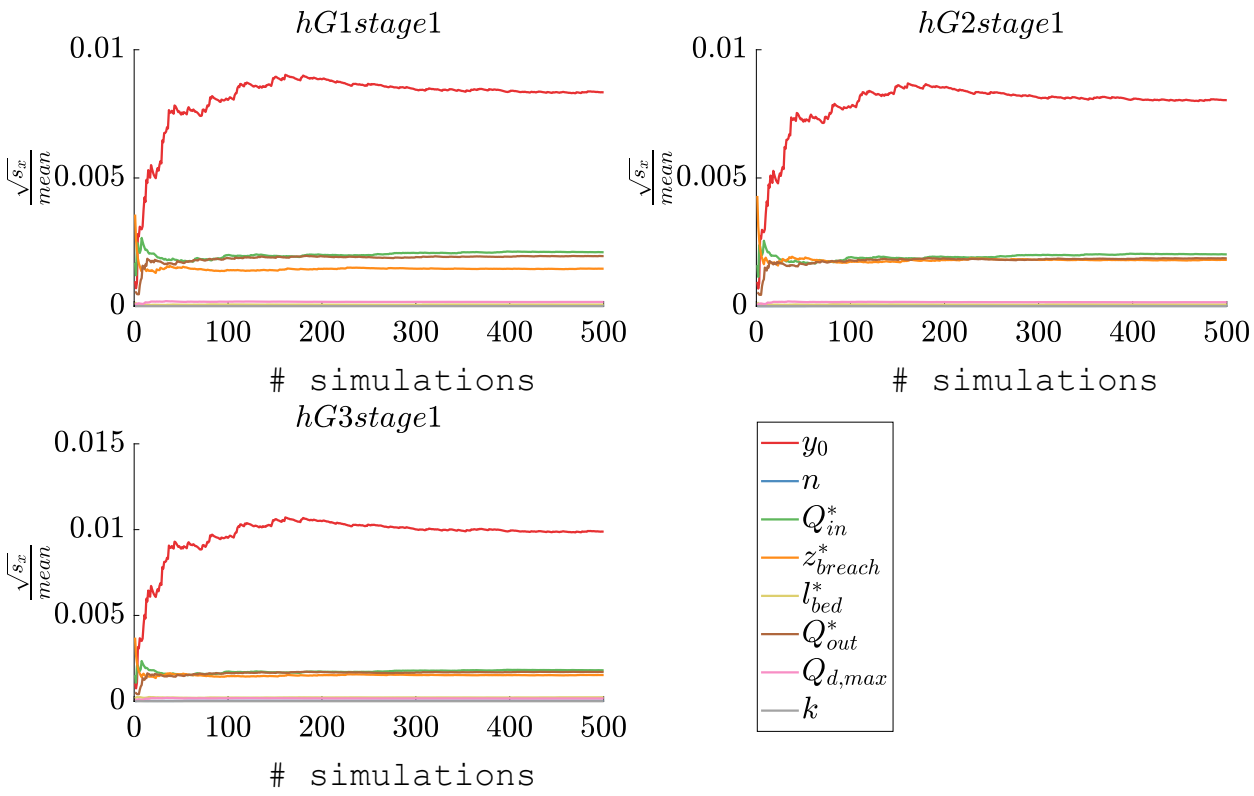

Figure 5.71: Convergence of the normalized significant descriptor results for water depth at different positions during stage 1 (1D model).

Stage 1					
h_{G1} [%]		h_{G2} [%]		h_{G3} [%]	
y_0	0.83	y_0	0.80	y_0	0.99
Q_{in}	0.21	Q_{in}	0.20	Q_{in}	0.18
Q^*_{out}	0.20	Q^*_{out}	0.19	Q^*_{out}	0.17
z^*_{breach}	0.15	z^*_{breach}	0.18	z^*_{breach}	0.15
$Q_{d,max}$	0.017	$Q_{d,max}$	0.016	l^*_{bed}	0.023
l^*_{bed}	0.0064	l^*_{bed}	0.0067	$Q_{d,max}$	0.016
n	0.0026	n	0	n	0.0029
k	0	k	0	k	0

Table 5.9: Normalized significant descriptor results for the water depth at stage 1 (1D model).

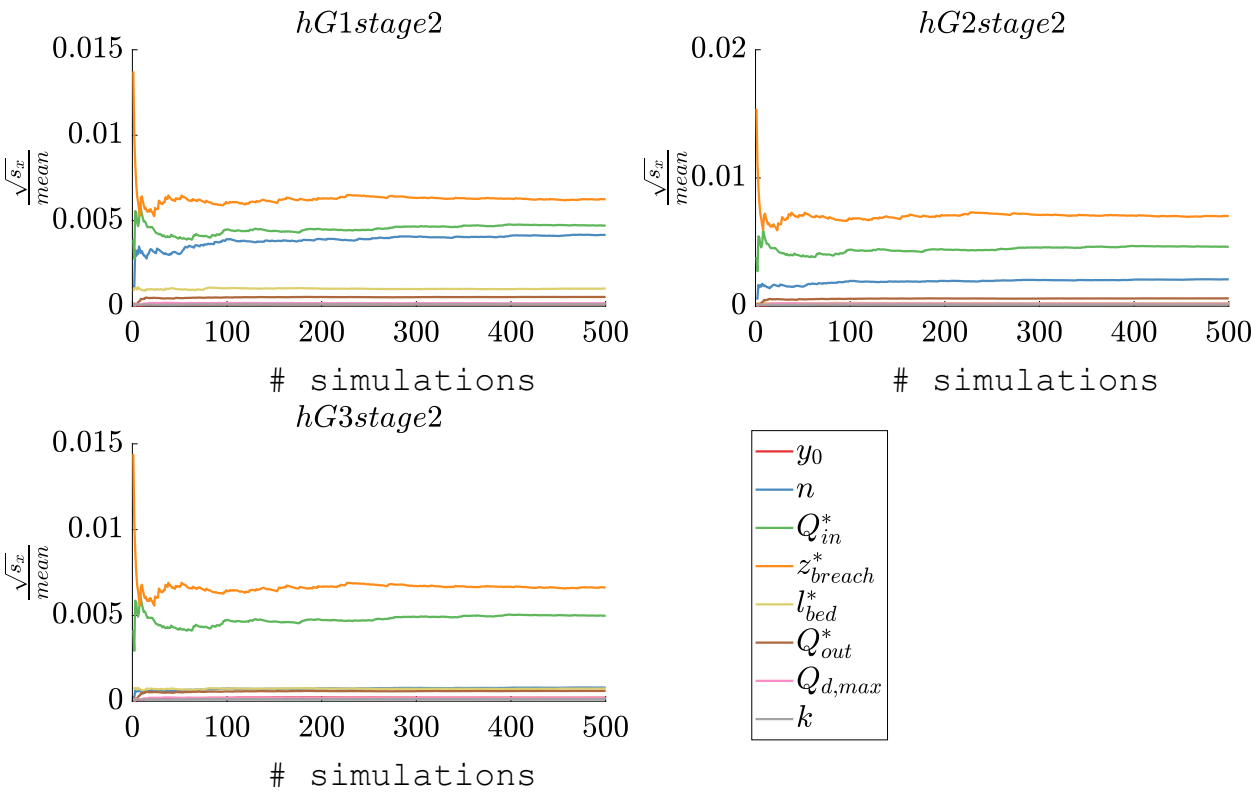

Figure 5.72: Convergence of the normalized significant descriptor results for water depth at different positions during stage 2 (1D model).

Stage 2					
h_{G1} [%]		h_{G2} [%]		h_{G3} [%]	
z^*_{breach}	0.63	z^*_{breach}	0.70	z^*_{breach}	0.66
Q_{in}	0.47	Q_{in}	0.46	Q_{in}	0.50
n	0.42	n	0.21	n	0.080
l^*_{bed}	0.10	Q^*_{out}	0.061	l^*_{bed}	0.074
Q^*_{out}	0.054	l^*_{bed}	0.024	Q^*_{out}	0.060
$Q_{d,max}$	0.017	$Q_{d,max}$	0.020	y_0	0.020
k	0.012	y_0	0.015	$Q_{d,max}$	0.019
y_0	0.011	k	0.013	k	0.012

Table 5.10: Normalized significant descriptor results for the water depth at stage 2 (1D model).

5.4 Overview of the results

Having established the analysis and discussion of the results, it seems appropriate to synthesize the different points described earlier. For this purpose, FIGURE 5.73 represents a summary of the studies carried out. It highlights the most effective and least effective formulations associated with the corresponding numerical model for each test. Accurate formulae are highlighted by a check mark (✓) and the most inaccurate ones are represented by a red cross (x). In order to draw more general conclusions, the best associations between formula and model giving results closest to the experimental results are indicated in bold shaded font.

For tests with a fixed breach geometry with zero lateral crest height, the most effective formula for predicting breach discharge is Subramanya and Awasthy (1972). For the most effective prediction, the 0D model should be used for Roger et al. (2009) and Mignot et al. (2020) Op2 tests. For Michelazzo et al. (2015) tests, the combination of this formulation with the 1D model is more relevant. For water depths, the spatially-distributed model provides more accurate results. A combination with the Yu-Tech (1972) formula is recommended for Roger et al. (2009) and Michelazzo et al. (2015) tests. The use of Hager (1987) formula is recommended for Mignot et al. (2020) Op2 experiments. For either breach discharge or depth, and for both numerical models, it is not recommend to use Singh et al. (1994) formula, as it does not allow obtaining relevant results.

For the tests with fixed breach geometry and non-zero lateral crest height, the results obtained were not sufficiently satisfactory (at least for the breach discharge). Nevertheless, the recommendations described below provide the least poor results. For the breach discharge, the use of the lumped model combined with Singh et al. (1994) formulation seems adequate. For the water depth, the 0D model combined with the Hager (1987) formula gives the best results. The 1D model does not give convincing results for this type of experiment.

For dynamic breach tests, the spatially-distributed model combined with Hager (1987) formula provides the most accurate peak breach discharge. This formula can also be used with the lumped model although the results are slightly less accurate. Ranga Raju et al. (1979) formulation should be avoided for both models. The depth obtained during stage 2 has been also analyzed. The 0D model is able to give good results. The most accurate formula is Ranga Raju et al. (1979) expression. As described above, the water depth predictions in stage 2 with the 1D model are not good. It is therefore not recommended to use this model in this context.

This synthesis finally illustrates the best combinations between formulae and models. In some cases, it appears that a formula is the most accurate for the breach discharge and the most inaccurate for the water depth (or conversely). This is the reason why it is important to consider carefully what is being looked for. Some formulations show a good general behavior. As this information is difficult to summarize, it is necessary to refer to figures highlighting the exact accuracy of the formulations (e.g. FIGURES 5.38 or 5.50).

In addition, a ranking of the formulations according to their accuracy, in terms of breach discharge, is shown in FIGURE 5.74. This figure provides an explicit representation of the performance of each formula for a specific numerical and experimental configuration. For the experimental configurations with fixed breach geometry and zero lateral crest height, Subramanya and Awasthy (1972) formula provides the best overall results. It is interesting to note that the Jalili and Borghei (1996) formula is performing quite well and consistently over the various experiments. For non-zero crest height configurations, the ranking is clear: the formulations of Singh et al. (1994), Ranga Raju et al. (1979) and Nandesamoorthy and Thomson (1972) are the most accurate formulae. For dynamic breach opening configurations, the most effective ones are those of Hager (1987), Jalili and Borghei (1996) and Singh et al. (1994).

		Roger et al. (2009)	Michelazzo et al. (2015)	Mignot et al. (2020) Op2
Q_l	0D	☑ **Subramanya and Awasthy (1972)**	☑ Subramanya and Awasthy (1972)	☑ **Subramanya and Awasthy (1972)**
		☒ Singh et al. (1994)	☒ Nandesamoorthy and Thomson (1972)	☒ Singh et al. (1994)
	1D	☑ Nandesamoorthy and Thomson (1972)	☑ **Subramanya and Awasthy (1972)**	☑ Nandesamoorthy and Thomson (1972)
		☒ Singh et al. (1994)	☒ Emiroglu et al. (2011)	☒ Singh et al. (1994)
h	0D	☑ Nandesamoorthy and Thomson (1972)	☑ Subramanya and Awasthy (1972)	☑ Ranga Raju et al. (1979)
		☒ Singh et al. (1994)	☒ Singh et al. (1994)	☒ Singh et al. (1994)
	1D	☑ **Yu-Tech (1972)**	☑ **Yu-Tech (1972)**	☑ **Hager (1987)**
		☒ Singh et al. (1994)	☒ Singh et al. (1994)	☒ Singh et al. (1994)

		Mignot et al. (2020) Op1
Q_l	0D	☑ **Singh et al. (1994)**
		☒ Borghei et al. (1999)
	1D	☑ Singh et al. (1994)
		☒ Borghei et al. (1999)
h	0D	☑ **Hager (1987)**
		☒ Singh et al. (1994)
	1D	☑ Borghei et al. (1999)
		☒ Singh et al. (1994)

		Rifai (2018)
$Q_{b,peak}$	0D	☑ Hager (1987)
		☒ Raju et al. (1979)
	1D	☑ **Hager (1987)**
		☒ Raju et al. (1979)
h STAGE 2	0D	☑ **Ranga Raju et al. (1979)**
		☒ Swamee et al. (1994b)
	1D	*Not relevant*

Figure 5.73: Identification of accurate (✓) or inaccurate (x) empirical formulae according to the numerical model used and the hydraulic variable considered for each experimental test. For each hydraulic variable of each test, a combination of the numerical model and the formulation giving the best results is also provided (bold shaded formula). The coloreds legend used for each formula throughout the thesis is also indicated.

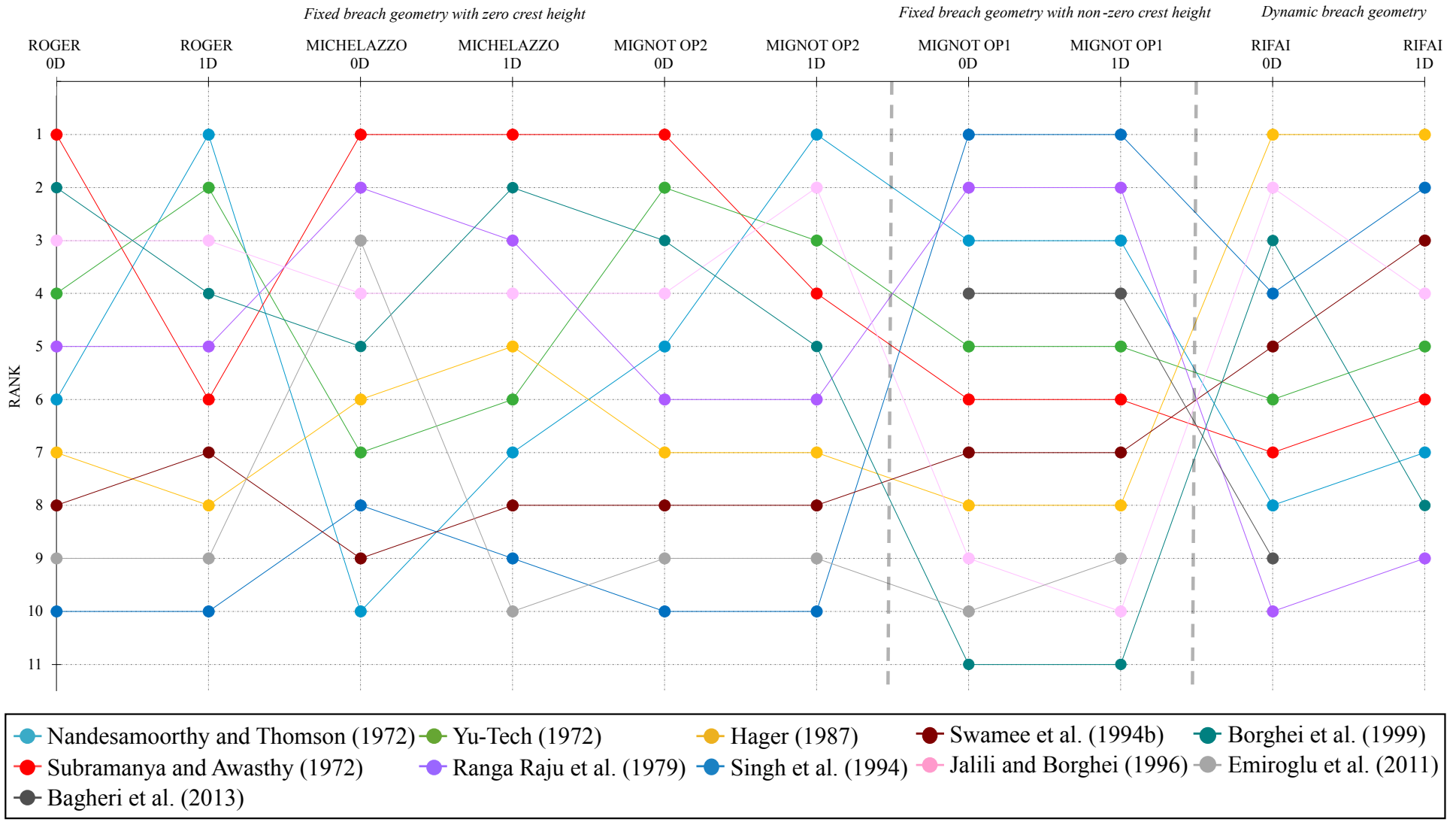

Figure 5.74: Breach discharges ranking performance of the formulations according to the test and the hydrodynamic model considered.

6 | Perspectives

Different perspectives emerge from this work.

One of the short-term perspectives of this work is to find physically meaningful modifications to the spatially-distributed model to improve the stationary phase behavior. As described in the analysis of the results, the 1D model gives remarkable results in terms of peak breach discharge and water depths during stage 1. However, in the stationary phase (stage 2), this model does not give convincing results for water depths. Further investigations of the model are required to find convincing reasons to explain this deficiency. Nevertheless, some tentative solutions have been provided in the discussion of this problem. It is possible that a limitation on the use of the formulations has been discovered. More investigations are needed to confirm this hypothesis.

It is also necessary to focus on the stationary phase of the breach development, which gives an indication of the stationary phase breach discharge. This discharge can be used to quantify the volumes of water involved in the flow through the breach and subsequently determine the impacts on the floodplain. Large discharges would result in large volumes of water. The spatially-distributed model gives an underestimation of this discharge.

A major perspective is undoubtedly the addition of a morphodynamic model to the numerical models implemented. The models used in dynamic breach opening focus only on the breach openings measured during the Rifai (2018) experiments. Therefore, it only simulates the laboratory experiments without taking into account the morphodynamic processes underlying the dike openings. It is currently impossible with the implemented models to take into account an arbitrary breach opening. This is one of the limitations of the developed numerical models.

By incorporating a morphodynamic module, the models would be much more sophisticated. Indeed, they would be able to predict the breach opening theoretically without relying on experimental measurements. One possibility may be to include a redesigned version of the Wu (2013) model as a morphodynamic module. Once this module is integrated, it will be necessary to also carry out a study of the various discharge coefficient formulations like the one carried out throughout this work.

In addition to this, the results obtained with this more complete model (integrated hydrodynamic and morphodynamic modules) could be compared with results obtained with more advanced numerical models such as *WOLF* 2D or TELEMAC-2D. By comparing these results, it underlines the different advantages and limitations of the implemented model.

7 | Conclusion

This work enabled the implementation of hydrodynamic models based on empirical formulations for the discharge coefficient at a breach in a fluvial dike. The models were evaluated against existing experimental observations of dike failure due to overtopping. Several steps were followed to achieve these objectives.

First of all, the significance of the dike failure phenomenon was highlighted by several concrete examples. The most popular example is Hurricane Katrina, which hit New Orleans in 2005 and caused dike breaches. But it is not the only one. Chapter 1 underlined many examples of dike breaches. These events prove that the dike failure phenomenon is a current and important topic.

Having demonstrated the importance of the subject through examples, a theoretical investigation was conducted. This research has enabled the presentation of the fundamental theoretical elements relating to the development of dike breaches. Fundamental notions such as the type of dike, the consequences of a breach, the breach mechanisms and their respective frequencies, as well as the different stages of breach development were highlighted throughout Chapter 2. In addition, some models that have been developed/used in recent years were also described. This section showed a non-exhaustive list of existing model examples. This supported the need to implement other numerical models to study the dynamics of dike failure.

Once the theoretical and historical bases of dike failure were established, the implementation of the different models was described (Chapter 4). Each of the numerical models is based on a purely hydraulic theory. During the development of these models, a fundamental unknown appeared: the discharge coefficient. To overcome this, empirical formulations were found in literature. These formulations have been tested and compared in the various experiments shown in this thesis.

Four independent series of experiments, comprising a total of 24 experiments, were considered. Each of the experiments was not selected by coincidence. Indeed, each experiment brought an additional specificity. The experimental set-ups used were detailed in Chapter 3. The first experiments included channel flows with a lateral opening and zero crest height. The flow conditions as well as the dimensions of the opening were different for each experiment, which made it possible to validate the models in simple situations and to test the formulations in a context close to the one used to elaborate these formulae. Then, a transition was made before moving on to the experiments with breach openings. The experiments used during this transition were aimed at validating the formulations for experiments with non-zero crest height. Finally, experimental tests close to the real observed dike failure were used.

After analyzing the results, several conclusions could be drawn, both in terms of models and formulae. For each type of test, conclusions were made. All these analyses were described in Chapter 5.

For the simple case of fixed breaches with zero lateral crest height, the results obtained with the different models are quite similar. However, the spatially-distributed model offers more advantages than the lumped model because the spatial variation of the hydraulic variables is known with this model. The lumped model does not offer this possibility. In terms of water depths, this model gives the water depth averaged over the entire length of the channel. In general, the spatially-distributed model gives better results for this kind of hydraulic variables. The lumped model, on the other hand, succeeds in predicting the breach discharge with an error below 10-15%, depending on the formula used, despite its simplicity and without calibration.

Regarding the formulations for the case of experiments with fixed breach with zero lateral crest height, formulae by Emiroglu et al. (2011) and Singh et al. (1994)) were discarded because they can lead respectively to error exceeding 30% and 60%, whereas all other formulae predict the lateral discharge with an error below 15%.

The conclusions drawn for the tests with zero lateral crest height are not valid for the experiments with non-zero crest height. In this context, the lumped model gives better results. Nevertheless, the results obtained are much less convincing than in the previous experiments. The formulations identified as effective in the tests with zero crest height are therefore less effective in the experiments with lateral crest: 20% or more error in breach discharge. There is even a radical change in the best formulation for predicting breach discharge as Singh et al. (1994) formula appears to be the most effective in this case (less than 15% error on breach discharge). In general, the results of the experiments with non-zero crest height are worse than those without crest.

The results obtained for the more complex tests with dynamic breach opening are quite convincing for the lumped model as the results almost perfectly match the experimental data. The accuracy obtained for the estimation of the breach discharge varies between 3 and 20% for the best tests. The results are quite similar for the formulations used.

The 1D model provides breach discharges closer to the experimental data than the 0D model. These vary with an accuracy of 0.5 to 19% for all tests. The spatially-distributed model generally gives better results with regard to breach discharge. The performance of this model is quite good in stage 1. However, the stationary phase (stage 2) is not well represented. The water depths are overestimated by 60% upstream of the channel. This means that the model is unable to predict the water depth in the main channel during this period. As these variables are underestimated, the results cannot be used as it is. An overestimation of the results would have been safer.

A sensitivity analysis was carried out on both models for fluvial dike failure experiments. This revealed that the uncertainties in the input parameters have a limited influence ($\approx 1\%$) on the uncertainties in the hydraulic variables of interest (only for experimental configurations). Other input parameters could have been taken into consideration. Nevertheless, this analysis took into account the major part of the most influential parameters.

A synthesis of the results obtained was carried out in order to identify, for each test and model, which empirical formulation is the most and least relevant in terms of breach discharge. An identification of the best combination (model/formulation) for each test was also provided in this synthesis of results. For more complex cases of dike breaches, Hager (1987) formulation combined with the 1D model enables the peak breach discharge to be obtained with a difference from the experimental results of less than 10%. For a simplified model using an empirical discharge coefficient formula not developed in this context, these results are very encouraging.

In addition, a ranking of all the formulations according to their performance in terms of breach discharge was carried out. Subramanya and Awasthy (1972) and Jalili and Borghei (1996) formulations are accurate for fixed beach geometry with zero crest height. For the configurations with non-zero crest height, formulations of Singh et al. (1994), Ranga Raju et al. (1979) and Nandesamoorthy and Thomson (1972) are the most accurate formulae. For dynamic breach opening configurations, the most effective formulations are those of Hager (1987), Jalili and Borghei (1996) and Singh et al. (1994).

A major perspective of this work would be the addition of a morphodynamic model to the numerical models to take into account dike erosion and sediment transport. Afterwards, a comparison of the different numerical models will be performed to assess their relevance.

References

APNews (2019). Mississippi river breaches pin oak levee in winfield. https://apnews.com/article/58c1f3dec6b74a81b450600cc147ef55. Accessed: 04.06.21.

Arnst, M. and Ponthot, J.-P. (2014). An overview of nonintrusive characterization, propagation, and sensitivity analysis of uncertainties in computational mechanics. *International Journal for Uncertainty Quantification*, 4(5):387–421.

Bagheri, S., Kabiri-Samani, A., and Heidarpour, M. (2013). Discharge coefficient of rectangular sharp-crested side weirs part i: Traditional weir equation. *Flow Measurement and Instrumentation*, 35:109–115.

Borghei, S., Jalili, M., and Ghodsian, M. (1999). Discharge coefficient for sharp-crested side weir in subcritical flow. *Journal of Hydraulic Engineering*, 125:1051–1056.

CIRIA (2013). International levee handbook.

Danka, J. and Zhang, L. (2015). Dike failure mechanisms and breaching parameters. *Journal of Geotechnical and Geoenvironmental Engineering*, 141(9):1–11.

De Marchi, G. (1934). Essay on the performance of lateral weirs. *L'Energia Elettrica*, 11:849–860.

de Moel, H., Jongman, B., Kreibich, H., Merz, B., Penning-Rowsell, E., and Ward, P. (2015). Flood risk assessments at different spatial scales. *Mitig Adapt Strateg Glob Change*, 20:865–890.

Dewals, B. (2020). Natural and technological risks in civil engeneering (academic course).

Emiroglu, M., Agaccioglu, H., and Kaya, N. (2011). Discharging capacity of rectangular side weirs in straight open channels. *Flow Measurement and Instrumentation*, 22:319–330.

FEMA (2004). Federal guidelines for dam safety, glossary of terms. *Journal of Geotechnical and Geoenvironmental Engineering*.

Flóriàn, G., de Haan, W., Houben, R., Paape, A., Schiereck, G., de Smidt, J., and Vrouwenvelder, A. (1998). Fundamentals on water defences. *Technical advisory committee*.

Gaddie, V., Mierza, M., and Marr, J. (2021). California water boards: Levee failures in the sacramento-san joaquin river delta. https://www.waterboards.ca.gov/waterrights/water_issues/programs/bay_delta/california_waterfix/exhibits/docs/PPorgans/porgans_301.pdf. Accessed: 04.06.21.

Hager, W. (1987). Lateral outflow over side weirs. *Journal of Hydraulic Engineering*, 113:491–504.

Hallissy, E. (2005). Months of work after levees break / california lesson: Repairing breaches first step of long process. https://www.sfgate.com/news/article/MONTHS-OF-WORK-AFTER-LEVEES-BREAK-CALIFORNIA-2613638.php. Accessed: 04.06.21.

Hudson, P. (2005). Natural levees. *Encyclopedia of water science*, 10:1–4.

Jalili, M. and Borghei, S. (1996). Discussion: discharge coefficient of rectangular side weirs. *Journal of Irrigation and Drainage Engineering*, 122:132–132.

Kandaswamy, P. and Rouse, H. (1957). Characteristics of flow over terminal weirs and sills. *Journal of Hydraulics Division*, 83:1–13.

Knabb, R., Rhome, J., and Brow, D. (2005). Hurricane katrina 23-30 august 2005. *Tropical Cyclone Report*, pages 1–43.

Michelazzo, G. (2014). River levee breaching: Analytical flow modelling and experimental hydro-morphodynamic investigations (ph.d. dissertation).

Michelazzo, G., Oumeraci, H., and Paris, E. (2015). Laboratory study on 3d flow structures induced by zero-height side weir and implications for 1d modeling. *Journal of Hydraulic Engineering*, 141(10):1–11.

Mignot, E., Camusson, L., , and Riviere, N. (2020). Measuring the flow intrusion towards building areas during urban floods: Impact of the obstacles located in the streets and on the facade. *Journal of Hydrology*, 583:1–12.

Nandesamoorthy, T. and Thomson, A. (1972). Discussion of spatially varied flow over side weir. *Journal of the Hydraulics Division*, 98:2234–2235.

Nash, J. and Sutcliffe, J. (1970). River flow forecasting through conceptual models part i - a discussion of principles. *Journal of Hydrology*, 10:282–290.

Ranga Raju, K., Gupta, S., and Prasad, B. (1979). Side weir in rectangular channel. *Journal of the Hydraulics Division*, 105:547–554.

Rifai, I. (2018). Overtopping induced fluvial dike failure (ph.d. dissertation).

Rifai, I., El kadi Abderrezzak, K., Erpicum, S., Archambeau, P., Violeau, D., Pirotton, M., and Dewals, B. (2019). Flow and detailed 3d morphodynamic data from laboratory experiments of fluvial dike breaching. *Scientific Data*, 6:53:1–11.

Rifai, I., Erpicum, S., Archambeau, P., Violeau, D., Pirotton, M., El Kadi Abderrezzak, K., and Dewals, B. (2017). Discussion of "laboratory study on 3d flow structures induced by zero-height side weir and implications for 1d modeling" by giovanni michelazzo, hocine oumeraci, and enio paris. *Journal of Hydraulic Engineering*, 143(3):1–2.

Rifai, I., Schmitz, V., Erpicum, S., Archambeau, P., Violeau, D., Pirotton, M., Dewals, B., and El Kadi Abderrezzak, K. (2020). Continuous monitoring of fluvial dike breaching by a laser profilometry technique. *Water Resources Research*, 56:1–16.

Rijksmuseum (2021). Master of the st. elizabeth panels. `https://www.rijksmuseum.nl/`. Accessed: 04.06.21.

Roger, S., Dewals, B., Erpicum, S., Schwanenberg, D., Schüttrumpf, H., Köngeter, J., and Pirotton, M. (2009). Experimental and numerical investigations of dike-break induced flows. *Journal of Hydraulic Research*, 47(3):349–359.

RTBF (2010). Chine: la rupture d'une digue menace 12 000 personnes. `https://www.rtbf.be/info/monde/detail_chine-la-rupture-d-une-digue-menace-12-000-personnes?id=5032143`. Accessed: 04.06.21.

RTBF (2012). Brésil: 4000 évacuations après la rupture d'une digue. https://www.rtbf.be/info/monde/detail_bresil-4000-evacuations-apres-la-rupture-d-une-digue?id=7341503. Accessed: 04.06.21.

Schmitz, V. (2021). Influence of the drain discharge (working paper).

Schmitz, V., Erpicum, S., El kadi Abderrezzak, K., Rifai, I., Archambeau, P., Pirotton, M., and Dewals, B. (2021). Overtopping-induced failure of non–cohesive homogeneous fluvial dikes: effect of dike geometry on breach discharge and widening (under review).

Singh, R., Manivannan, D., and Satyanarayana, T. (1994). Discharge coefficient of rectangular side weirs. *Journal of Irrigation and Drainage Engineering*, 120:814–819.

Subramanya, K. and Awasthy, S. (1972). Spatially varied flow over side-weirs. *Journal of the Hydraulics Division*, 98:1–10.

Swamee, P., Pathak, K., and Ali, M. (1994a). Side-weir analysis using elementary discharge coefficient. *Journal of Irrigation and Drainage Engineering*, 120:742–755.

Swamee, P., Pathak, K., Mohan, M., Agrawal, S., and Ali, M. (1994b). Subcritical flow over rectangular side weir. *Journal of Irrigation and Drainage Engineering*, 120:212–217.

TenCate (2021). Geosynthetics. https://www.tencategeo.eu/en/. Accessed: 04.06.21.

Weerts, H., Cohen, K., and Kleinhans, M. (2012). The 1421 st.elisabeth flooding 'event' and the loss of "de groote waard", the netherlands. *4th International Geologica Belgica Meeting 2012*, Session06(138):86.

Wu, W. (2013). Simplified physically based model of earthen embankment breaching. *Journal of Hydraulic Engineering*, 139(8):837–851.

Yu-Tech, L. (1972). Discussion of spatially varied flow over side weir. *Journal of the Hydraulics Division*, 98:2046–2048.

A | Appendix

A.1 Results comparison of the different rating curves for Michelazzo et al. (2015) tests

This section is dedicated to the comparison of the results obtained with the following 4 rating curves: Michelazzo et al. (2015) rating curve, rating curve reconstructed by regression of series A & B results, reconstructed by regression of series B results and constructed using the sluice gate formula.

A.1.1 Lumped model

Figures A.1 and A.2 illustrate the results in terms of breach discharge. Figures A.3 and A.4 show the results in terms of water depths.

For the Michelazzo et al. (2015) rating curve, the difference obtained decreases considerably beyond the B12 test with a difference of less than 5% for the various formulations (except for Singh et al. (1994) formulation).

The other three rating curves have quite similar results except for the B7 test. The difference observed is at most about 10%. For tests below the B12 test, the observed differences are under 5%.

In terms of water depths, the results are very similar. For the tests from B7 to B12, the 3 reconstructed rating curves give better results (i.e. the difference with the experimental results is lower).

In general, the results obtained with the different rating curves are similar. The choice of one over the other can be justified for each of the rating curves.

A.1.2 Spatially-distributed model

The same kind of analysis as for the lumped model can be done for the spatially-distributed model (Figures A.5 and A.6). Again, the results are quite similar. However, for some formulations, the Michelazzo et al. (2015) rating curve observes larger differences than the other rating curves. The B7 test is again worse for the Michelazzo et al. (2015) rating curve. Apart from this test, for the most accurate simulations, the differences observed for each of the rating curves are well below 10%.

A notable difference with the Michelazzo et al. (2015) rating curve is that the breach discharge is always underestimated (except for Emiroglu et al. (2011) formulation).

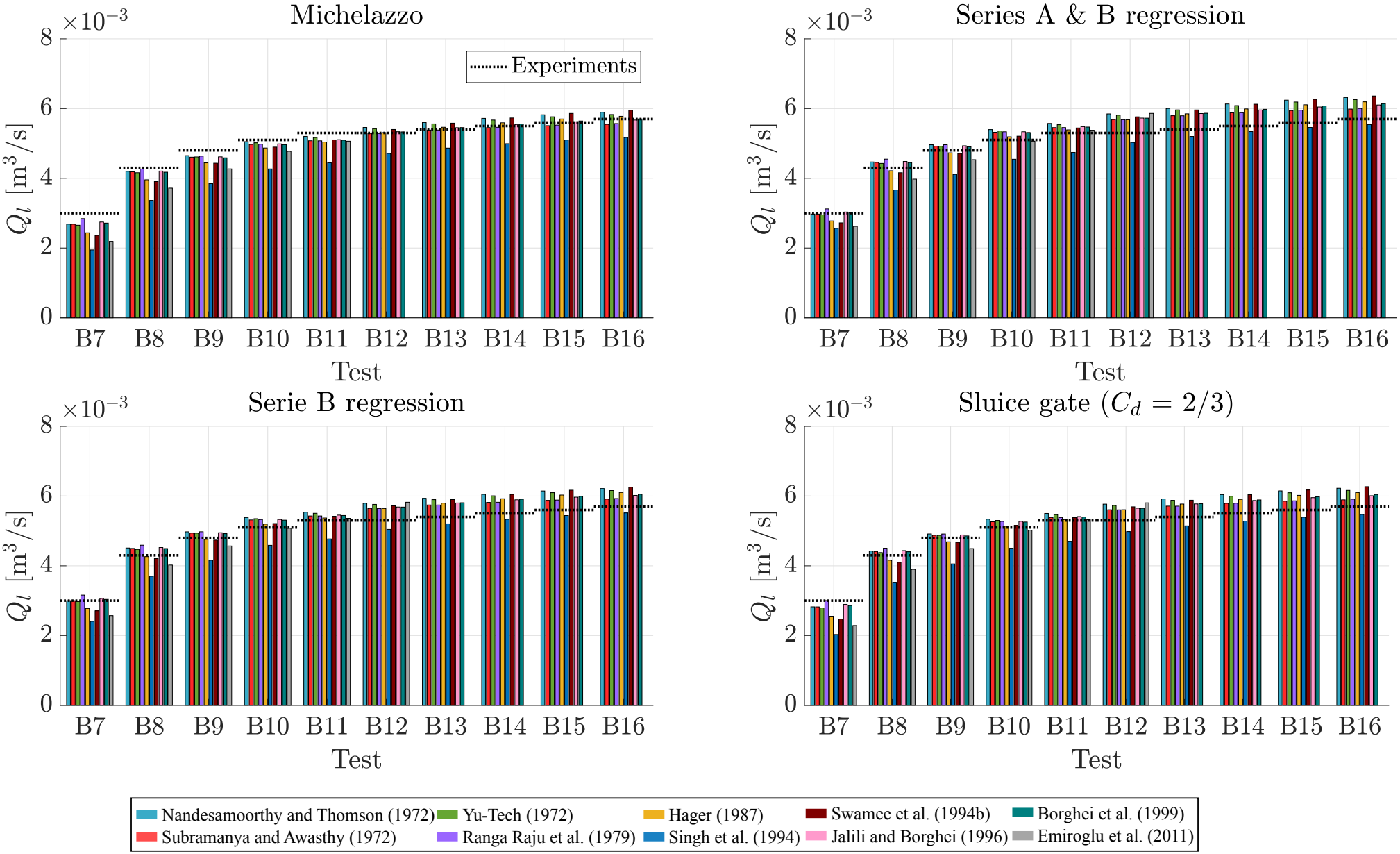

Figure A.1: Breach discharge results (0D model) for the 4 rating curves of Michelazzo et al. (2015) tests.

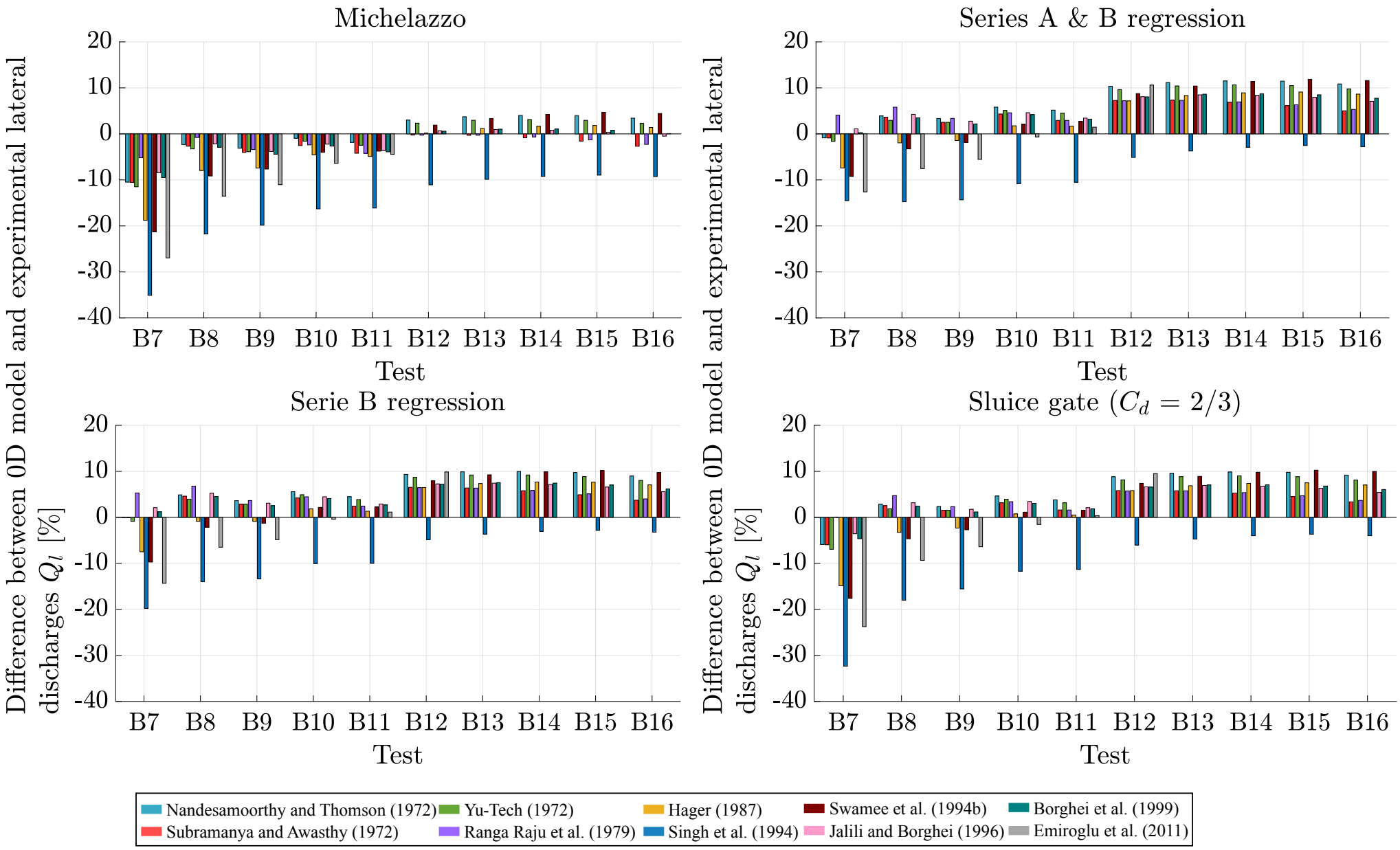

Figure A.2: Difference between numerical (0D model) and measurement breach discharge results for the 4 rating curves of Michelazzo et al. (2015) tests.

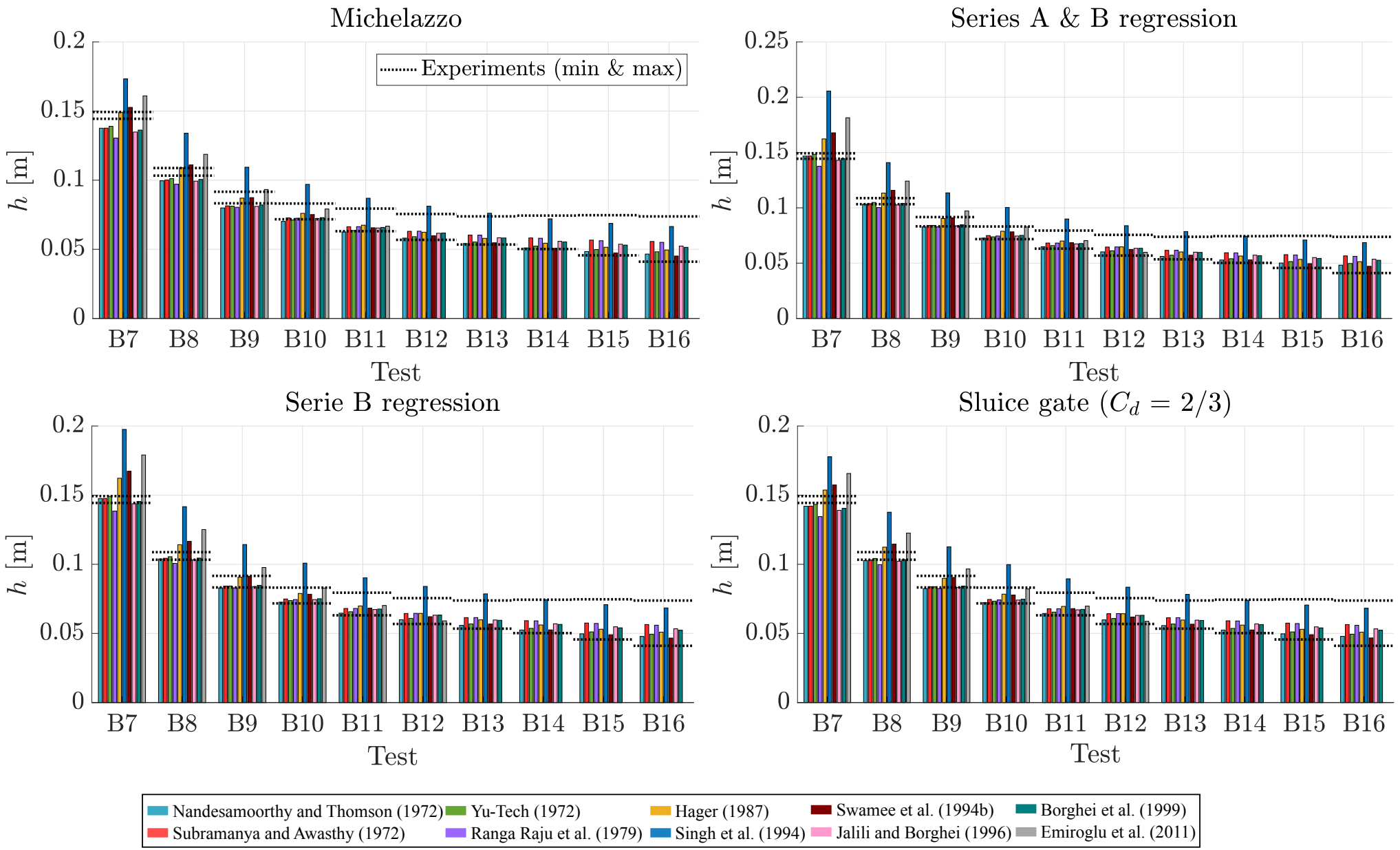

Figure A.3: Water depth results (0D model) for the 4 rating curves of Michelazzo et al. (2015) tests.

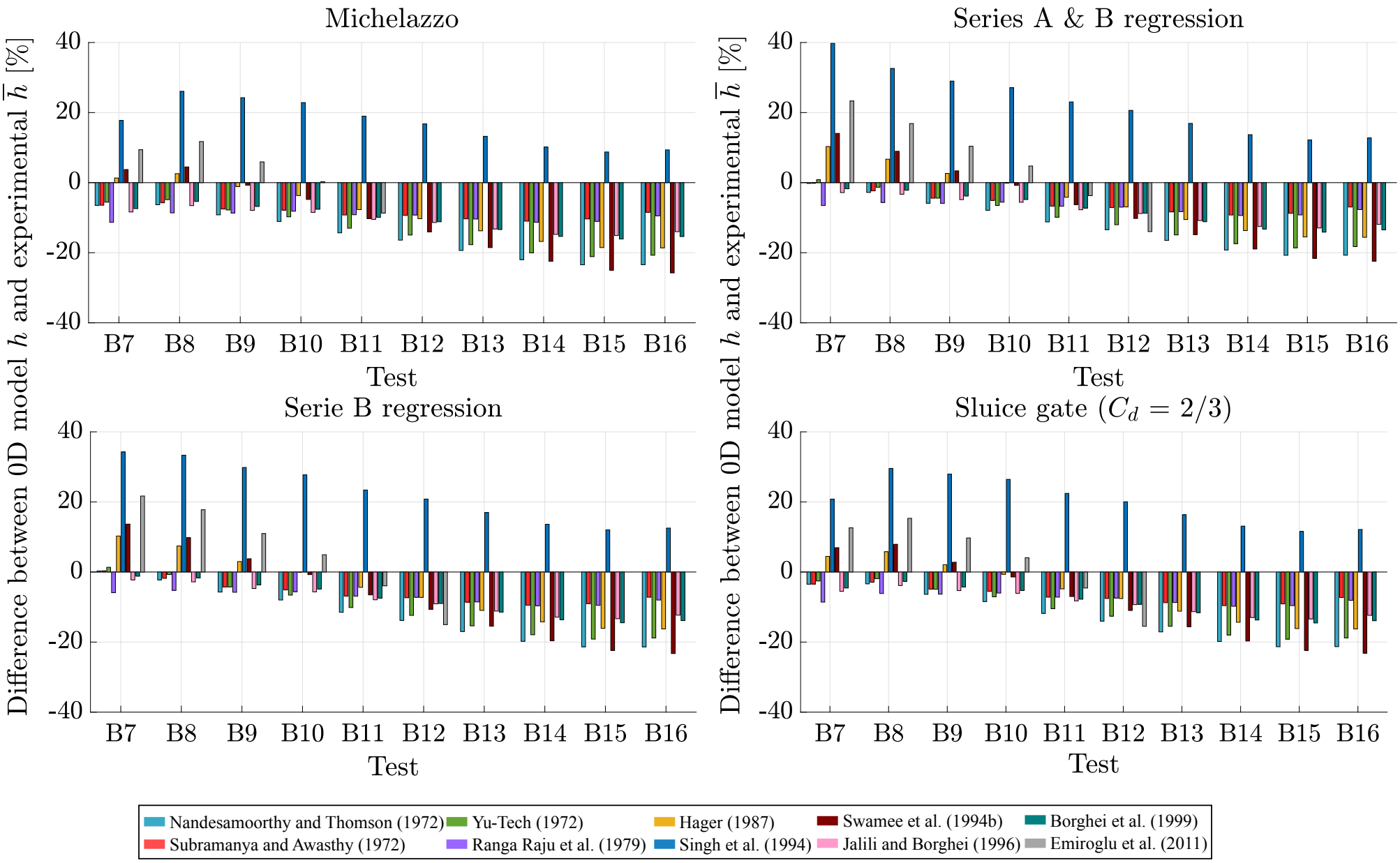

Figure A.4: Water depth difference between numerical (0D model) and experimental average for the 4 rating curves of Michelazzo et al. (2015) tests.

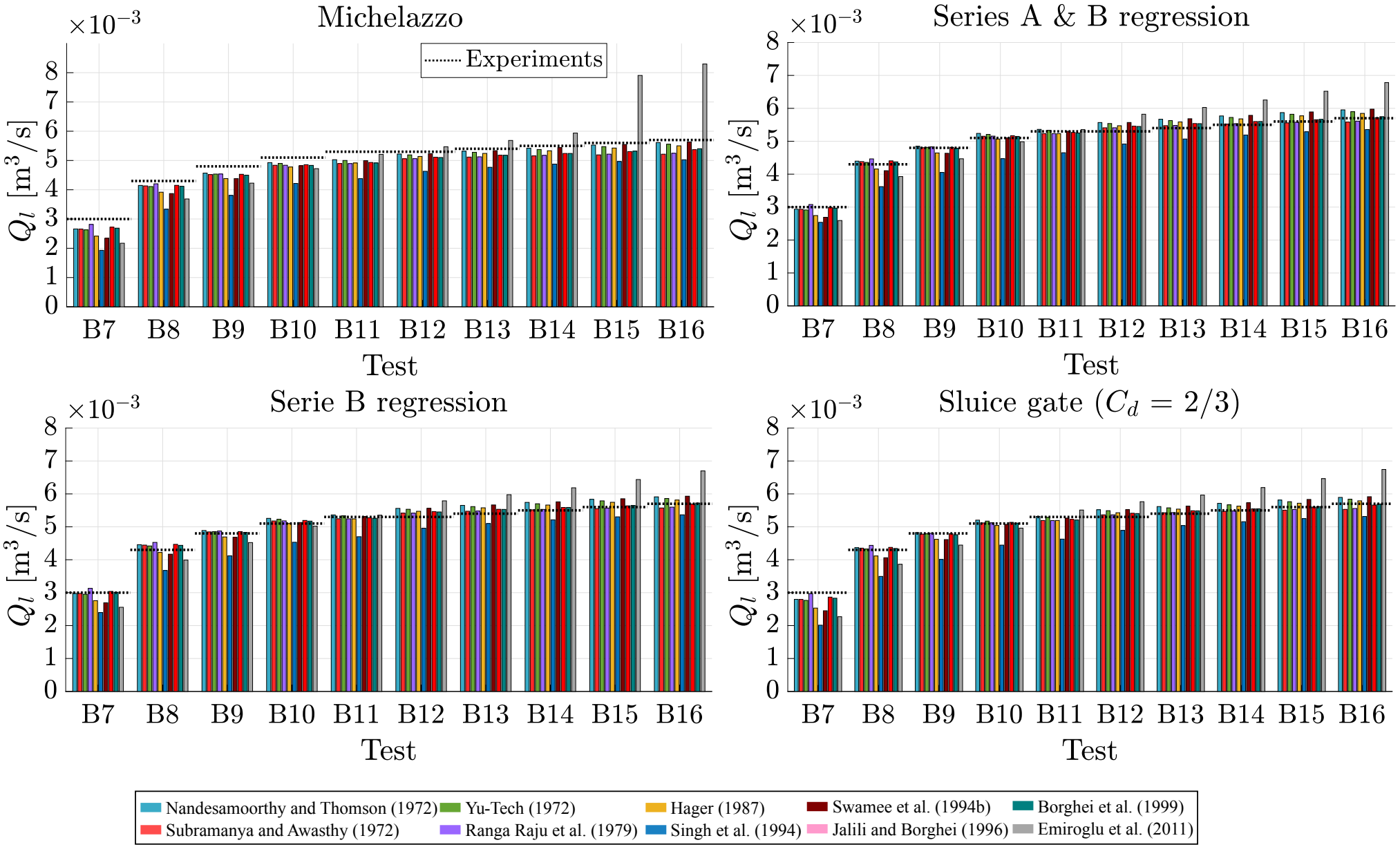

Figure A.5: Breach discharge results (1D model) for the 4 rating curves of Michelazzo et al. (2015) tests.

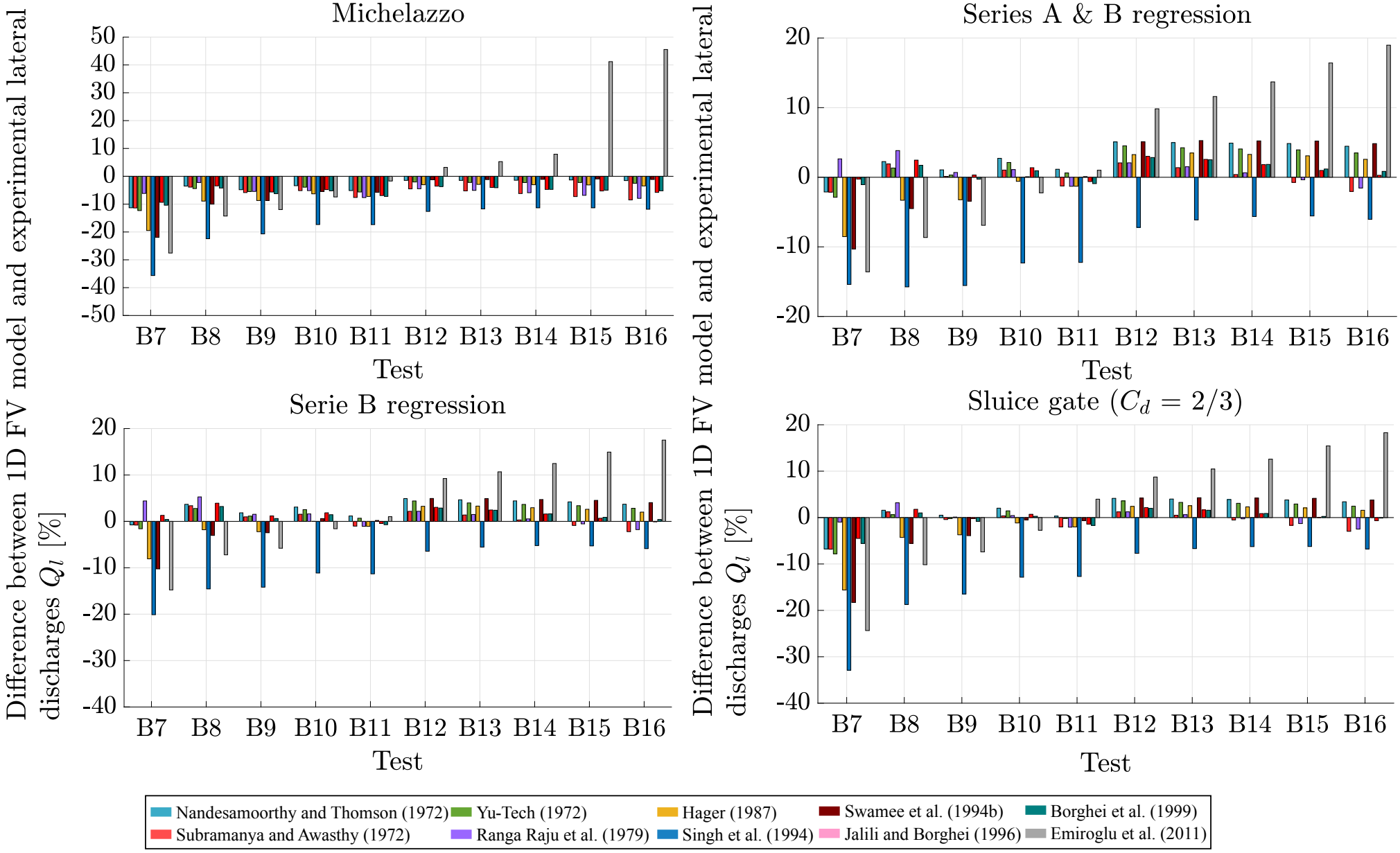

Figure A.6: Breach discharge difference between numerical (1D model) and measurement for the 4 rating curves of Michelazzo et al. (2015) tests.

A.2 PDF used for sensitivity analyses

The following figures (FIGURES A.7, A.8 and A.9) illustrate the probability density functions of the different input parameters for each sensitivity analysis performed (different models/α). In addition to the probability density functions, the random draws performed using the Beta law are also represented. As a reminder, 1000 random draws were made for the lumped model and 500 for the spatially-distributed model.

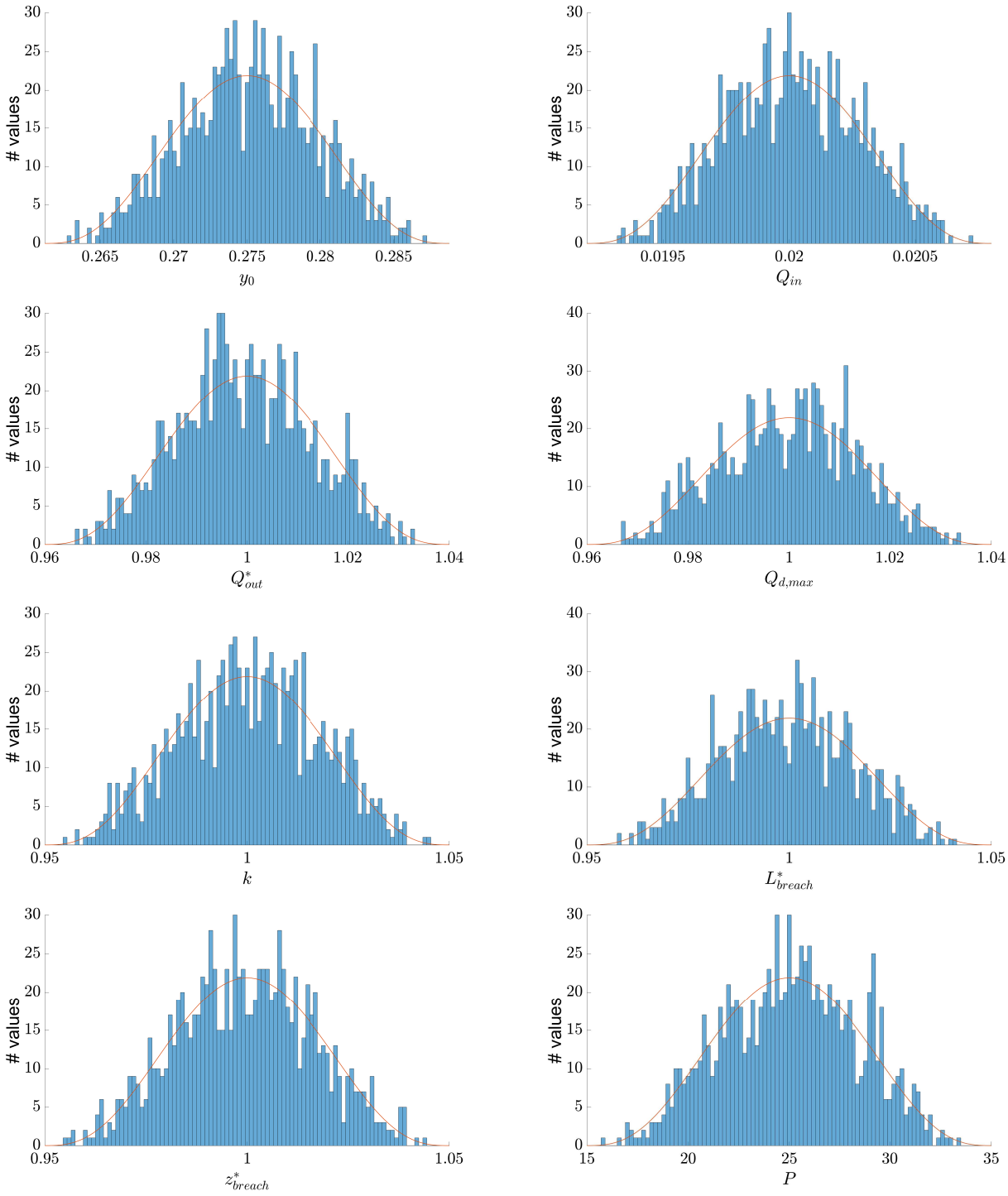

Figure A.7: PDF for all input parameters (in orange) and the distribution of the thousand random draws made (blue bars) for 0D model with $\alpha = 4$.

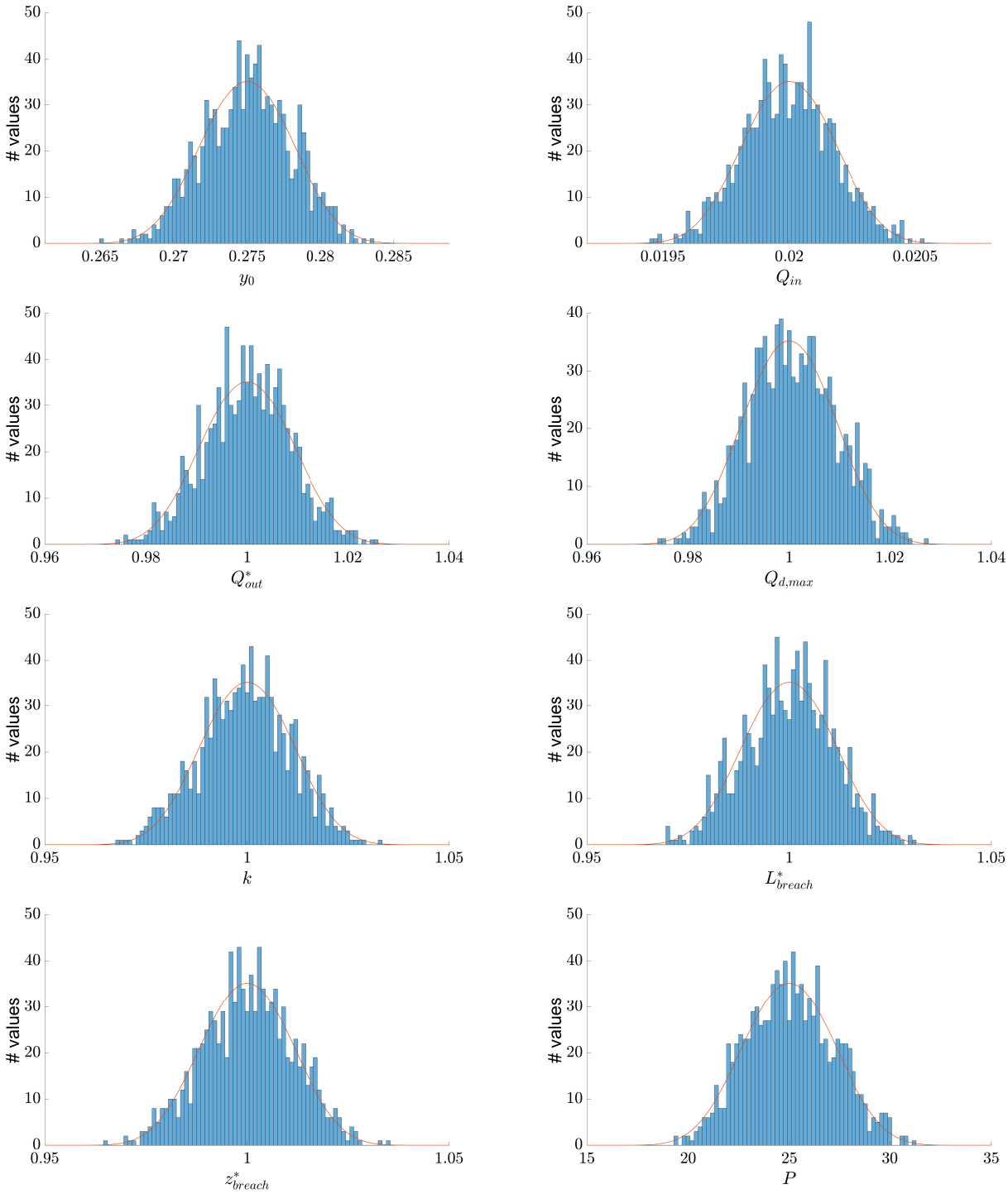

Figure A.8: PDF for all input parameters (in orange) and the distribution of the thousand random draws made (blue bars) for 0D model with $\alpha = 10$.

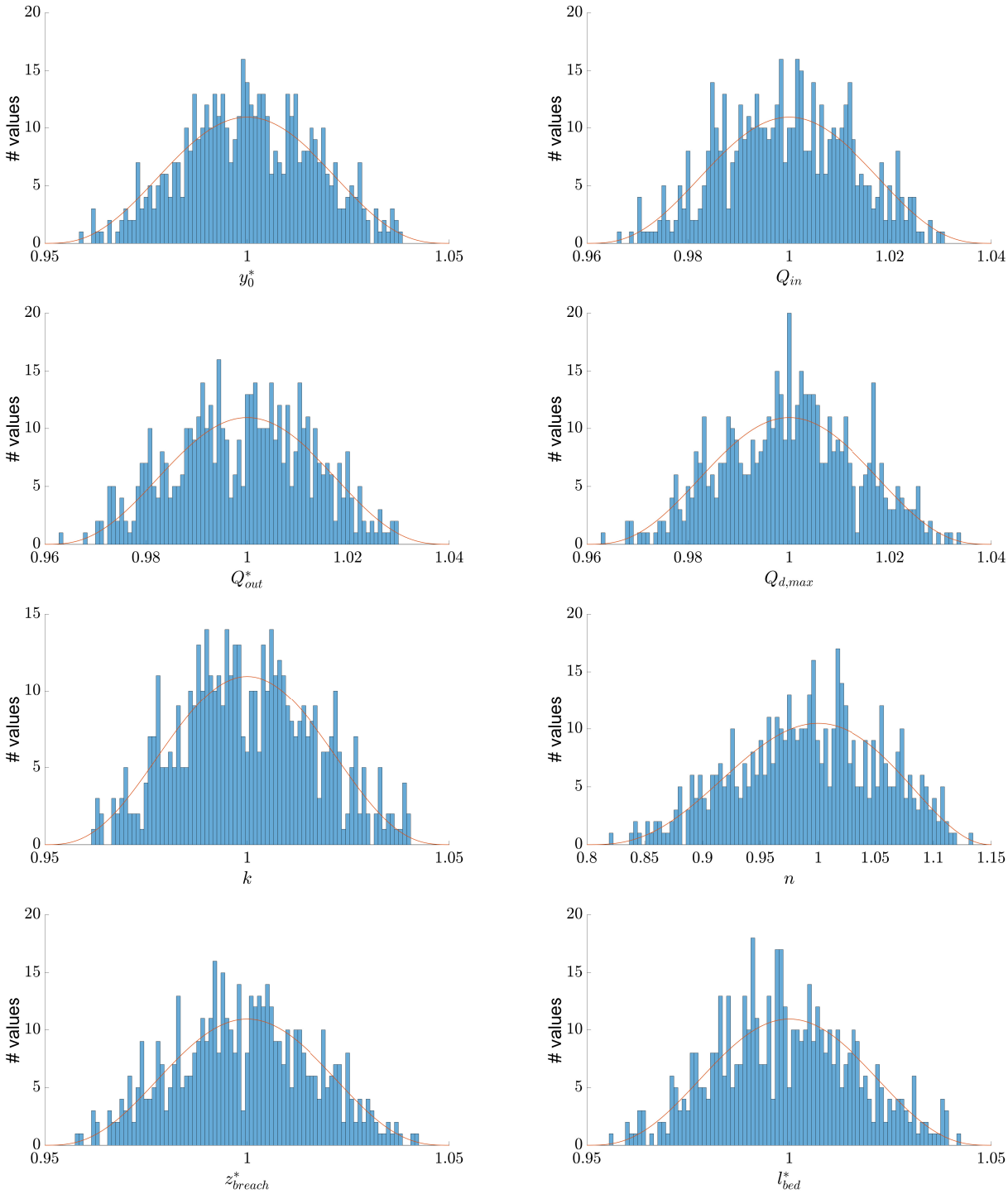

Figure A.9: PDF for all input parameters (in orange) and the distribution of the five hundred random draws made (blue bars) for 1D model with $\alpha = 4$.